POST-ENTRY DETERMINANTS OF MAMMALIAN ORTHOREOVIRUS REPLICATION

By

Laura Sue Ooms

Dissertation

Submitted to the faculty of the

Graduate School of Vanderbilt University

in partial fulfillment of the requirements

for the degree of

DOCTOR OF PHILOSOPHY

in

Pathology

August 2012

Nashville TN

Approved:

Dr. James D. Chappell, M.D., Ph.D.

Dr. Christopher R. Aiken, Ph.D.

Dr. Terence S. Dermody, M.D.

Dr. W. Gray Jerome, Ph.D.

Dr. Michael Laposata, M.D., Ph.D.

To my parents

ACKNOWLEDGEMENTS

I would not have been able to accomplish this body of work without the support of many people and to them I owe many thanks.

I would like to first thank my mentor, Jim Chappell, for his tireless dedication and support to my graduate training. Jim has to be one of hardest working and busiest people I know, yet he has always made time for me when I needed guidance. I have very much appreciated his commitment to my scientific training and career development. The Chappell lab has been a great place to train largely due to the great people who I have had the opportunity to work with. I would like to thank Sam Naik, the original Chappell lab manager, who not only supported the lab scientifically, but also made it a fun place to be. I thank Charles Martinez for our many scientific discussions and his help with experimental troubleshooting. I would like to thank Sandy Alvarez, our current lab manager. I am very thankful not only for her support to my work but also our friendship.

I would like to thank Terry Dermody who essentially has been a second mentor to me. Terry has included me in his lab group and treated me like one of his graduate students. I have greatly appreciated his critical feedback, helpful suggestions, and encouragement. His mentorship has significantly enhanced my graduate training. I would like to thank all the members of the Dermody lab for their support through my time in graduate school. Takeshi Kobayashi laid down the foundation for my project and provided me with the tools I needed to get started. Past members Karl Boehme, Pranav Danthi, Kristen Guglielmi, Geoff Holm, Liz Johnson, Denise Wetzel and present members Alison Ashbrook, Magda Bokiej, Josh Doyle, Johnna Frierson, Mine Ikizler,

Jason Iskarpatyoti, Solomiia Khomandiak, Jen Konopka, Caroline Lai, Bernardo Mainou, Andrea Pruijssers, Laurie Silva, Jen Stencel, Danica Sutherland, Greg Wilson, and Paula Zamora. Thank your for your technical support, helpful contributions in lab meetings and working groups, and friendship.

I would also like to thank the members of my dissertation committee: Drs. Mike Laposata, Jay Jerome, Chris Aiken, and Terry Dermody. Their critical input and advice were very helpful in guiding me throughout my graduate work and have significantly enhanced the quality of my training.

I am very grateful for the financial support of the departments of Pathology, Microbiology, & Immunology and Pediatric Infectious Diseases. Additional support was provided by the Elizabeth B. Lamb Center for Pediatric Research and Public Health Service awards K08 AI062862 (J. Chappell) and R0I AI32539 (T. Dermody).

During my time in Nashville I have made friends with some amazing people. I would like to thank Katie Larson; I value our friendship, the fun we have together, and her willingness to listen when I am struggling through something. I would like to thank the people I live with, Erin, Ritch, and Ritchie Gillespie. They have become like family to me and I am very thankful that I have such great place to live. I would also like to thank Daniel Larson, Erin Bruton, Margaret Parrish, Dana McIntosh, Erin Martinez, Anna Cummings, and all my other friends from West End Community Church. Thank you all for your encouragement and reminder that there is life outside of the lab.

I would like to thank my faculty advisor and research mentor from Trinity Christian College, Dr. Robin Pals-Rylaarsdam. Dr. Robin introduced me to scientific research and encouraged me to go to graduate school. Her mentorship very much defined

my scientific training in college and provided me with the tools I needed to succeed in graduate school.

I have been very blessed with a wonderful family. I would like to thank my grandparents, Bill and Christine Ooms and Marv and Pearl Vis, Uncle Bob, Auntie Sharon, Auntie Lu, and cousins, Lisa, Amy, Jonathan, and Alex, for their love and support. I have two fantastic older sisters, Marcia and Rachel. Marcia is one of my biggest encouragers and I have greatly appreciated her support over the years. When it came to school, Rachel strove for perfection and gave her best to her studies; I don't think I would have had as much academic success without learning from her example. I may not have always appreciated my sisters growing up, but they helped make me who I am today and I am so glad that we are not just sisters but friends. My brother-in-law Jeremy has made an awesome addition to our family and my niece Leah is such a joy and I am so excited to watch her grow up.

Finally, I would like to thank my parents, Bill and Joan Ooms. They deserve the credit for so much of what I am today. They taught me how to work hard and believe in myself and have encouraged me through every challenge I have faced. They have made many sacrifices to provide for me including ensuring that I had an excellent education. I thank them for their unconditional love and support.

TABLE OF CONTENTS

LIST OF TABLES

LIST OF FIGURES

LIST OF ABBREVIATIONS

AGMK	African green monkey kidney
Ch	chimera
DK	dog kidney
ds	double-stranded
HDV	hepatitis delta virus
IFN	interferon
IRF	interferon regulatory factor
L cell	murine L929 cell
L1	λ3-expressing gene
M1	μ2-expressing gene
MDBK	Madin Darby bovine kidney
MDCK	Madin Darby canine kidney
MOI	multiplicity of infection
NTP	nucleotide triphosphate
NTPase	nucleotide triphosphatase
P2 stock	second passage stock of virus
PFU	plaque forming unit
RdRp	RNA-dependent RNA-polymerase
Reovirus	mammalian Orthoreovirus
rs	recombinant strain
RTPase	RNA triphosphatase

RT-qPCR	Reverse transcription-quantitative PCR
SCID	severe combined immunodeficient
ss	single-stranded
ts	temperature-sensititve
T1	type 1 Lang
T3	type 3 Dearing
T7P	T7 RNA polymerase promoter
TEM	transmission electron microscopy
VP	virion particle

CHAPTER I

BACKGROUND

Introduction

In this research, I have focused on post-entry determinants of mammalian Orthoreovirus (reovirus) replication. These studies have contributed to unifying principles of RNA virus biology within three major categories: post-entry mediated virus tropism, compartmentalization of viral replication machinery into specialized sites in the cytoplasm, and viral replication protein structure and function. I have focused primarily on reovirus protein μ2, a replication protein that contributes to reovirus tropism and organization of transcriptional machinery and modulates diverse functions during the viral life cycle.

Viral tropism, defined by the range of hosts, tissues, and cells productively infected, creates natural biologic groupings among viruses that correlate with infection pathology, clinical disease expression, and epidemiology. Viral tropism has historically been thought to be governed by receptor engagement via the virus attachment protein. Receptor-dependent tropism has been characterized for many virus families (118); however, receptor engagement does not ensure successful replication as productive interaction with the cellular machinery at each step in the viral life cycle is required (70). Species-, tissue- and cell-type specific differences leading to non-productive viral interaction with cellular factors and thus reduced replication efficiency can be thought of as post-entry determinants of viral tropism.

A notable example of a post-entry mediated viral tropism has been described for influenza virus replication (82, 83). Replication of avian influenza virus is inhibited in human cells (82, 83). The viral determinants controlling replication capacity in avian vs. human cells reside within the proteins that comprise the RNA-dependent RNA-polymerase (RdRp), and inhibition of replication is observed during post-entry stages of the influenza life cycle (70). Picornaviruses also display post-entry mediated tropism; for example, poliovirus does not replicate in heart, lung, and kidney tissue despite high expression of the poliovirus receptor (122). Tissue-specific picornavirus tropism is thought to be determined by cell type-specific differences in factors required for IRES-mediated translation (53, 64, 90). These examples highlight two models of virus cell tropism regulated at post-entry steps in the virus life cycle. Despite a few key examples where the basis of viral, cellular, or host-species tropism has been clearly delineated in molecular terms, the vast diversity of viral replication strategies and tropic patterns suggests that mechanisms of cell- and tissue-specific permissivity to viral infection remain largely undefined.

A second major theme of my dissertation work is the capability of viruses to form specialized sites within a host cell to complete viral replication. RNA-containing viruses are challenged by the requirement for a unique biochemical apparatus that orchestrates the complex, and potentially competing, processes of genome amplification and new particle assembly while protecting viral RNAs from nuclease-mediated destruction. Furthermore, the replication program must proceed against potent antiviral defenses trained on molecular patterns and replicative intermediates shared by virtually all RNA viruses. Among single-stranded (ss) RNA viruses, a common strategy to coordinate RNA

regulation is compartmentalization of the viral replication machinery within reorganized cellular membranes. These structures recruit genomic RNAs, concentrate viral proteins and RNA for assembly, and likely shield viral products from the cellular antiviral response (1, 29, 81). Analogously, animal double-stranded (ds) RNA viruses generate nonmembranous intracytoplasmic structures—termed inclusions or factories—that have a characteristic morphology, contain viral proteins and RNA, and constitute the presumed site of (-)-strand RNA synthesis and particle assembly (24, 89, 110). Little is known about the nature of inclusions of dsRNA virus replication, including the individual and corporate roles of viral proteins.

The third major theme of my work is the organization of RNA virus functional domains that coordinate replication activities. The nature of RNA virus genomes dictates a sophisticated interplay of transcription, translation, replication, and encapsidation involving contributions by virus and cell to a biochemical apparatus that integrates these complex events required for productive viral infection. While the RNA replication proteins of different viral families coordinate similar replicative activities, the way in which their respective functional domains are arranged into proteins can be quite different. For example, rotavirus and reovirus are related dsRNA viruses that display similar life cycles; however, the viral proteins that mediate inclusion formation, protein recruitment to inclusions, and nucleotide triphosphatase (NTPase) activity are uniquely organized into two (rotavirus nsp2 and nsp5) or three (reovirus μNS, μ2, and σNS) proteins (113). A common strategy used by RNA viruses to organize replication domains is to encode multifunctional proteins that perform diverse activities during the viral life cycle. For example, the N protein of bunyaviruses binds viral RNA, interacts with the

viral polymerase, modulates ribonucleoprotein complex assembly, and interacts with proteins involved in cellular metabolism (56, 97). RNA viruses use a surprisingly small number of viral proteins to accomplish genome transcription and replication and often multifunctional proteins are a necessity. However, much remains unknown about the unique strategies used by RNA virus replication proteins to organize and coordinate diverse functions during the viral life cycle.

These three themes have been integrated throughout my study of post-entry determinants of reovirus replication. Reoviruses are non-enveloped, dsRNA viruses that display broad cell, tissue, and host tropism and serve as tractable models for the study of virus-cell interactions that dictate unique tropic properties. Critical checkpoints mediating reovirus tropism are governed both at receptor engagement and post-entry steps in the viral life cycle (7, 41, 55, 93, 128). The majority of the viral life cycle following entry takes place within viral cytoplasmic inclusions, which are biosynthetic centers of genome multiplication and new particle assembly (24); therefore, post-entry mediated reovirus tropism is likely governed by steps that occur with viral inclusions. Reovirus replication protein μ2 has many functional and biochemical properties that are essential to post-entry steps in the viral life cycle (24). μ2 is a structurally minor subunit of the virion core (25) found both in the cytoplasm and nucleus of infected cells (60, 68). Additionally, μ2 is a polymerase cofactor, an essential component of viral inclusions (61, 88), and a regulator of virulence (44, 49, 103, 104). Investigation of the mechanism by which μ2 coordinates its diverse functions throughout the reovirus life cycle intersects the three themes of RNA virus biology described above. Therefore, my studies have expanded our understanding

of post-entry mediated tropism, formation and organization of viral inclusions, and viral replication protein structure and function.

When this work was initiated, it was known that numerous strain-specific differences in reovirus replication potential for primary and transformed cells segregate with the μ2-encoded M1 gene, along with other components of the viral core (66, 67, 93, 101-103). A study performed by Rodgers et al. using T1 x T3 reassortant viruses showed that the λ3-encoding L1 and μ2-encoding M1 genes segregate with differences in the replication efficiency of T1 and T3 infection of Madin Darby canine kidney (MDCK) cells (93). Interestingly, the S1 gene, encoding the attachment protein σ1, was not genetically linked to this tropism phenotype. λ3 and μ2 are thought to form the viral RdRp; therefore, it was hypothesized that replication in MDCK is restricted at a later time point of infection when these proteins carry out their functions. This dichotomy presented a useful experimental platform to rigorously address the individual and cooperative roles of μ2 and λ3 in reovirus cell tropism and identify μ2-sensitive steps in the viral life cycle.

In my dissertation research, I have attempted to elucidate viral determinants of reovirus tropism for MDCK cells. Data presented in Chapter II identifies contributions of individual reovirus gene segments to replication efficiency in MDCK cells and sequence polymorphisms of μ2 that affect replication efficiency. Furthermore, replication experiments that provide initial clues into the cellular determinants mediating tropism for MDCK cells are reported. Chapter III outlines a systematic analysis of post-entry steps in the reovirus life cycle and identifies the specific stage that T3 fails to complete in MDCK cells. In Chapter IV, the functionally abnormal inclusions formed in T3-infected cells are

characterized using transmission electron microscopy (TEM), and the effect of temperature on T3 replication in MDCK cells is determined. These studies further an understanding of the role of μ2 in the viral life cycle to include initiation of particle assembly within viral inclusions. Furthermore, these studies indicate that this step in the viral life cycle is subject to regulation by cellular factors.

General Characteristics of Reovirus Biology

The reovirus virion (Fig. 1.1A) is a non-enveloped, icosahedral particle consisting of two

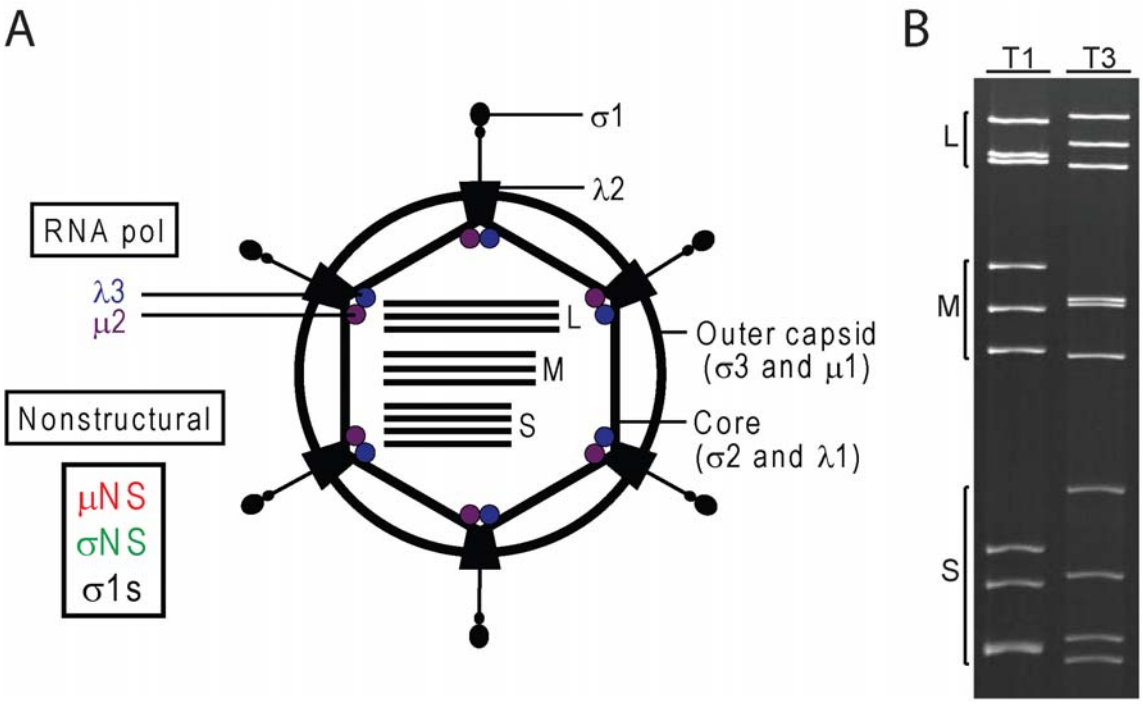

Figure 1.1. The reovirus virion particle. (A) Schematic of the reovirus virion. The virion is made of two concentric protein shells, the outer capsid and inner core which enclose the 10 dsRNA viral gene segments. The polymerase complex is located at the base of the vertex at the 5-fold axis of symmetry. The virus also encodes three nonstructural proteins. (B) Electropherotype of prototype strains of reovirus, type 1 Lang (T1) and type 3 Dearing (T3). Positions of L, M, and S gene segments are indicated.

protein shells, the outer capsid and inner core. The core encloses ten double-stranded RNA gene segments, which encode eight structural proteins and three nonstructural proteins (69, 96). Gene segments are separated into three size classes based on their electrophoretic mobility in polyacrylamide gels (Fig. 1.1B)–small, medium, and large (S, M, L)–which encode the σ, μ, and λ proteins, respectively (69, 79, 100). The virion core is formed by the λ1, λ2, λ3, μ2, and σ2 proteins. λ1 and σ2 form the shell of the core. Pentamers of λ2 form turrets at the five-fold axes of symmetry; one copy of λ3 and presumably two copies of μ2 are located at the base of these turrets. The outer capsid consists of μ1-σ3 heterohexamers that overlay the core. Attachment protein σ1 forms trimers that extend from the λ2 turrets (31, 34, 91) (Fig. 1.1A). Reovirus also encodes three nonstructural proteins: μNS, σNS, and σ1s (52).

Four reovirus serotypes have been identified based on neutralization and hemagglutination studies (4, 94, 95). The prototype strains for serotypes 1 and 3 are type 1 Lang (T1) and type 3 Dearing (T3), respectively. T1 and T3 display numerous phenotypic differences, including receptor usage, activities of viral replication proteins, regulation of the interferon response to reovirus infection, apoptosis induction, growth in various types of primary and transformed cells, virulence, dissemination pathways, and cell and tissue tropism in newborn mice (96). The genetic basis of several biological polymorphisms has been defined using reassortant viruses derived from co-infections of T1 and T3 (96). Such analyses have provided key insights into viral replication and disease mechanisms.

Reovirus Replication

The reovirus replication cycle (Fig. 1.2) begins with virion attachment to the host cell through interaction of reovirus protein σ1 with proteinaceious or carbohydrate receptors followed by receptor-mediated endocytosis (28). Following internalization of virions, the viral outer capsid disassembles within the endosome to generate transcriptionally active core particles (111), which are released into the cytoplasm. The viral cores synthesize full-length, message-sense, capped and nonpolyadenylated ssRNAs corresponding to

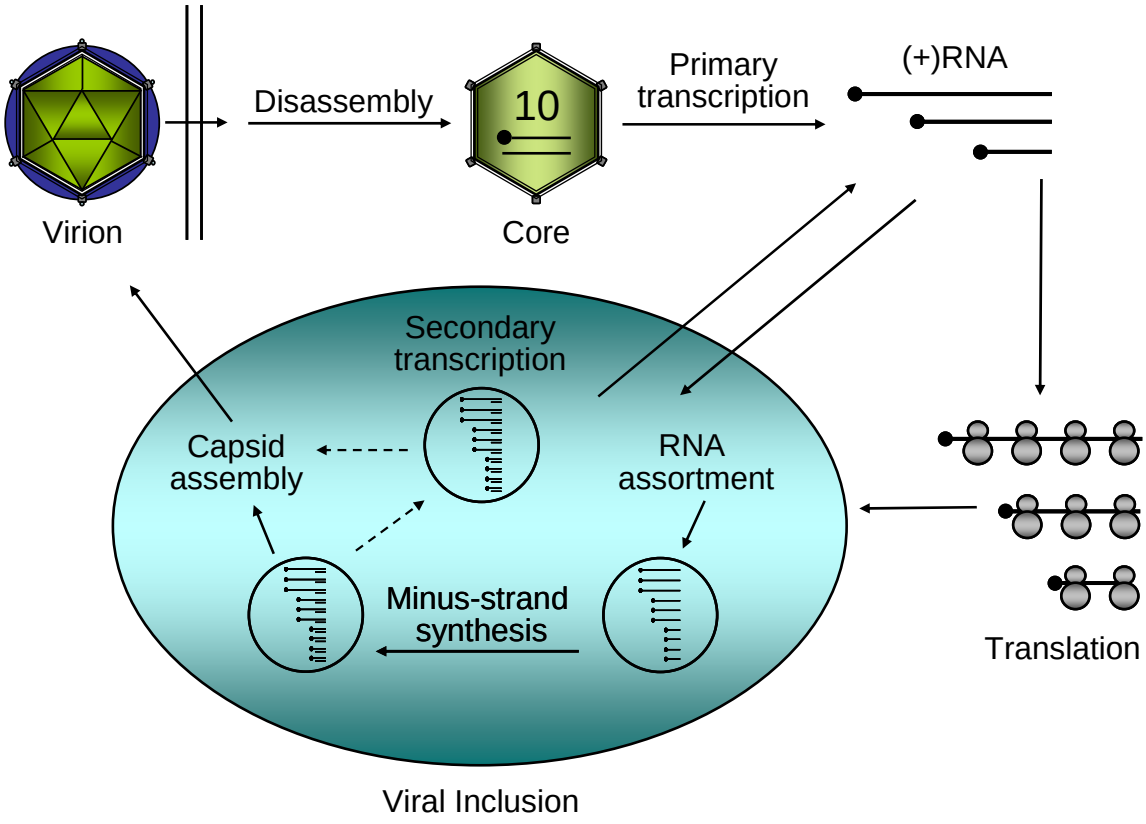

Figure 1.2. Model of reovirus replication. Following entry, transcriptionally active core particles initiate a primary round of transcription, generating 10 full-length, positive-sense, capped, and non-polyadenylated RNAs that serve as templates for translation and dsRNA synthesis. Nascent viral mRNA and protein localize to cytoplasmic viral inclusions where RNA assortment, minus strand synthesis, secondary transcription, and viral assembly take place.

each viral gene segment (86, 99, 106). These RNAs serve as templates for both translation and negative-strand synthesis. Newly synthesized viral RNA and protein are recruited to viral intracytoplasmic inclusions. Reovirus dsRNA synthesis and assembly are thought to occur within inclusions (96), which strictly depend on nonstructural proteins σNS and μNS and structural protein μ2 for proper formation and function in reovirus-infected cells (3). Viral inclusions are detectable within 4 h post-infection, lack a delimiting membrane, and contain viral proteins and dsRNA, virion particles at various stages of morphogenesis, and at late times of infection, paracrystalline arrays of virion particles (27, 35, 42, 92, 98, 105). Particle assembly is completed by the addition of outer capsid proteins to subviral particles. The mechanism of viral egress is unknown (24).

Reovirus Inclusions

The μNS, μ2, and σNS proteins participate in inclusion formation and maturation as indispensable components of viral replication (8, 9, 17, 60, 88). In infected cells, inclusions assume either filamentous or globular morphology depending upon residue 208 of μ2 (Fig. 1.3). Virus strains that produce filamentous inclusions, such as T1, encode a Pro at position 208 of μ2, whereas strain T3, which produces globular inclusions, encode Ser208 (61, 88). T1 μ2 binds and stabilizes microtubules, and this property is thought to be responsible for the formation of filamentous inclusions (88). Studies of expressed proteins have defined the role of μNS, σNS, and μ2 in inclusion formation. μNS forms small oligomers when free in solution, and globular inclusion-like structures form following transfection of cells with μNS-expressing plasmid (17). In contrast, σNS and μ2 display diffuse cytoplasmic localization (and nuclear in the case of

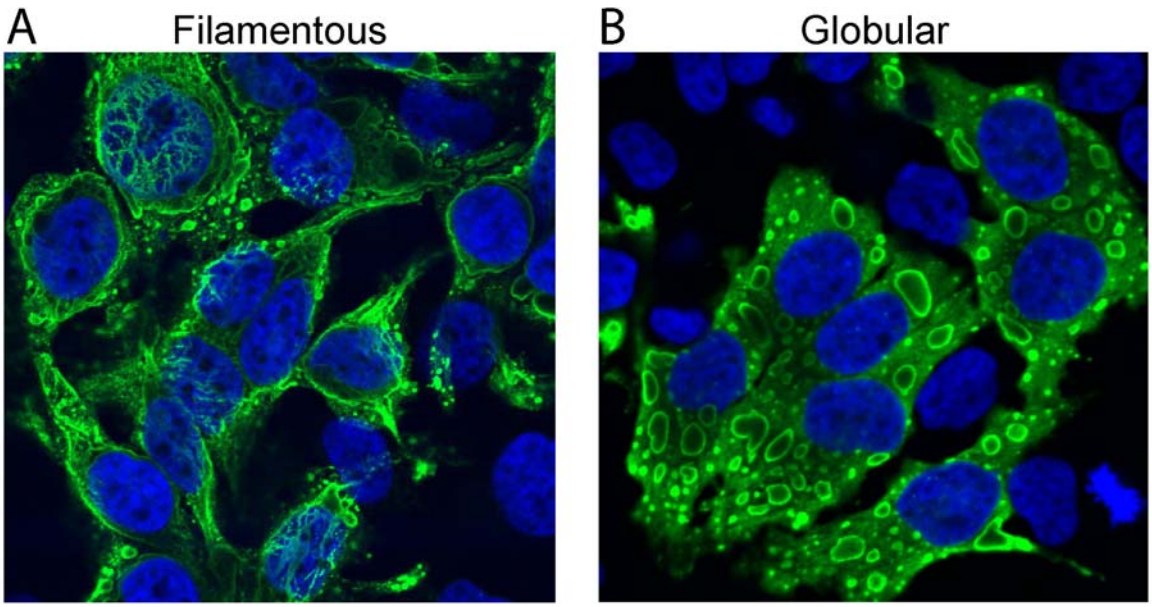

Figure 1.3. Morphology of reovirus inclusions. HeLa cells were infected with reovirus strain T3 (A) or T3-T1M1 (B) at an MOI of 20 PFU/cell, fixed at 24 h post-infection, and stained with anti-σNS antibody (green) and ToPro3 (blue, nucleus). Reovirus viral inclusions assume characteristic morphology, filamentous (A) or globular (B), based on amino acid residue 208 of μ2.

μ2) localization when individually expressed in cells (9, 74). If σNS and μNS are co-expressed in cells, the two proteins co-localize in globular inclusion-like structures (9, 74). Interaction between σNS and μNS is likely RNA-mediated, as treatment with RNase diminishes the capacity of these proteins to co-precipitate with σNS and μNS antibodies (15). The localization of μ2 is also altered when co-transfected with μNS; the two proteins co-localize into inclusion-like structures. These structures assume inclusion morphology characteristic of the strain-origin of μ2 protein (88). In addition to recruiting σNS and μ2, μNS recruits λ1, λ2, λ3, σ2, and core particles to inclusions (15, 72). Taken together, these studies indicate that higher-order multimers of μNS establish viral inclusions by forming an essential matrix to which μ2, σNS, and other viral proteins are recruited. While significant progress has been made in determining how μNS, σNS, and

μ2 mediate inclusion formation, the precise role of viral inclusion-forming proteins in the reovirus replication pathway—including dsRNA synthesis, gene-segment assortment, genome packaging, and virion assembly—is poorly understood, owing largely to limited insights into structure-function relationship of these molecules.

Viral RNA assortment, genome replication, secondary transcription, and particle morphogenesis are presumed to occur within reovirus inclusions (2, 27, 31, 77, 78, 92, 130, 132). The process likely begins with assortment of positive-sense viral RNAs by a specific mechanism. Available data are congruous with an assembly model wherein equimolar amounts of the ten viral mRNAs associate with nonstructural and core proteins and condense to form nascent viral particles (2, 31), termed "replicase particles," which are capable of synthesizing complementary negative-sense RNA to generate the dsRNA genome. Populations of particles with distinctive complements of viral RNA and protein, as well as specific transcriptional activities (i.e., positive- or negative-strand synthesis), can be separated physiochemically and are thought to represent particle intermediates on a pathway toward formation of mature virions (77, 78, 130, 132). Current concepts of individual steps in particle assembly are rooted mainly in biochemical analysis of these subparticle forms. However, the proposed assembly intermediates have not been correlated with specific morphogenic events in viral inclusions.

Enzymatic Activity of the Reovirus Core

The reovirus core mediates production of capped, non-polyadenylated viral mRNAs representing each of the 10 gene segments. Viral mRNA is transcribed from the dsRNA genome template (6, 106) and extruded through the λ2 turrets of the core (40). λ3

is the catalytic subunit of the RNA-dependent RNA polymerase (33, 108, 112). It displays limited activity *in vitro* and likely must interact with μ2 and λ1 for complete functionality (108). The atomic structure of λ3 reveals an RdRp domain with right-handed thumb, core, and palm subdomains, similar to other polymerases (112). This catalytic domain in enclosed by N- and C-terminal domains creating several channels that allow entry of template and nucleoside triphosphates and exit of template and newly synthesized mRNA (112). The structure of λ3 also suggests that it functions as a helicase, unwinding dsRNA prior to transcription; however, core shell protein λ1 exhibits some *in vitro* helicase activity (12). Following transcription, the 5' γ-phosphate of the newly synthesized transcript is removed by an RNA triphosphatase (RTPase) to initiate capping. λ1 is thought to mediate this activity as the transcript is directed out of the core through a channel in the λ1 shell located at the base of the λ2 turret at the icosahedral vertex of the particle (11, 126). Capping is thought to be completed as the transcript exits through the λ2 turret because λ2 has both guanylyltransferase and methyltransferase activities (21, 65, 112).

Reovirus Replication Protein μ2

The reovirus μ2 protein is a multifaceted regulator of reovirus replication and essential for the successful completion of the reovirus replication program. In addition to its role as an inclusion matrix protein, it is thought to be a polymerase cofactor, is a determinant of virulence, and is associated with tropism for a number of different cell types (14, 58, 61, 66, 67, 84, 85, 88, 102, 104, 123). The μ2 protein is a component of the reovirus core, which contains approximately 24 molecules of μ2 per virion particle (25).

Although the precise position of μ2 is unknown, several lines of evidence from biochemical, structural, and genetic studies suggest that μ2 resides at the vertex base in close approximation to λ3 (23, 58, 85, 91, 123, 126). μ2 is the only reovirus structural protein whose crystal structure has yet to be defined; nevertheless, numerous functional domains been mapped to the μ2 protein using biochemical and genetic studies (Fig.1.3) Although the μ2 protein coordinates diverse events during the reovirus replication cycle, a mechanistic understanding of the role of μ2 in replication remains unknown, primarily because its individual functional domains have not been linked to specific steps in the life cycle.

The μ2 protein has been hypothesized to be part of the RdRp complex based on genetic analyses linking the M1 gene to strain-specific characteristics of T1 and T3 replication and biochemical analysis of μ2 (14, 48, 58, 61, 84, 123, 124). Genetic association of the M1 gene with the λ3-expressing L1 gene was shown in an analysis of a

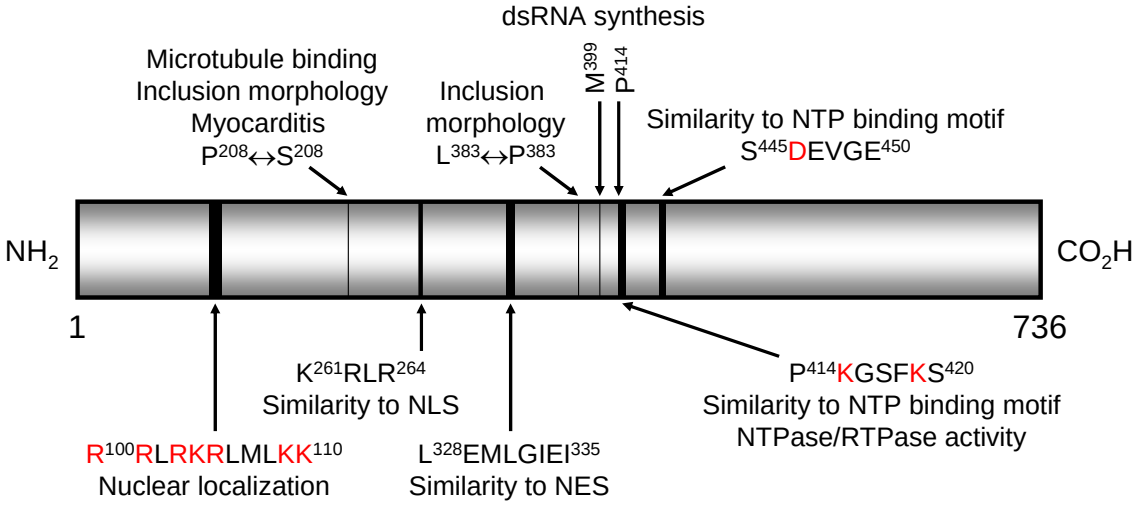

Figure 1.4. Sequence-function correlations of reovirus μ2 protein. Sequences associated with recognized functions and motifs are indicated. Amino acids highlighted in red have been shown to influence the efficiency of viral growth.

large panel of reassortant viruses (84). The M1 and L1 genes displayed nonrandom segregation, suggesting specific protein-protein, protein-RNA or RNA-RNA interactions among μ2 and λ3 proteins and M1 and L1 gene segments (84).

Despite showing significant sequence conservation between T1 and T3 (124), the M1 gene has been linked to numerous strain-specific phenotypes. The M1 gene determines the different temperature optima of *in vitro* transcription displayed by T1 and T3 cores (123). The L1 and M1 genes are also associated with the absolute amount of transcripts produced by cores *in vitro* (123). Reovirus replication displays strain-specific sensitivity to mycophenolic acid (which decreases intracellular levels of guanine nucleotides), with T1 being less sensitive than T3 (48). This phenotype maps to M1, and based on the mechanism of action of mycophenolic acid, suggests that μ2 may aid in the uptake and processing of GTP in viral transcription (48). *In vitro* nucleotide NTPase and RTPase activity (85) are also linked to the M1 gene and will be discussed further below. These genetic associations of M1 with strain-specific differences in transcription-related activities support the idea that μ2 is a cofactor of the viral RdRp.

Biochemical evidence supporting the polymerase cofactor model of μ2 function includes RNA binding activity (14), NTPase and RTPase activity (58, 85), and λ3-binding capacity (58). Expressed μ2 has RNA-binding activity *in vitro*; it binds ssRNA in a non-sequence specific manner, and it binds dsRNA and ssRNA analogs (14). μ2 has classical Walker A and Walker B nucleotide-binding motifs (Fig. 1.4) (85, 119), which are found in conserved regions of the μ2 protein (124). These motifs are associated with NTPase and RTPase activity, which is the removal of the γ-phosphate from the 5' end of either an NTP or RNA molecule, respectively. NTPase activity is often associated with

helicase activity, and RTPase activity is required to initiate the addition of a 5'cap onto an mRNA molecule (37, 125). *In vitro*, reovirus cores display NTPase activity, and differences in T1 and T3 NTPase activity profiles based on NTP substrate, reaction temperature, and pH have been mapped to the M1 and λ1-encoding L3 genes (85). Furthermore, Kim et al. showed that purified μ2 is a divalent cation-dependent NTPase and RTPase (58). Mutation of lysine residues to alanine at positions 415 and 419 within the proposed Walker A motif abolished NTPase activity (58) and diminished viral replication capacity (61). The addition of purified λ3 stimulates μ2 triphosphatase activity, and μ2 and λ3 proteins display *in vitro* binding capacity to one another in co-immunoprecipitation studies (58). Taken together, these biochemical data suggest that μ2 modulates many activities performed by the reovirus core and may itself mediate enzymatic functions, thus supporting a model whereby μ2 acts as a polymerase cofactor.

In addition to its central place in viral replication, μ2 regulates reovirus cell tropism and virulence. Strain-dependent viral replication efficiency has been genetically linked to μ2 in studies using primary and transformed cells, including murine cardiac myocytes (67, 102, 104), bovine aortic endothelial cells (66), human umbilical vein endothelial cells (66), and MDCK cells (93). Strain-specific virulence in severe combined immunodeficient (SCID) mice is determined by the S1, L2, M1, and L1 genes; M1 was independently important for virulence, including viral titer in the liver and severity of hepatitis (44).

The capacity of reovirus to cause myocarditis in neonatal mice is regulated by μ2 and tied to the innate antiviral response. Genetic analysis of myocarditic and nonmyocarditic reoviruses has identified M1 as a determinant of myocarditic potential

(102, 104). In cardiac myocytes, nonmyocarditic reoviruses induce greater levels of interferon (IFN)-β and are more sensitive to its antiviral affects (104). Furthermore, nonmycarditic reoviruses can cause myocarditis in mice depleted of IFN-α/β (104), showing that the IFN response to reovirus is essential for protection of the heart following infection. Reovirus strain-specific differences in induction of and sensitivity to IFN-α/β are associated with the viral M1, L2, and S2 genes. The μ2 protein of myocarditic strains such as T1 antagonizes the IFN response by mediating nuclear sequestration of interferon regulatory factor (IRF)-9, a key component of the complex that mediates the expression of IFN signaling genes (128), thus providing one possible explanation for the differences in myocarditic potential among reovirus strains. Furthermore, residue 208 of μ2 determines repression of IFN signaling in cardiac myocytes and modulates myocarditis in neonatal mice (49).

Reovirus Reverse Genetics System

I began my dissertation work shortly after a fully plasmid-based reovirus reverse genetics system was developed (59). This system is a powerful tool for carrying out reovirus research because it allows reoviruses with specific sequences to be designed and generated. The original system consisted of ten plasmids, each containing a full-length reovirus gene segment cDNA under transcriptional control of bacteriophage T7 RNA polymerase promoter and fused at the 3′ terminus with hepatitis delta virus (HDV) ribozyme sequences (Fig. 1.5A). These plasmids are thought to generate transcripts identical to reovirus-generated (+)-strand RNAs that serve as templates for translation and dsRNA synthesis in infected cells. In the original system, a primary round of reovirus

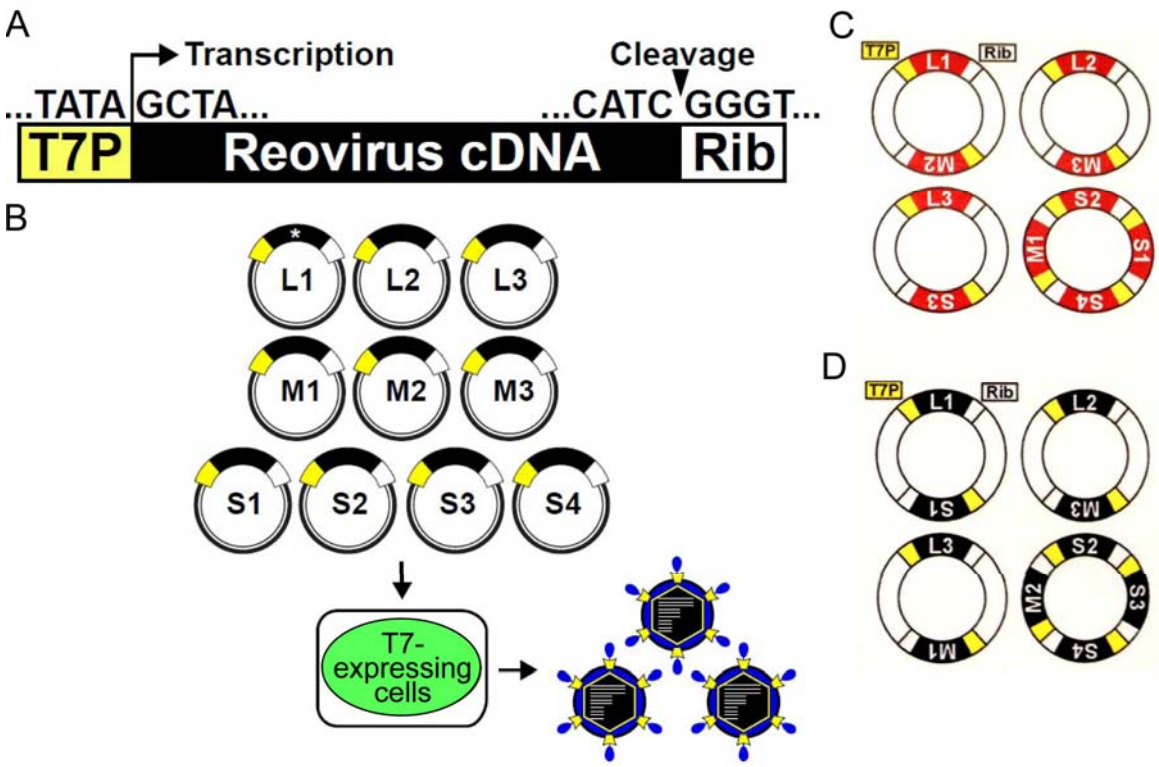

Figure 1.5. Experimental strategy to generate reovirus from cloned cDNAs. (A) Prototype reovirus gene segment cDNA in plasmid. Cloned cDNAs representing each of the 10 full-length reovirus gene segments are flanked by the bacteriophage T7 RNA polymerase promoter (T7P) and the antigenomic hepatitis delta virus ribozyme (Rib). (B) Schematic of the approach using 10 reovirus cDNA constructs. Constructs are transfected into T7-RNA polymerase-expressing cells. Nascent transcripts contain the viral mRNA 5' native end. Self-cleavage by HDV ribozyme generates the viral native 3'end. Rescued viruses are recovered from cell lysates by plaque assay. (C, D) Two or four gene transcription cassettes encoding reovirus cDNAs flanked by the T7 RNA polymerase promoter and HDV ribozyme sequences were combined into single plasmids, creating four plasmids for the T1 (C) and T3 (D) reverse genetics systems. Image adapted from Kobayashi et al. 2007, Kobayashi et al. 2010.

replication is initiated by co-transfection of all ten plasmids into murine L cells infected with replication-defective vaccinia virus (rDIs-T7pol) expressing T7 RNA polymerase. Following five days of incubation, recombinant strain (rs) viruses are isolated from co-transfection lysates by plaque assay using L cells (Fig. 1.5B). A second generation reverse genetics system was also developed which improved efficiency of virus recovery. In the improved system, the number of required plasmids was reduced from ten to four. Two or four gene transcription cassettes, each encoding T1 or T3 reovirus cDNAs flanked by the T7 RNA polymerase promoter and HDV ribozyme, were combined in a single plasmid (Fig. 1.5C, D). The new system also replaced rDis-T7pol-infected L cells with BHK-T7 cells that constitutively express T7 RNA polymerase. The improved system enhanced efficiency of virus recovery by reducing time to virus isolation and supporting increased total yields (62). Enhanced efficiency of the reverse genetics system has allowed for the recovery of viruses that were unrecoverable using the ten-plasmid system. For example, T1-T3M1, a virus with nine T1 gene segments and a T3 M1, could only be isolated using the improved methodology. The reovirus reverse genetics system has been crucial to my dissertation work as all of the viruses used were obtained through this means.

Significance of my Research

Viruses are constantly evolving to ensure continued propagation in a host system. Over the course of its evolution, each virus customizes a specific set of strategies to efficiently reprogram a host cell to further its proliferation. Divergent and convergent evolutionary processes lead to optimal strategies of replication. Therefore, diverse viruses

may exhibit similar strategies at certain points in their life cycles creating generalized themes of viral replication. Lessons learned from studies of the role of μ2 in reovirus inclusions that influence cell tropism can contribute to the identification of general mechanisms of post-entry-mediated cell tropism, compartmentalization of replication machinery within a host cell, and viral replication protein structure and function. For example, by the very nature of their genomes, reovirus (dsRNA) and influenza virus (negative-sense RNA) must utilize different mechanisms of replication. However, both reovirus and influenza virus display post-entry-mediated cell tropism that is controlled by viral polymerase proteins. Studies of reovirus can also inform studies of related dsRNA viruses such as the important human pathogen rotavirus. Rotavirus displays similar morphogenic and biochemical features to reovirus including confinement of enzymes required for transcription and replication within the inner capsid of the particle and completion of most post-entry steps of the viral life cycle within cytoplasmic inclusions. In this way, conclusions reached from work on reovirus have clear implications on strategies used by rotaviruses. Thus, studies of μ2 function, its interaction with other viral and cellular proteins, and its role in determining tropism contribute to virological principles that can be generally applied to many viruses.

In addition to advancing general virological principles, an exciting potential application of this work is development of reovirus for clinical use. Reovirus is oncolytic and currently undergoing clinical trials for cancer therapy (22, 109, 114). Reovirus is also being developed as a vaccine vector, targeting important human pathogens such as HIV (59). With the advent of reovirus reverse genetics as well as the availability of characterized strains with distinct phenotypes, it is conceivable that manipulation of the

μ2 protein and the viral replication machinery may facilitate the generation of reoviruses with favorable replication and tropism characteristics. Consequently, an understanding of reovirus replication properties in diverse cellular backgrounds may prove useful for application of reoviruses for clinical purposes.

CHAPTER II

ANALYSIS OF REOVIRUS REPLICATION IN MDCK CELLS

Introduction

Productive viral infection requires a complex interplay between viral and cellular factors at each step in the viral life cycle. Cell-, tissue-, and host-specific differences can affect the capability of a virus to utilize cellular machinery and lead to distinct patterns of virus tropism. Conceivably, each step of the viral life cycle could determine tropic differences; however, the role of viral replication proteins in mediating tropism is not well defined. In a study of reovirus infection of MDCK cells, it was found that strains T1 and T3 differ in their capacity to productively infect these cells (93). T1 efficiently replicates in MDCK cells but T3 does not. Analysis of a panel of T1 x T3 reassortant viruses showed that differences in replication efficiency between the two viruses in MDCK cells segregate primarily with the λ3-expressing L1 gene segment and secondarily with the μ2-expressing M1 gene segment (93). This phenotype presents a useful experimental model to study the individual and cooperative roles of μ2 and λ3 in reovirus cell tropism.

In this work, I investigated the viral determinants of replication potential in MDCK cells. Using viruses generated by reverse genetics I examined the involvement of individual gene segments and μ2-polymorphisms that contribute to the replication phenotype. My studies indicate that μ2 is the primary determinant of viral replication efficiency in MDCK cells and that λ3 is a conditional co-regulator of μ2 function

depending on the viral genetic background. Furthermore, residue 347 is the primary determinant of μ2-mediated replication in these cells. Additionally, I conducted replication experiments to initially characterize cellular determinants of the restriction of T3 replication in MDCK cells. I found that T3 replication efficiency is increased if infection is initiated with a low dose of virus and no differences were observed in IFN-β induction between permissive and non-permissive infections. These results enhance our understanding of the viral replication apparatus and the viral and cellular requirements crucial for its activity.

This work was done is collaboration with Dr. Takeshi Kobayashi, a former postdoctoral fellow in the laboratory of Dr. Terry Dermody. Dr. Kobayashi generated many of the viruses used in these studies and was involved in the initial characterization of monoreassortant viruses in MDCK cells.

Results

Reovirus strain-specific replication in MDCK cells – The original study identifying the strain-specific capacity of reovirus T1 and T3 to replicate in MDCK cells used laboratory stocks of native T1 and T3 viruses (93). To confirm that viruses recovered using the plasmid-based reverse genetics system (59, 62) recapitulate growth characteristics of native T1 and T3 in MDCK cells, recombinant strain T1 and recombinant strain T3 were used to infect MDCK cells at a multiplicity of infection (MOI) of 2 plaque forming units (PFU)/cell, and viral titers in cell lysates were monitored over the course of infection. Consistent with previous findings, strain T1 achieved an approximately 100-fold increase in viral titer over 48 h of incubation (Fig. 2.1A). Conversely, strain T3 exhibited a

minimal increase in titer during the course of infection. In contrast to growth in MDCK cells, both strains replicated with similar kinetics and produced equivalently high titers in L cells (Fig. 2.1B). These results demonstrate that differences in tropism for MDCK cells displayed by the native viruses are recapitulated by the recombinant strains. Table 2.1 provides the composition of all recombinant strain reoviruses used in these studies.

Identification of reovirus gene segments that influence replication in MDCK cells – To more fully understand the contributions of individual reovirus genes to viral replication efficiency in MDCK cells, monoreassortant viruses (containing nine gene segments from one strain, denoted first in the virus name, and one gene derived from a different strain, indicated second in the virus name) were generated, and production of infectious progeny virions was quantified. L1, M1, and S1 monoreassortant viruses were generated in both

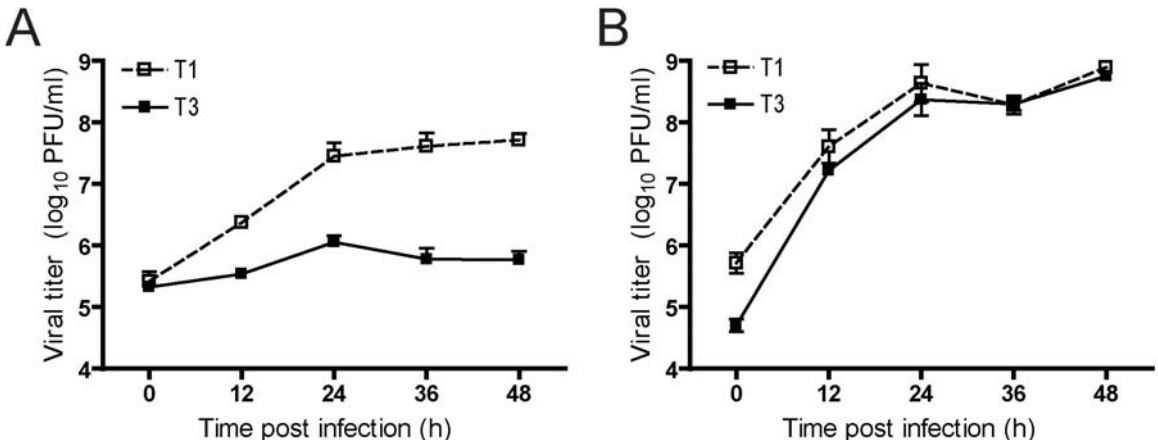

Figure 2.1. Growth of reovirus in cultured cells. MDCK cells (A) or L cells (B) were infected at an MOI of 2 PFU/cell, and viral titers in cell lysates were determined at the time points shown by plaque assay using L cell monolayers. Results represent the mean of triplicate experiments. Error bars indicate S.D.

Table 2.1 Genetic composition of reovirus strains used for these studies

	Gene Segment Origin									
Virus Strain	L1	L2	L3	M1	M2	M3	S1	S2	S3	S4
T1	1	1	1	1	1	1	1	1	1	1
T3	3	3	3	3	3	3	3	3	3	3
T1-T3L1	3	1	1	1	1	1	1	1	1	1
T1-T3M1	1	1	1	3	1	1	1	1	1	1
T1-T3L1M1	3	1	1	3	1	1	1	1	1	1
T3-T1L1	1	3	3	3	3	3	3	3	3	3
T3-T1M1	3	3	3	1	3	3	3	3	3	3
T3-T1L1M1	1	3	3	1	3	3	3	3	3	3
Chimera 1	3	3	3	Ch1	3	3	3	3	3	3
Chimera 2	3	3	3	Ch2	3	3	3	3	3	3
Chimera 3	3	3	3	Ch3	3	3	3	3	3	3
Chimera 4	3	3	3	Ch4	3	3	3	3	3	3
T1 V300M	1	1	1	V300M	1	1	1	1	1	1
T1 Q342R	1	1	1	Q342R	1	1	1	1	1	1
T1 F347L	1	1	1	F347L	1	1	1	1	1	1
T3 M300V	3	3	3	M300V	3	3	3	3	3	3
T3 R342Q	3	3	3	R342Q	3	3	3	3	3	3
T3 L347F	3	3	3	L347F	3	3	3	3	3	3
T1-T3L1-M1F347L	3	1	1	F347L	1	1	1	1	1	1
T3-T1L1-M1 L347F	1	3	3	L347F	3	3	3	3	3	3

T1 and T3 genetic backgrounds. L1 and M1 were exchanged because these genes were previously identified as determinants of reovirus tropism for MDCK cells (93). Monoreassortant viruses encoding reciprocal exchanges of the S1 gene, encoding viral attachment protein σ1 and nonstructural protein σ1s, were tested for growth in MDCK cells since receptor engagement is responsible for differences in the infectivity of type 1 and type 3 reoviruses for a variety of cells and tissues (32, 57, 96, 115, 121). Parental and monoreassortant viruses were used to infect MDCK cells at an MOI of 2 PFU/cell, followed by quantification of viral yields after 24 h of incubation. Consistent with the

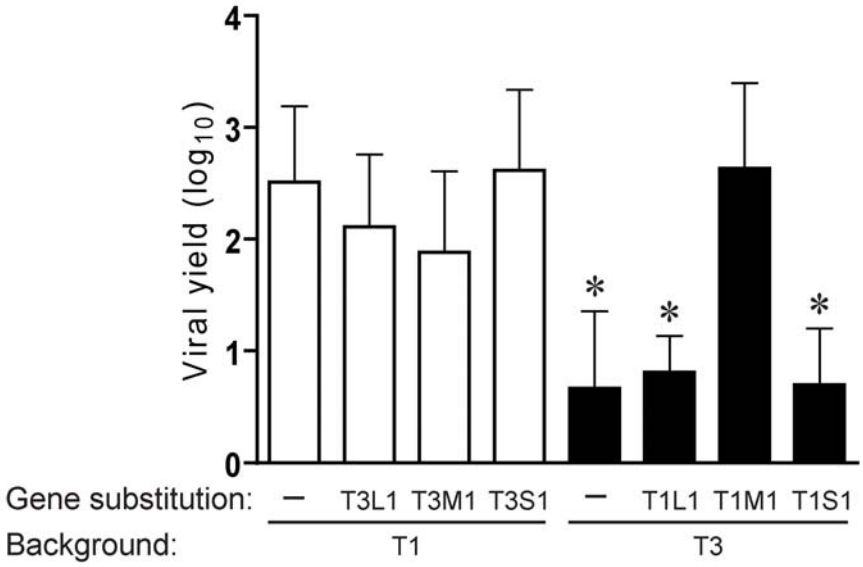

Figure 2.2. Growth of monoreassortant viruses in MDCK cells. Cells were infected with L1, M1, or S1 monoreassortant viruses at an MOI of 2 PFU/cell, and viral yields (relative to 0 h) at 24 h post-infection were determined by plaque assay using L cell monolayers. Results represent the mean of triplicate experiments. Error bars indicate S.D. *, $p < 0.05$ in comparison with strain T1 (Student's *t* test).

earlier mapping study, the T1 M1 gene was sufficient to support growth of T3 to the level of T1, whereas the S1 gene was not associated with strain-specific differences in viral yield (Fig. 2.2). However, contrary to previous findings, an independent association of the L1 gene with viral replication was not observed using L1 monoreassortant viruses; T1-T3L1 and T3-T1L1 displayed high and low yields, respectively, mimicking their parental strains. Furthermore, the effect of M1 on viral replication was unidirectional; the T3 M1 gene segment, alone, did not diminish T1 yield. These results indicate that the μ2 protein regulates reovirus replication efficiency in MDCK cells, but the effects of μ2 on replication are subject to modulation by other viral determinants.

To test the hypothesis that there is cooperativity between the L1 and M1 genes in governing viral yield, experiments using L1/M1 double reassortant viruses in the T1 (T1-

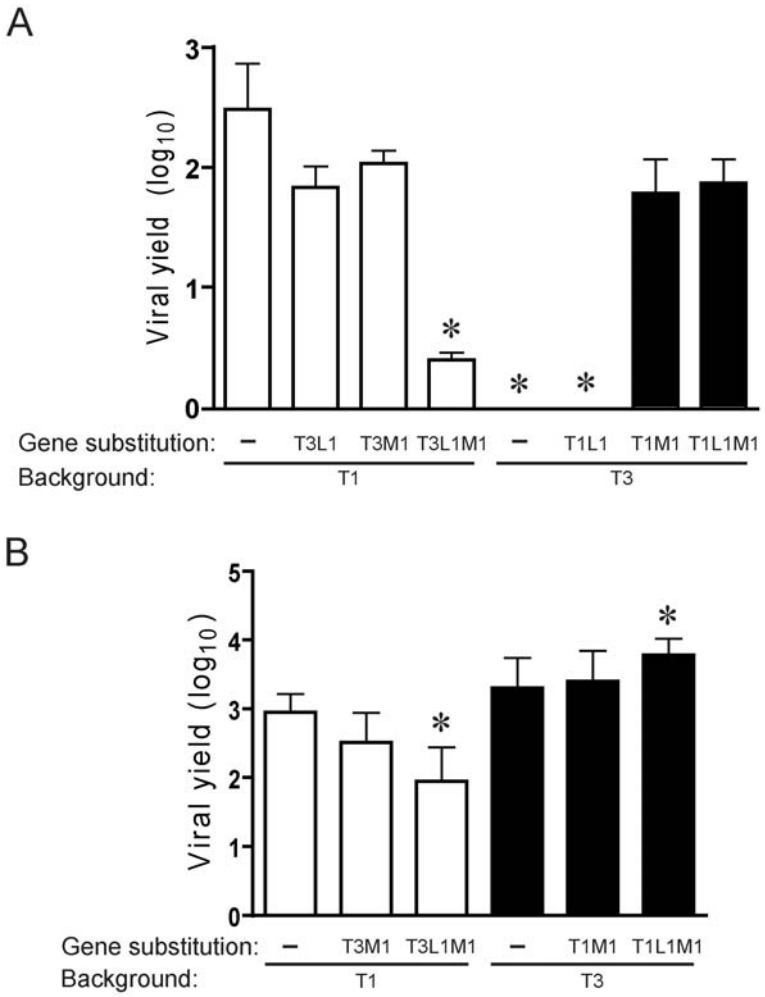

Figure 2.3. Yields of L1/M1 reassortant viruses in cultured cells. MDCK cells (A) or L cells (B) were infected at an MOI of 2 PFU/cell, and viral yields (relative to 0 h) were determined at 24 h post-infection by plaque assay using L cell monolayers. Results represent the mean of triplicate experiments. Error bars indicate S.D. *, $p < 0.05$ in comparison with strain T1 (Student's *t* test).

T3L1M1) and T3 (T3-T1L1M1) backgrounds were performed. Pairing T3 L1 and T3 M1 genes in the T1 background significantly reduced T1 viral yield in MDCK cells at 24 h post-infection (Fig. 2.3A). In contrast, growth of T3-T1M1 was unaffected by the strain origin of the L1 gene. Yields of M1 monoreassortant and L1/M1 double-reassortant viruses were also determined using L cells to control for potential constitutive effects of

the T1 and T3 L1 and M1 genes on viral replication. In these experiments, all strains produced high yields in L cells (Fig. 2.3B). Reassortant strain T1-T3L1M1 grew less efficiently in L cells compared to the T1 parental strain. However, the reduction in viral yield was 10-fold compared to a 100-fold difference in MDCK cells. The yield of T3-T1L1M1 exceeded that of T3 by approximately 3-fold, but this difference was modest compared to the 70-fold increase in MDCK cells. Taken together, results of experiments using M1 and L1 reassortant viruses indicate that μ2 is a key determinant of reovirus tropism for MDCK cells and, additionally, provide evidence for co-regulation of viral replication by polymerase protein λ3, conditioned on the viral genetic background.

Identification of sequences in μ2 that mediate reovirus tropism for MDCK cells – To identify μ2 sequence features of reovirus replication efficiency in MDCK cells, a panel of T1 x T3 μ2-chimeric viruses was generated in the T3 genetic background (Fig. 2.4A). Chimera (Ch) 1 and Ch2, containing T3 μ2-derived sequences 1-126 and 1-208, respectively, produced high viral yields similar to T1, whereas Ch3 and Ch4, containing T3 μ2-derived sequences 1-389 and 1-600, respectively, produced low yields similar to T3 (Fig. 2.4B). Relative replication efficiencies of the four chimeric viruses suggest that μ2 sequences regulating reovirus replication in MDCK cells are bounded by amino acid residues 209 and 389.

Three sequence polymorphisms with respect to T1 and T3—300, 342, and 347—are present within the μ2 region that controls viral replication efficiency in MDCK cells (Fig. 2.4C). The relative contribution of these amino acids to viral yield was assessed by reciprocal exchanges between the μ2 proteins of T1 and T3 using reverse genetics.

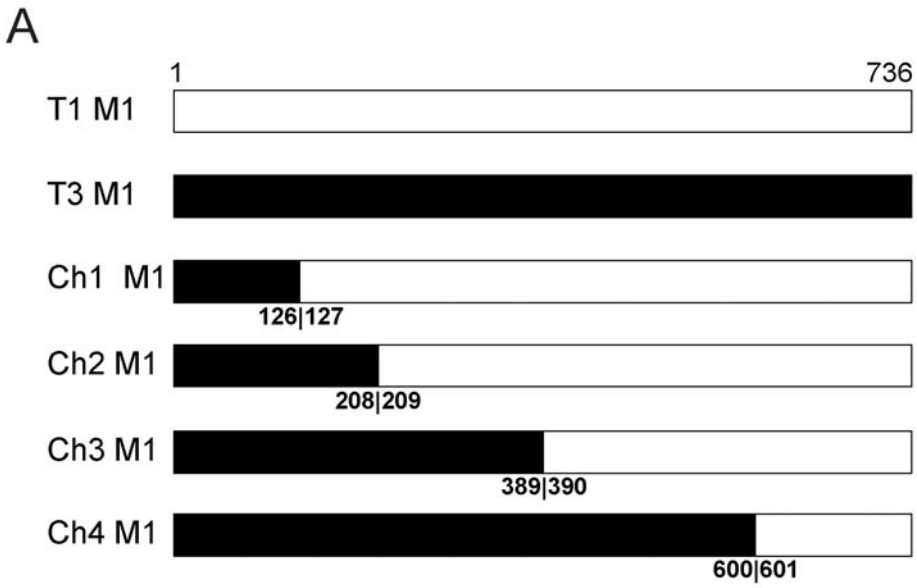

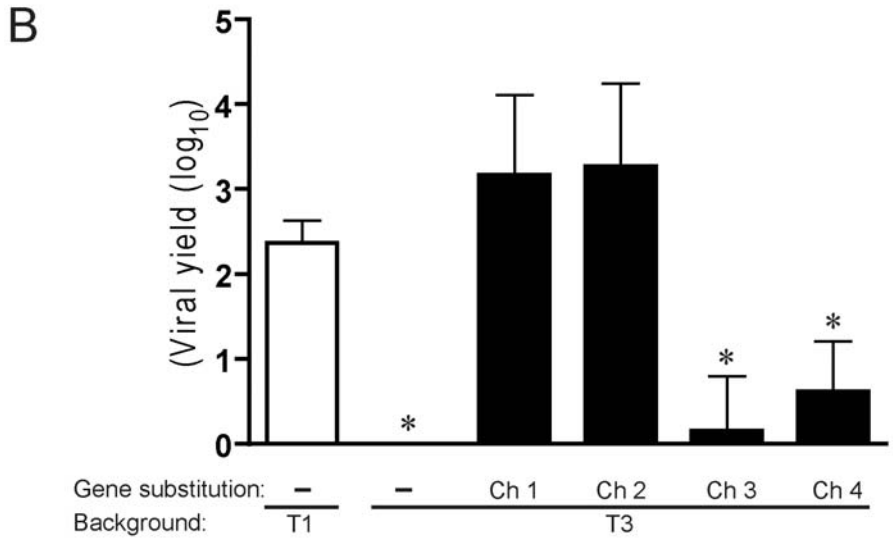

C

	93	208	300	342	347	434	458	652	726
T1	V	P	V	Q	F	V	H	M	N
T3	A	S	M	R	L	I	Q	I	S

Figure 2.4. Identification of a μ2 domain that mediates reovirus tropism for MDCK cells. (A) Schematic of T1 x T3 chimeric (Ch) M1 gene segments. Chimeric junctions were introduced at the nucleotide position corresponding to the amino acid numbers shown. Viruses containing M1 chimeric gene segments were generated in a T3 strain background. (B) MDCK cells were infected with M1 chimeric viruses at an MOI of 2 PFU/cell, and viral yields (relative to 0 h) were determined at 24 h post-infection by plaque assay using L cell monolayers. Results represent the mean of triplicate experiments. Error bars indicate S.D. *, $p < 0.05$ in comparison with strain T1 (Student's *t* test). (C) T1 and T3 μ2 proteins differ at nine amino acid positions.

Moderately increased yields (approximately 4-fold) resulted from replacement of T3 μ2 amino acids with the corresponding T1 μ2 residues at positions 300 and 342. In contrast, substitution of Leu347 in T3 μ2 with Phe (T3-M1L347F), which is found at this position in T1 μ2, enabled T3 to replicate equivalently to T1 (approximate 100-fold yield). Conversely, the yield of T1-M1F347L, isogenic to T1 except for Leu at μ2 amino acid position 347, approximated that of T1 (Fig. 2.5A). Yields of μ2 point-mutant viruses T1-M1Q342R and T1-M1F347L, which contain T3 residues at μ2 amino acid positions 342 and 347, were modestly reduced in L cells relative to parental strain T1 (Fig. 2.5C). However, the other μ2 point-mutant strains and the parental viruses all exhibited equivalently high yields in L cells; no influence of the L1 gene was detected (Figs. 2.5C, D). Therefore, constitutive replication defects are unlikely to account for disparities in yields of μ2-mutant viruses when propagated in MDCK cells.

Consistent with the cooperative relationship of wild type λ3 and μ2 proteins in viral growth (Fig. 2.3), a functional interaction was observed between λ3 and mutant μ2 governed by the specific viral genetic environment; yield of T1-M1F347L in MDCK cells was reduced relative to wt parental strain T1 when the mutant μ2 protein was accompanied by the T3 (strain T1-T3L1-M1F347L), but not T1 (strain T1-M1F347L), λ3 protein (Figs. 2.5A, 2.5B). Interestingly, the T1 λ3 protein acted synergistically with the μ2 L347F mutation to moderately suppress (approximately 13-fold reduction in yield) the growth of T3 (T3-T1L1- M1L347F) (Fig. 2.5B), which further substantiates the functional linkage of λ3 and μ2 in reovirus tropism for MDCK cells. These results indicate that a sequence polymorphism at amino acid position 347 is the primary determinant of μ2-mediated reovirus replication efficiency in MDCK cells. Furthermore,

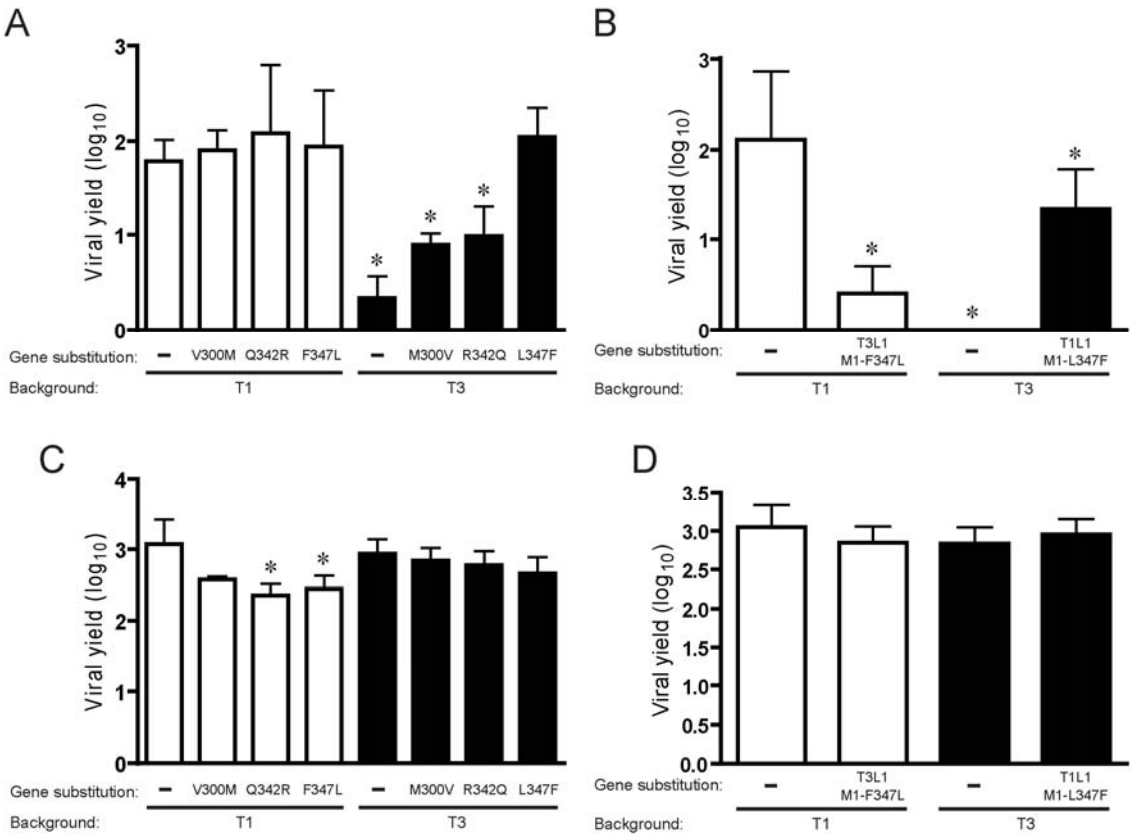

Figure 2.5. Identification of residues in μ2 that mediate reovirus tropism for MDCK cells. MDCK cells (A) or L cells (C) were infected with μ2 point-mutant viruses at an MOI of 2 PFU/cell, and viral yields (relative to 0 h) were determined at 24 h post-infection by plaque assay using L cell monolayers. MDCK cells (B) or L cells (D) were infected at an MOI of 2 PFU/cell with L1 monoreassortant viruses containing point mutations at residue 347 of μ2, and viral yields (relative to 0 h) were determined at 24 h post-infection by plaque assay using L cell monolayers. Results represent the mean of triplicate experiments. Error bars indicate S.D. *, $p < 0.05$ in comparison with strain T1 (Student's *t* test).

the λ3 protein acts as a modifier of tropic phenotypes manifested by sequence variation at this position in μ2.

Dose-dependent reovirus replication in MDCK cells – In order to determine if the amount of virus initiating infection in MDCK cells alters the capacity of T3 to replicate

in MDCK cells, replication kinetics in MDCK cells following infection at different MOIs were quantified. MDCK cells were infected with T1 or T3 at an MOI of 0.02, 0.2, 2, or 20 PFU/cell, and titer was monitored over 48 h (MOI of 2 or 20) or 120 h (MOI 0.02 or 0.2) infection (Fig. 2.6A, B). Interestingly, at an MOI of 0.02, an approximate 300 fold

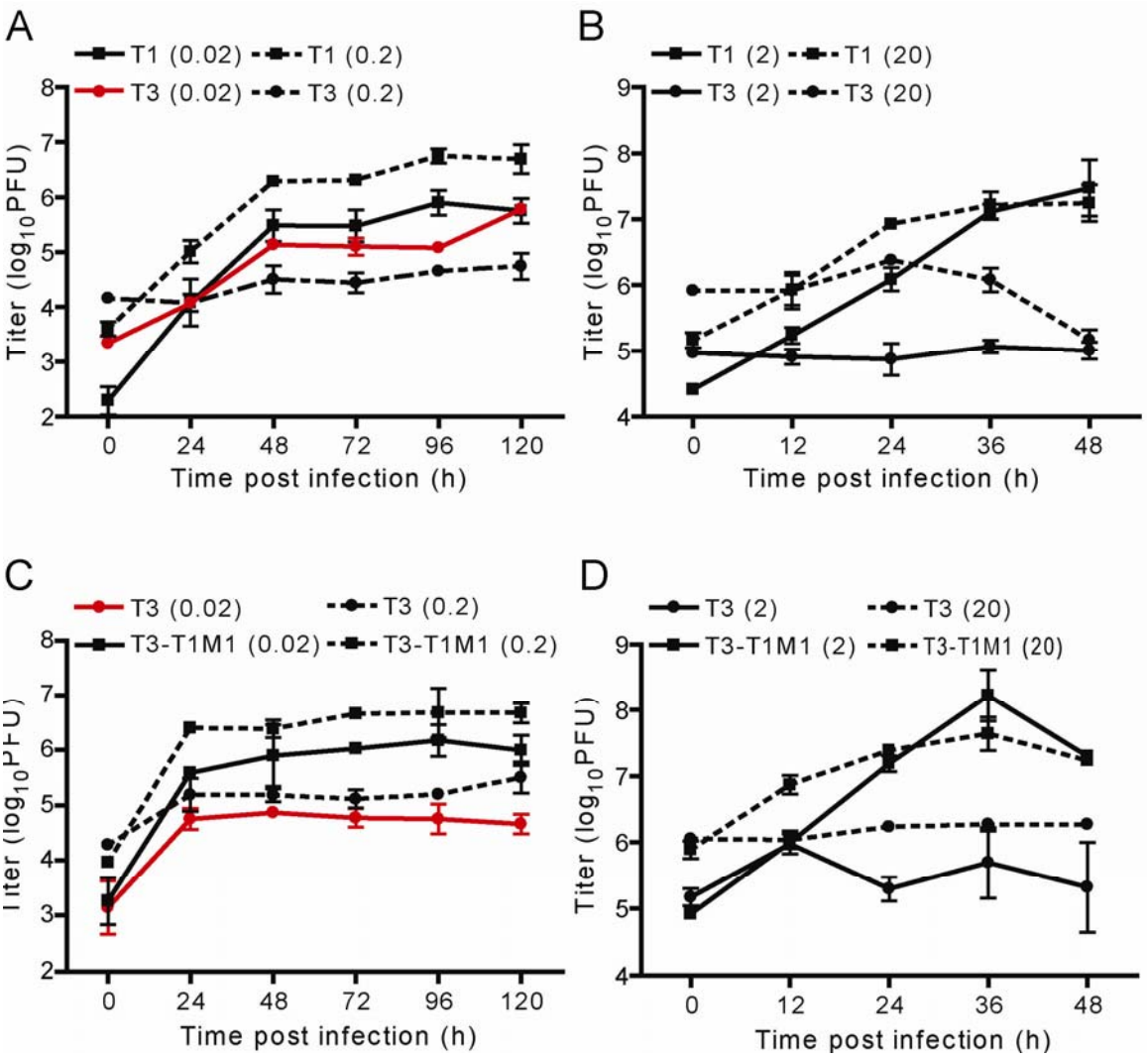

Figure 2.6. MOI-dependent replication of reovirus in MDCK cells. MDCK cells were infected with T1 and T3 (A, B) or T3 and T3-T1M1 (C, D) at an MOI of 0.02, 0.2 (A, C) 2 or 20 (B, D).Viral titers in cell lysates were determined at the time points shown by plaque assay using L cell monolayers. Results represent the mean of triplicate experiments. Error bars indicate S.D.

increase in titer of T3 was observed by 120 h post-infection compared to a 3000 fold increase in titer by T1. When the infection was initiated with an MOI of 0.2, 2, or 20 PFU/cell, no substantial increase in T3 titer was observed over the time course of infection (Fig. 2.6A, B). This experiment was also carried out with T3 and T3-T1M1 (Fig. 2.6C, D). T3-T1M1 displayed similar replication kinetics to T1, again highlighting the capacity of the T1 M1 gene to overcome the replication block in MDCK cells. Furthermore, a similar pattern of T3 dose-dependent replication was observed, whereby the greatest increase in T3 titer occurred following infection initiated at an MOI of 0.02 PFU/cell. These results suggest that the restriction of T3 replication in MDCK cells is dependent on the inoculum of virus initiating the infection.

Interferon-β production in MDCK cells – One hypothesis consistent with the observation of dose-dependent restriction of T3 replication in MDCK cells is that a negative regulator is induced following infection and a critical threshold of virus must be present produce enough factor to reduce viral replication. A common cellular defense mechanism against viruses is the production of type I IFN (α and β), which stimulates gene expression to establish an antiviral state within the host (38). Reovirus infection triggers IFN expression, and strains differ in the capacity to induce IFN in some cell types (104, 107). To assess IFN induction in MDCK cells, IFN-β mRNA was measured using reverse transcription quantitative PCR (RT-qPCR). MDCK cells were infected with T3 or T3-T1M1 at an MOI of 0.02 or 2 PFU/cell and IFN-β mRNA was quantified in cell lysates after 24 h (Fig. 2.7). In mock-infected cells, IFN-β mRNA was barely detectable with a Ct value of 37.2. In cells infected at an MOI of 2 PFU/cell, the Ct values were much

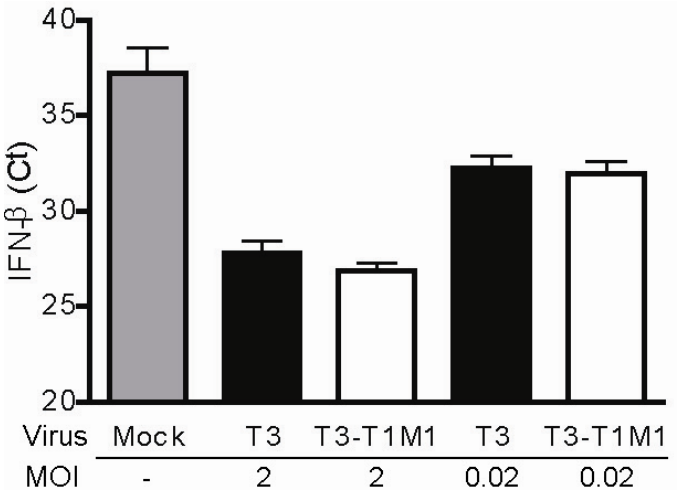

Figure 2.7. IFN-β production in MDCK cells. MDCK were infected with T3 or T3-T1M1 at an MOI of 2 or 0.02, and IFN-β mRNA was measured in cell lysates by RT-qPCR. Results represent the mean of triplicate experiments. Error bars indicate S.D.

lower than mock, 27.8 for T3 and 26.7 for T3-T1M1, indicating that IFN-β mRNA is produced following infection. In cells infected at an MOI of 0.02 PFU/cell, Ct values were approximately 32, indicating that some IFN-β mRNA was produced but at lower levels in cells infected at an MOI of 2 PFU/cell. No significant differences in IFN-β mRNA production were observed between the two viruses. These results indicate that MOI inversely correlates with T3 viral yield, and induction of IFN-β gene expression and increased IFN-β mRNA production following infection initiated at high multiplicities leads to a stronger IFN-stimulated response. It is possible that the block to T3 replication in MDCK cells may involve the type I IFN response and that T3 may be more sensitive to the IFN-induced antiviral state than T1. In other experimental systems, T3 is more sensitive to the IFN-stimulated antiviral response (104), and T1 μ2 has been shown to specifically antagonize components of the IFN-signaling pathway, whereas T3 does not (128). Therefore, the observation that less IFN-β is produced at the lower MOI is

compatible with a model in which infection initiated at a low MOI does not induce a strong enough antiviral state required to inhibit replication of T3.

Characterization of the MDCK cell-mediated restriction of T3 replication – Additional experiments have been carried out in order to better understand the nature of the replication block in MDCK cells. All preceding experiments described were performed using second-passage (P2) L cell-lysate stocks of virus. It is possible that a constituent of the L cell lysate causes MDCK cells to respond in such a way that impedes T3 replication. To test this hypothesis, MDCK cells were infected with T1 or T3 from P2 L cell-lysate stocks or virion particles (VPs) purified using CsCl gradients, and viral yields were quantified 24 h post-infection (Fig. 2.8A). No differences were observed between infections initiated with P2 vs. VP stocks of virus, indicating the block is not caused by a component of the infected L cell lysate.

If the replication block is mediated by an inducible factor, it is possible that the factor is only induced by T3 but T1 is still susceptible to it. To test this hypothesis, MDCK cells were infected with T3, T3-T1M1 (T3-T1M1 was used as a surrogate of T1 to specifically test the contribution of M1 to the phenotype), or co-infected with T3 and T3-T1M1, and viral yields were quantified 24 h post-infection (Fig. 2.8B). The mixed infection displayed a similar viral yield to T3-T1M1. These results do not confirm or refute the possibility that T3 specifically induces a restriction factor. However, if an inducible restriction factor exists, T3-T1M1 is not susceptible to it whether induced only by T3 or both T3 and T3-T1M1.

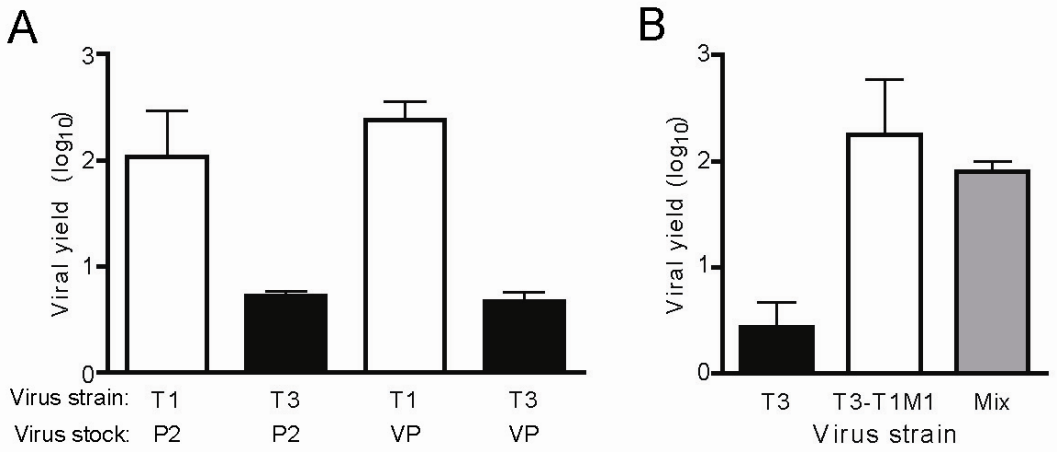

Figure 2.8. Viral yield of reovirus in MDCK cells. (A) MDCK cells were infected at an MOI of 2 PFU/cell with virus from P2 L cell-lysate stocks virion particles (VPs) purified on CsCl gradients, and viral yields (relative to 0 h) at 24 h post-infection were determined by plaque assay using L cell monolayers. (B) MDCK cells were infected with T3, T3-T1M1, or co-infected (Mix) with these strains at an MOI of 2 PFU/cell, and viral yields (relative to 0 h) at 24 h post-infection were determined by plaque assay using L cell monolayers. Results represent the mean of triplicate experiments. Error bars indicate S.D.

Discussion

Initial studies of reovirus replication in MDCK cells revealed a genetic association of the λ3 and μ2 proteins with viral replication efficiency using classical reassortant analysis (93). Subsequent development of a reverse genetics system for reovirus has permitted the generation of viruses containing specific combinations of T1 and T3 gene segments which clearly defined the relative contributions of μ2 and λ3 to this phenotype (Figs. 2.2 and 2.3). T1 μ2 is associated with efficient reovirus replication in MDCK cells irrespective of the viral genetic background. The influence of T3 μ2 on viral replication is more complex; its quantitative effect on production of infectious progeny undergoes modulation by T3 λ3. The μ2 protein is thought to be a cofactor of the viral RdRp (14, 23, 58, 85, 123). However, there is limited insight into interactions

between μ2 and λ3. Biochemical data have shown that the NTPase and RTPase activities of μ2 are enhanced in the presence of λ3, and the two proteins interact in immunoprecipitation assays (58). Furthermore, the L1 and M1 genes display nonrandom segregation in T1 x T3 reassortant viruses (84), suggesting co-evolution of λ3 and μ2 to optimize concerted roles in viral replication. Data presented in this chapter showing the unidirectional μ2-mediated regulation of replication efficiency in MDCK cells and viral background-dependent co-regulation by λ3 suggest a unique structural or functional interaction between μ2 and λ3 in specific viral and cellular contexts. These findings provide additional genetic evidence linking the function of these two proteins and implicate the role of the polymerase complex in determining viral cell tropism.

Using recombinant viruses containing chimeric and point-mutant μ2 proteins, I systematically defined sequence determinants of reovirus replication efficiency in MDCK cells. The results indicate that residue 347 is primarily responsible (Fig. 2.5A). The influence of this polymorphic position on viral replication potential is modulated by λ3 in a manner consistent with the effect of λ3 on full-length μ2 (Fig. 2.5B). A crystal structure of μ2 has not been reported; however, a number of functional sequence determinants have been defined (Fig. 1.4, [23, 49, 58, 61, 85, 88]). It is possible that critical residues identified in this study are part of a larger domain of μ2 that controls reovirus tropism for different types of cells. For example, a temperature-sensitive (ts) strain of reovirus (tsH11.2) containing mutations at residues 399 and 414 of μ2 displays defective dsRNA synthesis at restrictive temperatures. The sequence proximity of these residues to amino acid position 347 raises the possibility that all three are part of a functional unit responsive to the host cell environment. Residue 347 is also near a predicted leucine-rich

nuclear export signal spanning residues 328-335 (NetNES 1.1 [63]). Since μ2 is localized to both the cytoplasm and nucleus (61, 88) and contains two predicted nuclear localization signals, one of which has been shown to be important for viral replication (61), it is plausible that a polymorphism at position 347 could deleteriously shift the nucleocytoplasmic balance of μ2.

It is not possible to rule out an interaction of residue 347 with other structural or functional domains distantly located in primary sequence, such as the nucleotide binding motifs located at residues 414-420 and 445-450 (58). These sequences are required for NTPase and RTPase activities of μ2 (58) and are necessary for viral replication using an RNAi trans-complementation system (61). Therefore, changes at μ2 residue 347 plausibly could alter the function of these domains, with a resultant impact on viral replication efficiency in MDCK cells.

RdRp complexes of diverse RNA viruses may function in viral adaptation to different intracellular environments (71, 82, 83). In the influenza A paradigm, host-range restriction involves an active inhibitory process that protects against cross-species transmission of non-adapted viruses. It is provocative that reovirus strains T1 and T3 sharply contrast in their capacity to grow in canine cells, whereas both strains productively infect cells derived from several other species, including mouse (L [Fig. 2.1]), human (HeLa and 293T [18, 60]), and non-human primates (Vero and CV-1 [10, 19]), raising the possibility that μ2 is a host-range determinant of reovirus infection. However, this hypothesis awaits formal testing.

The capacity of MDCK cells to discriminate reovirus strains T1 and T3 in a μ2- and λ3-dependent manner indicates the existence of a tightly controlled post-entry

replication checkpoint responsive to structural or functional features of the viral polymerase complex. Conceivably, the regulatory mechanism could be positive or negative, i.e. active stimulation of T1 replication or suppression of T3 replication. A passive mechanism also is possible in which MDCK cells fail to provide a function essential for T3, but not T1, replication. The mediator of replication permissivity might be as simple as a single protein or as complex as a biochemical pathway.

One factor determining species-specific retroviral infection occurs through the anti-viral activity of TRIM5α (80), which mediates restriction of retroviruses at a post-entry step in the viral replication cycle. A key experiment in the characterization of TRIM5α regulation of infection was high-dose infection. When non-permissive cells were infected a high MOI, the replication block could be overcome, suggesting the presence of a dominant, saturable restriction factor (45, 80). In an effort to characterize the blockade to T3 in MDCK cells, I tested the affect of MOI to determine if a similar mechanism was occurring. Interestingly, altering the MOI had the opposite effect. High MOI did not enhance replication; however, at low MOI, T3 displayed greater replication efficiency (Fig. 2.6). This result is consistent with a model whereby reovirus infection of MDCK cells induces a restriction factor that blocks T3 infection. As the IFN signaling pathway is a common anti-viral defense mechanism, it plausible that the hypothetical restriction factor is IFN-inducible. Initial experiments commonly used to assess the involvement of IFN-stimulated genes on a phenotype involve stimulation of the IFN signaling pathway with exogenous IFN-α/β or blocking IFN signaling with anti-IFN-α/β antibody. However, neither canine-specific IFN nor anti-IFN-antibody was readily available. Therefore, I designed an RT-qPCR assay to measure production of IFN-β

mRNA. No strain-specific differences were observed in IFN-β production (Fig 2.7); however, these results do not preclude the possibility of different levels of activity of downstream mediators of the IFN signaling pathway. Indeed, in L cells, T1, but not T3, antagonizes IFN signaling by causing IRF-9 accumulation in the nucleus (128). Less IFN-β mRNA production was observed in low MOI infection, which is consistent with the notion that an IFN-induced restriction factor is not expressed at a high enough level to fully block T3 replication under these conditions. However, further experimentation is required to fully understand the involvement, if any, of the IFN signaling pathway on reovirus replication efficiency in MDCK cells.

The purpose of this study was to define the functional domains of reovirus genes that govern reovirus cell tropism. The main findings emerging from this study are the following: 1) μ2 controls efficiency of reovirus growth in MDCK cells; 2) residue 347 is the primary determinant of μ2-mediated viral replication potential in these cells; 3) polymerase protein λ3 is a co-regulator of viral replication in a strain-dependent manner; and 4) replication efficiency is increased when infection is initiated at a low MOI. These findings suggest a unique structural or functional interaction between μ2 and λ3 that facilitates productive viral replication in a manner responsive to specific viral and host-cell environments. A key question raised by this study is what is the mechanism whereby T3 replication is blocked In MDCK cells? Experiments addressing this question are described in Chapters III and IV.

CHAPTER III

IDENTIFICATION OF THE μ2-SENSITIVE STEP OF VIRAL REPLICATION IN MDCK CELLS

Introduction

Results presented in Chapter II indicate a unique structural or functional interaction between μ2 and λ3 that facilitates productive viral replication in a manner responsive to specific viral and host-cell environments. The strain-dependent capacity of reovirus to replicate in MDCK cells provided a useful experimental platform to systematically examine discrete steps in the viral replication program in permissive and non-permissive infection. As key viral mediators of this phenotype are replication proteins μ2 and λ3, I hypothesized that a post-entry step in the replication cycle is inhibited in T3-infected MDCK cells. I found this system of particular interest because post-entry determinants of reovirus tropism have not been defined. Following reovirus entry, the core mediates a primary round of transcription and translation. Viral inclusions are formed from newly synthesized viral proteins, and viral mRNA and protein and cores are recruited to inclusions. Within the inclusion RNA assortment and replication complex assembly, dsRNA synthesis, and secondary transcription and translation take place. These steps in the viral life cycle are plausible targets of a replication protein-determined block to infection based on known functions of μ2 and λ3. Capsid assembly and viral egress are also post-entry steps that could be inhibited; however, there is no evidence linking μ2 and λ3 to these final stages of the viral replication program.

Therefore, I designed experiments to study inclusion formation, viral RNA production, and viral protein synthesis to assess post-entry steps in the life cycle where T3 replication in MDCK cells may be blocked. I focused specifically on μ2 protein as T1 μ2 can independently enhance replication efficiency of T3 in MDCK cells. These studies provide insight into steps in the viral replication program that require μ2 function and are modulated by the host-cell environment.

Results

Viral inclusion formation in reovirus-infected cells – As an initial approach to define the μ2-sensitive step in viral replication in MDCK cells, I imaged viral inclusions over a time course of infection using confocal immunofluorescence microscopy. Cells were infected with T1 or T3, fixed at various intervals, and stained with anti-μ2 and anti-σNS antisera. In both T1- and T3- infected L cells, inclusions initially appeared as small, punctuate structures that gradually enlarged and assumed strain-dependent filamentous and globular features characteristic of T1 and T3, respectively (Fig. 3.1). Strain-dependent morphology was observed in MDCK cells; however, T1 inclusions in MDCK cells also displayed globular structures intermingled with filamentous forms, resulting in a more intermediate phenotype. Although the progress of inclusion formation for both T1 and T3 was slightly delayed in MDCK cells in comparison to L cells, inclusion development was comparable between MDCK cells and L cells by 12 h post-infection. Thus, kinetics of T3 inclusion maturation in MDCK cells was not overtly impaired. Typical inclusion maturation and abundant expression of σNS, a nonstructural protein, in

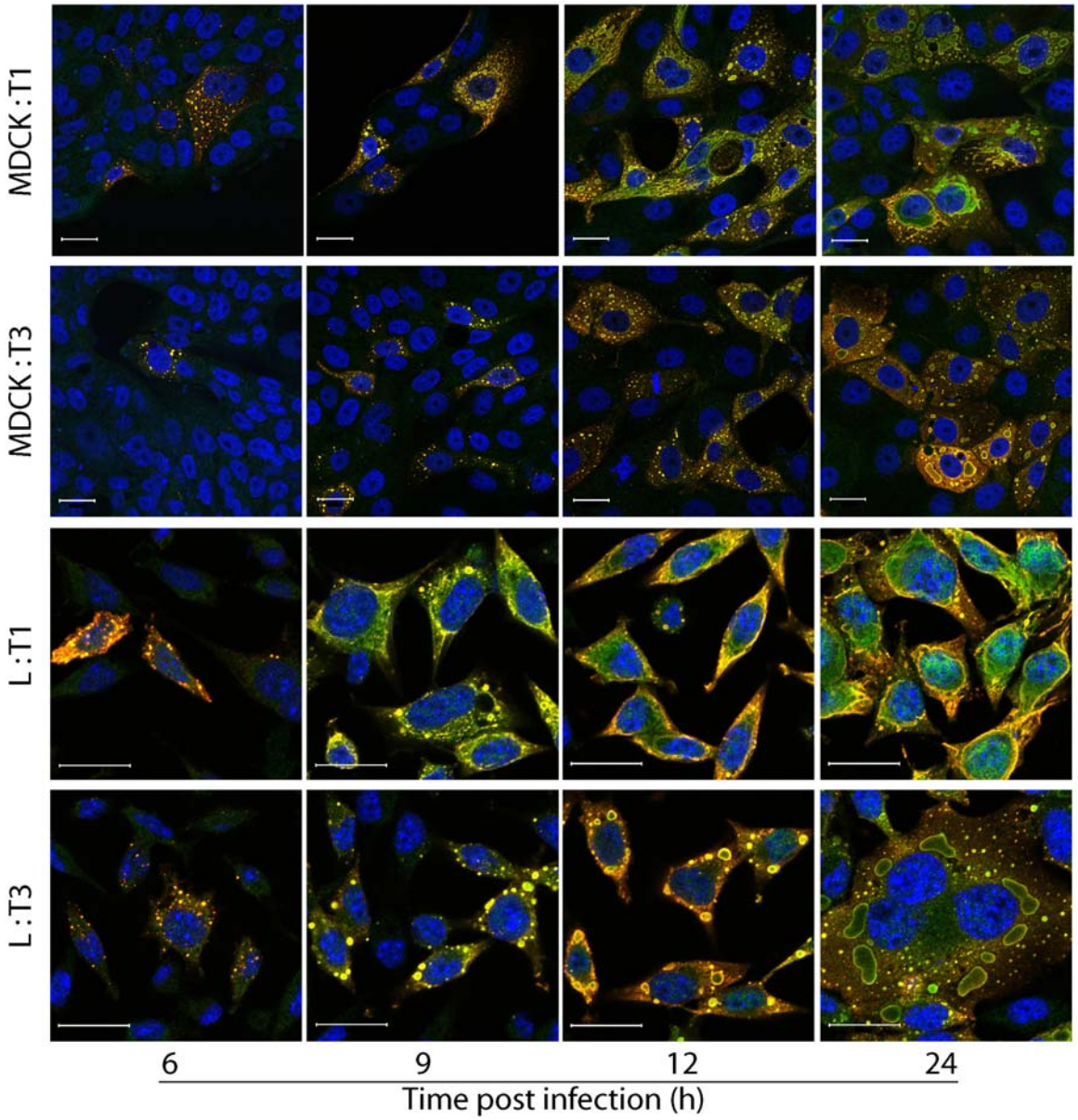

Figure 3.1. Reovirus inclusion formation. MDCK or L cells were infected with T1 or T3 at an MOI of 20 PFU/cell, fixed at the time points shown, stained with anti-μ2 (green) and anti-σNS (red) antibodies and ToPro3 (blue, nuclear), and imaged using confocal microscopy. Scale bars, 20 μm.

T3-infected MDCK cells indicate that viral attachment, entry, and early rounds of transcription and translation proceed normally.

Trafficking of viral proteins to inclusions – The analysis of inclusion formation presented in Figure 3.1 indicates normal kinetic and morphologic development of viral inclusions in T3-infected MDCK cells. However, as only σNS and μ2 were visualized, the possibility of aberrant inclusion composition or localization of other viral proteins cannot be ruled out from these results. To more precisely characterize viral inclusions in T3-infected MDCK cells, I visualized the localization of other viral proteins using confocal microscopy. Strain T3-T1M1 served as a reference for efficient μ2-regulated reovirus replication. Consistent with previous experiments (Fig. 2.2, 2.3), T3-T1M1 replicated to high titers, whereas T3 exhibited minimal titer increase over a 48 h incubation interval (Fig. 3.2A). Nonstructural proteins σNS and μNS physically associate in the formation of an inclusion scaffold (74). In cells infected with T3 or T3-T1M1, large inclusions with usual strain-dependent morphology were observed using σNS- and μNS-specific antisera to stain cells at 24 h post-infection (Fig. 3.2B, C). No alterations in σNS or μNS localization were apparent in T3-infected cells. These data indicate that the viral proteins required to form inclusions are properly recruited and assembled in T3-infected MDCK cells.

The localization of viral core proteins μ2 and λ2 and outer-capsid proteins μ1 and σ3 in T3- and T3-T1M1-infected MDCK cells (Fig. 3.3A) and L cells (Fig. 3.3B) was examined. In MDCK cells, the μ2 and λ2 proteins of both T3 and T3-T1M1 were found throughout the cytoplasm and concentrated in viral inclusions (Fig. 3.3A). A similar distribution of these proteins was observed in L cells. Outer-capsid protein σ3 was highly abundant in both T3- and T3-T1M1-infected MDCK cells. It was found distributed throughout the cytoplasm, colocalized with σNS in inclusion puncta, and frequently in

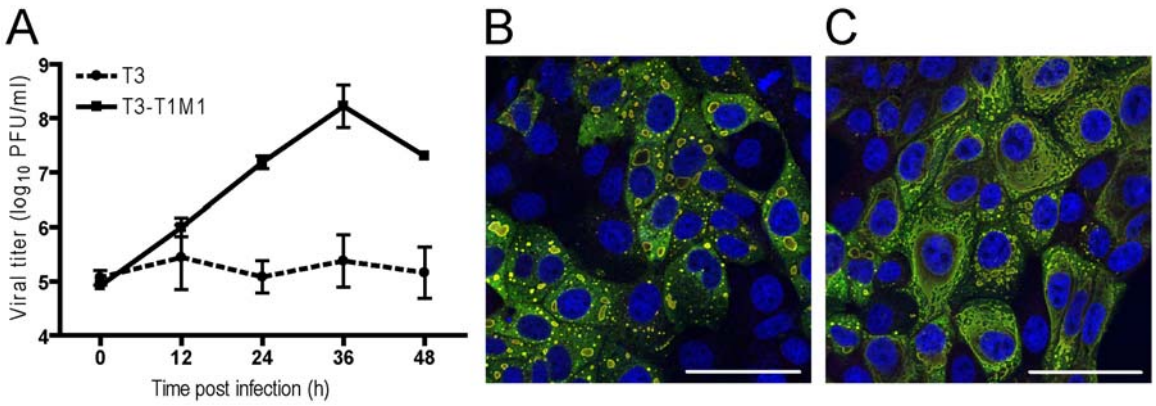

Figure 3.2 Replication and inclusion formation of T3 and T3-T1M1. (A) MDCK cells were infected with T3 or T3-T1M1 at an MOI of 2 PFU/cell, and viral titers in cell lysates were determined at the time points shown by plaque assay using L cells. Results represent the mean of triplicate experiments. Error bars indicate S.D. (B, C) MDCK cells were infected with T3 (B) or T3-T1M1 (C) at an MOI of 100 PFU/cell, fixed at 24 h post-infection, stained with anti-σNS (green) and anti-μNS (red) antibodies and ToPro3 (blue, nuclear), and imaged using confocal microscopy. Scale bar, 50 μm.

the nucleus (Fig. 3.3A). The distribution of σ3 in L cells was similar except for reduced distribution to the nucleus compared with MDCK cells. Outer-capsid protein μ1 was observed diffusely throughout the cytoplasm and in punctate structures associated with inclusions (Fig. 3.3). Fewer μ1-containing punctate structures were observed in T3- vs. T3-T1M1-infected MDCK cells (Fig. 3.3A). However, this quantitative difference correlates with diminished levels of μ1 expression overall (Fig. 3.5). In summary, no qualitative differences in the distribution of non-structural, core, or outer-capsid viral proteins were discernable in comparison of T3- and T3-T1M1-infected MDCK cells, indicating that viral protein recruitment to inclusions in cells infected by both strains occurs normally.

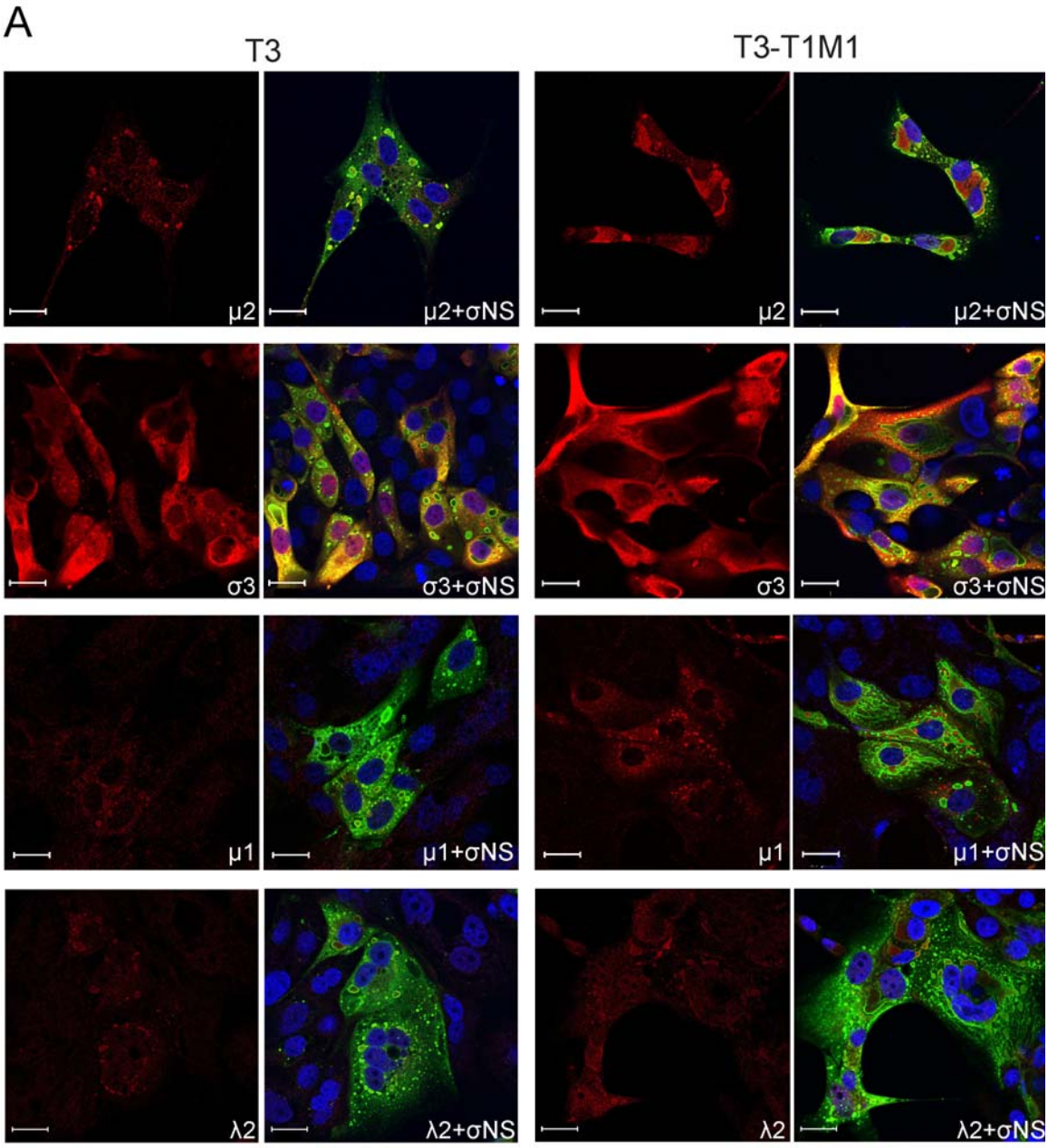

Figure 3.3. Distribution of reovirus proteins μ2, σ3, μ1, and λ2 in infected cells. MDCK cells (A) and L cells (B) were infected with either T3 or T3-T1M1 at an MOI of 20 PFU/cell, fixed at 24 h post-infection, stained with anti-σNS (green) and anti-μ2, anti-σ3, anti-μ1, or anti-λ2 (red) antibodies. Nuclei were visualized using ToPro3 (blue). Images were captured using confocal microscopy. Scale bar, 20 μm.

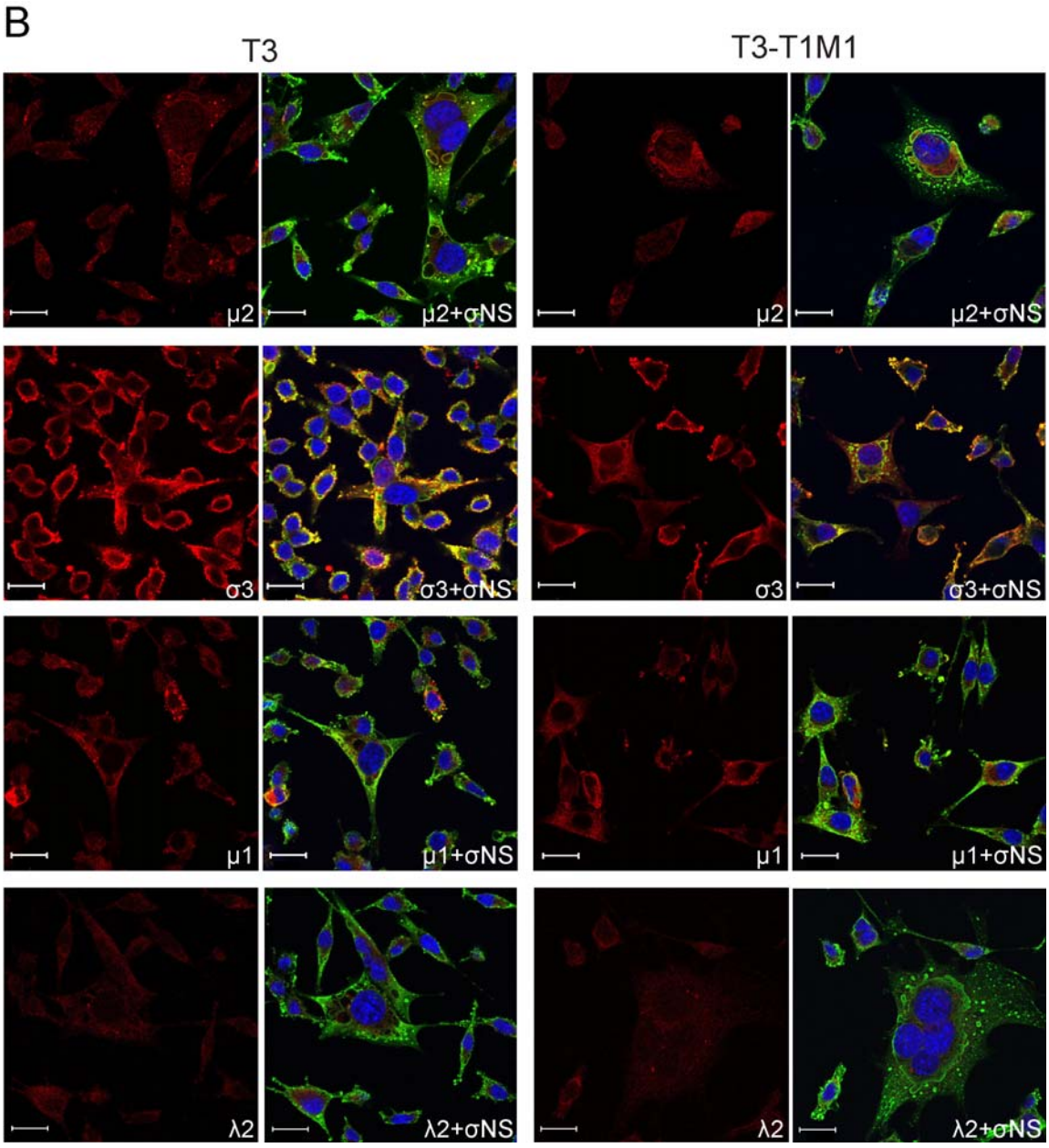

Quantification of reovirus RNA in infected cells – While the presence of viral inclusions in T3-infected MDCK cells confirms that viral transcription and translation occur, these findings cannot distinguish possible temporal defects occurring during primary and secondary rounds of gene expression. To monitor production of viral RNA over the

course of infection, I developed an RT-qPCR approach to specifically quantify positive- and negative-sense S4-gene RNA, which encodes viral structural protein σ3. Standard curves relating total viral genomic RNA to Ct were used for calculations of S4 total, double-stranded, and mRNA in RNA extracts from virus-infected cells. MDCK cells and L cells were infected at an MOI of 10 PFU/cell with either T3-T1M1 or T3. Strain T3-T1M1 was used in place of T1 because the T3 and T3-T1M1 S4 alleles are identical. At 12 h post-infection and following time points, high levels of total S4 RNA were detected in T3-T1M1-infected MDCK cells compared to the minimal amount of RNA produced in T3-infected cells (Fig. 3.4A). Conversely, in L cells, significant levels of total RNA were present in both T3-T1M1- and T3-infected cells at 12 h post-infection and beyond (Fig. 3.4B). Similar patterns of S4 dsRNA production by T3-T1M1 and T3 were observed in L cells (Fig. 3.4C, D). Significant levels of S4 mRNA were detected in MDCK cells at 12, 18, and 24 h post-infection with strain T3-T1M1 (Fig. 3.4E), whereas little S4 mRNA was detected in T3-infected cells at 12 and 18 h post-infection (Fig. 3.4E). The amount of S4 mRNA in T3-infected cells at 24 h post-infection was below the limit of detection (<10 copies of S4 RNA). These results indicate roughly equivalent efficiencies of early viral RNA synthesis in T3-T1M1 and T3-infected MDCK cells. However, late RNA synthesis is markedly diminished in T3-infected cells in comparison to that in T3-T1M1-infected cells, consistent with attenuated dsRNA production by T3 in MDCK cells.

Protein synthesis in reovirus-infected cells – Viral protein synthesis in infected MDCK cells and L cells was assessed by radiolabelling proteins during the course of infection. Strains T1 and T3 differ in the capacity to inhibit host cell protein synthesis, a phenotype

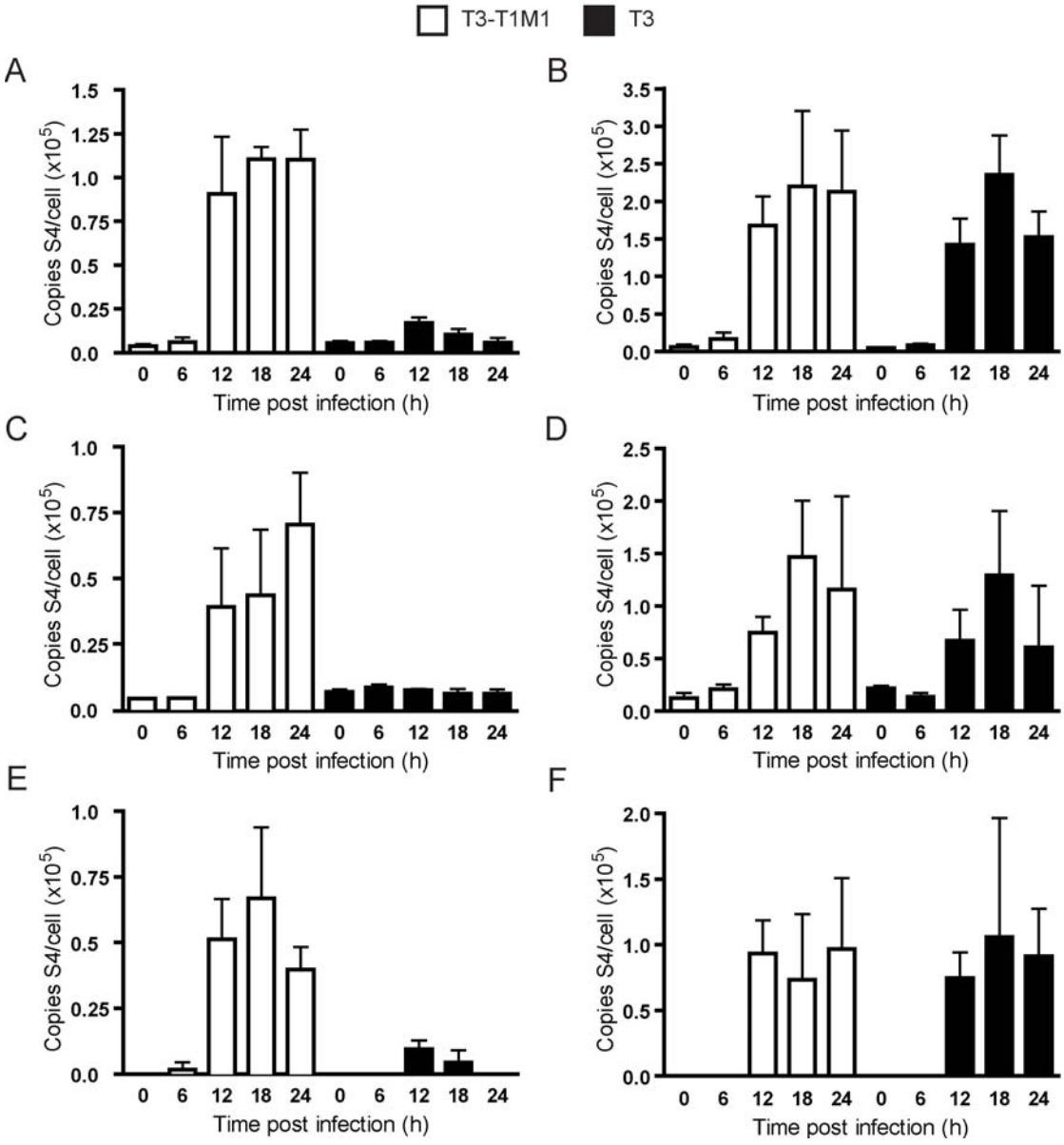

Figure 3.4. Analysis of viral RNA synthesis. Cells were infected with T3-T1M1 or T3 at an MOI of 10 PFU/cell, and total RNA was extracted from cell lysates at the indicated time points. RT-qPCR of total S4 RNA in MDCK cells (A) and L cells (B) was performed using an S4-specific reverse primer (complementary to the (+)-strand) in the reverse transcription step, followed by qPCR. A standard curve relating Ct to the amount of S4 RNA isolated from purified virion particles was used to determine S4 (+)-strand RNA copy number. RT-PCR of dsRNA in infected MDCK cells (C) and L cells (D) was performed using an S4-specific forward primer (complementary to the (–)-strand) in the reverse transcription step, followed by qPCR. A standard curve relating Ct to the amount of S4 RNA isolated from purified virion particles was used to determine S4 (–)-strand RNA copy number. Amounts of viral mRNA in MDCK cells (E) and L cells (F) are expressed as the difference between total RNA and dsRNA at each time point shown. Results represent the mean of triplicate experiments. Error bars indicate S.D.

unrelated to the M1 gene segment (98, 131). Therefore, T3-T1M1 was used instead of T1 to eliminate this possible confounder. MDCK cells and L cells were infected at an MOI of 100 PFU/cell with either T3-T1M1 or T3. One hour prior to harvest, cells were incubated with [^{35}S]methionine-cysteine, and solublized whole-cell proteins were resolved using SDS-PAGE followed by autoradiography. New viral protein synthesis was observed at 12, 18, and 24 h post-infection in T3-T1M1-infected MDCK cells, yet only at 12 h post-infection in T3-infected cells (Fig. 3.5A). These data generally mirror T3-T1M1 and T3 RNA production in MDCK cells. In contrast, the kinetics and magnitude of new viral protein synthesis by T3-T1M1 and T3 did not significantly differ in infected L cells (Fig. 3.5B). Thus, early viral protein synthesis was roughly equivalent between T3-T1M1 and T3 in MDCK cells, but late protein synthesis by T3 was undetectable, consistent with diminished mRNA production at later time points.

Discussion

In this chapter, I set out to elucidate the role of μ2 protein in viral replication efficiency and cell tropism by determining the step in the viral replication program blocked in T3 replication. Additionally, the precise steps in the viral life cycle that occur following the release of transcriptionally active core particles into the cytoplasm and release of progeny virions remain poorly defined. Therefore, I designed experiments to assess inclusion morphology and kinetics, viral protein localization, and viral RNA and protein synthesis in T3-infected MDCK cells. The results indicate normal morphologic and kinetic formation of viral inclusions and normal viral protein recruitment to inclusions. Furthermore, no apparent alteration of initial transcription and translation

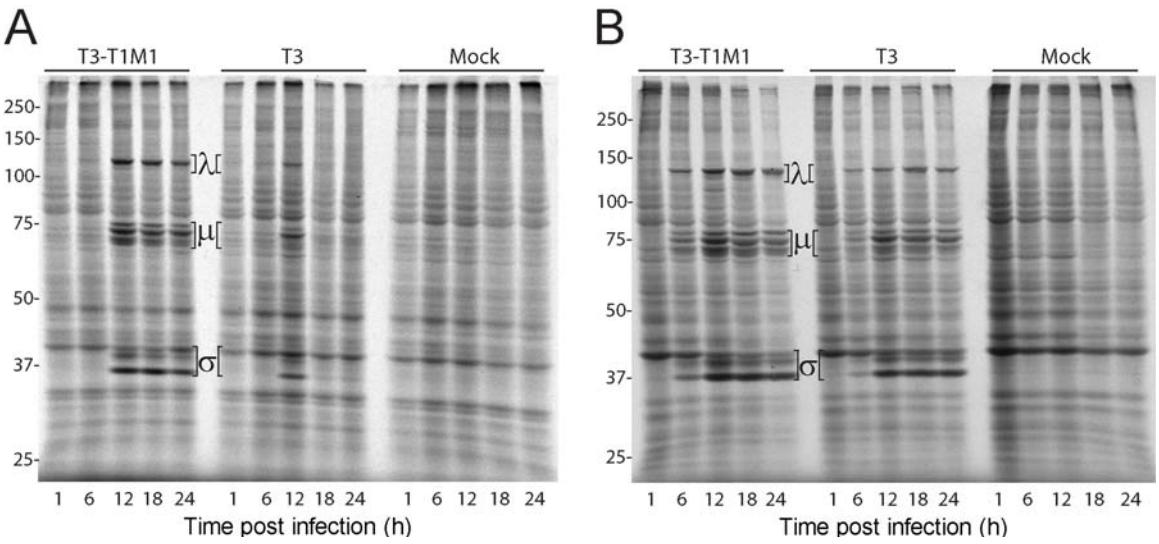

Figure 3.5. Analysis of viral protein synthesis. MDCK cells (A) or L cells (B) were infected at an MOI of 100 PFU/cell with reovirus strain T3-T1M1 or T3 and incubated for 1 h with [^{35}S]methionine/cysteine at the indicated times post-infection. Radiolabeled polypeptides were resolved by SDS-PAGE and visualized using autoradiography. Positions of viral λ, μ, and σ proteins are indicated. Molecular mass standards (in kDa) are shown.

was observed; however, secondary rounds of transcription and translation and dsRNA synthesis were significantly diminished in T3-infected MDCK cells. Collectively, these results indicate that the μ2-sensitive step in replication occurs at a point in the reovirus life cycle subsequent to primary rounds of viral transcription and translation but prior to dsRNA synthesis.

As an initial step to characterize the replication block in T3-infected MDCK cells, I used confocal microscopy to assess inclusion formation and kinetics. Interestingly, no differences in kinetics of inclusion formation were observed between T1 and T3 (Fig. 3.1). As expected, T1 and T3 displayed characteristic strain-dependent inclusion morphology. In this initial experiment, only σNS and μ2 were visualized. Normal localization of these two proteins does not ensure typical localization of other viral

proteins. Therefore, I conducted a more comprehensive analysis of viral protein trafficking to inclusions to determine whether one or more inclusion components display abnormal localization in non-productively infected MDCK cells. Using confocal microscopy, no discernable cell-type-specific differences in the distribution of μ2, other major inclusion proteins (μNS and σNS), core protein λ2, or outer-capsid proteins μ1 and σ3 were observed in T3-infected MDCK cells (Figs. 3.2, 3.3A). Although a relative reduction (compared with T3-T1M1) in the expression of μ1 was observed, the significance of this reduction to T3 replication in MDCK cells is unclear, as expression of all viral proteins markedly declines at late times post-infection (Fig. 3.5). Thus, results of confocal microscopy studies confirm the expected pattern of viral protein localization to T3 inclusions in MDCK cells, indicating structurally or functionally abnormal interactions within the inclusion that prevent production of infectious progeny.

An unexpected finding of this study was the co-existence of filamentous and globular inclusions in T1-infected MDCK cells (Fig. 3.1-3.3). Such mixture of inclusion morphologies contrasts with the uniformly filamentous appearance of T1 inclusions in previous studies using L, CV-1, Mv1Lu, and HEK 293T cells (60, 61, 88). Thus, inclusion morphologic phenotypes may be cell-type, as well as virus-strain, dependent. The significance of this novel pattern is unclear but congruous with previous studies that failed to show a relationship between viral replication capacity and inclusion morphology (61).

While negative-stand RNA synthesis and particle assembly have been ascribed to viral inclusions, the discrete series of steps that occur between entry of transcriptionally active core particles into the cytoplasm and appearance of mature progeny particles

within viral inclusions remains poorly defined. The absence of detectable viral RNA and protein synthesis at late times of infection in T3-infected MDCK cells (Figs. 3.2 and 3.3) despite normal-appearing inclusions (Fig. 3.1) indicates that the impasse occurs at one or more of these undefined steps.

Several potential but non-mutually exclusive mechanisms can be proposed to explain the replication block in T3-infected MDCK cells, including 1) mislocalization of RNA, 2) malfunction of the viral replicase during positive- or negative-strand synthesis, and 3) defective genome packaging or particle assembly. Significant effort was made to visualize RNA production in reovirus-infected cells to determine whether RNA is mislocalized in MDCK cells. Newly synthesized RNA can be visualized in infected cells by short-term labeling with 5'-bromouridine 5'-triphosphate (BrUTP) (47). In this method, cellular transcription is inhibited by actinomycin D, and BrUTP-containing viral RNA is visualized using BrdU-specific antibodies. This technique has been used to visualize production of reovirus RNA, and newly synthesized RNA was found to co-localize with viral inclusions (73). Unfortunately, I was unable to successfully use this technique because specific detection of BrUTP-labeled RNA, both viral and cellular, was not observed. Experiments designed to answer the second possible mechanism—malfunction of the viral replicase during positive- or negative-strand synthesis—also were not conducted; however, studies addressing this question may lead to further mechanistic understanding of the reovirus transcription machinery. Experiments designed to answer the third possible mechanism, defective genome packaging or particle assembly, are presented in Chapter IV.

Based on these results, the capacity of μ2 to mediate viral tropism at the post-entry level can be added to the list of μ2 functions in the reovirus replication program. Further investigation of μ2 interactions with the viral and cellular metabolic machineries will provide sharper insights into mechanisms of cellular permissivity to reovirus infection.

CHAPTER IV

REOVIRUS REPLICATION PROTEIN μ2 INFLUENCES CELL TROPISM BY PROMOTING PARTICLE ASSEMBLY WITHIN VIRAL INCLUSIONS

Introduction

Results presented in Chapter II implicate the μ2 and λ3 proteins as key viral determinants of reduced T3 replication efficiency in MDCK cells. The blockade to T3 replication takes place subsequent to primary transcription and translation but prior to dsRNA synthesis (Chapter III). Steps between these two stages of the viral life cycle likely take place within the reovirus inclusion; therefore, T3 infection of MDCK cells provides an excellent model to better understand the function of viral inclusions and how these novel organelles influence viral tropism.

In work described here, thin-section transmission electron microscopy (TEM) was used to more precisely define the role of μ2 protein in productive reovirus replication and virion particle production. The results indicate that particle assembly in T3-infected MDCK cells is defective and dependent on μ2 protein in a cell type-specific and temperature-dependent manner. Thus, reovirus infection of some cells is governed by interactions between viral replication proteins and the unique cell environment that promote genesis of functional viral inclusions.

This work was assisted by Dr. Jay Jerome, director of the electron microscopy core in Vanderbilt's Cell Imaging Shared Resource. Dr. Jerome provided guidance in

analyzing electron micrographs of reovirus-infected cells and determining appropriate quantitative methods to analyze inclusion ultrastructure.

Results

Ultrastructural analysis of viral inclusions – As confocal microscopy did not reveal overt abnormalities in the morphology or viral protein composition of T3 inclusions in MDCK cells, I used thin-section TEM to visualize viral particles within inclusions. In both T3- and T3-T1M1-infected cells, mature virion particles (i.e., containing electron-dense centers representing genomic viral RNA (27, 92) and empty virion particles were observed in a variety of arrangements. Some sections contained only a few mature virions scattered in the cytoplasm (Fig. 4.1A, B). Virus was occasionally visualized outside of the cell, attached to, or near the plasma membrane (Fig. 4.1B). Other sections contained large groups of viral particles surrounded by material having a heterogeneous consistency clearly distinct from cytoplasm (Fig. 4.2). The latter structures presumably correspond to the filamentous or globular inclusions observed using confocal microscopy; these are referred to as particle-containing inclusions. Representative images of particle-containing inclusions in T3-T1M1-infected MDCK cells are shown in Fig. 4.2A. These large aggregates of virions contain a significant fraction of complete particles in paracrystalline arrays. Occasionally, particles were interspersed with coated microtubules (Fig. 4.1C), which have been previously described in reovirus infected cells (27). This coat is thought to be composed primarily of viral protein μNS (16, 76). The arrangement of particles in T3-infected MDCK cells sharply contrasted with that observed in T3-T1M1-infected MDCK cells. Sections containing only a few scattered particles were most frequently

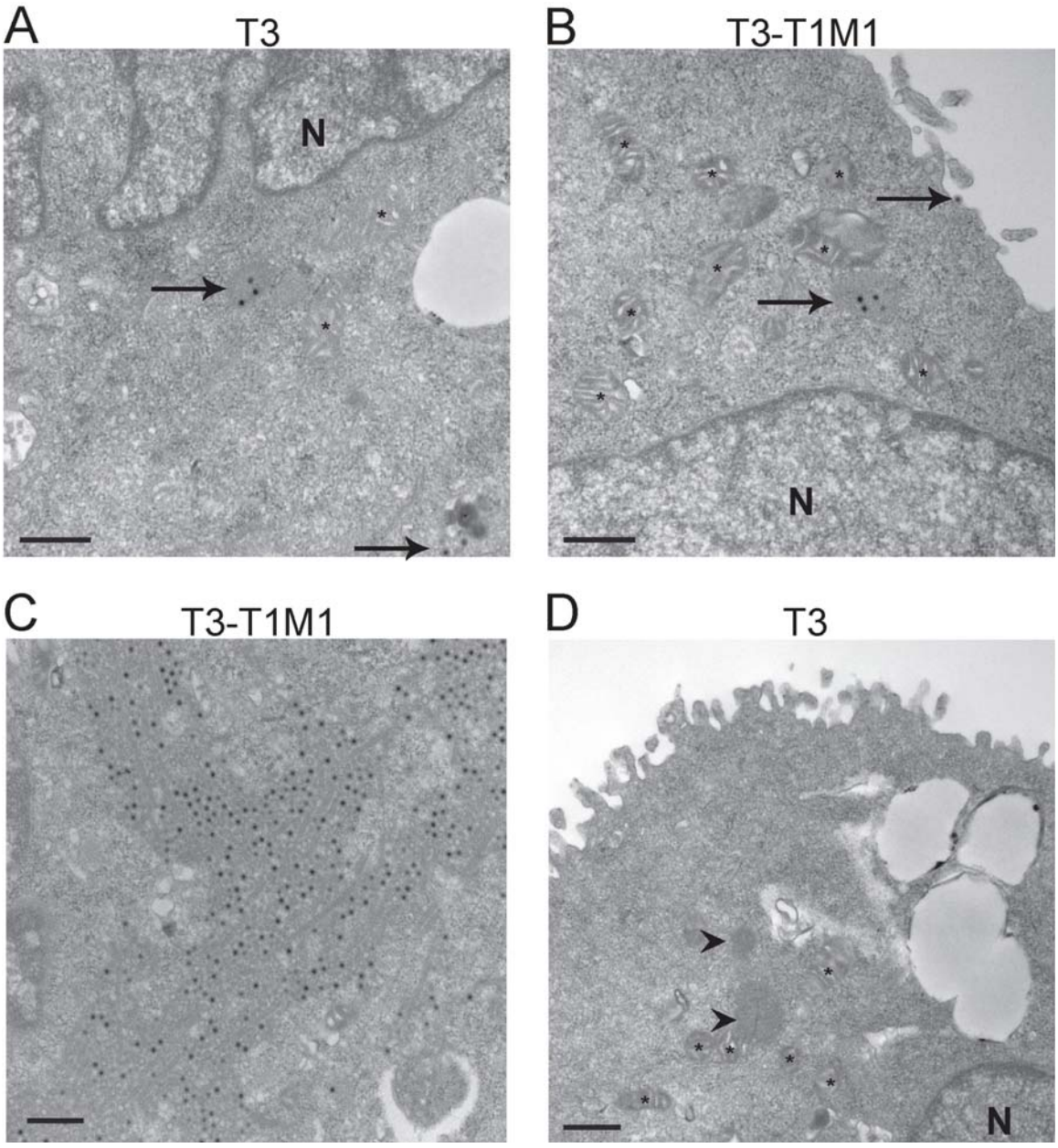

Figure 4.1. Ultrastructural analysis of viral inclusions. MDCK cells were infected with either T3 (A, D) or T3-T1M1 (B, C) at an MOI of 100 PFU/cell and fixed at 24h post-infection. Ultra-thin sections (65-70 nm) were examined using transmission electron microscopy. (A, B) Sections containing small numbers of particles scattered within the cytoplasm or outside of the cell. (C) Inclusion containing particles and coated microtubules. (D) Section depicting a presumed "particle-free" inclusion. Black arrows indicate particles. Asterisks, mitochondria. N, nucleus. Arrow heads indicate particle-free inclusions. Scale bar, 500 nm.

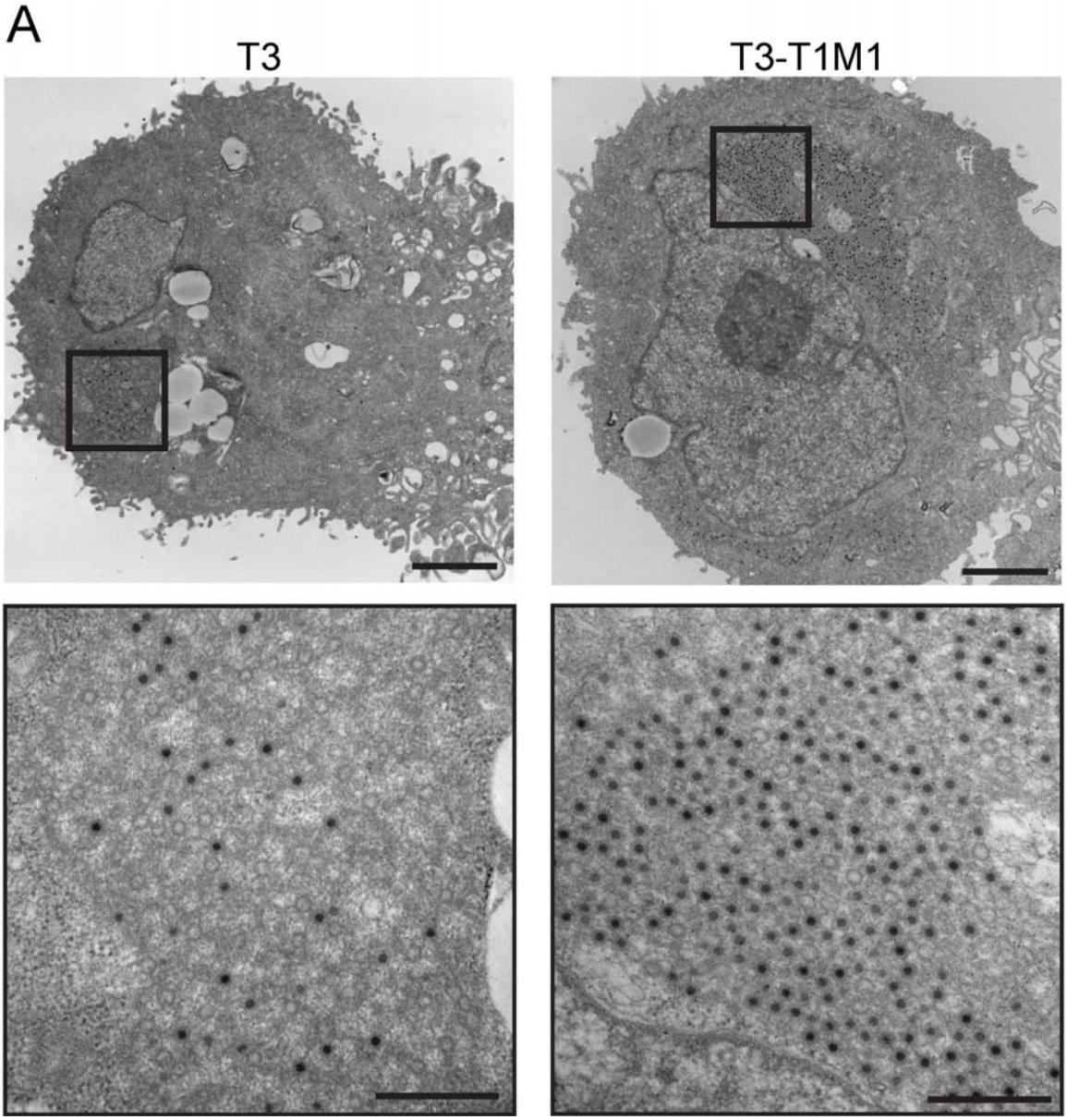

Figure 4.2. Large particle-containing inclusions in infected cells. MDCK cells (A) and L cells (B) were infected with either T3 or T3-T1M1 at an MOI of 100 PFU/cell and fixed at 24 h post-infection. Ultra-thin sections (65-70 nm) were examined using transmission electron microscopy. Boxed regions correspond to high-magnification images shown below. Scale bars: low-magnification images, 2 μm; high-magnification images, 500 nm.

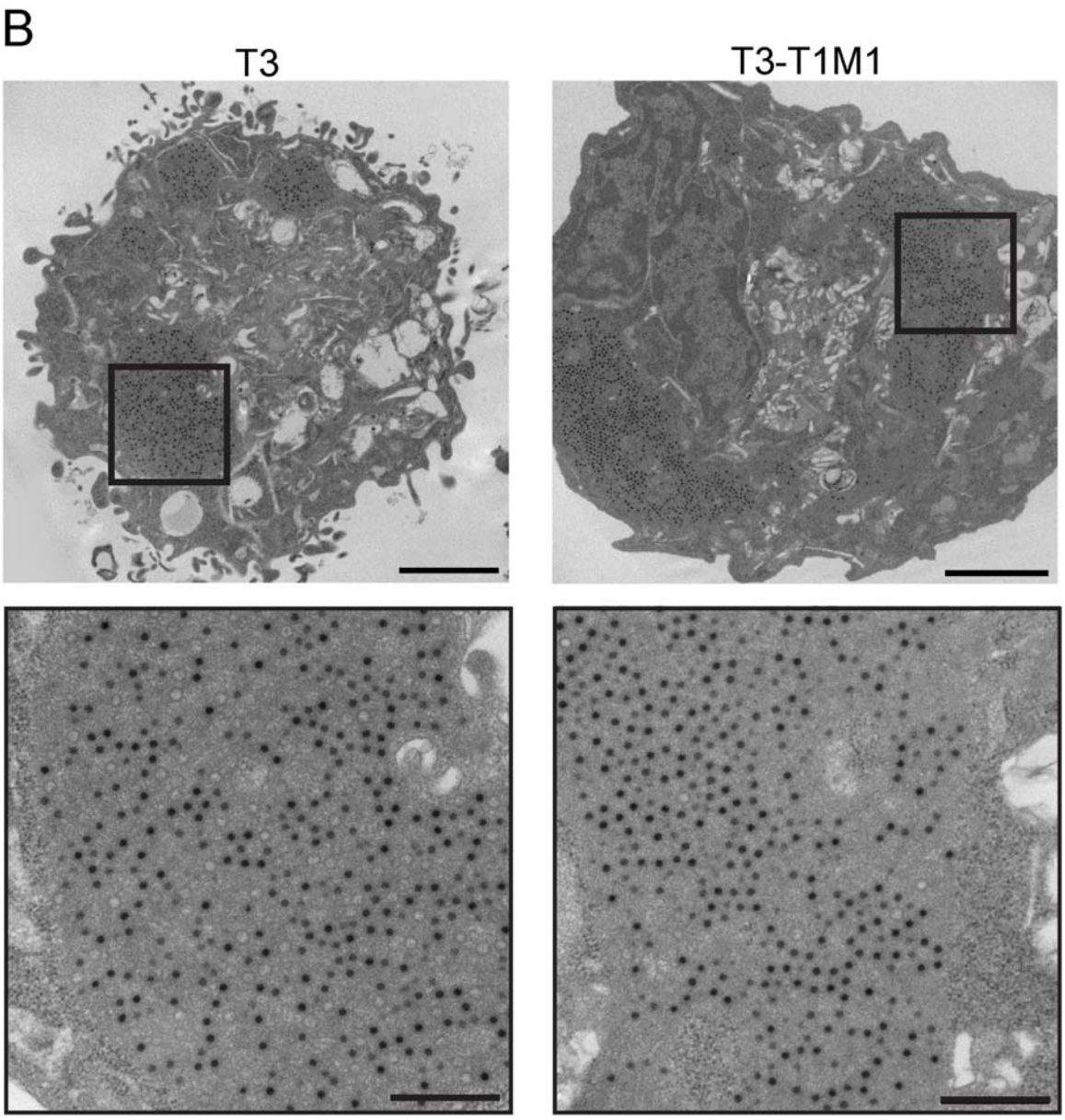

observed (Fig. 4.1A), although some organized particle-containing inclusions were detected (Fig. 4.2A). Inclusions in T3-infected cells were less frequent, smaller, displayed decreased organization, and harbored fewer genome-containing particles compared to T3-T1M1-infected cells. The size, frequency, and particle content of T3 and T3-T1M1

inclusions in L cells were similar to each other and to those in T3-T1M1-infected MDCK cells (Fig. 4.2B).

Quantification of ultrastructural features in infected cells – To validate observations of T3 and T3-T1M1 ultrastructural morphology, certain features of inclusions captured in electron micrographic images were quantified. The fraction of cytoplasm containing virion particles or inclusion matrix was measured using the point counting stereology method (120). I defined the viral fraction of cytoplasm to be viral particles and surrounding milieu (i.e., inclusion matrix) that was clearly distinct from normal cytoplasm. Structures resembling viral inclusions but devoid of viral particles (Fig. 4.1D) were counted as cytoplasm since I could not be certain that these were of viral origin. However, such "empty inclusions" were not observed frequently. This experiment was performed on two separate occasions. In T3-T1M1-infected MDCK cells, 19.2% or 13.5% of the cytoplasm was occupied by inclusion matrix, whereas this fraction was only 2.9% or 0.38% in T3-infected cells (Table 4.1). The corresponding values in L cells were 27.8% or 13.5% in T3-T1M1-infected cells and 14.9% or 11.4% in T3-infected cells. The proportion of inclusion matrix occupied by particles was 11.2% or 10.4% and 17.8% or 21.9% in T3- and T3-T1M1-infected MDCK cells, respectively, and 23.4% or 25.3% and 32.1% or 24.3% in L cells. These data are consistent with my observation that particles within inclusions of T3-infected MDCK cells were less densely packed. Following infection with either T3 or T3-T1M1, a spectrum of particle organization was observed, with the greatest degree of order being a paracrystalline array. Figure 4.3 depicts

inclusions in infected L cells with highly ordered particles. Particles in T3 inclusions did not achieve the same high degree of organization as particles in T3-T1M1 inclusions.

Table 4.1. Quantitative analysis of reovirus replication using thin-section electron micrographs of reovirus-infected cells*

Cell type	Exp.	Virus strain	Fraction of cytoplasm containing virion particles or inclusion matrix	Fraction of viral inclusion matrix occupied by particles	Mature fraction of virion particles
MDCK	1	T3	2.9%	11.2%	36.3%
MDCK	1	T3-T1M1	19.2%	17.8%	76.7%
MDCK	2	T3	0.38%	10.4%	32.1%
MDCK	2	T3-T1M1	13.5%	21.9%	55.0%
L	1	T3	14.9%	23.4%	79.7%
L	1	T3-T1M1	27.8%	32.1%	94.9%
L	2	T3	11.4%	25.3%	86.2%
L	2	T3-T1M1	13.5%	24.3%	91.8%

*28-36 images collected for each sample condition.

The ratios of complete and empty particles in inclusions formed in both cell types were determined. The fraction of complete particles in T3- and T3-T1M1-infected MDCK cells was 36.3% or 32.1% and 76.7% or 55%, respectively. The corresponding values in L cells were 79.7% or 86.2% and 94.9% or 91.8%, respectively. The smaller fraction of inclusion matrix observed in T3-infected MDCK cells suggests that particle assembly is defective and, furthermore, that this process is dependent on the μ2 protein. While some inter-experimental variability was observed, in all three quantitative categories, the overall trends were consistent. T3-infected cells displayed a smaller fraction of cytoplasm containing virion particles or inclusion matrix, viral inclusion

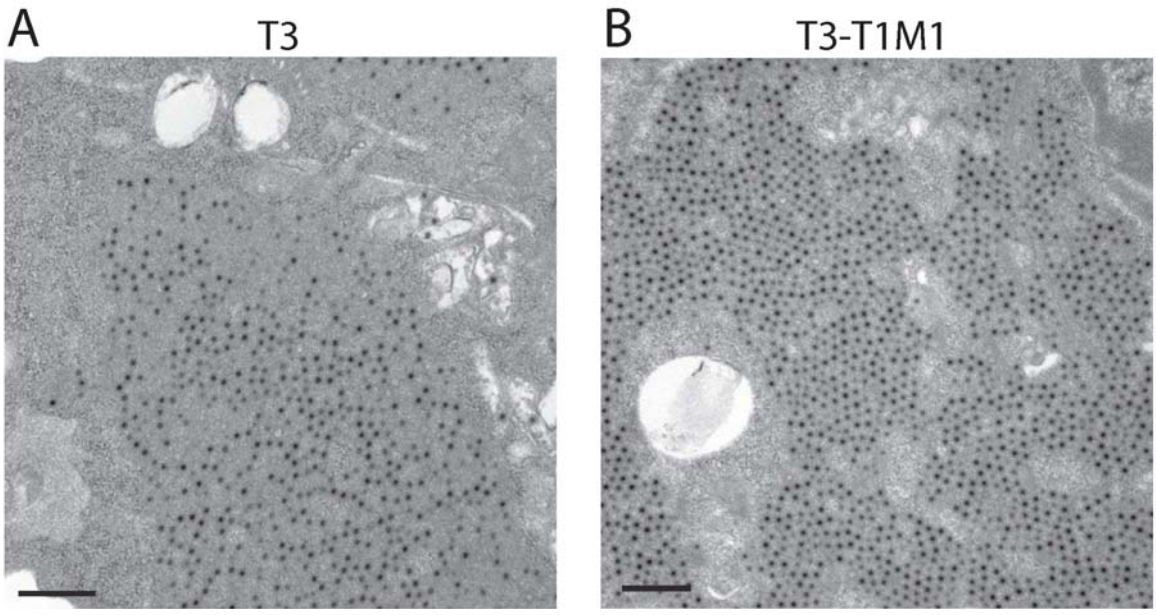

Figure 4.3. Paracrystalline arrangement of particles. L cells were infected with either T3 (A) or T3-T1M1 (B) at an MOI of 100 PFU/cell and fixed at 24 h post infection. Ultra-thin sections (65-70 nm) were examined using transmission electron microscopy. Paracrystalline arrays of particles are shown. Scale bar, 500 nm.

matrix occupied by particles, and mature fraction of virion particles in MDCK cells. Taken together, qualitative and quantitative TEM analysis of reovirus inclusions under conditions of productive and abortive infection of MDCK cells points to viral assembly as a μ2-sensistive step in viral replication.

Identification of size differences of reovirus particles in non-permissive infection – While examining the ultrastructure of reovirus inclusions in MDCK cells, I observed that empty T3 particles appeared smaller than empty T3-T1M1 particles. Therefore, complete and empty particle diameters were quantified and compared. A high-magnification image of virion particles in T3-T1M1-infected MDCK cells (Fig. 4.4) illustrates the specific

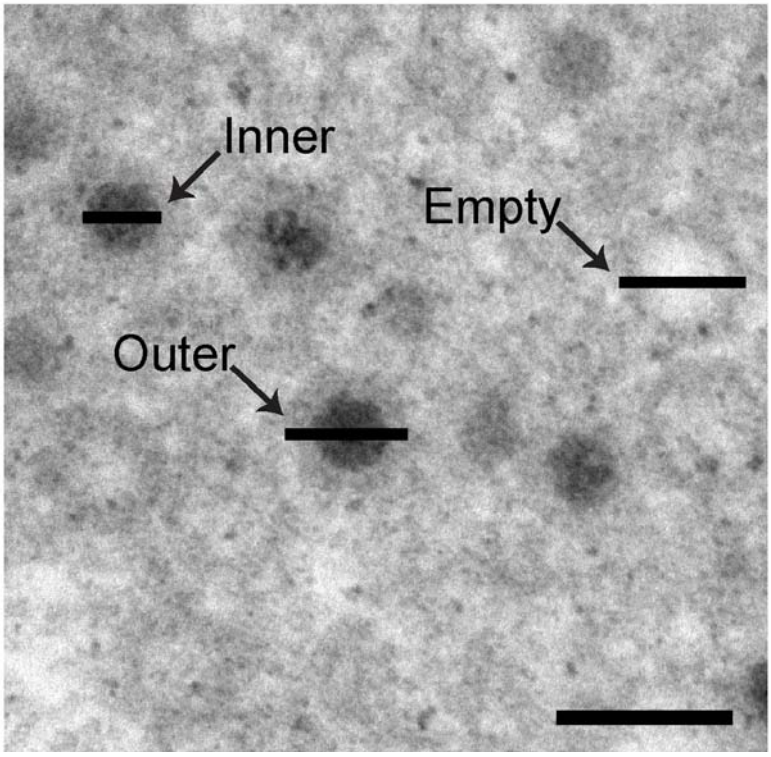

Figure 4.4. High-magnification image of T3-T1M1-infected MDCK cells. The diameter of the inner electron dense center of complete particles (Inner), the outer diameter of complete particles (Outer), and outer diameter of empty particles (Empty) are demarcated by horizontal bars. Scale bar (lower right), 100 nm.

diameter measurements recorded: 1) electron-dense centers of mature particles, 2) outer rim of mature particles, and 3) outer rim of empty particles. Large numbers of observations (86-1000) for each category were made to statistically validate size differences. This experiment was carried out on two separate occasions. The mean inner diameter of mature T3 and T3-T1M1 particles in both MDCK and L cells was approximately 38 nm, whereas the mean outer diameters of mature particles were approximately 71 – 72 nm (Table 4.2). In contrast, the mean diameter of empty particles in T3-infected MDCK cells was significantly less than the empty-particle diameters in T3-T1M1-infected MDCK cells, 67.3 ±0.27 nm vs. 73.5 ±0.34 nm in Experiment 1 and

67.8 ±0.25 nm vs 72.8 ±0.30 nm in Experiment 2. Diameters of empty particles of T3 and T3-T1M1 in L cells were not significantly different and were approximately 71 – 72 nm. These results reveal a difference in the size of T3 and T3-T1M1 empty particles produced in MDCK cells but not L cells, indicating that some aspects of T3 particle assembly in MDCK cells follow an anomalous path. Furthermore, these findings are consistent with a μ2-associated block to the morphogenesis of mature T3 virions in MDCK cells.

Table 4.2: Quantification of viral particle diameters in reovirus infected cells

Cell type	Exp.	Virus strain	Mature particle outer diameter (nm)*	n[§]	Mature particle inner diameter (nm)	n	Empty particle outer diameter (nm)	n
MDCK	1	T3	72.3 ± 0.44	110	38.3 ± 0.22	116	67.3 ± 0.27	306
	1	T3-T1M1	72.0 ± 0.21[#]	311	37.9 ± 0.12[#]	323	73.5 ± 0.34[&]	177
L	1	T3	71.3 ± 0.24	380	38.5 ± 0.11	417	71.2 ± 0.40	119
	1	T3-T1M1	71.0 ± 0.22[#]	385	38.3 ± 0.11[#]	413	72.0 ± 0.42[#]	138
MDCK	2	T3	71.3 ± 0.34	251	39.0 ± 0.15	329	67.8 ± 0.25	497
	2	T3-T1M1	71.1 ± 0.25[#]	657	38.9 ± 0.12[#]	985	72.8 ± 0.30[&]	445
L	2	T3	71.1 ± 0.25	496	38.4 ± 0.11	973	71.4 ± 0.78	86
	2	T3-T1M1	70.6 ± 0.19[#]	727	38.2 ± 0.08[#]	1000	70.8 ± 0.37[#]	163

*Values represent mean ± SEM
[§]n, number of particles measured
[#]*t*-test, not significant (vs. T3)
[&]*t*-test, $P < 0.0001$ (vs. T3)

Replication of reovirus at low temperature – A previous study suggested that the T3 μ2 protein is subject to temperature-dependent misfolding (75), which led us to consider whether strain-dependent differences in viral replication efficiency in MDCK cells might be influenced by the temperature of infection. To test this hypothesis, viral titers were monitored in MDCK cells (Fig. 5A, 5C) and L cells (Fig. 5B, 5D) infected with either T3 or T3-T1M1 and incubated at either 31ºC (Fig. 5A, 5B) or 37ºC (Fig. 5C,

5D) for 96 h post-infection. Replication of T3 in MDCK cells at 31ºC greatly exceeded that at 37ºC, closely approaching the yield of T3-T1M1 at 31ºC. In L cells infected at 31ºC, T3 displayed significantly lower yield at 24 h post-infection compared to T3-T1M1, but attained a similarly high level of replication at later times post-infection. T3-T1M1 replicated efficiently in both cell types at 31ºC. However, the rise in titer was

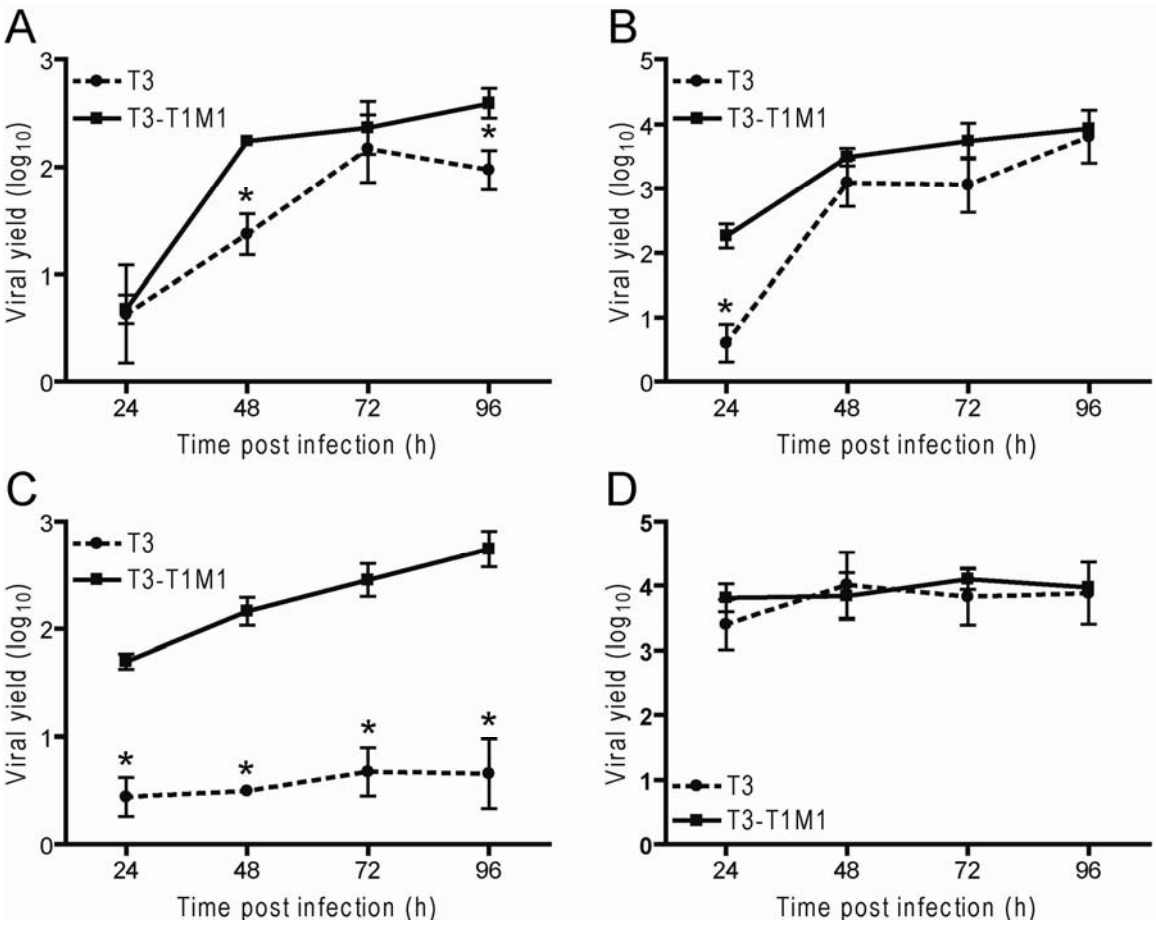

Figure 4.5. Temperature-dependence of reovirus replication in MDCK cells. MDCK cells (A, C) or L cells (B, D) were infected at an MOI of 2 PFU/cell and incubated at 31ºC (A, B) or 37ºC (C, D) for the times shown. Viral titers in cell lysates were determined by plaque assay using L cells. Viral yields were calculated as the difference between $\log_{10}$ titer at the indicated time points and $\log_{10}$ titer at 0 h. Results represent the mean of triplicate experiments. Error bars indicate S.D. *, $p < 0.05$ in comparison to T3-T1M1 (Student's *t* test).

delayed relative to 37ºC. Taken together, these results indicate that replication of T3 in MDCK cells is temperature-dependent.

One line of evidence that was used to suggest that T3 μ2 is subject to temperature-dependent folding (75) was the observation that T3 formed filamentous inclusions at low temperature. Confocal microscopy of MDCK cells infected at 31ºC was used to assess the effect of temperature on inclusion morphology in these cells. MDCK cells were infected with T3, T3-T1M1, and T3-M1L347F, incubated at 31ºC or 37ºC, and fixed at 24 h post-infection. At both temperatures, T3 displayed characteristic globular inclusions and T3-T1M1 displayed predominantly filamentous inclusions. T3-M1L347F, a virus

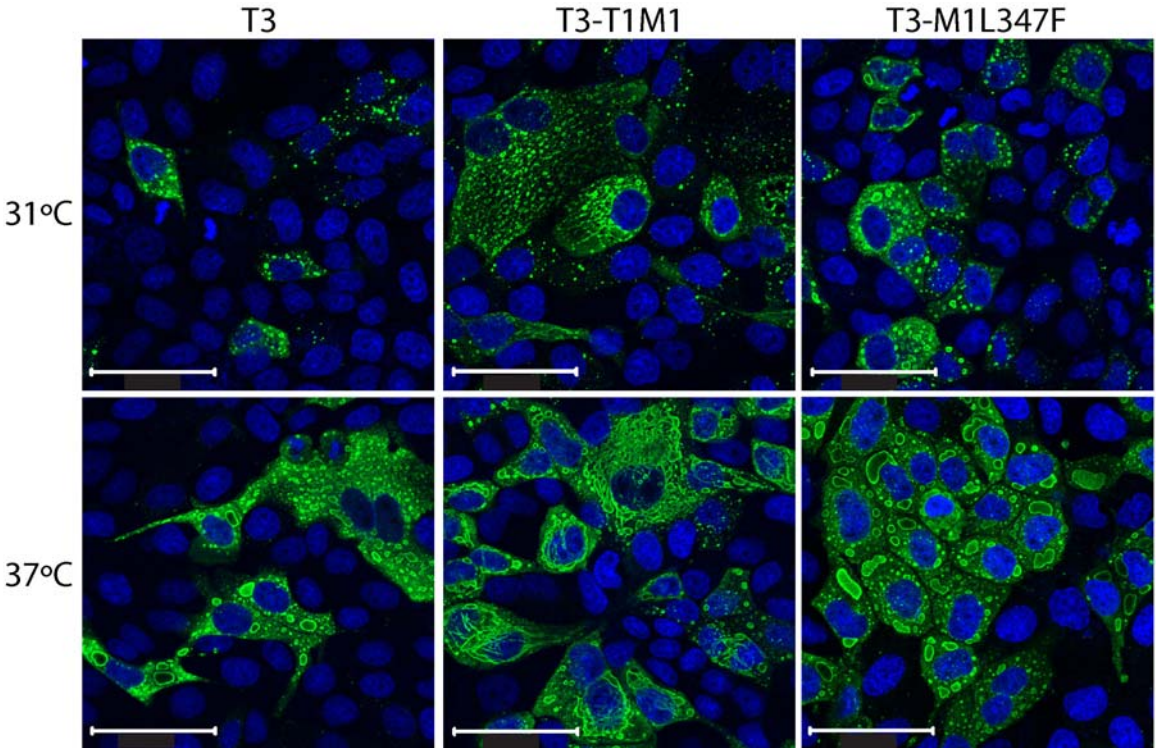

Figure 4.6. Confocal microscopy of viral inclusions in MDCK cells infected at low temperature. MDCK cells were infected with T3, T3-T1M1, or T3-M1L347F at an MOI of 20 PFU/cell, fixed 24 h post infection at 31ºC or 37ºC, stained with anti-σNS (green) antibody and ToPro3 (blue, nuclear), and imaged using confocal microscopy. Scale bars, 50 μm.

containing a single amino acid polymorphism in μ2 that confers replicative capacity in MDCK cells (Fig. 2.5), also displayed globular inclusions at both temperatures. In cells infected at 31ºC, inclusions were smaller and less developed than inclusions in cells infected at 37ºC. This observation is consistent with the slower kinetics of replication observed at 31ºC in comparison to 37ºC (Fig. 4.5); however, in contrast to results presented by Miller et al. (75), temperature did not affect inclusion morphology.

Ultrastructural analysis of viral inclusions in cells infected at low temperature – Thin-section TEM of MDCK cells infected at the lower temperature was used to determine whether enhanced replication kinetics of T3 in MDCK cells at 31ºC correlates with restoration of normal inclusion ultrastructure. Since the replication kinetics of infection are delayed at 31ºC, infected cells were fixed at 48 and 72 h post-infection. At both time points, large particle-containing inclusions enclosing mature and empty particles were observed in both T3- and T3-T1M1-infected cells (Fig. 4.7). At 48 h post-infection, the fraction of cytoplasm occupied by viral inclusion matrix was 13.0% and 27.0% in T3- and T3-T1M1-infected MDCK cells, respectively, while the proportion of inclusion matrix occupied by particles was 7.5% in T3-infected cells and 12.9% in T3-T1M1-infected cells (Table 4.3). Complete particles comprised 42.0% and 40.0% of total virions in T3- and T3-T1M1-infected cells, respectively. At 72 h post-infection, the fraction of cytoplasm occupied by viral inclusion matrix was 17% and 28.0% in T3- and T3-T1M1-infected cells, respectively, while the proportion of inclusion matrix occupied by particles was 12.7% in T3-infected cells and 16.8% in T3-T1M1-infected cells (Table 4.3). Complete particles comprised 29.7% and 36.3% of total virions in T3- and T3-T1M1-

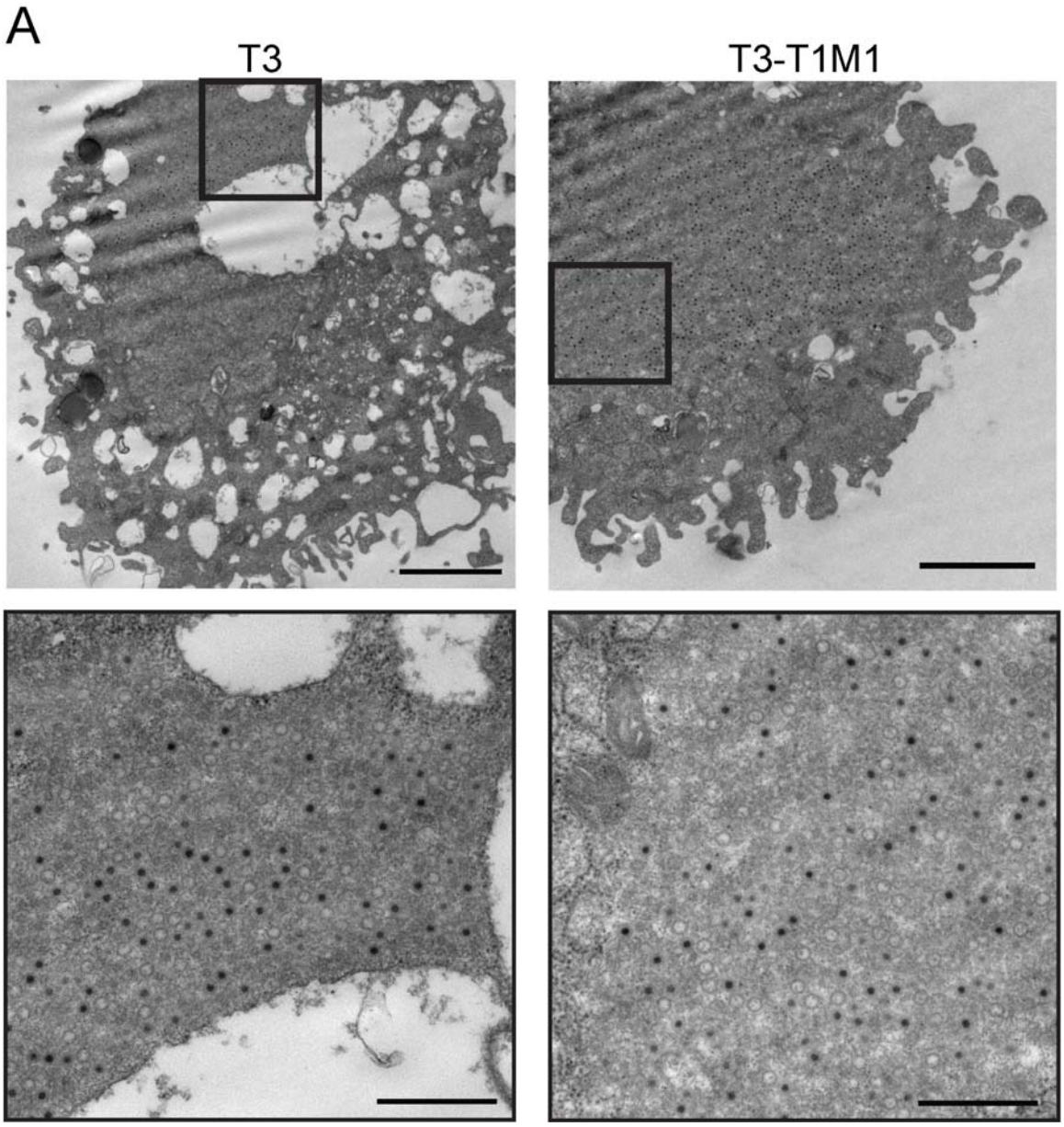

Figure 4.7**.** Ultrastructural analysis of viral inclusions in MDCK cells infected at low temperature. MDCK cells were infected with either T3 or T3-T1M1 at an MOI of 100 PFU/cell and fixed at 48 (A) or 72 (B) h post-infection. Ultra-thin sections (65-70 nm) were examined using transmission electron microscopy. Boxed regions correspond to high-magnification images shown below. Scale bars: low-magnification images, 2 μm; high-magnification images, 500 nm.

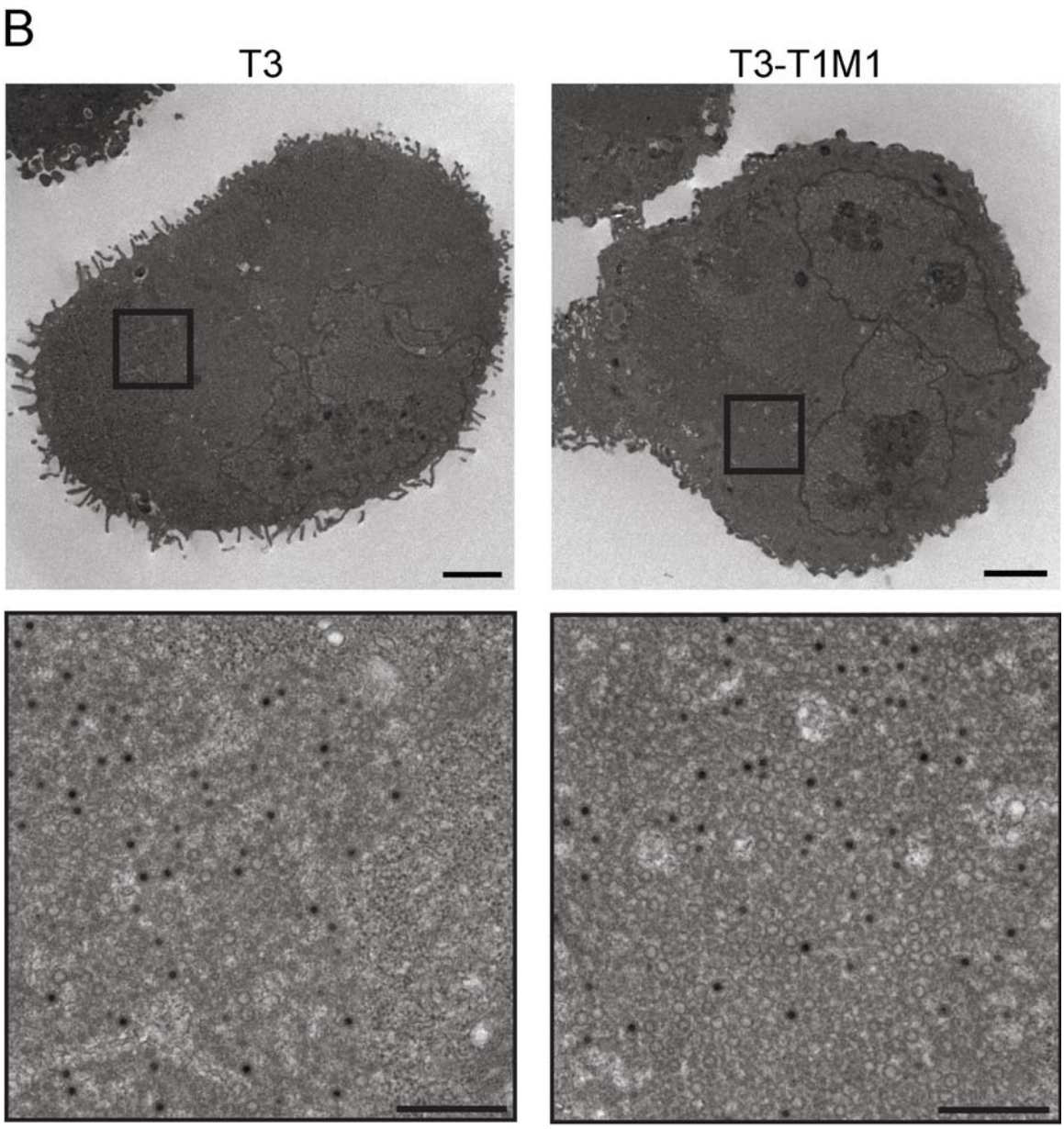

infected cells, respectively. The substantial increase in the fraction of inclusion matrix from 2.9% to 17.0% at 72 h post-infection in T3-infected MDCK cells incubated at 31ºC vs. 37ºC provides further evidence that the inhibition to T3 replication in MDCK cells is eased at low temperature. Additionally, the mean diameters of empty particles in MDCK cells infected with T3 (72.9 ± 0.22 nm [48 h], 72.6 ±0.29 nm [72 h]) and T3-T1M1 (73.3

± 0.21 nm [48 h], 71.9 ± 0.20 nm [72 h]) were equivalent at reduced incubation temperature (Table 4.4). Thus, lowering the temperature of infection partially relieved μ2-mediated restriction of T3 replication in MDCK cells and reversed the block to mature particle assembly, consistent with the hypothesis that the conformational state of μ2 influences success of the reovirus life cycle through a mechanism involving virion morphogenesis.

Table 4.3. Quantitative analysis of reovirus replication at 31ºC using thin-section electron micrographs of reovirus-infected MDCK cells*

Virus strain	Time post infection	Fraction of cytoplasm containing virion particles or inclusion matrix	Fraction of viral inclusion matrix occupied by particles	Mature fraction of virion particles
T3	48 h	13.0%	7.5%	42.0%
T3-T1M1	48 h	27.0%	12.9%	40.0%
T3	72 h	17.2%	12.7%	29.7%
T3-T1M1	72 h	28.0%	16.8%	36.3%

*36 images collected for each sample condition.

Table 4.4. Quantification of viral particle diameters following infection at 31ºC

Virus strain	Time post infection	Mature particle outer diameter (nm)*	n§	Mature particle inner diameter (nm)	n	Empty particle outer diameter (nm)	n
T3	48 h	72.2 ± 0.25	324	38.6 ± 0.12	360	72.9 ± 0.22	388
T3-T1M1	48 h	72.6 ± 0.21#	435	38.4 ± 0.17#	451	73.3 ± 0.21#	483
T3	72 h	71.9 ± 0.35	203	38.0 ± 0.16	225	72.6 ± 0.29	284
T3-T1M1	72 h	71.5 ± 0.23#	306	37.9 ± 0.13#	312	71.9 ± 0.20#	472

*Values represent mean ± SEM

§n, number of particles measured

#*t*-test, not significant (vs. T3)

Discussion

A common strategy of virus replication is the formation of neo-organelles—i.e., inclusions—that concentrate and protect viral components required for genome multiplication and particle assembly. An understanding of viral inclusion composition and organization is essential to illuminate strategies by which viruses direct a successful replication program. The specific steps that occur within reovirus inclusions have not been precisely defined; however, viral RNA assortment, genome replication, secondary transcription, and particle morphogenesis are presumed to occur within these structures (2, 27, 31, 77, 78, 92, 129, 130). In this study, I made use of a post entry-determined, strain-specific replication defect in MDCK cells to enhance knowledge of key activities within reovirus inclusions that are sensitive to the specific host cell milieu. These findings suggest that reovirus tropism for some types of cells is governed by interactions between viral replication proteins and the unique cell environment that favor development of inclusions capable of generating fully assembled infectious particles.

TEM analysis of MDCK cells infected with T3 revealed a much smaller fraction of cytoplasm containing particles and inclusion matrix compared with strain T3-T1M1 (0.38% - 2.9% vs 13.5% - 19.2%) (Fig. 4.2A, Table 4.1). Mature particles with electron-dense (i.e., genome-containing) centers and empty particles were observed in MDCK cells infected with either T3 or T3-T1M1. However, the mature fraction of T3 particles was less than that for T3-T1M1 (32.1% - 36.0% vs. 55.0% - 77%) (Table 4.1). Assembly intermediates that escape the blocked step appear competent to reach full structural maturity, consistent with the finding that conditions can be modified to permit partial relief of the restriction to T3 replication in MDCK cells. Collectively, the substantial

decrease in particle-containing inclusion matrix and mature virion particles suggest that assembly of T3 particles is blocked in MDCK cells, leading to a significant reduction in viral yield.

Although results of confocal microscopy studies indicate that a majority of cells are infected (Fig. 3.2), not all TEM sections contained identifiable viral structures. I defined inclusions in electron micrographs by the presence of virion particles. Structures resembling particle-free inclusions were rarely observed (Fig. 4.1D), and inclusion matrix could not be identified with complete confidence in the absence of particles. It is possible that the TEM method lacks the sensitivity necessary to identify particle-free inclusion matrix. Alternatively, the large difference in section thickness between the two methods (900 nm confocal z-slice vs. 70 nm EM thin section) may explain preferential detection of infected cells using confocal microscopy.

A higher degree of particle organization in T1- vs. T3-infected cells has been previously described (5). This difference is also observed in electron micrographs of cells infected with T3- vs. T3-T1M1 (Fig. 4.2). Increased organization of particles and a larger fraction of viral inclusion matrix occupied by particles in T3-T1M1-infected cells in comparison to T3-infected cells (Table 4.1) suggest that this phenotype can at least partially be attributed to μ2. Increased particle organization could be caused by a specific function of μ2 in inclusions or could be the result of increased particle numbers in cells infected with T1-μ2-containing viruses.

The observation that empty particles are smaller in T3- vs. T3-T1M1-infected MDCK cells offers corroborating evidence of aberrant assembly of T3 virion particles. It is not known whether the empty particles represent precursors to mature virions or

replication byproducts, but the latter possibility is generally favored (27, 46). In either case, these structures inevitably share some assembly steps with complete virion particles and signal the possibility for a global μ2-dependent defect in particle assembly. Possible explanations for the smaller size of empty T3 particles include missing or stoichiometrically incorrect protein subassemblies or misfolding of key protein constituents. The cell-type-specific nature of this phenotype further suggests that discrete cellular factors are essential to coordinate successful particle maturation.

The capacity of T3 to replicate in MDCK cells at 31ºC provides insight into a possible mechanism of the μ2-regulated replication phenotype. The T3 μ2 protein is highly ubiquitylated in a temperature-dependent manner, and ubiquitylation is reduced when the temperature of viral infection is lowered (75). These findings are consistent with the idea that T3 μ2 misfolds at higher temperature, causing increased aggregation and ubiquitylation. Enhanced yield of T3 in MDCK cells at 31ºC (Fig. 4.5) suggests that temperature-sensitive conformations of μ2 influence a important early step in viral assembly. Importantly, the μ2 ubiquitylation phenotype segregates with a polymorphism at amino acid position 208 (75), while temperature-dependent replication efficiency in MDCK cells is regulated by amino acid 347, with no detectable contribution by the residue at position 208 (Fig. 2.4). The effect of amino acid variability at position 347 on μ2 conformational states has not been examined; however, reversal of the block to T3 replication at decreased temperature suggests that a temperature-sensitive property of μ2, possibly protein-folding, governs reovirus strain-specific interactions with the host-cell environment during viral assembly. These interactions could involve stimulation of replication complexes containing T1 μ2 or inhibition of complexes containing T3 μ2.

Alternatively, the replication block could be passive in nature, caused by a failure of T3 μ2 to successfully interact with cellular factors. In either model, conformational variation in μ2 could conceivably influence a critical association of viral and host-cell factors required for virion assembly.

The non-productive infection of T3 in MDCK cells is similar to that of reovirus strain tsH11.2, which contains lesions in μ2 protein that restrict viral replication to low temperature (23). Like T3 infection of MDCK cells, tsH11.2 synthesizes normal amounts of ssRNA but displays significantly diminished dsRNA production and secondary translation (23). However, unlike T3 infection of MDCK cells, tsH11.2 μ2 does not concentrate in viral inclusions at restrictive temperature (68). Thus, the replication block to tsH11.2 might operate through mechanisms affecting μ2 localization. Although the precise step in viral replication blocked in tsH11.2 may differ from or complement that of T3 in MDCK cells at non-permissive temperature, both of these models of conditional reovirus replication confirm the importance of μ2 protein for progression of the viral life cycle beyond primary rounds of RNA and protein synthesis.

Reovirus inclusions are generally thought to contain cellular proteins repurposed for viral use. Nevertheless, identities of these putative host cell molecules remain largely unknown. Early studies using electron microscopy identified inclusion-associated cytoskeletal elements, including coated microtubules and thick, kinked fibrils interspersed among the particles (27, 35). Known cellular proteins recruited to reovirus inclusions include chaperone Hsc70 (54) and clathrin (51). Hsc70 associates with viral inclusions independent of its chaperone function (54), whereas clathrin recruitment results in disruption of its normal cellular function (51). However, the roles played by

these proteins in inclusion formation and function await further investigation. A comprehensive study of cellular factors required for reovirus replication, in particular those required for inclusion development and maturation, will further define post-entry mechanisms of viral tropism and the precise activities of μ2 and other viral replication proteins in virion morphogenesis.

In summary, microscopic techniques were used to characterize functionally abnormal reovirus inclusions that form in non-permissive cells to more fully understand the role played by μ2 in promoting productive viral replication and tropism for host cells. Findings presented in this chapter established that virion particle assembly is a μ2-regulated step in the reovirus replication program and suggested that a temperature-sensitive property of μ2, perhaps protein conformation, controls key events within inclusions that culminate in assembly of mature particles. Additional characterization of this system may identify novel cellular regulators of reovirus infection that participate in virion morphogenesis and serve as determinants of viral cell tropism.

CHAPTER V

SUMMARY AND FUTURE DIRECTIONS

Introduction

Coordination of viral replication requires successful and often complex interactions of viral proteins and cellular factors. Although much progress has been made in understanding the formation of specialized sites of replication where viral proteins and repurposed cellular factors direct genome multiplication and particle assembly, much remains unknown about the specific mechanisms of post-entry determinants of viral replication efficiency and cell tropism. The goal of my dissertation research has been to determine how reovirus μ2, and its cooperation with other viral proteins, support progression of the viral replication cycle and contribute to reovirus cell tropism. Toward that goal, I characterized the genetic basis of strain-dependent reovirus replication in MDCK cells (Chapter II). μ2 controls efficiency of reovirus replication in these cells, and amino acid residue 347 is the primary determinant. Furthermore, polymerase protein λ3 is a co-regulator of viral replication in a strain-dependent manner. I systematically tested post-entry steps in the reovirus life cycle to identify the critical step in reovirus tropism for MDCK cells (Chapter III). The replication block occurs following inclusion formation but prior to dsRNA synthesis, indicating that inclusions formed during non-permissive infection are morphologically normal but functionally abnormal. I also analyzed inclusion ultrastructure under permissive and non-permissive conditions of infection (Chapter IV) and found that particle assembly is inhibited in non-productively infected

cells. In this chapter I will discuss implications of this work and future directions for this research.

Model of Reovirus Replication in MDCK Cells

The precise mechanism regulating reovirus replication capacity in MDCK cells has not been fully defined; however, this body of work significantly advances an understanding of viral and cellular determinants governing reovirus replication in MDCK cells. Therefore, I will present several plausible models of reovirus replication in MDCK cells that are consistent with the current experimental evidence. It is possible that inhibition of T3 in MDCK cells is mediated by an inducible restriction factor that specifically recognizes T3 μ2 and not T1 μ2. Strain-dependent recognition of μ2 could occur because T3 μ2 is subject to temperature-dependent misfolding. When T3 μ2 is present in a misfolded conformation, it can be antagonized by a MDCK-specific factor that inhibits the assembly of replication complexes that mediate minus-strand synthesis and subsequently secondary transcription of viral mRNA. Reducing the temperature of infection prevents T3 μ2 from assuming an unfavorable conformation and therefore is not recognized by the restriction factor. In addition to lowering the temperature of infection, T3 μ2 could also be modulated to mediate productive infection by the presence of other T1 proteins such as λ3 (evidenced by the ability of T1-T3M1 to replicate efficiently in MDCK cells). Other mechanisms of inhibition of T3 in MDCK cells are also possible. For example, a μ2-containing complex could specifically antagonize an inducible restriction factor. At high temperature, T3 μ2 may assume an unfavorable conformation that can no longer mediate its function in blocking the factor. It is also conceivable that

the block to T3 μ2 replication is caused by failure of T3 μ2 to interact cooperatively with cellular components that provide an essential function during reovirus replication. Low temperature or interaction with other T1 proteins could modulate T3 μ2 to allow successful interaction with the required cellular components. This model of reovirus replication in MDCK cells still contains numerous testable hypotheses, some of which will be addressed by experiments proposed in the future directions outlined below.

Identification of Other Reovirus Determinants of Replication Capacity in MDCK Cells

The genetic analysis of recombinant virus strains presented in Chapter II thoroughly defines the determinants of μ2 that control replication efficiency in MDCK cells; however, the role of other viral proteins, determinants of λ3, and μ2-λ3 interactions in promoting replication efficiency in MDCK cells have yet to be defined.

T1 μ2 promotes efficient replication in MDCK cells irrespective of the viral genetic background. The influence of T3 μ2 on replication efficiency is more complex because its presence does not ensure poor replication. A schematic representation of replication capacity of reovirus strains in MDCK cells is presented in Figure 5.1 and highlights that each μ2/λ3 combination is present in two genetic backgrounds. T1-T3M1 and T3-T1L1 both have T1 λ3 and T3 μ2; however, T1-T3M1 replicates efficiently while T3-T1L1 does not. These results suggest that the viral genetic background in which T1 λ3 is presented to T3 μ2 influences its capacity to compensate for T3 μ2. To investigate which viral proteins modulate the effect of λ3 on μ2 function, reassortant viruses could be generated to ascertain which T1 genes, aside from M1, can enhance the replication of

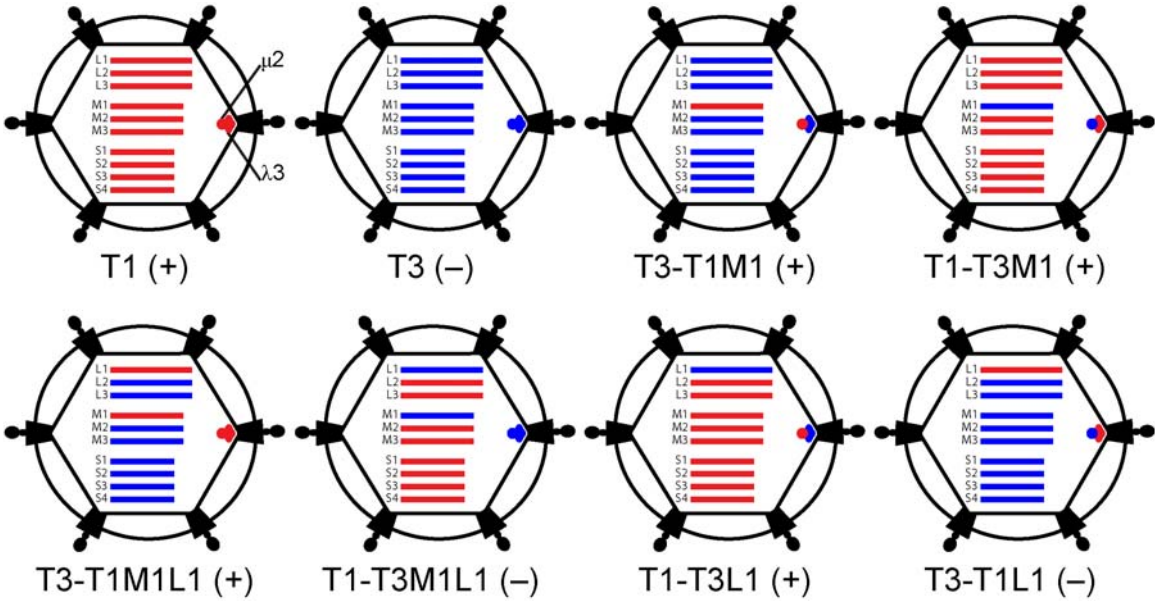

Figure 5.1. Schematic representation of T1 and T3 μ2/λ3 combinations in recombinant viruses tested in MDCK cells. Four possible combinations of μ2 and λ3 from strains T1 and T3 are depicted and each combination is present in two different virus genetic backgrounds. Red represents strain T1 and blue represents strain T3. (+), replicates efficiently in MDCK cells. (–), replicates inefficiently in MDCK cells.

T3-T1L1 and which T3 genes, aside from L1, reduce the replication of T1-T3M1. Based on their proximity to μ2 and λ3 within in the virion, other core proteins –λ2, λ1, and σ2– are likely determinants of this phenotype. Other possible determinants are σNS and μNS, as these proteins are thought to be involved in assortment and initial core assembly within the inclusion (2, 26, 50). Identification of other proteins that influence replication efficiency in MDCK cells will provide further insight into mechanisms by which μ2 controls replication efficiency and may illuminate important interactions between other reovirus proteins that control replication activities within inclusions.

The conditional regulation of μ2 function by λ3 during replication in MDCK cells raises the question of what determinants of λ3 confer replication capacity. T1-T3M1 replicates efficiently, whereas T1-T3M1L1 does not. Which domains and ultimately

residues of T1 λ3 bestow enhanced replication capacity to T1-T3M1? To address this question, T1 x T3 L1 chimeras could be generated in a T1-T3M1 background. The λ3 protein contains 3 domains: N-terminal (N), central polymerase (P), and C-terminal bracelet (C) (112), which would make logical junctions for T1 x T3 L1 chimeras. Viruses containing chimeric L1 genes, T3 M1, and the remaining 8 T1 gene segments can be obtained using reverse genetics, and the replication capacity of the resultant viruses can be compared to T1-T3M1 and T1-T3M1L1. If one region of L1 confers replication capacity, T1 x T3 polymorphisms can be tested by generating viruses with individual point mutations and testing viral yield in MDCK cells. The structure of λ3 is known (112); therefore, domains or individual polymorphisms that modulate replication may provide insight into the mechanism of regulation and identify potential points of contact between μ2 and λ3.

Several lines of evidence from biochemical and genetic studies suggest that μ2 and λ3 functionally cooperate. L1 and M1 genes display nonrandom segregation in reassortant viruses (84). NTPase and RTPase activities of μ2 are enhanced in the presence of λ3, and the two proteins co-immunoprecipitate (58). Genetic linkage of the M1 and L1 genes to replication efficiency in MDCK cells (Chapter II, [93]) provides further evidence that these proteins functionally if not directly interact with one another. However, further study is required to understand the role μ2-λ3 interactions in viral infection. The co-immunoprecipitation studies of μ2 and λ3 were carried out *in vitro* using purified proteins (58). However, it is unknown if this interaction would be maintained in the complex cellular milieu. The capacity of μ2 and λ3 from different genetic backgrounds—i.e., T1 or T3—to interact is also unknown. To test whether μ2 and

λ3 interact within cells and whether strain differences affect this putative interaction, the four combinations of T1 and T3 μ2 and λ3 proteins could be expressed in permissive cells, followed by immunoprecipitation of μ2 or λ3. Antibodies that can effectively immunoprecipitate μ2 and λ3 are not available; therefore, μ2 and λ3 expression plasmids might be generated containing HA or FLAG N-terminal tags. Following transfection of tagged μ2 and λ3 proteins in L cells, HA or FLAG antibodies can be used to immunoprecipitate μ2 or λ3, and immunoblots of immunoprecipitated complexes can be used to visualize μ2 and λ3. Any results identified using this technique should be confirmed by an *in cyto* strategy as a potential caveat of this experiment is the opportunity for abnormal association of μ2 and λ3 due to overexpression or the presence of tags. If direct interactions are observed in permissive cells, these experiments could be repeated in MDCK cells to determine if there are differences in μ2-λ3 interaction that correlate with tropism. Additionally, genetic analysis can be used to determine domains that determine differential interactions. These studies may reveal unique interactions between μ2 and λ3 and possibly other viral and cellular proteins that have yet to be functionally linked to μ2.

Cellular Determinants of Post-entry Mediated Reovirus Tropism

Much of my dissertation work has been focused on deciphering viral genetic determinants of tropism for MDCK cells and understanding the mechanisms that leads to reduced T3 replication in MDCK cells. An equally intriguing question is what are the cellular determinants of restriction of T3 replication in MDCK cells. I have suggested that there is a factor in MDCK cells that interacts differentially with T1 and T3 μ2

leading to the strain-specific difference in reovirus replication efficiency exhibited in these cells. This factor could be as simple as a single protein or as complex as a biochemical pathway. It is possible that μ2-mediated replication capacity is only a MDCK-associated phenomenon. However, this phenotype could represent a host-species (canine) or tissue-type (kidney) tropism. To test this possibility, the capacity of T1 and T3 to replicate in a panel of available cell types was ascertained. Cell types tested included L cells (mouse fibroblast), AGMK (African green monkey kidney), Caco-2 (human colorectal adenocarcinoma), HEK293 (human embryonic kidney), MA104 (Rhesus monkey kidney), MDBK (Madin Darby bovine kidney), and DK (dog kidney) (Fig. 5.2). Replication of T1 and T3 was similar in all cells with the exception of AGMK

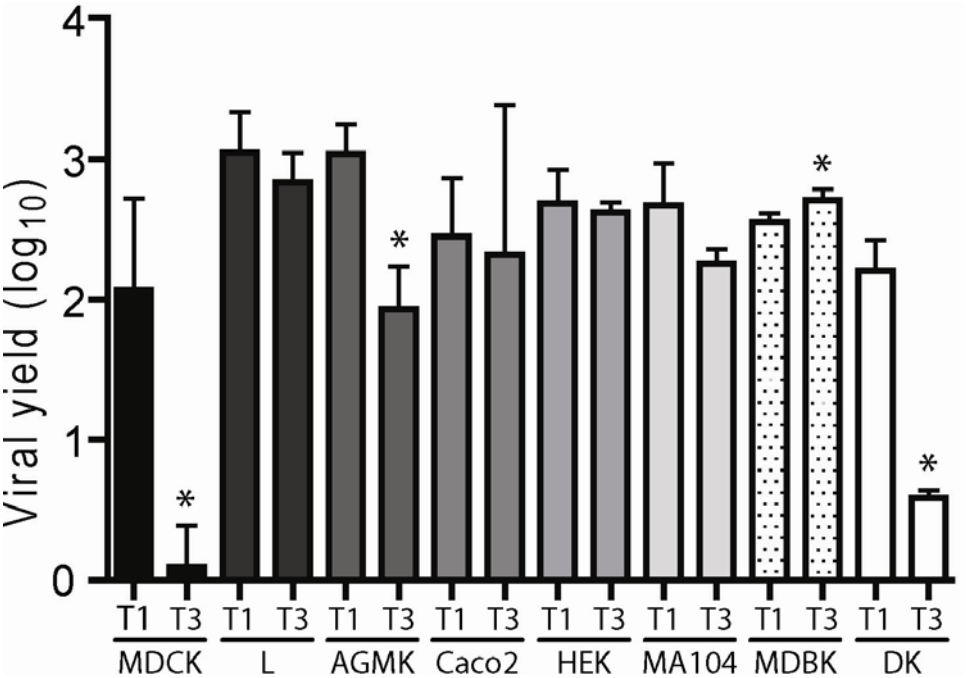

Figure 5.2. Yields of T1 and T3 viruses in cultured cells. A. The indicated cell line was infected with T1 or T3 at an MOI of 2 PFU/cell, and viral yields (relative to 0 h) at 24 h post-infection were determined by plaque assay using L-cell monolayers. Results represent the mean of triplicate experiments. Error bars indicate S.D. *, $p < 0.05$ in comparison with strain T1 in corresponding cell line (Student's *t* test).

and DK cells. In AGMK cells, the yield of T1 exceeded that of T3 by ~10 fold. However, T3 achieved an ~100 fold increase in viral titer by 24 h post-infection, which is significantly greater than that measured in T3-infected MDCK cells. Replication of T1 and T3 in DK cells was similar to MDCK cells. A precise characterization of DK cells is unavailable, and it is possible that DK cells represent the same kidney cell type as MDCK cells. Therefore, this result neither confirms nor contradicts the hypothesis that the block is canine-specific. A number of kidney cell lines are represented in this panel; therefore, the inhibition of T3 replication is likely not related to a kidney-specific factor.

Many other cell types could be obtained and tested; however, a potentially more productive approach to study questions of μ2-dependent cell-type specific tropism would utilize the neonatal mouse model of reovirus pathogenesis. Previous studies have linked the M1 gene to virulence and liver tropism in adult severe combined immunodeficient (SCID) mice (44) and myocarditis in newborn immunocompetent mice (102, 103) using classical reassortant analysis. The M1 gene also independently modulates myocarditis in newborn mice (49). However, the importance of μ2 and other reovirus replication proteins have not been systematically investigated *in vivo*. One possible approach to characterize the role of μ2 *in vivo* would be to monitor survival and organ-specific replication and pathology following infection with T1 and T1-T3M1 or T3 and T3-T1M1. If differences in μ2-determined organ-specific replication efficiency or tropism are identified, further experimentation using viruses containing T1 x T3 μ2-polymorphisms can be used to identify specific μ2 residues involved. Primary cells of target organs displaying these differences can be used to investigate the replication cycle using the imaging and PCR strategies utilized in Chapters III and IV. These studies will

allow differences in replication efficiency and tropism to be correlated with patterns of disease expression and will enhance our understanding of the role of μ2 in reovirus pathogenesis.

Identification of the specific cellular component or components responsible for strain-specific replication capacity in MDCK cells will provide insight into the role of cellular factors in promoting or inhibiting reovirus replication steps that occur within inclusions. The proposed MDCK-specific factor could work actively, by antagonizing T3 μ2, or passively by failing to interact with T3 μ2. Classification of the mechanism of action of the MDCK-specific factor as active or passive will provide the rationale required to design a discovery-based approach for factor identification. Analysis of reovirus replication in heterokaryons generated from permissive and non-permissive cells could be used to distinguish if the factor acts through an active or passive mechanism.

During the course of this work, some progress was made in generating heterokaryons of MDCK cells and HeLa cells (protocol modified from Gottesman et al. [43]) (Fig. 5.3). Fusion was mediated by co-culturing fluorescently dyed, MDCK and HeLa cells that transiently expressed vesicular stomatitis virus G protein. Fused and unfused cells were separated by flow cytometry. Results of experiments using heterokaryons may provide evidence into the regulatory mechanism present in MDCK cells that facilitates the discrimination of T1 and T3. If the factor specifically inhibits T3 replication, it is expected that T3 will fail to replicate in MDCK-HeLa heterokaryons. A logical discovery-based approach would utilize a siRNA screen to identify the factor that, when knocked down, rescues replication of T3. Alternatively, if replication block is mediated by an inability of MDCK cells to support T3 replication, it is expected that T3

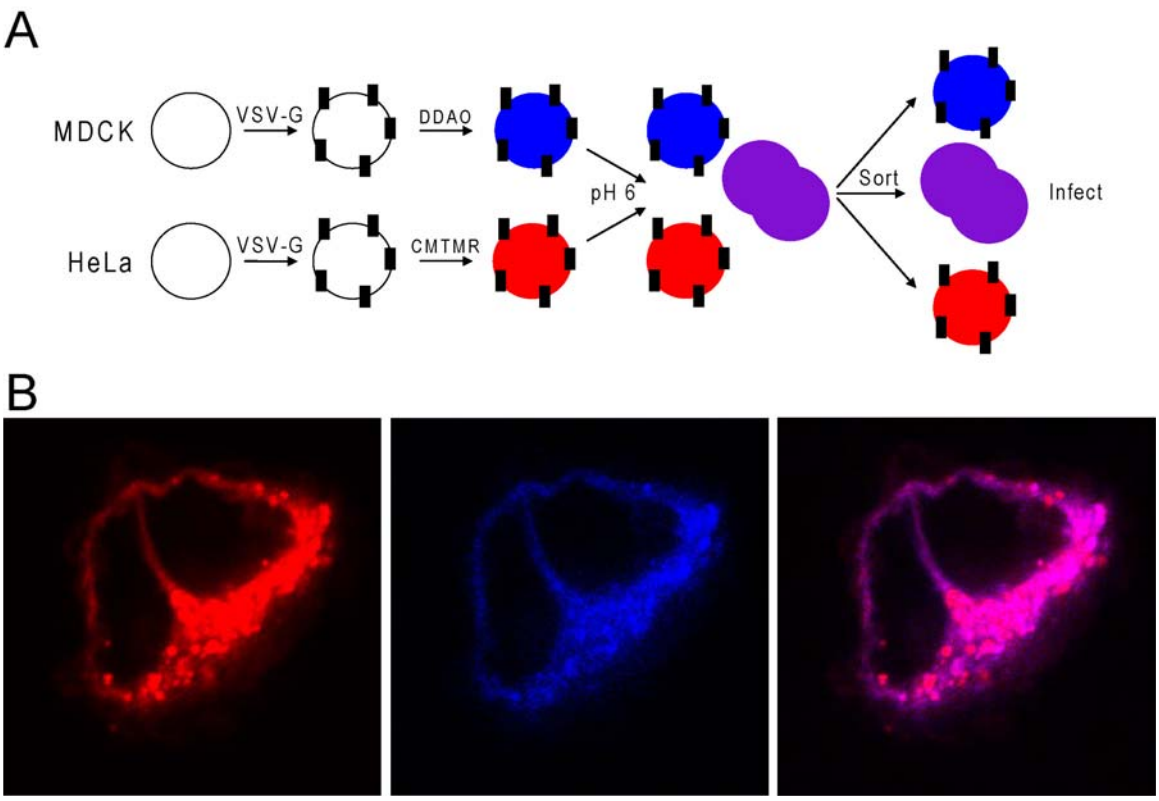

Figure 5.3. Formation of MDCK-HeLa cell heterokaryons. A. Schematic of heterokaryon generation. MDCK cells and HeLa cells are individually transfected with a vesicular stomatitis virus G protein-expressing plasmid, stained with CellTrace Far Red DDAO or CellTracker Orange CMTMR, and then co-cultured. Fusion was initiated by washing with pH 6 fusion buffer. Single positive and double positive cells were sorted by flow cytometry into culture dishes. B. Heterokaryon visualized by confocal immunofluorescence microscopy. Images obtained using 543 nm laser channel (CMTMR, left), 633nm laser channel (DDAO, middle), and overlay (right).

would replicate in heterokaryons. Therefore, a rational method would use a HeLa cell cDNA library transfected in MDCK cells to identify the cellular components that enhance T3 replication. Very little is known about the identity and function of cellular proteins in viral inclusions. Therefore, discovery of an MDCK-specific factor that mediates the discrimination of reovirus strains will illuminate a cellular target or targets that interact with reovirus during post-entry steps of the life cycle.

Analysis of Inclusion Architecture

An understanding of the composition and organization of viral inclusions is essential to elucidate strategies by which viruses direct a successful replication program. Findings presented in Chapter IV suggest that reovirus tropism for some types of cells is governed by interactions between viral replication proteins and the unique cell environment that favor development of inclusions capable of generating fully assembled infectious particles. However, these results also highlight our limited understanding of inclusion architecture, including the organization of viral particles and replication intermediates within inclusions as well as cellular components in these structures. Significant advances in understanding the architecture of positive-sense RNA virus replication factories have been made using three-dimensional electron microscopy techniques (29). These advances have allowed the detailed characterization of cellular membrane reorganization induced by these viruses to form their replication factories (30). Three-dimensional reconstruction of serial sections of reovirus-infected cells using TEM imaging would significantly enhance an understanding of the unique architecture of reovirus inclusions. This technique could be used to image inclusions in infected MDCK cells and HeLa cells (or some other permissive cell line) following infection with either T3 or T3-T1M1. μ2 mediates differences in inclusion ultrastructure in both permissive and non-permissive cell lines. Therefore, the ability to analyze different inclusion phenotypes will provide significant strength to this analysis as comparison of inclusions in permissive and non-permissive infection can be correlated with successful replication. These studies will further an understanding of viral inclusion composition and organization and illuminate strategies by which viruses coordinate productive infection.

Conclusions

My research has enhanced an understanding of post-entry determinants of reovirus replication. These studies have identified particle assembly within viral inclusions to be a key checkpoint of reovirus cell-type specific replication. This work has further expanded knowledge of the complex role that μ2 plays during the viral replication program as a determinant of replication efficiency and post-entry mediated tropism. Studies of reovirus replication in MDCK cells have also provided additional evidence for a functional interaction between the μ2 and λ3 proteins. However, many unanswered questions still exist, including: what specific biochemical functions does μ2 serve in reovirus replication? How does μ2 interact with other viral proteins to mediate productive infection? How does reovirus repurpose the cellular environment for its own benefit, and which cellular factors are involved? How are viral inclusions organized with respect to structure and function? Further experimentation, such as the studies outlined above, will reveal interconnections between μ2 and the host-cell machinery and provide insights into the molecular architecture and functional organization of reovirus inclusions. Additionally, these studies will contribute to the identification of fundamental strategies of post-entry mediated virus tropism, compartmentalization of viral replication machinery, and viral replication protein structure and function.

CHAPTER VI

MATERIALS AND METHODS

Cells and Viruses

L cells were grown in Joklik's modified Eagle's minimal essential medium (Lonza, Walkersville, MD) supplemented to contain 5% fetal calf serum (Cellgro, Manassas, VA), 2 mM L-glutamine (Gibco, Grand Island, NY), 100 U of penicillin G/ml (Gibco), 100 μg of streptomycin/ml (Gibco), and 0.25 μg amphotericin B/ml (Sigma, St. Louis, MO). MDCK, AGMK, Caco2, HEK293, MA104, MDBK, DK, and HeLa cells were grown in DMEM supplemented to contain 4.5g/L sodium pyruvate (Cellgro), 10% fetal calf serum, 2 mM L-glutamine, 100 U of penicillin G/ml, 100 μg of streptomycin/ml, and 0.25 μg amphotericin B/ml. BHK-T7 cells were grown in DMEM (Invitrogen, Eugene, OR) supplemented to contain 5% fetal calf serum, 2 mM $_{L}$-glutamine, 2% MEM Amino Acid Solution (Invitrogen), and 1 mg/ml geneticin (Invitrogen). Strains T1, T3, T1-T3M1, T3-T1M1, and all other reassortant strains used in this study were recovered by reverse genetics as described (59, 62). Virus was purified from L cells by CsCl gradient centrifugation (36). Viral titers were determined by plaque assay using $_{L}$-cell monolayers as described (116).

Construction of Mutant Viruses

T1 x T3 M1 chimeric cDNAs were generated by inserting the EcoRV-RsrII (Ch1), MfeI-RsrII (Ch2), PsiI-RsrII (Ch3), and NdeI-RsrII (Ch4) fragments of pT7-M1T1L (62)

into the pT7-M1T3D vector (59). M1 point mutants were generated using PCR with mutagenic primers and the pT7-M1T1L and pT7-M1T3D plasmids. Vectors containing mutant M1 genes were substituted for WT M1 to recover recombinant viruses using reverse genetics. Plasmid sequences of determined to confirm fidelity of mutagenesis and cloning.

Quantification of Virus Infectivity

Monolayers of cells (approximately 5 x 10^5 cells) seeded in 24-well plates (Costar, Corning, NY) were adsorbed with virus at an MOI of 2 PFU/cell (unless otherwise specified). After 1 h adsorption at room temperature, the viral inoculum was removed, cells were washed with PBS, and fresh medium was added. Cells were incubated at 37ºC (unless otherwise specified) for various intervals and removed to -80ºC. Viral titers in cell lysates were determined by plaque assay using L cells (116). Viral yield was calculated as the difference between $\log_{10}$ titer at the time indicated and $\log_{10}$ titer at 0 h. Negative differences were assigned a value of zero. For the purpose of calculating fold differences in viral yields, non log transformed data were used, and a yield of less than 1 was considered to be 1.

Quantification of IFN-β mRNA in MDCK Cells by Reverse Transcription-Quantitative PCR

Monolayers of MDCK cells (approximately 5 x 10^5 cells) seeded in 24-well plates were adsorbed with virus at an MOI of 0.02 or 2 PFU/cell. After 1 h adsorption at RT, the viral inoculum was removed, cells were washed with PBS, and fresh medium

was added. Following incubation at 37ºC for various intervals, cultures were placed at -80ºC, and total RNA was extracted from 140 µl of thawed lysate using an RNeasy Mini Kit (Qiagen, Valencia, CA). DNA contamination was removed by DNAse digestion (RNase Free DNase set, Qiagen). IFN-β RNA in 10 µl of RNA extract was quantified using the SuperScript III Platinum One-Step qRT-PCR System (Invitrogen). PCR reactions were prepared according to the manufacturer's specifications. The published canine IFN-β1 sequence (accession number: NM_001135787) was used to design an IFN-β-specific fluorogenic probe (5' d FAM-CCATGAGCAACGACTTG-BHQ-1 3'), forward primer (5' TGTATTTCTCCACCATGGCTCTT 3') and reverse primer (5' GCTGCTTAGCTGGGATCGAA 3').

Immunofluorescence Detection of Reovirus Infection

L cells plated on untreated glass coverslips and MDCK cells plated on poly-$_L$-lysine (Sigma)-treated glass coverslips in 24-well plates were adsorbed with virus at an MOI of 20 PFU/cell. Following incubation at 37ºC (or 31ºC were indicated) for various intervals, cells were fixed and stained with rabbit µ2-specific (127), guinea pig σNS-specific (8), rabbit µNS-specific (60), mouse σ3-specific (4F2, [117]), mouse µ1-specific (8H6, [117]), or rabbit λ2-specific (7F4, [116]) antibodies followed by Alexa 546-conjugated and Alexa 488-conjugugated secondary antibodies (Invitrogen). Nuclei were visualized with ToPro3 (Invitrogen). Images were acquired using a Zeiss LSM 510 META inverted confocal microscope.

Analysis of Viral RNA Production Using Reverse Transcription-Quantitative PCR

Monolayers of L or MDCK cells (approximately 5 x 10^5 cells) seeded in 24-well plates were adsorbed with virus at an MOI of 10 PFU/cell. After 1 h adsorption at room temperature, the viral inoculum was removed, cells were washed with PBS, and fresh medium was added. Following incubation at 37ºC for various intervals, cultures were frozen at -80ºC, and total RNA was extracted from 140 µl of thawed lysate using an RNeasy Mini Kit (Qiagen, Valencia, CA). RNA was incubated at 95ºC for 3 min and immediately placed on ice. Reovirus S4 RNA in 10 µl of RNA extract was quantified using the SuperScript III Platinum One-Step qRT-PCR System (Invitrogen). PCR reactions were prepared according to the manufacturer's specifications with minor modifications. The S4-specific fluorogenic probe used was 5' d FAM-AGCGCGCAAGAGGGATGGGA-BHQ-1 3' (Biosearch Technologies, Novato, CA). Either forward (S4 83F [5' CGCTTTTGAAGGTCGTGTATCA 3']) or reverse (S4 153R [5' CTGGCTGTGCTGAGATTGTTTT 3']) primer corresponding to the viral S4 gene was used for reverse transcription performed at 50ºC for 15 min. Following 3 min incubation at 95ºC, the second primer was added, and 40 cycles of quantitative PCR was performed at 95ºC for 15 sec followed by 60ºC for 30 sec. Total S4 RNA (combined dsRNA and mRNA) was quantified using the S4-specific reverse primer (complementary to the positive strand) in the reverse transcription step, and double-stranded S4 RNA was quantified using the S4-specfic forward primer (complementary to the negative strand) in the reverse transcription step. Inclusion of only the reverse or forward primer in the reverse-transcription step resulted in specific detection of the positive or negative strand of S4 RNA, respectively. Total S4 RNA is represented by the amount of positive-sense

template, whereas dsRNA is equivalent to the amount of negative-sense template. S4 mRNA was calculated by subtracting the amount of dsRNA from total RNA. Standard curves relating C*t* values to copies of positive- or negative-sense RNA template were generated using 10-fold dilutions of viral RNA extracted from purified virion particles (QIAamp Viral RNA Purification Kit [Qiagen]) and quantified by spectrophotometry. The amount of total and dsRNA in each sample was then extrapolated from standard curves generated with the reverse and forward primers, respectively. Standard curves generated using forward and reverse primers in the reverse-transcription step were consistently similar, reflecting comparable amplification efficiencies of S4 RNA positive- and negative-sense strands.

Analysis of Viral Protein Synthesis

Monolayers of L or MDCK cells (approximately 5 x 10^5 cells) seeded in 24-well plates were adsorbed with virus at an MOI of 100 PFU/cell. After 1 h adsorption at room temperature, the inoculum was removed, fresh medium was added, and cells were incubated at 37ºC for various intervals. Cells were incubated with 50 µCi [^{35}S]methionine-cysteine (PerkinElmer, Waltman, MA) in methionine-free medium (MP Biomedicals, Solon, OH) for 1 h prior to harvest, the medium was removed, and 50 µl lysis buffer (0.1M NaCl, 1mM EDTA, 10mM Tris [pH 7.4], and 0.5% IGEPAL) was added. Cell lysates were centrifuged at 14,000 x *g* at 4ºC for 15 min, and 20 µl of the resultant supernatant was mixed with an equal volume of Laemmli sample buffer (Bio Rad, Hercules, CA). Samples were incubated at 95ºC for 5 min and electrophoresed in a

10% SDS-polyacrylamide gel, which was dried onto filter paper and exposed to film (BioMax MR Film, Kodak, Rochester, NY).

Electron Microscopy

L cells or MDCK cells grown in T75 flasks (Corning) were adsorbed at an MOI of 100 PFU per cell using L-cell lysate stocks of virus. Following adsorption of virus at RT for 1h, cells were incubated at 31ºC or 37ºC for 24 or 72 h. Cells were trypsinized, pelleted, washed with PBS, fixed at room temperature for at least 1 h with 2.5% glutaraldehyde buffered with 0.1M sodium cacodylate, and stored at 4 ºC. Following fixation cells were washed in 0.1M sodium cacodylate, postfixed in 1% osmium tetroxide/0.1M sodium cacodylate for 1 h, washed in 0.1M sodium cacodylate, and dehydrated using a graded series of ethanol. After dehydration, cells were subjected to two changes of propylene oxide and embedded in epoxy resin. Ultra-thin (65-70 nm) serial sections obtained using a Leica Ultracut microtome were collected on copper grids. Samples were contrast stained with 2% uranyl acetate followed by Reynold's lead citrate and examined using a Phillips CM10 transmission electron microscope or FEI T-12 transmission electron microscope operated at 80 KeV.

Quantification of TEM Images

The fraction of cytoplasm containing virion particles or inclusion matrix in electron micrographs was quantified using point count stereology (120). Images were collected in a systematic, unbiased fashion using a FEI T-12 transmission electron microscope at a magnification of 30,000x. Thirty-six images were collected for each

sample. A grid of points was superimposed over the images (grid size 43 x 43nm), and points overlaying cytoplasm or virus-specific material were counted. The volume of virus-occupied cytoplasm was calculated by dividing the number of points that fell on virus-specific material by the total number points on the cytoplasm. Particle diameters were measured using ImageJ (http://rsb.info.nih.gov/ij/index.html). A Student's *t*-test was used to determine statistical significance between the different groups. The fraction of viral inclusion matrix occupied by particles was calculated from the images collected for point counting. Particle area was estimated by assuming that particles are spherical and calculating area using πr^2 where r is half the mean diameter of mature and empty particles measured using imageJ. Areas of mature and empty particles were calculated independently using appropriate diameters and combined to yield total particle area.

Generation of Heterokaryons

HeLa cells or L cells were transfected with a vesicular stomatitis virus G protein-expressing plasmid using TransIT-LT1 (Mirus Bio, Madison, WI). Two days post-infection, cells were trypsinized and resuspended in cell dyes diluted in incomplete DMEM at a concentration of $1x10^7$ cells/ml. HeLa cells were dyed with 20 μM CellTrace Far Red DDAO-SE (Invitrogen) and MDCK cells with 0.5 μM CellTracker Orange CMTMR (Invitrogen). HeLa and MDCK cells were dyed for 30 minutes, washed twice in PBS, resuspended in complete DMEM, and co-cultured. 1 day later, fusion was initiated with PBS, pH 6.0 (fusion buffer). After 30 minutes, fusion buffer was removed from cells and replaced with complete medium. Cells were incubated for 2 hours and sorted using a FACSAria III (BD Biosciences) cell sorter into 96-well plates (Costar) or 24-well plates

containing glass coverslips. Cells plated in 96-well plates were infected and viral infectivity was measured as described above. Cells plated in 24-well plates containing glass coverslips were fixed for confocal immunofluorescence microscopy as described above.

Mutagenesis and Expression of μ2

The μ2 expression vector, pM1T1L, in which the complete T1 μ2 open reading frame is cloned into pcDNA3, was generated using a T1 M1 cDNA originally obtained from Earl Brown (127). The expression vectors containing alanine substitutions in the NLS1 and NLS2 sequences were generated using the QuikChange Site-Directed Mutagenesis Kit (Stratagene), specific primers, and pM1T1L template. L cells were transfected with M1 constructs using Lipofectamine 2000 (Invitrogen, La Jolla, CA) according to the manufacturers' instructions. Distribution of μ2 was analyzed by confocal immunofluorescence microscopy as described above.

APPENDIX A

NUCLEAR LOCALIZATION OF μ2 PROTEIN

The reovirus replication cycle is thought to be entirely cytoplasmic (96); yet μ2 localizes to the nucleus of infected (61, 68) and transfected (15, 17, 61, 88) cells. The molecular mass of μ2 exceeds the exclusion limit for passive diffusion into the nucleus (~40kDa) (13, 87), suggesting that μ2 contains specific nuclear localization signals (NLSs). μ2 has two sequence motifs fitting the consensus NLS (124), which are sequences characterized by short stretches of basic amino acids (20, 39). The two predicted μ2 NLSs are R^{100}RLRKRLMLKK^{110} (NLS1) and K^{261}RLR^{264} (NLS2). NLS1 has the capacity to traffic GFP to the nucleus in the absence of other μ2 sequences. Expression of μ2 lacking the N-terminal l06 residues (pM1Δ1-106) resulted in diminished nuclear localization in comparison to wt μ2 expression (Appendix B, Fig. 6 [61]). However, mutagenesis of residues 100 and 101 or 103-105 did not disrupt the nuclear-cytoplasmic distribution of μ2 (Appendix B, Fig. 6 [61]). Conversely, mutation of basic residues in NLS1 diminished the capability of μ2 to support viral replication in trans-complementation assays (Appendix B, Fig. 5 [61]) indicating that these residues are essential for viral replication. The capacity of NLS2 to shuttle GFP to the nucleus or support replication was not tested.

The predominantly cytoplasmic localization of pM1Δ1-106 suggests that there is a nuclear localization signal within the μ2 protein that can be disrupted. To more fully test the capacity of NLS1 and NLS2 to direct nuclear localization, I replaced basic

A

M1 construct	NLS1	NLS2
WT	R^{100}RLRKRLMLKK^{110}	R^{260}KRLR^{264}
mNLSa	A^{100}ALAAALMLKK^{110}	R^{260}KRLR^{264}
mNLSb	A^{100}ALAAALMLAA^{110}	R^{260}KRLR^{264}
mNLSc	R^{100}RLRKRLMLKK^{110}	A^{260}AALA^{264}
mNLSd	A^{100}ALAAALMLAA^{110}	A^{260}AALA^{264}
mNLSe	R^{100}RLRKRAMAKK^{110}	R^{260}KRLR^{264}

B

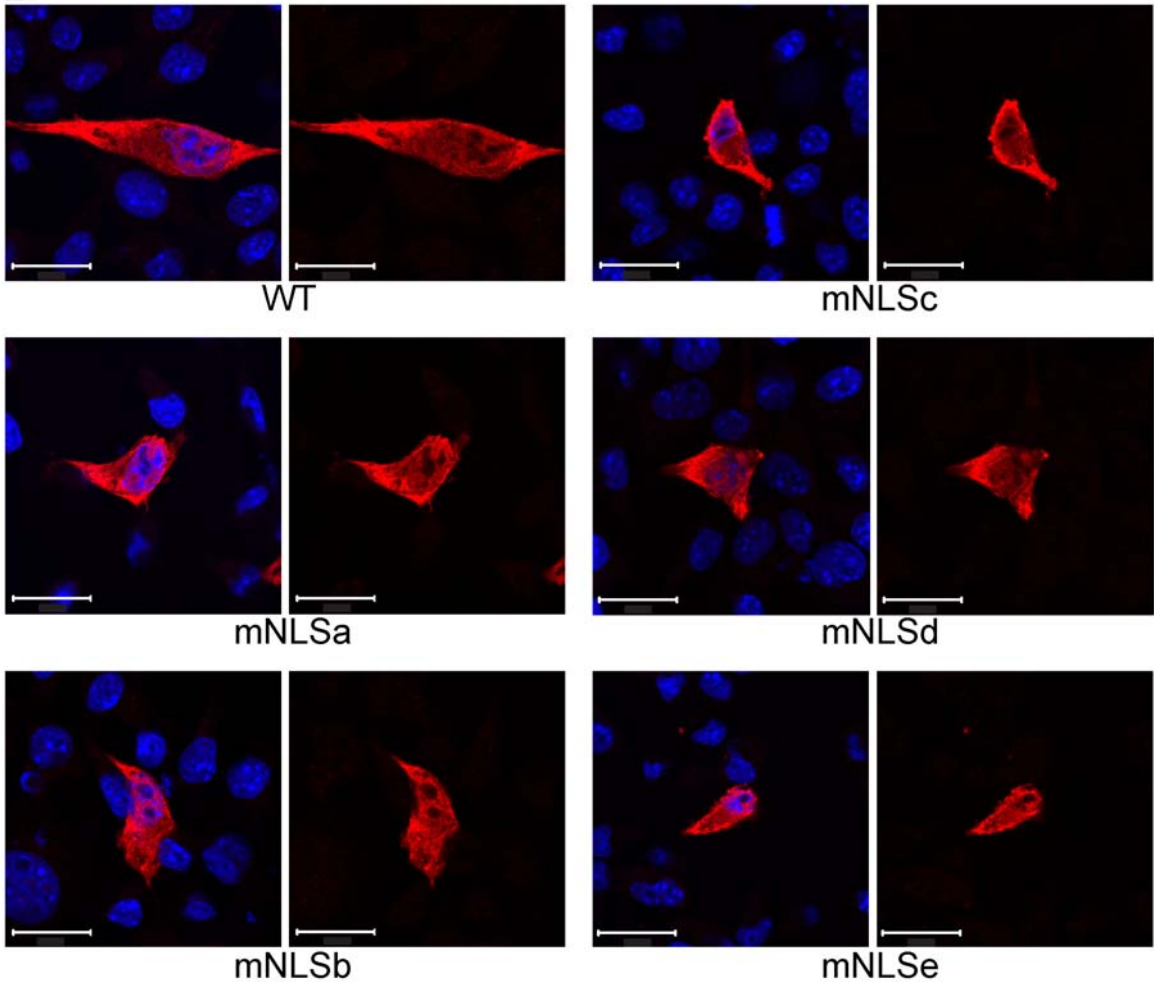

Figure A.1. Mutagenesis of putative μ2 NLSs. A. WT and mutant T1 μ2 constructs. Basic residues in putative NLSs were replaced with alanine residues (red). B. Intracellular distribution of WT and μ2-mutant proteins. L cells were transfected with plasmid constructs encoding the indicated μ2 proteins, fixed at 24 h post-transfection, and stained with anti-μ2 antibody (red). Nuclei were visualized using ToPro3 (blue). Images of μ2 expression are shown with (left) and without (right) nuclear staining.

residues within NLS1 and NLS2 with alanine residues (Fig. A.1A). L cells were transfected with wt μ2 or NLS mutant μ2 constructs. Cells were fixed and imaged using confocal microscopy at 24 h post-infection. No NLS mutant, including a mutant lacking all basic residues in NLS1 and NLS2, displayed significantly altered μ2 localization (Figure A1.B). From these results I concluded that sequences other than those within NLS1 and NLS2 possess the capacity to direct nuclear localization of μ2.

APPENDIX B

IDENTIFICATION OF FUNCTIONAL DOMAINS IN REOVIRUS REPLICATION PROTEINS μNS AND μ2

Takeshi Kobayashi, Laura S. Ooms, James D. Chappell, and Terence S. Dermody

Journal of Virology. 83(7) 2892-906; 2009

JOURNAL OF VIROLOGY, Apr. 2009, p. 2892–2906 Vol. 83, No. 7
0022-538X/09/$08.00+0 doi:10.1128/JVI.01495-08

Identification of Functional Domains in Reovirus Replication Proteins μNS and μ2[▽]

Takeshi Kobayashi,[1,2]† Laura S. Ooms,[2,3] James D. Chappell,[1,2,3]* and Terence S. Dermody[1,2,4]*

Departments of Pediatrics,[1] Pathology,[3] and Microbiology and Immunology,[4] and Elizabeth B. Lamb Center for Pediatric Research,[2] Vanderbilt University School of Medicine, Nashville, Tennessee 37232

Received 16 July 2008/Accepted 9 January 2009

Mammalian reoviruses are nonenveloped particles containing a genome of 10 double-stranded RNA (dsRNA) gene segments. Reovirus replication occurs within viral inclusions, which are specialized nonmembranous cytoplasmic organelles formed by viral nonstructural and structural proteins. Although these structures serve as sites for several major events in the reovirus life cycle, including dsRNA synthesis, gene segment assortment, and genome encapsidation, biochemical mechanisms of virion morphogenesis within inclusions have not been elucidated because much remains unknown about inclusion anatomy and functional organization. To better understand how inclusions support viral replication, we have used RNA interference (RNAi) and reverse genetics to define functional domains in two inclusion-associated proteins, μNS and μ2, which are interacting partners essential for inclusion development and viral replication. Removal of μNS N-terminal sequences required for association with μ2 or another μNS-binding protein, σNS, prevented the capacity of μNS to support viral replication without affecting inclusion formation, indicating that μNS-μ2 and μNS-σNS interactions are necessary for inclusion function but not establishment. In contrast, introduction of changes into the μNS C-terminal region, including sequences that form a putative oligomerization domain, precluded inclusion formation as well as viral replication. Mutational analysis of μ2 revealed a critical dependence of viral replication on an intact nucleotide/RNA triphosphatase domain and an N-terminal cluster of basic amino acid residues conforming to a nuclear localization motif. Another domain in μ2 governs the capacity of viral inclusions to affiliate with microtubules and thereby modulates inclusion morphology, either globular or filamentous. However, viral variants altered in inclusion morphology displayed equivalent replication efficiency. These studies reveal a modular functional organization of inclusion proteins μNS and μ2, define the importance of specific amino acid sequences and motifs in these proteins for viral replication, and demonstrate the utility of complementary RNAi-based and reverse genetic approaches for studies of reovirus replication proteins.

Mammalian reoviruses are the type species of the genus *Orthoreovirus*, within the *Reoviridae* family, which includes important human and veterinary pathogens, such as rotavirus and bluetongue virus, respectively. Reoviruses serve as highly tractable experimental models for studies of viral replication and pathogenesis (51). Reovirus virions are nonenveloped, double-shelled particles that display icosahedral symmetry and contain 10 segments of double-stranded RNA (dsRNA). Following internalization of virions by receptor-mediated endocytosis, the viral outer capsid undergoes acid-dependent proteolysis within endosomes to generate core particles containing all components of the viral transcriptional machinery (3, 18, 58). Transcriptionally active core particles released into the cytoplasm synthesize full-length, message-sense, single-stranded RNAs (ssRNAs) corresponding to each viral gene segment (4, 14). These ssRNAs are competent for translation and serve as templates for minus-strand synthesis to generate nascent genomic dsRNA (33, 52, 53). Synthesis of the complementary strand appears to be concomitant with assortment of the 10 genome segments into progeny particles (1). The viral replication cycle is completed by condensation of outer capsid proteins onto newly formed dsRNA-containing particles, producing fully assembled infectious progeny (70).

Reovirus replication and assembly are thought to occur within viral inclusions that form in the cytoplasm of infected cells (19). Viral inclusions contain dsRNA (56), viral proteins (19), and both complete and incomplete virion particles (19). The viral nonstructural proteins μNS and σNS and minor core protein μ2 are collectively required for the genesis and maturation of viral inclusions in reovirus-infected cells (2, 28). Expression of these proteins from cloned cDNAs in the absence of infection results in spontaneous assembly of intracytoplasmic structures exhibiting inclusion morphology (6, 39). Virus-like inclusions recruit constituent proteins of the viral core (10), indicating that viral inclusion-forming proteins create an organizing center for the ultimate development of a functional replication matrix. However, the precise role of viral inclusions in the reovirus replication pathway, including dsRNA synthesis, gene segment assortment, genome packaging, and virion assembly, is poorly understood, owing largely to limited mechanistic insight into the individual and corporate functions of inclusion-forming proteins.

The ~80-kDa μNS protein, encoded by the M3 genome

* Corresponding author. Mailing address: Lamb Center for Pediatric Research, D7235 MCN, Vanderbilt University School of Medicine, Nashville, TN 37232. Phone: (615) 343-9943. Fax: (615) 343-9723. E-mail for J. Chappell: jim.chappell@vanderbilt.edu. E-mail for T. Dermody: terry.dermody@vanderbilt.edu.

† Present address: Laboratory of Primate Model, Experimental Research Center for Infectious Diseases, Institute for Virus Research, Kyoto University, Sakyo-ku, Kyoto 606-8507, Japan.

▽ Published ahead of print on 28 January 2009.

segment, is 721 amino acid residues in length (38, 41). The μNS protein associates with viral mRNA (1), core protein μ2 (12), and nonstructural protein σNS (6, 39). Transiently expressed μNS, in the absence of other viral proteins, forms inclusion-like structures that are similar in appearance and localization to the globular inclusions observed in cells infected with prototype strain type 3 Dearing (T3D) (12). In addition, μNS associates with intact viral cores and recruits core proteins λ1, λ2, λ3, and σ2 into viral inclusion-like structures in transient-transfection assays (10, 12). Interactions of μNS with cores prevent assembly of the virion outer capsid and prolong transcription (11), which may benefit viral replication at earlier stages of infection by maximizing RNA and protein production. Thus, μNS protein plays a fundamental role in viral inclusion formation and provides a protected environment in which RNA replication, assortment, and packaging converge in particle assembly.

A truncated isoform of μNS naturally produced during reovirus infection, known as μNSC (32), lacks the 40 N-terminal residues and has been proposed to result from initiation of translation at an alternative in-frame AUG codon in M3 mRNA (64). The N-terminal 40 residues of μNS contain interacting domains for μ2 and σNS (12, 39), neither of which associates with μNSC (12, 39). Using RNA interference (RNAi)-based *trans*-complementation approaches, μNSC was found to be incapable of supporting viral growth in μNS-silenced cells (2, 28), pointing to the significance of interactions between μNS, μ2, and σNS for viral replication. However, the concerted activities of μNS and other replication proteins within inclusions have not been defined in structural or functional terms.

The approximately 83-kDa μ2 protein, encoded by the M1 genome segment, is 736 amino acid residues in length and forms a structurally minor component of the reovirus core (17, 38, 41). The μ2 protein binds ssRNA and dsRNA (8) and demonstrates both nucleoside triphosphatase (NTPase) and RNA 5′-triphosphatase (RTPase) activities (26). Reassortant studies suggest that μ2 determines viral strain differences in transcriptional efficiencies of core particles (66). Phenotypes associated with a temperature-sensitive lesion in μ2 indicate that it also participates in RNA replication and particle assembly (16).

The μ2 protein binds to cellular microtubules and determines virus strain-specific differences in inclusion morphology, either globular or filamentous, in infected cells (45, 67). Sequence analysis of M1 segments belonging to independent viral isolates has revealed a correlation between inclusion morphology and a single amino acid polymorphism at position 208 (45). Virus strains that produce filamentous inclusions, such as prototype strains type 1 Lang (T1L) and type 2 Jones (T2J), contain Pro^{208}, whereas strain T3D, which produces globular inclusions, contains Ser^{208} (45, 67). Inclusion-like structures arising from coexpression of plasmid-encoded μNS and μ2 in the absence of viral infection adopt a morphology predicted by the amino acid residue at position 208, independent of the μ2 strain origin (45). The presence of Pro at position 208 in μ2 is genetically linked to more efficient μ2-microtubule association and increased microtubule stabilization in reovirus-infected cells (45). In contrast, the μ2 proteins of strains encoding a Ser at position 208 are more prone to temperature-dependent misfolding that correlates with reduced efficiency of microtubule binding (39). Taken together, these findings indicate that amino acid position 208 of μ2 determines inclusion morphology by influencing its capacity to assume a conformation commensurate with microtubule binding and stabilization.

In studies reported here, we extended application of RNAi-based replication complementation and plasmid-based reverse genetics to define sequences and functional domains in μNS and μ2 proteins involved in viral replication. Our findings demonstrate the importance of extreme amino-terminal sequences in μNS that interact with μ2 and σNS proteins and sequences in the C-terminal one-half of μNS that mediate inclusion formation. Furthermore, these studies reveal the significance of μ2 sequences that specify or predict NTPase and RTPase activities, constitute a predicted nuclear localization motif, and determine inclusion morphology. An understanding of μNS and μ2 structure-function relationships gained through these studies will provide new insights into the genesis of viral inclusions and their role in reovirus replication.

MATERIALS AND METHODS

Cells, viruses, and antibodies. Murine L929 (L) cells were grown in Joklik's modified Eagle's minimal essential medium (Irvine Scientific, Santa Ana, CA) supplemented to contain 5% fetal calf serum (Gibco-BRL, Gaithersburg, MD), 2 mM L-glutamine, 100 U of penicillin G/ml, 100 μg of streptomycin/ml, and 0.25 μg of amphotericin B/ml (Gibco-BRL). Human embryonic kidney 293T cells stably expressing reovirus-specific short hairpin RNAs (shRNAs) were maintained as described previously (28).

Reovirus prototype strains T1L and T3D are laboratory stocks. Recombinant strain (rs) T3D is a stock rescued by plasmid-based reverse genetics from cloned T3D cDNAs (27). Viral titers were determined by plaque assay using L-cell monolayers (60). Attenuated vaccinia virus strain rDIs-T7pol expressing T7 RNA polymerase was propagated in chicken embryo fibroblasts (25).

The μ1/μ1C-specific monoclonal antibody 8H6 (61) and antisera to μNS (28) and μ2 (68) proteins have been described previously.

Plasmid construction. The construction of μNS expression vectors pM3 (encoding full-length μNS) and pM3(41-721) (encoding μNS amino acids 41 to 721), previously referred to as $pcM3_{1861m}$ and $pcM3_{dN138}$, respectively, has been described elsewhere (28). The expression vectors pM3(14-721) (encoding μNS amino acids 14 to 721), pM3(Δ14-40) (encoding μNS amino acids 1 to 13 and 41 to 721), pM3(1-675) (encoding μNS amino acids 1 to 675), and pM3(1-716) (encoding μNS amino acids 1 to 716) were generated by inserting PCR amplicons derived from pM3 into the KpnI-XhoI site of pcDNA3 (Invitrogen, Carlsbad, CA). The μNS expression vector pH570Q, H572S, containing His-to-Gln and His-to-Ser amino acid substitutions at positions 570 and 572, respectively, was generated using the QuikChange site-directed mutagenesis kit (Stratagene, La Jolla, CA) with specific primers and pM3 as template. Plasmid vector pT7-M3T3DM41I, which contains an ATG-to-ATC modification of the μNSC translation initiation codon, was generated using QuikChange with pT7-M3T3D template (27) and specific primers. This plasmid was used to recover the μNSC-negative virus rsT3D-μNSC-null.

The μ2 expression vector, pM1T1L, in which the complete T1L μ2 open reading frame is cloned into pcDNA3, was generated using a T1L M1 cDNA originally obtained from Earl Brown (68). The expression vectors containing single, double, or triple substitutions in the T1L μ2 protein—pK415A, pG416A, pK419A, pD446A, pG449A, pR100G,R101G, pRKR103-5GQG, pL106QL108Q, and pK109Q K110Q—were generated using QuikChange, specific primers, and pM1T1L template. The rescue vector pT7-M1T1L, encoding the entire T1L M1 gene, was constructed by inserting an M1 cDNA amplicon fused at its native 5′ terminus to the T7 RNA polymerase promoter into the SmaI-RsrII site of p3E5EGFP (62), resulting in complete replacement of sequences encoding green fluorescent protein (GFP) and the Ebola virus leader and trailer, thereby ligating the native M1 3′ terminus to the HDV ribozyme sequence. Two amino acid differences in the cDNA obtained from E. G. Brown (68), Phe^{302} and Leu^{383}, compared to the published T1L M1 sequence (45) were changed to match the published sequence (Phe^{302} to Leu and Leu^{383} to Pro) using QuikChange. QuikChange also was used to generate constructs for rescue of the following T1L and T3D μ2 mutant viruses (summarized in Table 1): pT7-M1T1LP208S (pT7-M1T1L template), pT7-M1T1LL383P (pT7-M1T1L tem-

TABLE 1. Reovirus strains used for studies of viral inclusion morphology

Virus strain	M1 gene derivation	Amino acid at μ2 position:		
		208	302	383
T1L	T1L	Pro	Phe	Leu
T3D	T3D	Ser	Phe	Leu
rsT3D	T3D	Ser	Phe	Leu
rsT3D-μ2S208P	T3D	Pro	Phe	Leu
rsT3D-μ2S208P+L383P	T3D	Pro	Phe	Pro
rsT3D-T1Lμ2	T1L	Pro	Phe	Leu
rsT3D-T1Lμ2P208S	T1L	Ser	Phe	Leu
rsT3D-T1Lμ2F302L	T1L	Pro	Leu	Leu
rsT3D-T1Lμ2L383P	T1L	Pro	Phe	Pro

plate), pT7-M1T1LF302L (pT7-M1T1L template), pT7-M1T3DS208P (pT7-M1T3D template) (27), and pT7-M1T3DS208P+L383P (pT7-M1T3D template) (27).

Expression constructs encoding μ2 protein mutagenized within the N-terminal region were generated using pM1T1L template, specific primers, and either QuikChange (substitution mutants) or PCR (N-terminal deletion mutant).

Expression plasmid pGFP-μ2(99-110), encoding GFP fused C-terminally to μ2 amino acid residues 99 to 110, was engineered by cloning oligonucleotides specifying D^{99}RRLRKRLMLKK^{110} into the XhoI-EcoRI site of pEGFP-C2 (Clontech, Mountain View, CA). Plasmid pGFP-μ2(99-110m), containing Ala substitutions of μ2 basic amino acids in pGFP-μ2(99-110), was generated using oligonucleotides encoding D^{99}AALAAALMLAA^{110}.

All mutations were confirmed by nucleotide sequence analysis. Primer sequences used for plasmid construction are available upon request.

Transient protein expression. 293T cells and L cells were transfected using Lipofectamine 2000 (Invitrogen) and TransIT-LT1 (Mirus, Madison, WI) transfection reagents, respectively, according to the manufacturers' instructions. To detect expressed proteins by immunofluorescence, cells grown on glass coverslips (Fisher Scientific, Pittsburgh, PA) were sequentially transfected with plasmid vectors, incubated for 24 h, fixed in 10% formalin, permeabilized with 1% Triton X-100, and incubated with antisera specific for viral proteins, a 1:1,000 dilution of Alexa Fluor anti-immunoglobulin G secondary antibody (Molecular Probes, Eugene, OR), and TO-PRO3 (Molecular Probes). GFP fusion proteins were detected by intrinsic GFP fluorescence. Cells were visualized using an inverted LSM510 confocal microscope (Carl Zeiss, New York, NY).

To detect expressed proteins by immunoblotting, lysates from transfected cells were prepared as described previously (28). Proteins were detected using enhanced chemiluminescence (Amersham Biosciences, Piscataway, NJ) following incubation with μNS- and μ2-specific antisera and appropriate secondary antibodies.

Infection with native and recombinant reovirus strains. Monolayers of L cells were infected with various reovirus strains at a multiplicity of infection (MOI) of 2 PFU/cell. Following 1 h of adsorption, cells were washed with phosphate-buffered saline (PBS) to remove the inoculum, and fresh medium was added. Cultures were harvested at various intervals for virus titration, immunofluorescence assay, and immunoblotting.

LMB treatment. Monolayers of L cells were adsorbed with rsT1L at an MOI of 10 (culture plates) or 20 (glass coverslips) PFU/cell. Following 1 h of adsorption, cells were washed with PBS to remove the inoculum, and fresh medium was added. At 8 h postinfection, growth medium was replaced with fresh medium containing 20 μg/ml leptomycin B (LMB), and cultures were processed 4 h later for plaque assay or confocal immunofluorescence microscopy.

Viability of uninfected and reovirus-infected cells in the presence of LMB was determined using the CellTiter 96 AQ_{ueous} assay (Promega, Madison, WI), which is based on the capacity of viable cells to metabolically reduce 3-(4,5-dimethylthiazol-2-yl)-5-(3-carboxymethoxyphenyl)-2-(4-sulfophenyl)-2H-tetrazolium (MTS). L cells were distributed into 96-well plates at a density of 5.5×10^4 cells/well and infected with rsT1L at an MOI of 10 PFU/cell. Following 1 h of adsorption, cells were washed with PBS to remove the inoculum, and fresh medium was added. LMB was added 8 h postinfection at a final concentration of 20 μg/ml, and the MTS assay was performed according to the manufacturer's instructions after 4 h of LMB exposure. Absorbance in reaction wells was recorded at 485 λ following 1 h of incubation.

The subcellular localization of shuttling reporter proteins was determined in the presence and absence of LMB using the GFP-based vectors $Rev_{68\text{-}90}$-GFP_2-M9 (24) and pXRGG (34). $Rev_{68\text{-}90}$-GFP_2-M9 contains sequences derived from the human immunodeficiency virus type 1 (HIV-1) Rev protein nuclear export signal (NES; amino acid residues 68 to 90) and heterogeneous nuclear ribonucleoprotein A1 (hnRNPA1) nuclear localization signal (NLS; M9). The pXRGG vector contains full-length HIV-1 Rev protein fused C-terminally to the hormone-responsive region of the rat glucocorticoid receptor, followed by GFP. Rev and the glucocorticoid receptor furnish pXRGG with one NLS and two NLSs, respectively, while Rev supplies an NES. L cells were transfected with plasmid vectors, and cultures were supplemented 20 h posttransfection with 20 μg/ml LMB. Cells were imaged 4 h later by confocal microscopy.

Complementation of reovirus replication in cells expressing reovirus shRNAs. *trans*-complementation of viral replication by transient expression of viral proteins was performed as described previously (28). 293T cells (10^6) stably expressing M1 or M3 shRNA were seeded into six-well plates (Costar, Cambridge, MA) approximately 24 h prior to transfection. Cells were transfected with expression plasmids encoding μ2 or μNS protein, incubated for 4 or 6 h, respectively, and adsorbed with T3D at an MOI of 10 PFU/cell. Following 1 h of adsorption, cells were washed with PBS to remove the inoculum, and fresh medium was added. Cultures were harvested 24 h after infection, and viral titers in cell lysates were determined by plaque assay.

Rescue of reovirus mutants from cloned cDNAs. Viruses containing engineered changes in μNS and μ2 proteins were generated from cloned cDNAs using plasmid-based reverse genetics (27). Recombinant viruses were isolated from cotransfection lysates at 5 days posttransfection by plaque assay using L cell monolayers.

RESULTS

Complementation of reovirus replication in cells stably expressing T3D M3 shRNA by transient expression of μNS. Previous studies revealed that the N-terminal 40 residues of μNS are required for association with viral replication proteins μ2 and σNS and that C-terminal sequences in μNS are required for inclusion formation (9, 12, 39). To determine whether these μNS domains are required for viral replication, expression plasmids encoding wild-type (wt) and mutant forms of μNS were generated for use in RNAi-based replication-complementation assays. We first assessed the intracellular distribution of viral proteins in transiently transfected 293T cells. At 24 h posttransfection, wt μNS and an N-terminally truncated μNS isoform corresponding to μNSC (amino acids 41 to 721) were present in globular inclusion-like structures, similar morphologically to inclusions present in strain T3D-infected cells (Fig. 1A). Likewise, truncation mutants lacking amino acids 1 to 13 or 14 to 40, which are required for interaction of μNS with σNS and μ2, respectively (12, 39), formed distinctive globular structures. This finding contrasts with the diffuse cytoplasmic distribution of μNS protein lacking the C-terminal 46 or 5 amino acid residues. Substitution of two histidine residues (His^{570} to Gln and His^{572} to Ser) possessing Zn^{2+}-binding potential and contained within a short sequence motif conserved among μNS proteins of orthoreoviruses and aquareoviruses (9) also resulted in a diffuse cytoplasmic pattern of protein localization. These results show that His^{570}, His^{572}, and C-terminal sequences, but not μ2- or σNS-interacting N-terminal sequences, of μNS are required for autoassembly into inclusion-like structures.

Cultures of 293T cells stably expressing M3 shRNA (28) were transiently transfected with wt T3D μNS expression plasmid pM3, which contains three silent point mutations within the shRNA target sequence, followed by infection 4 h posttransfection with T3D at an MOI of 10 PFU/cell. Viral titers in culture lysates were determined 24 h postinfection by plaque

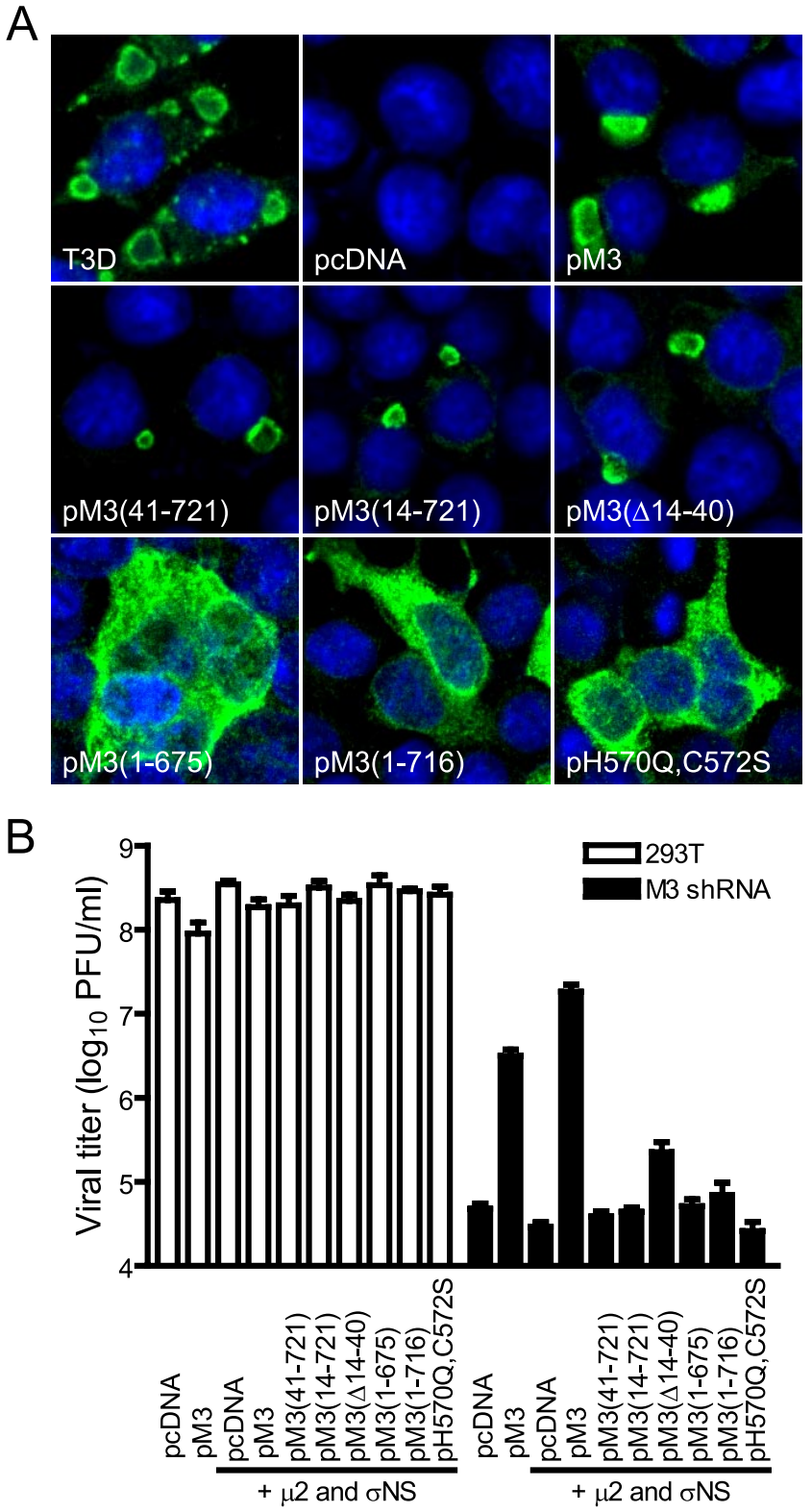

FIG. 1. *trans*-complementation of reovirus replication in cells expressing M3 (μNS-specific) shRNA. (A) Subcellular localization of mutant μNS proteins. 293T cells were infected with T3D at an MOI of 2 PFU/cell or transfected with the indicated plasmid constructs, and μNS expression was examined 24 h later by confocal immunofluorescence microscopy using μNS-specific antiserum (green). Nuclei were stained with TO-PRO3 (blue). pcDNA, nonrecombinant vector control; pM3, encodes full-length μNS; pM3(41-721), encodes μNS amino acids 41 to 721; pM3(14-721), encodes μNS amino acids 14 to 721; pM3(Δ14-40), encodes μNS amino acids 1 to 13 and 41 to 721; pM3(1-675), encodes μNS amino acids 1 to 675; pM3(1-716), encodes μNS amino acids 1 to 716; pH570Q, H572S, encodes full-length μNS containing His-to-Gln and His-to-Ser amino acid substitutions at positions 570 and 572, respectively. (B) Viral growth in cells expressing vector-encoded μNS proteins. Parental or M3 shRNA-expressing 293T cells were transfected with plasmids expressing wt or mutant μNS proteins, wt μ2, or wt σNS as indicated, followed by infection with T3D at an MOI of 10 PFU/cell. At 24 h postinfection, viral titers were determined by plaque assay. Results are mean viral titers from three independent experiments. Error bars denote standard deviations.

assay. Yields of T3D were diminished ~5,000-fold in shRNA-expressing cells transfected with nonrecombinant plasmid compared to an ~70-fold reduction in cells transfected with pM3 (Fig. 1B). Thus, μNS protein provided in *trans* restored ~98% of viral growth suppressed by treatment with M3 shRNA. An additional ~6-fold enhancement in yield was achieved by coexpression of μ2 and σNS proteins with μNS, suggesting that the abundance or accessibility of μNS-interacting partners is an important factor in complementation efficiency using this RNAi-based system.

We next assessed the capacity of mutant forms of ectopically supplied μNS protein to complement reovirus replication in μNS-silenced cells. Expression plasmids encoding mutant μNS proteins and wt μ2 and σNS proteins were cotransfected into M3 shRNA-expressing cells, followed by infection with T3D. Mutant μNS proteins lacking amino acids 1 to 13, 1 to 40, 676 to 721, or 717 to 721, or containing the double-point mutations His^{570}→Gln and His^{572}→Ser, were incapable of restoring reovirus yields above control vector, although expression of a deletion mutant lacking amino acids 14 to 40 resulted in a very modest (~5-fold) increase in viral titer (Fig. 1B). These results indicate that viral replication depends on the capacity of μNS to form inclusions and interact with μ2 and σNS proteins.

Importance of μNSC for viral replication in infected cells. We demonstrated previously that heterologous expression of a naturally occurring, internally initiated form of μNS lacking amino acids 1 to 40, known as μNSC, is incapable of supporting reovirus replication in an RNAi-based complementation system (28). However, the precise function of μNSC in the viral life cycle is unknown. To better understand the biologic role of μNSC, we used reverse genetics (27) to generate a virus incapable of μNSC expression, rsT3D-μNSC-null, by altering the in-frame μNSC initiation codon (corresponding to nucleotides 139 to 141 of the μNS open reading frame) to the isoleucine-encoding sequence, ATC. All remaining genes were derived from wt T3D. Immunoblot analysis of L cells infected with plaque-purified rsT3D and rsT3D-μNSC-null viruses revealed that μNS and μNSC were expressed by rsT3D, but only μNS was expressed in rsT3D-μNSC-null-infected cells (Fig. 2A). Inclusion formation (Fig. 2B) and growth kinetics (Fig. 2C) for the two viruses were virtually identical. These results indicate that μNSC is neither required for viral inclusion formation nor viral replication in reovirus-infected cells.

Complementation of reovirus replication in cells stably expressing T3D M1 shRNA. To develop a complementation system for studies of μ2 functions in viral replication, we established L cells constitutively expressing T3D M1-specific shRNA. A T1L μ2 expression plasmid containing a single silent nucleotide substitution within the shRNA target sequence (pM1T1L) was transfected into M1 shRNA-expressing cells, followed by infection 6 h posttransfection with T3D at an MOI of 10 PFU/cell. At 20 h postinfection, infected cells were subjected to immunofluorescence microscopy to detect outer capsid protein μ1/μ1C as a marker of viral replication. The μ1/μ1C protein was detected in shRNA-expressing cells transfected with pM1T1L but not in cells transfected with empty vector (Fig. 3A). Concordantly, transfection of cells with pM1T1L resulted in ~150-fold-increased viral yields compared to cells transfected with control vector (Fig. 3B), confirming that reovirus replication in μ2-silenced cells is rescued by ectopic μ2 expression.

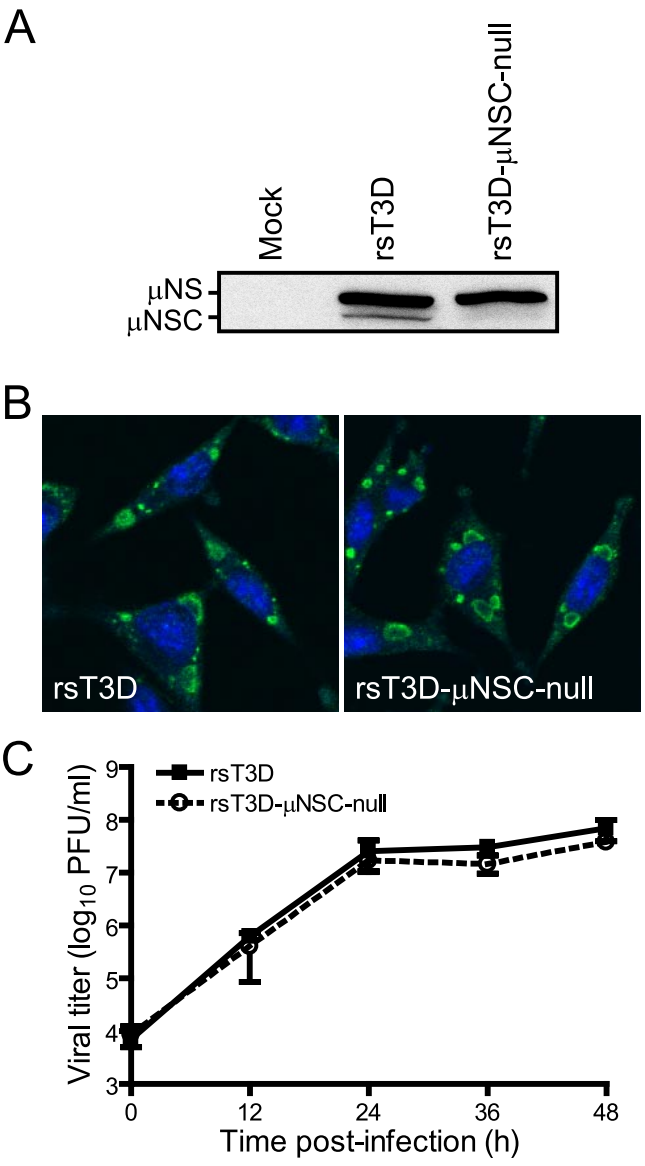

FIG. 2. Replication of a μNSC-null virus. (A) Immunoblot detection of μNS and μNSC expression in virus-infected cells. L cells were infected with rsT3D or rsT3D-μNSC-null at an MOI of 2 PFU/cell. At 24 h postinfection, cells were lysed and lysates were immunoblotted using μNS-specific antiserum. (B) Immunofluorescence detection of μNS and μNSC expression in virus-infected cells. L cells were infected as described for panel A and processed for confocal microscopy at 24 h postinfection using μNS-specific antiserum (green). Nuclei were stained with TO-PRO3 (blue). (C) Growth of rsT3D-μNSC-null. L cells were infected with rsT3D or rsT3D-μNSC-null at an MOI of 2 PFU/cell, and viral titers in culture lysates were determined by plaque assay at the intervals shown. Results are mean viral titers from three independent experiments. Error bars denote standard deviations.

Importance of an intact μ2 NTPase/RTPase domain for reovirus replication. The μ2 protein contains conserved regions of primary sequence, A^{411}VLPKGSFKS^{420} and D^{446}EVG^{449}, with similarity to the nucleotide-binding A and B motifs, respectively, of ATPases (26, 42). Previous studies

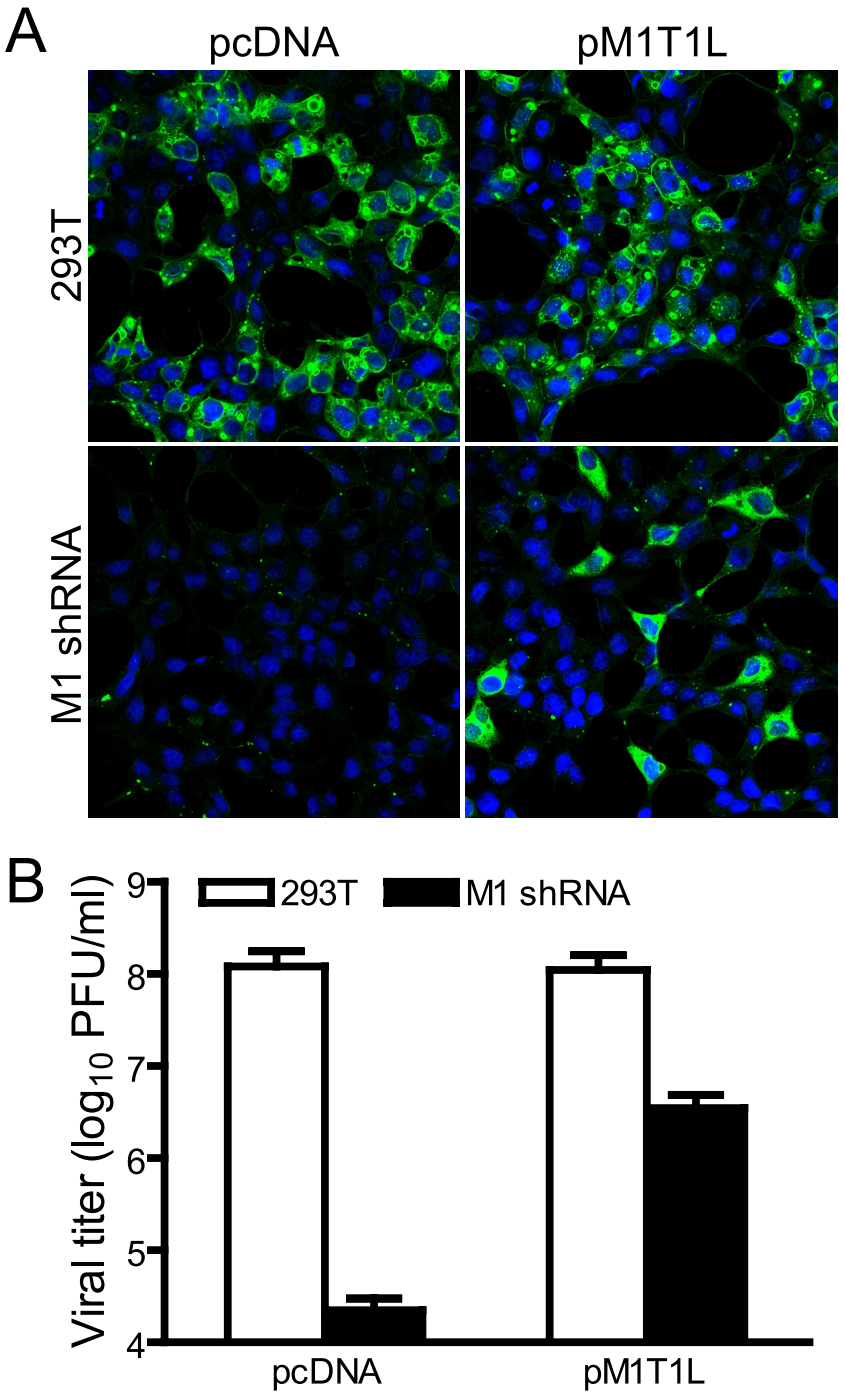

FIG. 3. *trans*-complementation of reovirus replication in cells expressing M1 (μ2-specific) shRNA. Parental or M1 shRNA-expressing 293T cells were transfected with empty vector (pcDNA) or T1L μ2-expressing vector (pM1T1L), followed by infection with T3D at an MOI of 10 PFU/cell. (A) Immunofluorescence analysis of viral replication. At 20 h postinfection, cells were visualized by confocal immunofluorescence microscopy using a monoclonal antibody specific for viral structural protein μ1/μ1C (green). Nuclei were stained with TO-PRO3 (blue). (B) Quantitation of viral growth. At 24 h postinfection, viral titers in culture lysates were determined by plaque assay. Results are mean viral titers from two independent experiments. Error bars denote standard deviations.

showed that baculovirus-expressed μ2 exhibits NTPase and RTPase activities and that both functions are abolished by dual Ala substitutions of conserved Lys residues at positions 415 and 419 (26). To ascertain the importance of μ2 putative nucleotide-binding motifs in virus replication, we replaced Lys^{415}, Gly^{416}, Lys^{419}, Asp^{446}, and Gly^{449} individually with Ala (Fig. 4A). Mutant μ2 proteins with Gly^{416} to Ala or Gly^{449} to Ala mutations retained the capacity to restore viral growth in μ2-deficient cells, whereas mutants with Lys^{415} to Ala, Lys^{419} to Ala, or Asp^{446} to Ala substitutions failed to support growth

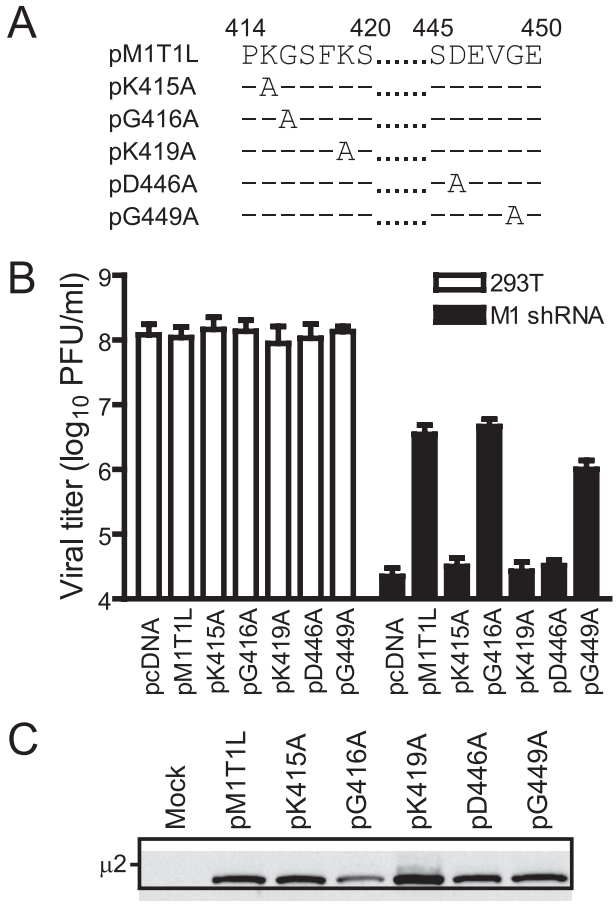

FIG. 4. *trans*-complementation of M1 (μ2-specific) RNAi with μ2 proteins containing mutations in a domain required for NTPase and RTPase activities. (A) Substitutions in predicted NTP-binding motifs of T1L μ2 protein. Changes are shown relative to the wt sequence encoded by the parental vector, pM1T1L. (B) Viral growth in cells expressing vector-encoded μ2 proteins. Parental or M1 shRNA-expressing 293T cells were transfected with empty vector (pcDNA) or T1L μ2-expressing vectors, followed by infection with T3D at an MOI of 10 PFU/cell. At 24 h postinfection, viral titers in culture lysates were determined by plaque assay. Results are mean viral titers from three independent experiments. Error bars denote standard deviations. (C) Confirmation of μ2 expression in transfected cells. Expression of μ2 proteins from *trans*-complementation vectors was verified by immunoblotting of protein extracts from transiently transfected cells using μ2-specific antiserum.

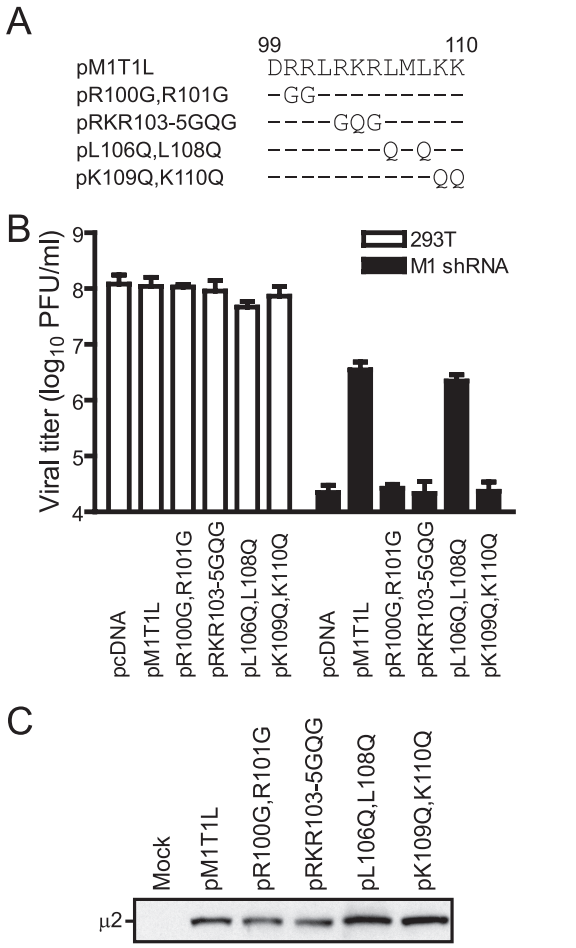

FIG. 5. *trans*-complementation of M1 (μ2-specific) RNAi with μ2 proteins containing mutations in a conserved N-terminal polybasic region. (A) Substitutions in a basic amino acid domain. Changes are shown relative to the wt sequence encoded by the parental vector, pM1T1L. (B) Viral growth in cells expressing vector-encoded μ2 proteins. Parental or M1 shRNA-expressing 293T cells were transfected with empty vector (pcDNA) or T1L μ2-expressing vectors, followed by infection with T3D at an MOI of 10 PFU/cell. At 24 h postinfection, viral titers in culture lysates were determined by plaque assay. Results are mean viral titers from three independent experiments. Error bars denote standard deviations. (C) Confirmation of μ2 expression in transfected cells. Expression of μ2 proteins from *trans*-complementation vectors was verified by immunoblotting of protein extracts from transiently transfected cells using μ2-specific antiserum.

above background levels (Fig. 4B). Differing complementation efficiencies among wt and mutant μ2 proteins were not explained by variations in expression levels, based on results of immunoblot assays (Fig. 4C). These findings indicate that both putative nucleotide-binding motifs in μ2 are vital to its function in viral replication, consistent with an essential role for μ2 NTPase/RTPase activity.

Importance of a μ2 N-terminal region basic cluster for reovirus replication. Alignment of μ2 sequences from reovirus strains representing serotypes 1, 2, and 3 reveals a highly conserved short stretch of predominantly basic amino acids that occupies positions 100 to 110 in the primary sequence, $R^{100}R$ $LRKRLMLKK^{110}$ (67). Such motifs are associated with nuclear targeting activities (15, 21). Therefore, we investigated the importance of $R^{100}RLRKRLMLKK^{110}$ in viral replication by using complementation methods (Fig. 5A). Viral yields in cells expressing a mutant μ2 protein substituted at two apolar positions, Leu^{106}/Leu^{108} to Gln^{106}/Gln^{108}, were equivalent to those expressing wt protein (Fig. 5B). In contrast, disruption of basic positions via double or triple substitution mutants—$R^{100}R^{101}$ to $G^{100}G^{101}$, R^{103} K^{104} R^{105} to $G^{103}Q^{104}G^{105}$, and $K^{109}K^{110}$ to $Q^{109}Q^{110}$—eliminated the capacity of vector-derived μ2 to restore viral growth in μ2-silenced cells despite equivalent expression levels of wt and mutant μ2 proteins (Fig. 5C). These results indicate that a cluster of basic residues near the N terminus of μ2 is critical for viral replication and support the idea that these conserved sequences are contained within a discrete functional domain.

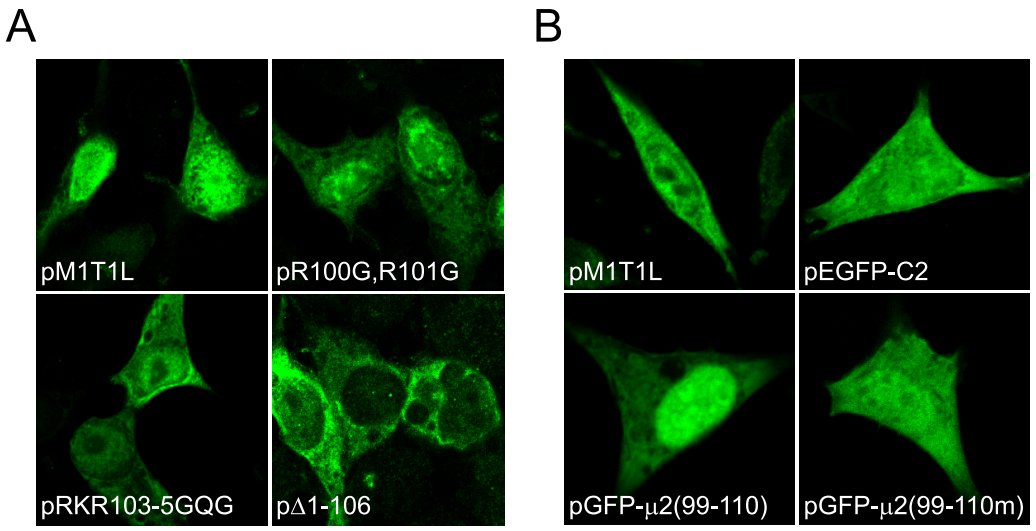

FIG. 6. Requirement for conserved N-terminal basic residues in μ2 subcellular localization. (A) Intracellular distribution of wt and mutant μ2 proteins. 293T cells were transfected with plasmid constructs encoding the indicated T1L-derived μ2 proteins, which were detected by confocal immunofluorescence microscopy using μ2-specific antiserum (green). pM1T1L, wt T1L μ2; pR100G,R101G, μ2 containing Arg^{100}-to-Gly and Arg^{101}-to-Gly substitutions; pRKR103-5GQG, μ2 containing Arg^{103}-to-Gly, Lys^{104}-to-Gln, and Arg^{105}-to-Gly substitutions; pΔ1-106, truncated μ2 protein lacking the N-terminal 106 amino acid residues. (B) Intracellular distribution of GFP fused to μ2 protein sequences. L cells were transfected with the indicated plasmid constructs. Expression of wt T1L μ2 protein was detected by confocal immunofluorescence microscopy using μ2-specific antiserum (green). Intrinsic GFP fluorescence was detected using confocal microscopy (green). pEGFP-C2, enhanced GFP; pGFP-μ2(99-110), EGFP appended at the C terminus with the μ2 putative nuclear localization sequence, D^{99}RRLRKRLMLKK^{110}; pGFP-μ2(99-110m), pGFP-μ2(99-110) containing Ala substitutions for μ2 basic residues.

Influence of μ2 N-terminal region basic sequences on protein subcellular distribution. To determine whether perturbations in protein nucleocytoplasmic compartmentalization contribute to the lethal phenotype of mutations introduced at positions occupied by basic residues between amino acids 100 and 110, we examined the distribution of μ2 in transiently transfected cells using confocal microscopy. Native μ2 protein was found in both the nucleus and cytoplasm of 293T cells with similar staining intensities (Fig. 6A). As the molecular mass of μ2 exceeds the exclusion limit for passive diffusion of molecules into the nucleus (~40 kDa) (7, 44), this finding is consistent with the presence of a functional NLS. Amino acid substitutions that abrogate the capacity of μ2 to *trans*-complement viral replication—$R^{100}R^{101}$ to $G^{100}G^{101}$ and R^{103} K^{104} R^{105} to $G^{103}Q^{104}G^{105}$—elicited a modest to moderate shift in the distribution of μ2 from the nucleus to cytoplasm. Moreover, an N-terminally truncated μ2 protein lacking the first 106 amino acid residues displayed almost exclusive cytoplasmic localization. These results provide evidence that N-terminal region sequences in μ2 harbor an NLS.

To directly determine whether the μ2 polybasic region and predicted NLS possess autonomous nuclear targeting activity, we examined the intracellular distribution of GFP extended at its C terminus with μ2 sequences, D^{99}RRLRKRLMLKK^{110} (Fig. 6B). In contrast to the homogeneous dispersion of unmodified GFP in L cells, there was marked nuclear accumulation of GFP fused to the μ2 predicted NLS. Ala substitution of basic residues in the appended μ2 sequences nullified their impact on GFP nuclear translocation, resulting in a uniform distribution of the GFP-μ2 fusion protein indistinguishable from wt GFP. These findings indicate that the N-terminal polybasic region in μ2 can independently function as an NLS. Furthermore, because mutations in this same region profoundly interfere with viral replication (Fig. 5B), results of the μ2 localization experiments suggest that nuclear targeting of μ2 is required for completion of the reovirus infectious cycle.

Effect of LMB on μ2 localization and reovirus replication. Because μ2 protein distributes to both the nucleus and cytoplasm (Fig. 6) (10, 12, 37, 39, 45), it is possible that μ2 shuttles between these compartments. The best-characterized and most commonly used nuclear export pathway is mediated by Crm1 (exportin 1), which facilitates translocation of cargos containing a Leu-rich NES, the Crm1 ligand (20, 30). LMB covalently associates with Crm1 and blocks binding to this NES (29). To determine whether Crm1-mediated nuclear export functions in μ2 subcellular distribution and viral replication, we examined the effect of LMB treatment on μ2 nuclear accumulation and viral replication in T1L-infected L-cell cultures. Addition of 20 μg/ml LMB at 8 h postinfection did not appreciably alter the nucleocytoplasmic distribution of μ2 at 12 h postinfection (Fig. 7A). Furthermore, viral yields in LMB-treated and control cells were virtually identical (Fig. 7C). The treatment conditions employed were adequate to induce nuclear sequestration of two GFP-based shuttling proteins, Rev_{68-90}-GFP_2-M9 and pXRGG, containing the Crm1-dependent NES of HIV-1 Rev (24, 34) (Fig. 7B). As an additional control, neither uninfected nor reovirus-infected cells displayed evidence of substantial LMB-induced cytotoxicity as judged by the capacity of treated cells to reductively metabolize MTS (Fig. 7D). Thus, experimental parameters commensurate with inhibition of Crm1-mediated nuclear export did not reveal spatial or functional evidence of Crm1-dependent μ2 nucleocytoplasmic shuttling.

Sequence polymorphisms in μ2 and viral inclusion morphology. The μ2-encoding M1 gene is a determinant of strain-

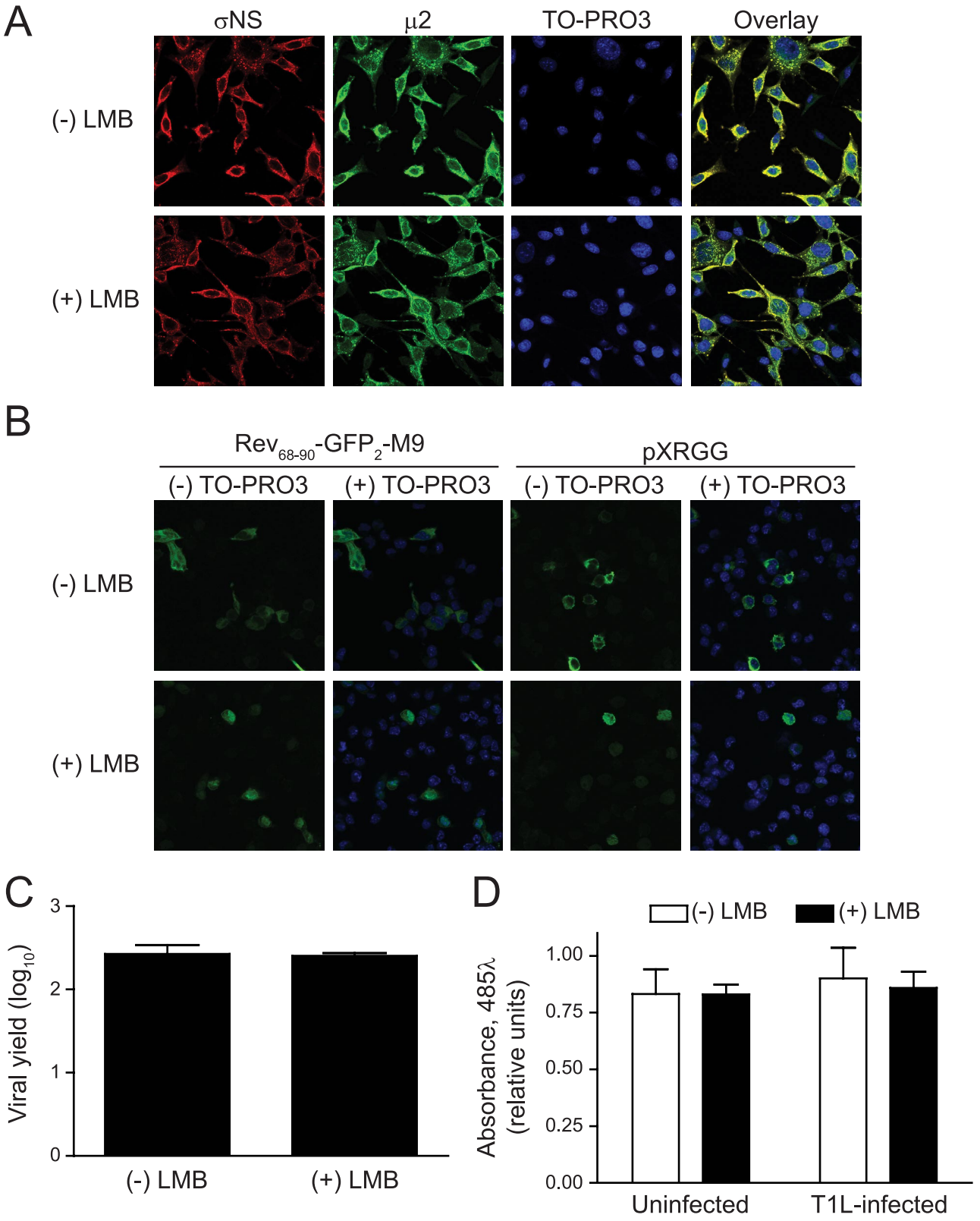

FIG. 7. Treatment of reovirus-infected cells with LMB. (A) Subcellular distribution of μ2. L cells were infected with T1L at an MOI of 20 PFU/cell. At 8 h postinfection, the culture medium was supplemented to contain 20 μg/ml LMB (+LMB) or left unsupplemented (-LMB). Cells were imaged 12 h postinfection using confocal immunofluorescence microscopy with σNS (red)- and μ2 (green)-specific antisera. Nuclei were stained with TO-PRO3 (blue). (B) Subcellular distribution of nuclear shuttling proteins. Modified GFPs enabled for nucleocytoplasmic shuttling were transfected into L cells. At 20 h posttransfection, the culture medium was supplemented to contain 20 μg/ml LMB (+ LMB) or left unsupplemented (-LMB). GFP was visualized 24 h posttransfection using confocal microscopy. Nuclei were left unstained (- TO-PRO3) or stained

specific differences in viral inclusion morphology (45), which has been correlated with the efficiency of μ2-microtubule interactions and a single amino acid polymorphism in μ2 at position 208 (45, 67). To determine the significance of the Pro^{208}/Ser^{208} polymorphism in viral replication, L cells were infected with wt and μ2-mutant viruses recovered by reverse genetics (Table 1) and subjected to immunofluorescence analysis at 24 h post infection. Consistent with patterns displayed by native viruses, rsT3D, which contains a Ser residue at μ2 position 208, produced exclusively globular inclusions, whereas recombinant virus containing the T1L-derived μ2 protein (rsT3D-T1Lμ2), in which Pro occurs at position 208, produced only filamentous inclusions (Fig. 8A). Moreover, this pattern was reversed upon reciprocal Ser^{208}-to-Pro and Pro^{208}-to-Ser substitutions in T3D (rsT3D-μ2S208P) and T1L (rsT3D-T1Lμ2P208S) μ2 proteins, respectively. These results confirm that the Pro/Ser polymorphism at position 208 in μ2 protein serves as an independent determinant of viral inclusion morphology in L cells.

Stocks of reovirus maintained in different laboratories exhibit polymorphisms in the μ2 protein (67). The T1L and T3D stocks used in our laboratory were acquired from the laboratory of Bernard Fields and contain Phe and Leu residues at μ2 positions 302 and 383, respectively. However, a cloned T1L μ2 cDNA derived from a reovirus stock maintained in the laboratory of Earl Brown contains Leu and Pro residues at positions 302 and 383, respectively (45). To determine whether sequence variability at μ2 positions 302 and 383 influences inclusion morphology, we generated T1L and T3D μ2-mutant viruses with substitutions at both sites (Table 1). Immunofluorescence analysis of L cells infected with rsT3D-T1Lμ2- and rsT3D-T1Lμ2F302L displayed filamentous inclusion morphology typical of T1L μ2 (Fig. 9A). However, infection with rsT3D-T1Lμ2L383P revealed only globular viral inclusions, whereas uniformly filamentous inclusions were observed in rsT3D-μ2S208P+L383P-infected cells (Fig. 9C). These findings show that an amino acid position in μ2 other than 208 modulates phenotypic effects of the Ser^{208}/Pro^{208} polymorphism in a sequence context-dependent fashion. Furthermore, the Phe^{302}-to-Leu substitution in rsT3D-T1Lμ2F302L serves as a specificity control for the effects of engineered changes on protein folding, which provides confidence that alterations in inclusion morphology associated with substitutions at positions 208 and 383 are unlikely to result from gross conformational changes in μ2. Thus, amino acid residues 208 and 383 are part of a functional, and possibly structural, domain involved in μ2-microtubule interactions.

Inclusion morphology and viral growth. To ascertain the relevance of inclusion morphology to viral replication, L cells were infected with wt and μ2-mutant rs viruses at an MOI of 2 PFU/cell, and viral growth was assessed by plaque assay at various times postinfection (Fig. 8B and 9B). Kinetics of viral growth and absolute titers of infectious particles did not differ significantly among wt and mutant viruses, indicating that neither μ2 sequence variability at positions 208, 302, or 383 nor inclusion morphology is a critical modulator of reovirus replication efficiency in L cells infected with isogenic μ2 mutant viruses.

DISCUSSION

The μNS protein forms distinct structures resembling viral inclusions when expressed in the absence of other viral proteins (12). Minimum sequences required for autoassembly of μNS protein into inclusion-like structures are contained within the 161 to 251 C-terminal amino acids (9). The C-terminal two to eight amino acid residues and a putative metal-chelating motif (perhaps selective for Zn^{2+}) involving His^{570} and Cys^{572} appear to play critical roles in this process (2, 9). These sequences may contribute to a dimerization domain perhaps involved in μNS homotypic or heterotypic interactions required to nucleate inclusions (9). We found that preservation of the μNS extreme C terminus and conservation of His^{570} and Cys^{572} are required for autoassembly of μNS into structures resembling viral inclusions. Furthermore, results of shRNA-based *trans*-complementation assays indicate that mutant μNS proteins failing to form inclusion-like structures are incapable of supporting viral growth in 293T cells, consistent with a recent study using a different *trans*-complementation methodology (2). Therefore, concordant results obtained in independent laboratories using different methods provide compelling functional evidence that establishment of cytoplasmic inclusions by μNS is a prerequisite to reovirus replication.

Although formation of inclusions is necessary for viral replication, results reported here indicate that inclusion formation is not sufficient. Our findings and those previously reported by Arnold et al. (2) show that μNSC, though capable of self-assembly into inclusion-like structures, cannot support viral replication. Such aspects of μNS structure-function relationships point to compulsory heterointeractions between μNS and μ2 and σNS proteins at one or more steps in the viral RNA life cycle, perhaps recruitment or retention of (+)-strand RNAs at sites of viral replication, dsRNA synthesis, or genome packaging. In support of this model, we previously found that selective RNAi-mediated elimination of μNS, μ2, or σNS from reovirus-infected cells inhibits viral dsRNA synthesis and production of infectious particles (28). We show here that removal of μNS N-terminal sequences specifically required for interac-

(blue) with TO-PRO3 (+ TO-PRO3). $Rev_{68–90}$-GFP_2-M9 contains sequences derived from the HIV-1 Rev protein nuclear export signal and the heterogeneous nuclear ribonucleoprotein A1 nuclear localization signal. The nuclear export signal for pXRGG is supplied by full-length Rev, and nuclear localization signals are furnished by both Rev and the rat glucocorticoid receptor hormone-responsive region. (C) Reovirus growth. L cells were infected with T1L at an MOI of 10 PFU/cell, and the culture medium was supplemented 8 h postinfection to contain 20 μg/ml LMB (+ LMB) or left unsupplemented (- LMB). Viral titers in culture lysates were determined at 0 and 12 h postinfection by plaque assay. Results are mean viral yields (relative to time zero) from three independent experiments. Error bars denote standard deviations. (D) Cell viability. L cells were infected with T1L at an MOI of 10 PFU/cell. At 8 h postinfection, culture medium was supplemented to contain 20 μg/ml LMB (+ LMB) or left unsupplemented (- LMB). Cell viability was determined 12 h postinfection with an MTS assay. Results are mean absorbances from three independent experiments. Error bars denote standard deviations. Reaction absorbance is directly proportional to cell viability.

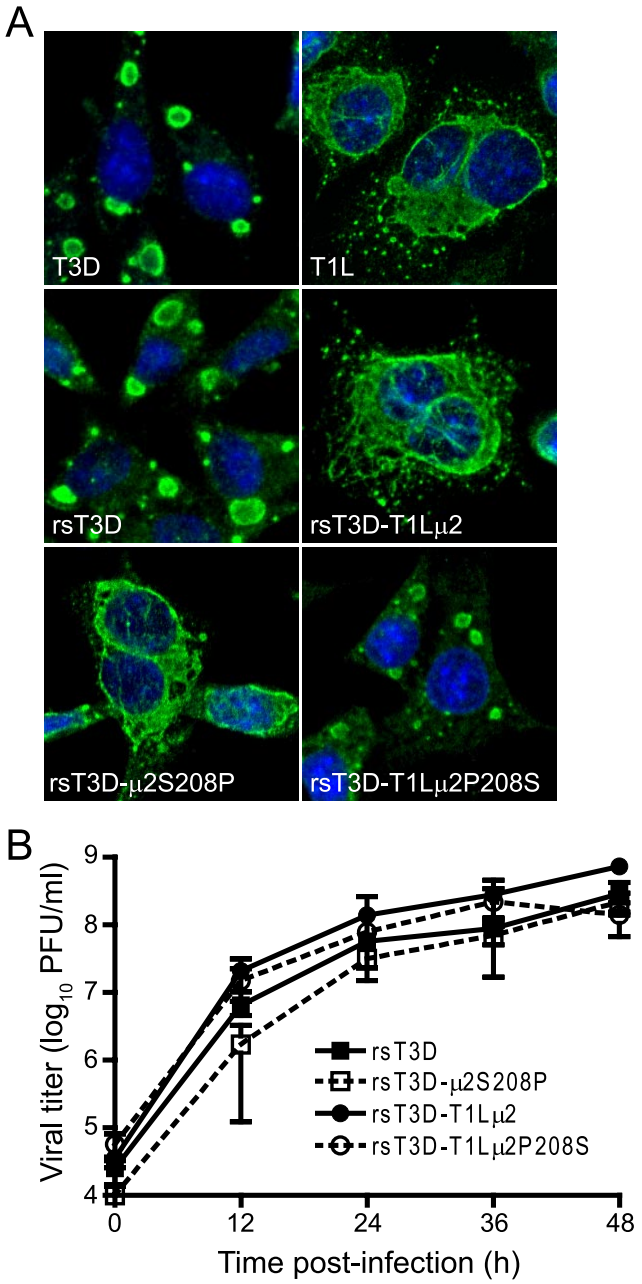

FIG. 8. Modulation of viral inclusion morphology by engineered changes at μ2 amino acid position 208. (A) Inclusion morphology of μ2 mutant viruses. L cells were infected at an MOI of 2 PFU/cell with wt viruses or viral mutants with substitutions at amino acid position 208 in the T1L and T3D μ2 proteins. At 24 h postinfection, cells were imaged using confocal immunofluorescence microscopy after staining with μNS-specific antiserum (green). Nuclei were stained with TO-PRO3 (blue). T3D and T1L, native viruses; rsT3D, wt strain; rsT3D-T1Lμ2, rsT3D containing T1L-derived μ2; rsT3D-μ2S208P, rsT3D containing a Ser^{208}-to-Pro substitution in μ2; rsT3D-T1Lμ2P208S, rsT3D-T1Lμ2 with a Pro^{208}-to-Ser substitution in μ2. (B) Growth of μ2 mutant viruses. L cells were infected with the indicated viruses at an MOI of 2 PFU/cell, and titers in culture lysates were determined by plaque assay at the intervals shown. Results are mean viral titers from three independent experiments. Error bars denote standard deviations.

tions with either σNS (1 to 13) or μ2 (14 to 40) (10, 39) also eliminates or drastically reduces the capacity of μNS to support viral growth, yet without compromising its capacity for inclusion formation.

Despite the failure of ectopically supplied μNSC to restore viral replication in μNS-depleted cells, μNSC might nevertheless contribute to viral inclusion formation or growth in infected cells. Thus, to unequivocally define the importance of μNSC in the viral infectious cycle, we characterized the replication of a μNSC-deficient mutant virus obtained using reverse genetics. In these experiments, we found that μNSC is neither required for normal viral inclusion development nor viral growth (Fig. 2). It is possible that μNSC promotes viral growth in certain cell or tissue types requisite to efficient spread within or between hosts. Alternatively, μNSC may modulate host defenses to reovirus infection at the intracellular or organismal level. We are currently investigating these possibilities.

RNAi-mediated reduction in μ2 expression is associated with marked retardation of viral inclusion development, inhibition of dsRNA synthesis, and virtual absence of progeny virion production (28). The exquisite responsiveness of reovirus replication to diminished μ2 levels permitted specific sequences in μ2 important for viral growth to be defined by complementation. We identified three short regions of sequence critical for viral replication: two predicted nucleotide-binding units with similarity to Walker A (A^{411}VLPKGS FKS^{420}) and B (D^{446}EVG^{449}) motifs of ATPases (26) and an N-terminal basic amino acid cluster conforming to a possible NLS (R^{100}RLRKRLMLKKDLRK^{114}) (15, 21). The Walker A- and B-like motifs are invariant among 14 reported μ2 sequences representing reovirus strains of all three serotypes, including the prototype strains (67). Single Ala substitutions at putative nucleotide-binding residues Lys^{415} and Lys^{419} in the A-like motif prevented viral replication, whereas mutation of the neutral position, Gly^{416}, was replication compatible. These results strongly suggest that μ2 NTPase/RTPase activity is requisite to viral replication and agree with recent findings by Carvalho et al. (13), who reported that introduction of the double mutation, Lys^{415}/Lys^{419}-to-Ala^{415}/Ala^{419}, into μ2 caused an ~10- to 100-fold viral titer reduction in CV-1 cells when they used an siRNA-based replication complementation system. Tolerance of a mutation at Gly^{449}, but not Asp^{446}, in the Walker B-like domain provides further evidence that viral replication is dependent on μ2 NTPase/RTPase functionality.

Our findings do not address specific steps in the viral infectious cycle disrupted by mutations in the Walker-like motifs. Considering that μ2 is a probable component of the core particle transcriptional machinery (8, 26, 66) as well as inclusion-associated protein (5, 10, 12, 37, 39, 40, 45) involved in genomic RNA synthesis and particle assembly (16), diminished NTPase/RTPase activities could interrupt progression of the replication program at multiple points during or following RNA (+)-strand synthesis. Introduction of Lys^{415}/Lys^{419}-to-Ala^{415}/Ala^{419} mutations into T1L μ2 does not interfere with its capacity to form filamentous inclusion-like structures when coexpressed with μNS in CV-1 cells (26). Interestingly, the NTPase function of rotavirus viroplasm-forming protein NSP2 is essential for productive rotavirus replication, but not viroplasm formation, in *trans*-complemented MA104 cells (59). Taken together, these findings suggest that disruption of μ2

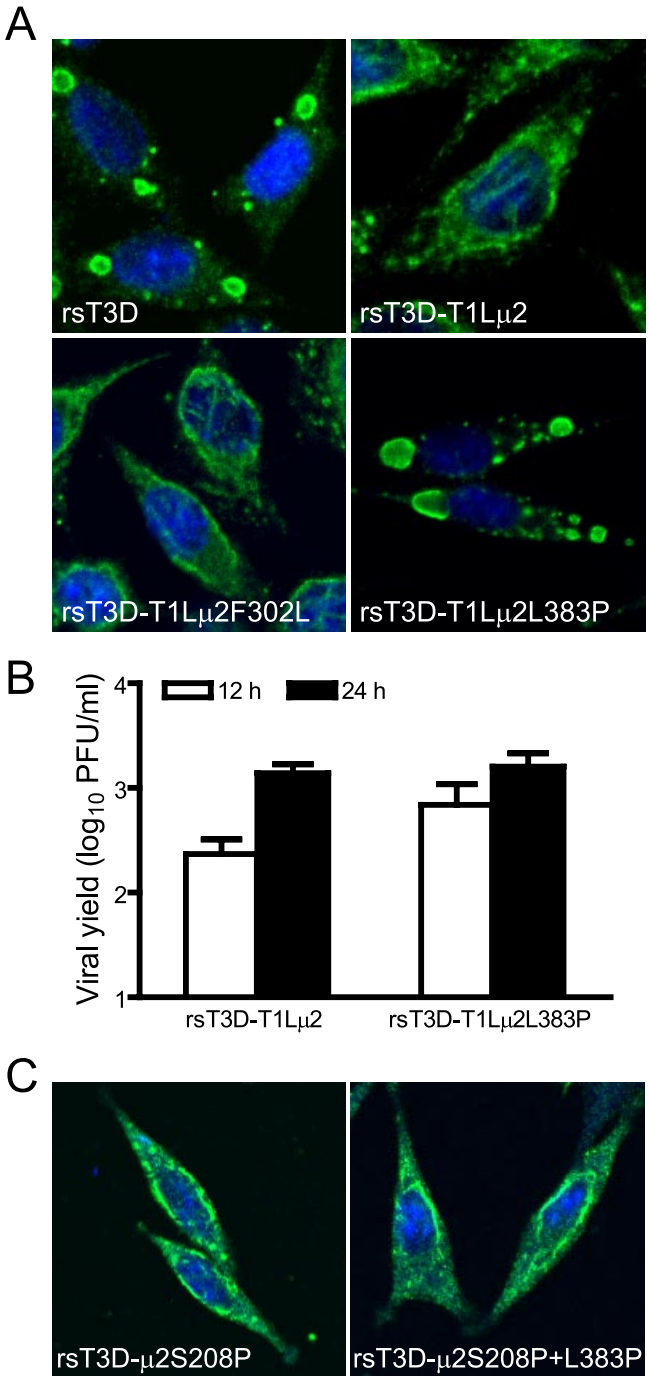

FIG. 9. Effect of altering μ2 amino acids other than at position 208 on viral inclusion morphology and growth. (A) Inclusion morphology of viruses with alterations in T1L μ2. L cells were infected at an MOI of 2 PFU/cell with wt viruses or viral mutants with substitutions at amino acid positions 302 and 383 in the T1L μ2 protein. At 24 h postinfection, cells were imaged using confocal immunofluorescence microscopy after staining with μNS-specific antiserum (green). Nuclei were stained with TO-PRO3 (blue). rsT3D, wt strain; rsT3D-T1Lμ2, rsT3D containing T1L-derived μ2; rsT3D-T1Lμ2F302L, rsT3D-T1Lμ2 with a Phe^{302}-to-Leu substitution in μ2; rsT3D-T1Lμ2L383P, rsT3D-T1Lμ2 with a Leu^{383}-to-Pro substitution in μ2. (B) Growth of virus with substitutions at amino acid position 383 of T1L μ2. L cells were infected with the indicated viruses at an MOI of 2 PFU/cell, and titers in culture lysates were determined by plaque assay after 0, 12, and 24 h of incubation. Results are mean viral yields (relative to time zero) from three independent experiments. Error bars denote standard deviations. (C) Inclusion morphology of viruses with alterations in T3D μ2. L cells were infected with the indicated viruses and imaged 24 h later as described for panel A. rsT3D-μ2S208P, rsT3D containing a Ser^{208}-to-Pro substitution in μ2; rsT3D-μ2S208P+L383P, rsT3D with Ser^{208}-to-Pro and Leu^{383}-to-Pro substitutions in μ2.

NTPase/RTPase activity blocks reovirus replication at a point subsequent to inclusion formation, for example, synthesis or packaging of dsRNA.

We found that nonconservative substitutions at charged, but not apolar, positions in the more N-terminal of two basic clusters in μ2 completely prevented transiently expressed μ2 from restoring viral growth in μ2-deficient cells. These changes produced a mild nuclear-to-cytoplasmic shift in the subcellular distribution of transiently expressed μ2 protein, suggesting that other sequences also regulate nuclear localization. One such possibility is the slightly more C-terminal NLS-like sequence element, K^{261}RLR^{264}, but additional nuclear-targeting activities may reside proximal to the N terminus of μ2, as very little mutant protein lacking the N-terminal 106 residues was present in the nucleus. Nevertheless, we found that the oligopeptide D^{99}RRLRKRLMLKK^{110} is sufficient to direct a heterologous protein (GFP) to the nucleus. Thus, this region of μ2 possesses intrinsic capacity for nuclear localization. Classical (i.e., basic) NLSs are recognized by importin-α, and NLS-presenting proteins are translocated through the nuclear pore in a complex containing importin-α and importin-β (57). These findings are consistent with a physical interaction between μ2 and components of the nuclear import apparatus.

A functional role for μ2 nuclear entry is not apparent from our studies. However, it is noteworthy that μ2 protein has been genetically linked to viral strain-specific differences in the induction of alpha/beta interferon (IFN-α/β) expression in cardiac myocytes and reovirus sensitivity to the antiviral effects of IFN in these cells (55). A recent report by Zurney et al. (69) provided evidence that the μ2 protein of strain T1L, but not T3D, antagonizes signal transduction from the IFN-α/β receptor by favoring the nuclear accumulation of a key signaling molecule, IFN regulatory factor 9 (IRF9), which partners with signal transducer and activator of transcription 1 (STAT1) and STAT2 to form a heterotrimeric inducer of IFN-stimulated gene (ISG) expression (49). The nuclear phase of μ2 might benefit viral replication by directly or indirectly perturbing the normal cycle of IRF9 nucleocytoplasmic translocation, thereby suppressing the expression of ISGs. Activities of μ2 in the nucleus might also involve cellular processes unrelated to innate immunity, such as regulation of transcription or the cell cycle, congruous with diverse functional interactions between proteins encoded by cytoplasmically replicating RNA viruses and nuclear structures and proteins (23).

The most commonly used and best-characterized pathway for exporting nuclear cargo to the cytoplasm is dependent on Crm1, which recognizes hydrophobic, typically Leu-rich, NESs and translocates NES-containing proteins through the nuclear pore as part of a heteromeric complex containing GTP-bound Ran protein (57). A number of viral proteins are shuttled in a Crm1-dependent fashion (20, 46, 48, 63, 65), and like μ2, these

proteins are frequently involved in viral RNA regulation or subversion of the IFN response. A specific inhibitor of Crm1 nuclear export activity, LMB (29, 30), did not significantly affect viral replication or the distribution of μ2 protein in T1L-infected L cells under treatment conditions adequate to induce nuclear retention of two different GFP-based reporter molecules containing the HIV-1 Rev NES. Nonetheless, our results do not exclude the possibility of bidirectional movement of μ2 between the cytoplasm and nucleus. It is possible that variation in the sequence of μ2 (or other proteins) among different viral strains (67) influences the extent or kinetics of μ2 nucleocytoplasmic shuttling and, therefore, sensitivity to LMB. Another possibility is that μ2 export from the nucleus occurs through a nonclassical pathway (43), reminiscent of Crm1-indpendent nuclear export of morbillivirus N proteins containing Leu-rich NESs (50). We note the presence of a sequence element in μ2, L^{328}EMLGIEI^{335}, which exhibits similarity to a Leu-rich NES (31) and is highly conserved among 14 published μ2 sequences except that belonging to strain T2J (67).

The μ2 protein binds and stabilizes microtubules and anchors inclusions of the majority of characterized reovirus strains to the cytoskeleton, resulting in filamentous inclusion morphology (12, 45, 67). However, a Pro^{208}-to-Ser change present in some viral strains is associated with the covariant phenotypes of diminished microtubule binding by μ2 (45) and globular inclusion morphology (45, 67). We rescued isogenic viruses containing single amino acid substitutions in μ2 and found that the Pro^{208}/Ser^{208} polymorphism is indeed an independent determinant of inclusion morphology. We further observed that a Leu/Pro polymorphism at position 383, identified in the cloned M1 cDNA sequence from a laboratory isolate of T1L (45), also determines inclusion morphology of rescued viruses expressing T1L μ2 and that the simultaneous presence of Pro and Leu at positions 208 and 383, respectively, is required to produce filamentous inclusions. Similar studies performed using viruses expressing T3D μ2 protein yielded the somewhat surprising result that the polymorphism at position 383 in T3D μ2 does not affect inclusion morphology dictated by amino acid 208. There are nine amino acid differences between the T1L- and T3D-derived μ2 proteins used for our studies (T1L/T3D amino acids: Val^{93}/Ala^{93}, Pro^{208}/Ser^{208}, Val^{300}/Met^{300}, Gln^{342}/Arg^{342}, Phe^{347}/Leu^{347}, Val^{434}/Ile^{434}, His^{458}/Gln^{458}, Met^{652}/Ile^{652}, and Asn^{726}/Ser^{726}), one or more of which must control the differential effects of residue 383 on inclusion morphology. Detailed structural models of the μ2 protein are needed to fully explain these strain-specific effects, but one logical hypothesis is that amino acid residues 208 and 383 are proximal in the μ2 structure and contribute to the microtubule-binding or microtubule-stabilizing region of μ2. Neighboring polymorphic positions may influence the interactions of amino acid residues 208 and 383 with microtubules or each other.

We were unable to correlate inclusion morphology with total viral yields or replication kinetics by using rescued μ2 mutant viruses, which grew equivalently to wt regardless of the inclusion morphotype or strain origin of μ2. These findings contrast with those reported by Carvalho et al. (13), which showed that viral growth in an RNAi-based *trans*-complementation system was significantly enhanced when complementation was performed with μ2 protein containing Pro rather than Ser at position 208. The mechanistic basis for these differential effects of Pro^{208} versus Ser^{208} on the capacity of transiently expressed μ2 to restore viral replication was not evident in those studies, but rescue of viral growth was sensitive to nocodazole, indicating dependence on intact microtubules. The requirements for microtubule binding by μ2 may be cell type dependent. In this regard, previous experiments were performed with primate kidney-derived (CV-1) cells, whereas we used murine fibroblast (L) cells. The μ2-encoding M1 gene is a determinant of differences between strains T1L and T3D with respect to viral growth in MDCK cells (47), murine cardiac cells (36), and bovine aortic endothelial cells (35); reovirus-induced myocarditis in immunocompetent mice (54); and organ-specific viral growth and injury in SCID mice (22). Thus, μ2-mediated recruitment of viral factories to microtubules might be necessary for efficient reovirus growth in some types of cells. Although a mechanistic explanation for such a requirement is not obvious, concentration of viral proteins and RNA on the cytoskeleton may facilitate genome replication and particle assembly or, perhaps, shield viral components from recognition by the intracellular pathogen surveillance system.

In this study, we combined RNAi-based and reverse genetics strategies to define the role of functional domains in the viral inclusion-forming proteins μNS and μ2 in reovirus replication. Both proteins display modular architectures built from what appear to be functionally and structurally unique sequence domains involved in discrete steps of inclusion development and viral replication. Recombinant reoviruses systematically altered in the μNS, μ2, and other viral proteins will foster new insights into the viral replication machinery and may reveal posttranscriptional determinants of viral pathogenesis.

ACKNOWLEDGMENTS

We thank Sam Naik for his assistance with studies of μ2 subcellular localization and members of our laboratories for many helpful discussions about this project. We thank Ralph Kehlenbach, University of Gottingen, for kindly providing the GFP shuttling constructs.

This work was supported by Public Health Service awards K08 AI062862 (J.D.C.) and R01 AI32539 from the National Institute of Allergy and Infectious Diseases, the Naito Foundation (T.K.), the Elizabeth B. Lamb Center for Pediatric Research, and the Vanderbilt University Department of Pathology. Additional support was provided by Public Health Service awards CA68485 for the Vanderbilt-Ingram Cancer Center and DK20593 for the Vanderbilt Diabetes Research and Training Center. Acquisition and analysis of confocal imaging data were performed in part through the use of the Vanderbilt University Medical Center Imaging Shared Resource.

REFERENCES

1. **Antczak, J. B., and W. K. Joklik.** 1992. Reovirus genome segment assortment into progeny genomes studied by the use of monoclonal antibodies directed against reovirus proteins. Virology **187:**760–776.
2. **Arnold, M. M., K. E. Murray, and M. L. Nibert.** 2008. Formation of the factory matrix is an important, though not a sufficient function of nonstructural protein μNS during reovirus infection. Virology **375:**412–423.
3. **Baer, G. S., D. H. Ebert, C. J. Chung, A. H. Erickson, and T. S. Dermody.** 1999. Mutant cells selected during persistent reovirus infection do not express mature cathepsin L and do not support reovirus disassembly. J. Virol. **73:**9532–9543.
4. **Banerjee, A. K., and A. J. Shatkin.** 1970. Transcription in vitro by reovirus-associated ribonucleic acid-dependent polymerase. J. Virol. **6:**1–11.
5. **Becker, M. M., M. I. Goral, P. R. Hazelton, G. S. Baer, S. E. Rodgers, E. G. Brown, K. M. Coombs, and T. S. Dermody.** 2001. Reovirus σNS protein is required for nucleation of viral assembly complexes and formation of viral inclusions. J. Virol. **75:**1459–1475.
6. **Becker, M. M., T. R. Peters, and T. S. Dermody.** 2003. Reovirus σNS and

μNS proteins form cytoplasmic inclusion structures in the absence of viral infection. J. Virol. **77:**5948–5963.
7. **Bonner, W. M.** 1978. Protein migration and accumulation in nuclei, p. 97–148. *In* H. Busch (ed.), The cell nucleus, vol. 6. Academic Press, New York, NY.
8. **Brentano, L., D. L. Noah, E. G. Brown, and B. Sherry.** 1998. The reovirus protein μ2, encoded by the M1 gene, is an RNA-binding protein. J. Virol. **72:**8354–8357.
9. **Broering, T. J., M. M. Arnold, C. L. Miller, J. A. Hurt, P. L. Joyce, and M. L. Nibert.** 2005. Carboxyl-proximal regions of reovirus nonstructural protein μNS necessary and sufficient for forming factory-like inclusions. J. Virol. **79:**6194–6206.
10. **Broering, T. J., J. Kim, C. L. Miller, C. D. Piggott, J. B. Dinoso, M. L. Nibert, and J. S. Parker.** 2004. Reovirus nonstructural protein μNS recruits viral core surface proteins and entering core particles to factory-like inclusions. J. Virol. **78:**1882–1892.
11. **Broering, T. J., A. M. McCutcheon, V. E. Centonze, and M. L. Nibert.** 2000. Reovirus nonstructural protein μNS binds to core particles but does not inhibit their transcription and capping activities. J. Virol. **74:**5516–5524.
12. **Broering, T. J., J. S. Parker, P. L. Joyce, J. Kim, and M. L. Nibert.** 2002. Mammalian reovirus nonstructural protein μNS forms large inclusions and colocalizes with reovirus microtubule-associated protein μ2 in transfected cells. J. Virol. **76:**8285–8297.
13. **Carvalho, J., M. M. Arnold, and M. L. Nibert.** 2007. Silencing and complementation of reovirus core protein μ2: functional correlations with μ2-microtubule association and differences between virus- and plasmid-derived μ2. Virology **364:**301–316.
14. **Chang, C. T., and H. J. Zweerink.** 1971. Fate of parental reovirus in infected cell. Virology **46:**544–555.
15. **Chelsky, D., R. Ralph, and G. Jonak.** 1989. Sequence requirements for synthetic peptide-mediated translocation to the nucleus. Mol. Cell. Biol. **9:**2487–2492.
16. **Coombs, K. M.** 1996. Identification and characterization of a double-stranded RNA-reovirus temperature-sensitive mutant defective in minor core protein μ2. J. Virol. **70:**4237–4245.
17. **Coombs, K. M.** 1998. Stoichiometry of reovirus structural proteins in virus, ISVP, and core particles. Virology. **243:**218–228.
18. **Ebert, D. H., J. Deussing, C. Peters, and T. S. Dermody.** 2002. Cathepsin L and cathepsin B mediate reovirus disassembly in murine fibroblast cells. J. Biol. Chem. **277:**24609–24617.
19. **Fields, B. N., C. S. Raine, and S. G. Baum.** 1971. Temperature-sensitive mutants of reovirus type 3: defects in viral maturation as studied by immunofluorescence and electron microscopy. Virology **43:**569–578.
20. **Fukuda, M., S. Asano, T. Nakamura, M. Adachi, M. Yoshida, M. Yanagida, and E. Nishida.** 1997. CRM1 is responsible for intracellular transport mediated by the nuclear export signal. Nature **390:**308–311.
21. **Garcia-Bustos, J., J. Heitman, and M. Hall.** 1991. Nuclear protein localization. Biochim. Biophys. Acta **1071:**83–101.
22. **Haller, B. L., M. L. Barkon, G. P. Vogler, and H. W. Virgin, IV.** 1995. Genetic mapping of reovirus virulence and organ tropism in severe combined immunodeficient mice: organ-specific virulence genes. J. Virol. **69:**357–364.
23. **Hiscox, J. A.** 2003. The interaction of animal cytoplasmic RNA viruses with the nucleus to facilitate replication. Virus Res. **95:**13–22.
24. **Hutten, S., S. Wälde, C. Spillner, J. Hauber, and R. H. Kehlenbach.** The nuclear pore component Nup358 promotes transportin-dependent nuclear import. J. Cell. Sci., in press.
25. **Ishii, K., Y. Ueda, K. Matsuo, Y. Matsuura, T. Kitamura, K. Kato, Y. Izumi, K. Someya, T. Ohsu, M. Honda, and T. Miyamura.** 2002. Structural analysis of vaccinia virus DIs strain: application as a new replication-deficient viral vector. Virology **302:**433–444.
26. **Kim, J., J. S. Parker, K. E. Murray, and M. L. Nibert.** 2004. Nucleoside and RNA triphosphatase activities of Orthoreovirus transcriptase cofactor μ2. J. Biol. Chem. **279:**4394–4403.
27. **Kobayashi, T., A. A. R. Antar, K. W. Boehme, P. Danthi, E. A. Eby, K. M. Guglielmi, G. H. Holm, E. M. Johnson, M. S. Maginnis, S. Naik, W. B. Skelton, J. D. Wetzel, G. J. Wilson, J. D. Chappell, and T. S. Dermody.** 2007. A plasmid-based reverse genetics system for animal double-stranded RNA viruses. Cell Host Microbe **1:**147–157.
28. **Kobayashi, T., J. D. Chappell, P. Danthi, and T. S. Dermody.** 2006. Gene-specific inhibition of reovirus replication by RNA interference. J. Virol. **80:**9053–9063.
29. **Kudo, N., N. Matsumori, H. Taoka, D. Fujiwara, E. P. Schreiner, B. Wolff, M. Yoshida, and S. Horinouchi.** 1999. Leptomycin B inactivates CRM1/exportin 1 by covalent modification at a cysteine residue in the central conserved region. Proc. Natl. Acad. Sci. USA **96:**9112–9117.
30. **Kudo, N., B. Wolff, T. Sekimoto, E. P. Schreiner, Y. Yoneda, M. Yanagida, S. Horinouchi, and M. Yoshida.** 1998. Leptomycin B inhibition of signal-mediated nuclear export by direct binding to CRM1. Exp. Cell. Res. **242:**540–547.
31. **la Cour, T., L. Kiemer, A. Molgaard, R. Gupta, K. Skriver, and S. Brunak.** 2004. Analysis and prediction of leucine-rich nuclear export signals. Protein Eng. **17:**527–536.
32. **Lee, P. W. K., E. C. Hayes, and W. K. Joklik.** 1981. Characterization of anti-reovirus immunoglobulins secreted by cloned hybridoma cell lines. Virology **108:**134–146.
33. **Li, J. K.-K., P. P. Scheible, J. D. Keene, and W. K. Joklik.** 1980. The plus strand of reovirus gene S2 is identical with its in vitro transcript. Virology **105:**282–286.
34. **Love, D. C., T. D. Sweitzer, and J. A. Hanover.** 1998. Reconstitution of HIV-1 Rev nuclear export: independent requirements for nuclear import and export. Proc. Natl. Acad. Sci. USA **95:**10608–10613.
35. **Matoba, Y., W. S. Colucci, B. N. Fields, and T. W. Smith.** 1993. The reovirus M1 gene determines the relative capacity of growth of reovirus in cultured bovine aortic endothelial cells. J. Clin. Investig. **92:**2883–2888.
36. **Matoba, Y., B. Sherry, B. N. Fields, and T. W. Smith.** 1991. Identification of the viral genes responsible for growth of strains of reovirus in cultured mouse heart cells. J. Clin. Investig. **87:**1628–1633.
37. **Mbisa, J. L., M. M. Becker, S. Zou, T. S. Dermody, and E. G. Brown.** 2000. Reovirus μ2 protein determines strain-specific differences in the rate of viral inclusion formation in L929 cells. Virology **272:**16–26.
38. **McCrae, M. A., and W. K. Joklik.** 1978. The nature of the polypeptide encoded by each of the ten double-stranded RNA segments of reovirus type 3. Virology **89:**578–593.
39. **Miller, C. L., T. J. Broering, J. S. Parker, M. M. Arnold, and M. L. Nibert.** 2003. Reovirus σNS protein localizes to inclusions through an association requiring the μNS amino terminus. J. Virol. **77:**4566–4576.
40. **Miller, C. L., J. S. Parker, J. B. Dinoso, C. D. Piggott, M. J. Perron, and M. L. Nibert.** 2004. Increased ubiquitination and other covariant phenotypes attributed to a strain- and temperature-dependent defect of reovirus core protein μ2. J. Virol. **78:**10291–10302.
41. **Mustoe, T. A., R. F. Ramig, A. H. Sharpe, and B. N. Fields.** 1978. Genetics of reovirus: identification of the dsRNA segments encoding the polypeptides of the μ and σ size classes. Virology **89:**594–604.
42. **Noble, S., and M. L. Nibert.** 1997. Core protein μ2 is a second determinant of nucleoside triphosphatase activities by reovirus cores. J. Virol. **71:**7728–7735.
43. **Ossareh-Nazari, B., C. Gwizdek, and C. Dargemont.** 2001. Protein export from the nucleus. Traffic **2:**684–689.
44. **Paine, P. L., L. C. Moore, and S. B. Horowitz.** 1975. Nuclear envelope permeability. Nature **254:**109–114.
45. **Parker, J. S., T. J. Broering, J. Kim, D. E. Higgins, and M. L. Nibert.** 2002. Reovirus core protein μ2 determines the filamentous morphology of viral inclusion bodies by interacting with and stabilizing microtubules. J. Virol. **76:**4483–4496.
46. **Pasdeloup, D., N. Poisson, H. Raux, Y. Gaudin, R. W. H. Ruigrok, and D. Blondel.** 2005. Nucleocytoplasmic shuttling of the rabies virus P protein requires a nuclear localization signal and a CRM1-dependent nuclear export signal. Virology **334:**284–293.
47. **Rodgers, S. E., E. S. Barton, S. M. Oberhaus, B. Pike, C. A. Gibson, K. L. Tyler, and T. S. Dermody.** 1997. Reovirus-induced apoptosis of MDCK cells is not linked to viral yield and is blocked by Bcl-2. J. Virol. **71:**2540–2546.
48. **Rodriguez, J. J., C. D. Cruz, and C. M. Horvath.** 2004. Identification of the nuclear export signal and STAT-binding domains of the Nipah virus V protein reveals mechanisms underlying interferon evasion. J. Virol. **78:**5358–5367.
49. **Sadler, A. J., and B. R. G. Williams.** 2008. Interferon-inducible antiviral effectors. Nat. Rev. Immunol. **8:**559–568.
50. **Sato, H., M. Masuda, R. Miura, M. Yoneda, and C. Kai.** 2006. Morbillivirus nucleoprotein possesses a novel nuclear localization signal and a CRM1-independent nuclear export signal. Virology **352:**121–130.
51. **Schiff, L., M. Nibert, and K. L. Tyler.** 2007. Orthoreoviruses and their replication, p. 1853–1915. *In* D. M. Knipe and P. M. Howley (ed.), Fields virology, 5th ed. Lippincott Williams & Wilkins, Philadelphia, PA.
52. **Schonberg, M., S. C. Silverstein, D. H. Levin, and G. Acs.** 1971. Asynchronous synthesis of the complementary strands of the reovirus genome. Proc. Natl. Acad. Sci. USA **68:**505–508.
53. **Shatkin, A. J., and M. Kozak.** 1983. Biochemical aspects of reovirus transcription and translation, p. 79–106. *In* W. K. Joklik (ed.), The Reoviridae. Plenum Press, New York, NY.
54. **Sherry, B., and M. A. Blum.** 1994. Multiple viral core proteins are determinants of reovirus-induced acute myocarditis. J. Virol. **68:**8461–8465.
55. **Sherry, B., J. Torres, and M. A. Blum.** 1998. Reovirus induction of and sensitivity to beta interferon in cardiac myocyte cultures correlate with induction of myocarditis and are determined by viral core proteins. J. Virol. **72:**1314–1323.
56. **Silverstein, S. C., and P. H. Schur.** 1970. Immunofluorescent localization of double-stranded RNA in reovirus-infected cells. Virology **41:**564–566.
57. **Sorokin, A. V., E. R. Kim, and L. P. Ovchinnikov.** 2007. Nucleocytoplasmic transport of proteins. Biochemistry (Moscow) **72:**1439–1457.
58. **Sturzenbecker, L. J., M. L. Nibert, D. B. Furlong, and B. N. Fields.** 1987. Intracellular digestion of reovirus particles requires a low pH and is an essential step in the viral infectious cycle. J. Virol. **61:**2351–2361.
59. **Taraporewala, Z. F., X. Jiang, R. Vasquez-Del Carpio, H. Jayaram, B. V. V. Prasad, and J. T. Patton.** 2006. Structure-function analysis of rotavirus NSP2 octamer by using a novel complementation system. J. Virol. **80:**7984–7994.

60. **Virgin, H. W., IV, R. Bassel-Duby, B. N. Fields, and K. L. Tyler.** 1988. Antibody protects against lethal infection with the neurally spreading reovirus type 3 (Dearing). J. Virol. **62:**4594–4604.
61. **Virgin, H. W., IV, M. A. Mann, B. N. Fields, and K. L. Tyler.** 1991. Monoclonal antibodies to reovirus reveal structure/function relationships between capsid proteins and genetics of susceptibility to antibody action. J. Virol. **65:**6772–6781.
62. **Watanabe, S., T. Watanabe, T. Noda, A. Takada, H. Feldmann, L. D. Jasenosky, and Y. Kawaoka.** 2004. Production of novel Ebola virus-like particles from cDNAs: an alternative to Ebola virus generation by reverse genetics. J. Virol. **78:**999–1005.
63. **Wells, G., and A. Malur.** 2008. Expression of human parainfluenza virus type 3 PD protein and intracellular localization in virus infected cells. Virus Genes. **37:**358–367.
64. **Wiener, J. R., J. A. Bartlett, and W. K. Joklik.** 1989. The sequences of reovirus serotype 3 genome segments M1 and M3 encoding the minor protein μ2 and the major nonstructural protein μNS, respectively. Virology **169:**293–304.
65. **Wolff, B., J.-J. Sanglier, and Y. Wang.** 1997. Leptomycin B is an inhibitor of nuclear export: inhibition of nucleo-cytoplasmic translocation of the human immunodeficiency virus type 1 (HIV-1) Rev protein and Rev-dependent mRNA. Chem. Biol. **4:**139–147.
66. **Yin, P., M. Cheang, and K. M. Coombs.** 1996. The M1 gene is associated with differences in the temperature optimum of the transcriptase activity in reovirus core particles. J. Virol. **70:**1223–1227.
67. **Yin, P., N. D. Keirstead, T. J. Broering, M. M. Arnold, J. S. Parker, M. L. Nibert, and K. M. Coombs.** 2004. Comparisons of the M1 genome segments and encoded μ2 proteins of different reovirus isolates. Virol. J. **1:**6.
68. **Zou, S., and E. G. Brown.** 1996. Stable expression of the reovirus μ2 protein in mouse L cells complements the growth of a reovirus ts mutant with a defect in its M1 gene. Virology **217:**42–48.
69. **Zurney, J., T. Kobayashi, G. H. Holm, T. S. Dermody, and B. Sherry.** 2008. The reovirus μ2 protein inhibits interferon signaling through a novel mechanism involving nuclear accumulation of interferon regulatory factor-9. J. Virol. **82:**2178–2187.
70. **Zweerink, H. J., E. M. Morgan, and J. S. Skyler.** 1976. Reovirus morphogenesis: characterization of subviral particles in infected cells. Virology **73:**442–453.

APPENDIX C

AN IMPROVED REVERSE GENETICS SYSTEM FOR MAMMALIAN ORTHOREOVIRUSES

Takeshi Kobayashi*, Laura S. Ooms*, Mine Ikizler, James D. Chappell, Terence S. Dermody

Virology. 398(2) 194-200; 2010.

*Authors contributed equally to this manuscript

Virology 398 (2010) 194–200

Contents lists available at ScienceDirect

Virology

journal homepage: www.elsevier.com/locate/yviro

An improved reverse genetics system for mammalian orthoreoviruses

Takeshi Kobayashi [a,d,1,2], Laura S. Ooms [b,d,1], Mine Ikizler [a,d], James D. Chappell [b,d,*], Terence S. Dermody [a,c,d,*]

[a] Department of Pediatrics, Vanderbilt University School of Medicine, Nashville, TN 37232, USA
[b] Department of Pathology, Vanderbilt University School of Medicine, Nashville, TN 37232, USA
[c] Department of Microbiology and Immunology, Vanderbilt University School of Medicine, Nashville, TN 37232, USA
[d] Elizabeth B. Lamb Center for Pediatric Research, Vanderbilt University School of Medicine, Nashville, TN 37232, USA

ARTICLE INFO

Article history:
Received 23 October 2009
Returned to author for revision
12 November 2009
Accepted 20 November 2009
Available online 29 December 2009

Keywords:
Reverse genetics
Reovirus
dsRNA
T7 RNA polymerase
Reassortment

ABSTRACT

Mammalian orthoreoviruses (reoviruses) are highly useful models for studies of double-stranded RNA virus replication and pathogenesis. We previously developed a strategy to recover prototype reovirus strain T3D from cloned cDNAs transfected into murine L929 fibroblast cells. Here, we report the development of a second-generation reovirus reverse genetics system featuring several major improvements: (1) the capacity to rescue prototype reovirus strain T1L, (2) reduction of required plasmids from 10 to 4, and (3) isolation of recombinant viruses following transfection of baby hamster kidney cells engineered to express bacteriophage T7 RNA polymerase. The efficiency of virus rescue using the 4-plasmid strategy was substantially increased in comparison to the original 10-plasmid system. We observed full compatibility of T1L and T3D rescue vectors when intermixed to produce a panel of T1L×T3D monoreassortant viruses. Improvements to the reovirus reverse genetics system enhance its applicability for studies of reovirus biology and clinical use.

Introduction

One of the most transformative technologic advancements in virology has been the development of reverse genetics systems for nearly all major groups of RNA- and DNA-containing viruses. Although the molecular design and methodologic details of these systems vary, their common feature is the availability of cloned cDNAs encoding viral genomes that can be manipulated and subsequently used to isolate viruses containing engineered changes in genomic nucleic acids. RNA virus rescue systems typically entail intracellular transcription of full-length genomic or antigenomic RNAs from plasmids transfected into permissive cells, frequently in conjunction with transient expression of essential components of the viral replicase (Bridgen and Elliott, 1996; Collins et al., 1995; Fodor et al., 1999; Garcin et al., 1995; Lawson et al., 1995; Neumann et al., 1999; Racaniello and Baltimore, 1981; Schneider et al., 2005; Schnell et al., 1994; Whelan et al., 1995; Yoneda et al., 2006). Furthermore, translational competence of (+)-strand RNA virus genomes has enabled rescue of infectious virus from cells following introduction of *in vitro*-generated genomic RNAs free of viral proteins (Almazan et al., 2000; Coley et al., 2005; Gritsun and Gould, 1995; Kinney et al., 1997; Racaniello and Baltimore, 1981; Rice et al., 1989; Yount et al., 2003; Yun et al., 2003). Development of a fully plasmid-based reverse genetics strategy for double-stranded (ds) RNA viruses of mammalian species, which include coltiviruses, orbiviruses, reoviruses, and rotaviruses, has trailed other major systems owing in part to the technical complexities involved in manipulation of a multipartite genome containing 10 or more segments. We have developed a reverse genetics system for mammalian reovirus (Kobayashi et al., 2007), a nonenveloped, double-layered particle containing 10 dsRNA gene segments (Schiff et al., 2007), and used this system to engineer changes in both structural and nonstructural proteins for studies of reovirus replication and pathogenesis (Boehme et al., 2009; Danthi et al., 2008a; Danthi et al., 2008b; Kirchner et al., 2008; Kobayashi et al., 2007, 2009; Zurney et al., 2009).

The implications of targeted alterations of the reovirus genome are highly significant to current research focused on therapeutic use of reovirus as an oncolytic agent (Kelly et al., 2009) and to conceptualization of reovirus-vectored vaccines. Goals for our continuing work with this technology include performance improvement in the form of increased efficiency of virus recovery, broadened scope of dissectible viral properties and phenotypes, expanded spectrum of nonviral nucleic acids inserted into the viral genome, shortened time to virus recovery, and reduced reagent preparation time and expense.

* Corresponding authors. Lamb Center for Pediatric Research, D7235 MCN, Vanderbilt University School of Medicine, Nashville, TN 37232, USA. Fax: +1 615 343 9723.
E-mail addresses: jim.chappell@vanderbilt.edu (J.D. Chappell), terry.dermody@vanderbilt.edu (T.S. Dermody).
[1] These authors contributed equally to this manuscript.
[2] Current address: Institute for Virus Research, Kyoto University, Kyoto 606-8507, Japan.

0042-6822/$ – see front matter © 2009 Elsevier Inc. All rights reserved.
doi:10.1016/j.virol.2009.11.037

Progress in these key aspects of the rescue system will accelerate basic studies of reovirus biology and development of reovirus for clinical applications.

The reovirus reverse genetics system is based on the serotype 3 prototype strain, type 3 Dearing (T3D; Kobayashi et al., 2007), and consists of 10 plasmids, each containing a full-length reovirus gene-segment cDNA under transcriptional control of the bacteriophage T7 RNA polymerase promoter and fused at the 3′ terminus with hepatitis delta virus (HDV) ribozyme sequences. These plasmids are presumed to generate transcripts identical in sequence to reovirus-generated (+)-strand RNAs that serve as templates for translation and dsRNA synthesis in infected cells. The primary round of reovirus replication is initiated by co-transfection of all 10 plasmids into murine L929 (L) cells infected with a replication-defective vaccinia virus expressing T7 RNA polymerase. Following 5 days of incubation, recombinant strain (rs) viruses are isolated from co-transfection lysates by plaque assay using L cells. The global replication behavior and strain-specific phenotypes of rs viruses studied to date are qualitatively and quantitatively consistent with the natural parental isolates (Danthi et al., 2008a; Kobayashi et al., 2007, 2009). These results demonstrate that the reovirus reverse genetics system is a biologically plausible approach to study viral replication and pathogenesis, optimize viral oncotropism, and develop reovirus as a live, naturally attenuated vaccine vector for diverse pathogenic microorganisms.

Reovirus strain type 1 Lang (T1L) serves as the prototype for serotype 1 reoviruses. Like T3D, T1L infection has been extensively studied using cultured cells and *in vivo*. T1L and T3D display numerous phenotypic differences including receptor usage, activities of viral replication proteins, regulation of the interferon response to reovirus infection, apoptosis induction, growth in various types of primary and transformed cells, virulence, dissemination pathways, and cell and tissue tropism in newborn mice (Schiff et al., 2007). Reassortant viruses derived from co-infections of T1L and T3D have been used to define the genetic basis of several of these biologic polymorphisms. Such analyses have provided key insights into viral replication and disease mechanisms. A marker rescue system for T1L does not exist. However, the availability of tools to derive infectious T1L particles starting with plasmid templates would greatly expand the potential utility of reovirus reverse genetics by permitting any desired combinatorial exchange of T1L and T3D gene segments and providing an alternative genetic background to optimize cell targeting and vectoring capacity.

A reduction in the total number of plasmids necessary to initiate the reovirus replication cycle would improve certain practical aspects of the reverse genetics system including effort and costs associated with reagent preparation. A decreased plasmid requirement also theoretically carries the possibility of increased co-transfection efficiency resulting in enhanced virus isolation, which is particularly relevant to recovery of viruses that replicate poorly. Introduction of changes that handicap reovirus replicative fitness is a productive approach to the elucidation of structure–function relationships in viral proteins (Kirchner et al., 2008; Kobayashi et al., 2006, 2009). Therefore, technical enhancements such as construct consolidation that potentially lower the efficiency barrier to virus replication should strengthen system performance and broaden its utility.

In this report, we describe the establishment of reverse genetics for strain T1L and validate performance of this system by isolation of viable rsT1L and rsT3D single-gene reassortant viruses using plasmid vectors. We improved the reovirus reverse genetics system by consolidating viral gene-segment cDNAs into four plasmids. Compared to the 10-plasmid system, this strategy permits more efficient virus recovery than the 10-plasmid system from L cells using recombinant vaccinia virus as a source of T7 RNA polymerase. Finally, we show that both T1L and T3D can be recovered following plasmid transfection of baby hamster kidney (BHK) cells in which the T7 RNA polymerase is constitutively expressed. These enhancements to reverse genetics for reovirus represent a significant advance for this technology.

Results

Plasmid-based reverse genetics for reovirus T1L

To generate T1L from cloned cDNAs, plasmids encoding each gene segment were engineered in similar fashion to T3D cDNAs used for reverse genetics (Kobayashi et al., 2007; Fig. 1). Each plasmid contains one full-length gene-segment cDNA placed under control of the bacteriophage T7 RNA polymerase promoter and appended with the HDV ribozyme at the 3′terminus. These plasmids are anticipated to generate full-length (+)-sense RNAs containing native 5′ and 3′ ends following transcription with T7 RNA polymerase. L cells were infected with replication-defective T7 RNA polymerase-expressing vaccinia virus strain rDIs-T7pol 1 h prior to co-transfection with the 10 T1L cDNA plasmids. Recombinant viruses were recovered from cell-culture supernatants by plaque assay using L cell monolayers. Thus, rsT1L can be recovered from plasmid-transfected cells.

Characterization of T1L obtained using reverse genetics

Genomic dsRNA segments of different reovirus strains produce characteristic electrophoretic patterns when resolved using SDS–PAGE (Barton et al., 2001). To confirm that rsT1L contains the correct combination of gene segments, genomic dsRNA isolated from native T1L and rsT1L virions was electrophoresed in an SDS–polyacrylamide gel and visualized by ethidium bromide staining (Fig. 2A). The electropherotype of rsT1L was indistinguishable from that of native strain T1L. To exclude the possibility that rsT1L represents

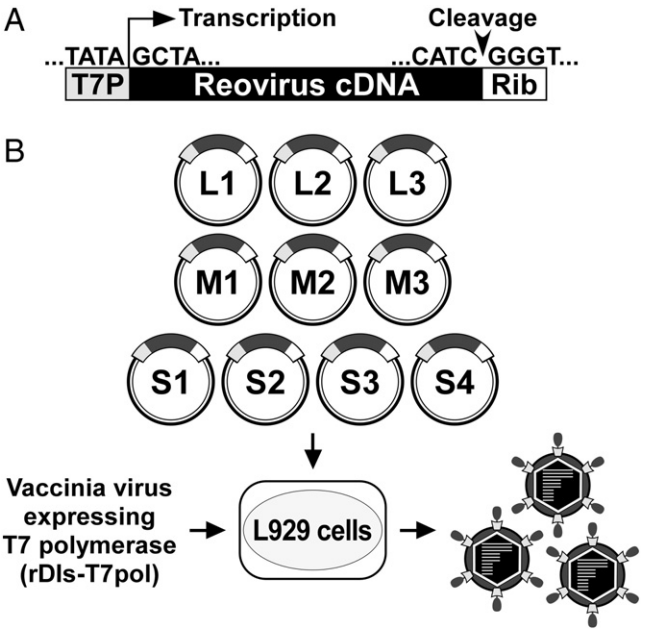

Fig. 1. Experimental strategy to generate reovirus type 1 Lang (T1L) from cloned cDNAs. (A) Rescue plasmids containing T1L gene-segment cDNAs. Vectors contain cDNAs representing each of the 10 full-length T1L gene segments. Reovirus cDNAs are flanked by the bacteriophage T7 RNA polymerase promoter (T7P) and the antigenomic hepatitis delta virus (HDV) ribozyme (Rib). (B) Reverse genetics procedure. The 10 T1L cDNA constructs are transfected into murine L cells that express T7 RNA polymerase from recombinant vaccinia virus strain DIs-T7pol. Plasmid-derived transcripts correspond to viral mRNAs with native 5′ termini. The 3′ termini of nascent transcripts are fused to HDV ribozyme sequences, which generate authentic 3′ ends through autocatalytic cleavage. After 5 days of incubation, transfected cells are lysed by freeze–thaw, and recombinant strain (rs) viruses are isolated from lysates by plaque assay using L cells.

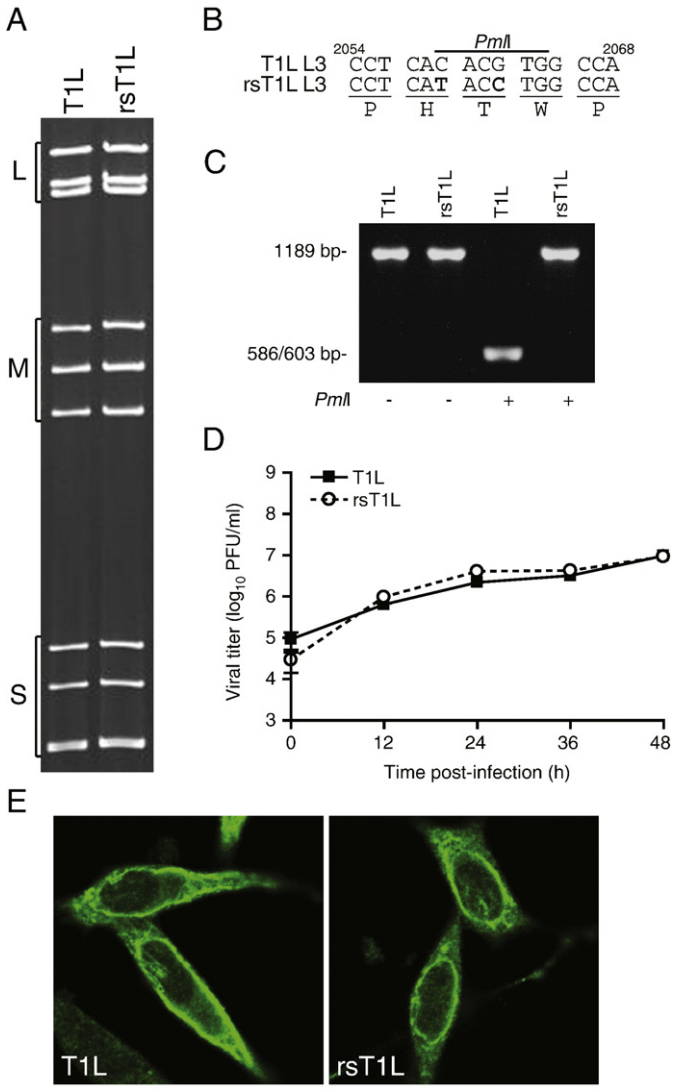

Fig. 2. Characterization of T1L viruses derived using reverse genetics. (A) Electropherotypes of native T1L and plasmid-derived rsT1L. Purified virions were electrophoresed in an SDS–polyacrylamide gel, followed by ethidium bromide staining to visualize viral gene segments. Size classes of gene segments (L, M, S) are indicated. (B) Novel mutations in the L3 gene of rs viruses. The C→T change at nucleotide 2059 and G→C change at nucleotide 2062 eliminate a unique PmlI site. (C) Digestion of the L3 gene RT-PCR products of T1L and rsT1L with PmlI to confirm the presence or absence of a unique restriction site. Size markers are indicated. (D) Growth of T1L and rsT1L. L cells were adsorbed with T1L or rsT1L at an MOI of 2 PFU/cell, and viral titers in cell lysates were determined by plaque assay at the times shown. Results are presented as mean viral titers for triplicate experiments. Error bars indicate S.D. (E) Immunofluorescence analysis of cells infected with T1L and rsT1L. L cells were adsorbed with either T1L or rsT1L and stained at 24 h post-infection with μNS-specific antiserum followed by a fluorophore-conjugated, goat-anti-rabbit secondary antibody to visualize reovirus inclusions. Representative images of T1L- and rsT1L-infected cells are shown.

contamination by native T1L, a unique PmlI site in the L3 gene was destroyed by the introduction of two silent point mutations into the L3 rescue plasmid: C to T at nucleotide 2059 and G to C at nucleotide 2062 (Fig. 2B). A 1189-bp fragment of the L3 gene was amplified using RT-PCR of viral dsRNA extracted from T1L and rsT1L virions. The L3 gene RT-PCR product derived from T1L was digested with PmlI to produce 586- and 603-bp fragments, whereas the L3 product derived from rsT1L was not (Fig. 2C), indicating that rsT1L originated from plasmids. To ascertain whether rsT1L and native T1L have similar replication kinetics, yields of rsT1L and T1L were quantified following infection of L cells at an MOI of 2 PFU/cell (Fig. 2D). Titers of rsT1L and T1L were virtually identical at all time points tested.

Reoviruses form characteristic cytoplasmic inclusions in infected cells (Becker et al., 2003; Kobayashi et al., 2009; Miller et al., 2004). These inclusions are thought to represent sites of viral genome replication and vary in morphology dependent on the infecting strain. T1L forms filamentous inclusions, whereas the inclusions formed by T3D are globular (Parker et al., 2002). To determine whether rsT1L inclusions are similar to those produced by T1L, L cells were infected with each virus, fixed at 24 h post-infection, and imaged using confocal microscopy (Fig. 2E). Inclusions formed by rsT1L and T1L were indistinguishable and displayed filamentous morphology. Taken together, these data demonstrate comparable replication characteristics of rsT1L and native T1L.

Generation of an improved reverse genetics system using four plasmid vectors

To reduce the number of plasmids required for reverse genetics, two or four T1L gene transcription cassettes encoding reovirus cDNAs flanked by the T7 RNA polymerase promoter and HDV ribozyme were combined in a single plasmid (Fig. 3A). Specifically, L1 and M2 (pT7-L1-M2T1L), L2 and M3 (pT7-L2-M3T1L), L3 and S3 (pT7-L3-S3T1L), and S1, S2, S4, and M1 (pT7-M1-S1-S2-S4T1L) transcription cassettes were jointly introduced into the rescue backbone plasmid using PCR to generate requisite restriction enzyme recognition sites compatible with multiplex cloning (Fig. 3A).

To assess rescue efficiency of the 4-plasmid system, L cells were infected with vaccinia virus strain rDIs-T7pol 1 h prior to transfection with the 4- or 10-plasmid vector set, and viral titers in transfected cell lysates were determined at 24 and 48 h post-transfection by plaque assay using L cell monolayers. Viral titers following transfection with 10 plasmids encoding the T1L genome were 10 and 1000 PFU/ml at 24 and 48 h, respectively. However, viral titers following transfection with the 4-plasmid T1L cDNA vector set were markedly higher at both 24 h (1000 PFU/ml) and 48 h (10,000 PFU/ml) post-transfection (Fig. 3B). Thus, transfection with four plasmids substantially enhances rescue efficiency.

A 4-plasmid reverse genetics system was also developed for T3D. Using this strategy, L1 and S1 (pT7-L1-S1T3D), L2 and M3 (pT7-L2-M3T3D), L3 and M1 (pT7-L3-M1T3D), and M2, S2, S3, and S4 (pT7-M2-S2-S3-S4T3D) gene cassettes were introduced into individual plasmids (Fig. 3C). To compare the efficiency of the T3D rescue systems, the T3D 4-plasmid and 10-plasmid vector sets were independently transfected into rDIs-T7pol-infected L cells, and viral titers in culture lysates were determined by plaque assay at 24 and 48 h. Viral titers in cultures transfected with 10 plasmids were below the limit of detection at 24 h and ~100 PFU/ml at 48 h. In contrast, L cell cultures transfected with four plasmids produced ~100 PFU/ml of virus at 24 h and ~1000 PFU/ml at 48 h (Fig. 3D). From these data, we conclude that both T1L and T3D can be recovered using four plasmids and that a reduction in plasmid number substantially improves rescue efficiency.

Generation of rsT1L×rsT3D monoreassortant viruses

Using a combination of the 4-plasmid and 10-plasmid rescue systems, we generated a panel of 20 rsT1L×rsT3D monoreassortant viruses. These viruses contain nine genes from one parental strain and one gene from the other. Genotypes of recovered viruses were confirmed using a combination of gene-segment electrophoretic mobility and sequence analysis (data not shown). The electrophoretic pattern of a representative monoreassortant, rsT1L-T3M1, which contains the T3D M1 gene segment in an otherwise T1L background, clearly shows co-migration of the M1 RNA with that of T3D (Fig. 4). Conversely, the M1 RNA of the reciprocal reassortant virus, rsT3D-T1M1, co-migrates with T1L M1. The generation of T1L×T3D monoreassortant viruses demonstrates the versatility of the reverse

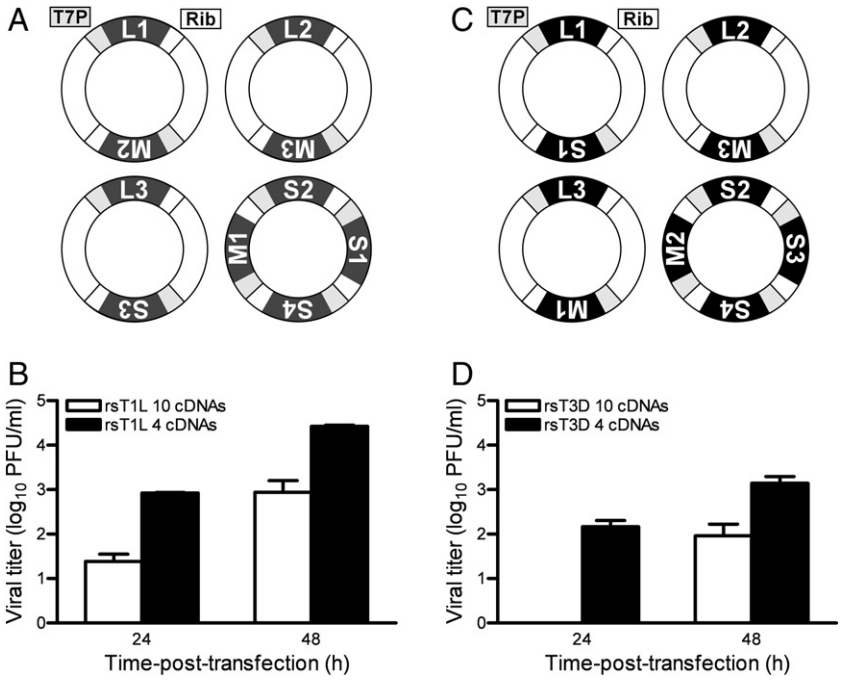

Fig. 3. Improved reverse genetics for reovirus strains T1L and T3D. (A, C) Two or four gene transcription cassettes encoding reovirus cDNAs flanked by the T7 RNA polymerase promoter and HDV ribozyme sequences were combined into single plasmids, creating four plasmids for the T1L and T3D reverse genetics systems. (B, D) L cells expressing T7 polymerase were co-transfected with either 4 or 10 rescue plasmids corresponding to the T1L (A,B) and T3D (C,D) genomes. Following 24 or 48 h incubation, transfected cells were lysed by freeze–thaw, and viral titers in cell lysates were determined by plaque assay. Results are presented as mean viral titers for triplicate experiments. Error bars indicate S.D.

genetics system to potentially rescue viruses with any desired genetic combination, including monoreassortants, which have traditionally been the most difficult to obtain by co-infection of cells with T1L and T3D.

Generation of rs viruses using BHK-T7 cells

BHK cells have been engineered to stably express T7 RNA polymerase (BHK-T7) under control of a cytomegalovirus promoter (Buchholz et al., 1999). To determine whether these cells allow recovery of viable reovirus following plasmid transfection, thus eliminating the requirement for rDIs-T7pol, we transfected BHK-T7 cells with the T1L or T3D 4-plasmid vector sets in the absence of rDIS-T7pol and determined viral titers in transfected cell lysates by plaque assay at 48 h post-transfection (Fig. 5). We found that transfection with either T1L or T3D cDNAs led to substantial viral titers at 48 h post-transfection. From these results, we conclude that BHK-T7 cells can be used as an alternative to rDIs-T7pol-infected L cells for the recovery of reovirus using plasmid vectors.

Discussion

The prototype strain for type 1 reovirus, T1L, has been studied extensively in replication and pathogenesis models. Therefore, a primary goal of this study was to generate a reverse genetics system for T1L. As demonstrated for strain T3D (Boehme et al., 2009; Danthi et al., 2008a, 2008b; Kirchner et al., 2008; Kobayashi et al., 2007, 2009; Zurney et al., 2009), development of a reverse genetics system for T1L affords an opportunity to leverage an extensive knowledge base of virus structure and biology toward further acceleration of basic and applied reovirus research. Here, we show production of T1L virions from cloned cDNAs. Similar to rsT3D and native T3D, the replication characteristics of rsT1L reflect native T1L. Growth kinetics, total yields, inclusion morphology, and genomic electrophoretic signatures were indistinguishable between T1L and rsT1L. These results further validate retention of native viral properties by plasmid-derived viruses. Moreover, development of the T1L rescue system will expand the utility of reverse genetics for studies of reovirus biology.

Analysis of a large panel of T1L×T3D reassortant viruses has shown that reovirus gene segments display nonrandom segregation upon co-infection of L cells by the parental strains (Nibert et al., 1996). This observation suggests that there may be interactions among viral proteins, RNAs, or both that influence reovirus evolution. Additionally, compensatory mutations that promote viral replication efficiency may be necessary to stabilize certain genetic combinations (Roner et al., 1995). Prior to this study, it was unclear whether generation of all 20 single-gene T1L×T3D reassortant viruses would be feasible due to uncertainties about the replicative fitness of gene constellations not previously isolated in T1L×T3D reassortant panels. Development of a fully plasmid-based rescue system for T1L will now allow systematic characterization of gene-segment co-evolution and may facilitate isolation of viruses with replication impediments or combinations of T1L and T3D genes normally disfavored in mixed infections (Nibert et al., 1996).

Establishment of reverse genetics for reovirus has allowed engineering of mutations into structural and nonstructural reovirus proteins and provided an opportunity to observe the effects of these mutations on viral replication and pathogenesis in the context of infection. However, the current system is limited by the inefficiency of transfection of 10 plasmids (Kobayashi et al., 2007). Therefore, a second goal of this study was to improve viral yields by reducing the number of plasmids required for virus recovery. This goal was accomplished by combining two or four transcriptional cassettes in a single plasmid, reducing the total number of plasmids from 10 to 4. Compared to the first-generation marker rescue system, the 4-plasmid strategy enhanced efficiency of virus recovery by reducing time to virus isolation and supporting increased total yields. The improved reverse genetics system also offers the economic advantage of requiring fewer reagents and less preparation time. Interestingly, recovery of T1L appears to be more efficient than T3D using either the 4- or 10-plasmid reverse genetics system. While the simplest explanation is that T1L exhibits an intrinsic replication advantage

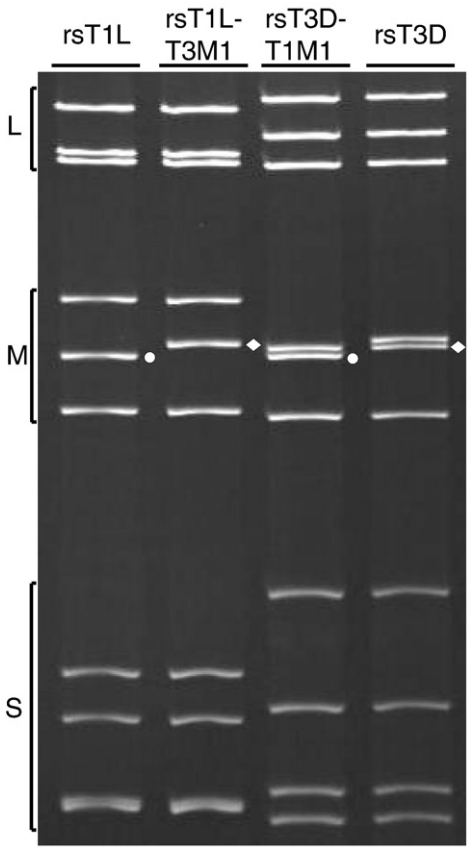

Fig. 4. Representative electropherotype of recombinant monoreassortant viruses. Purified virions of rsT1L, rsT3D, and T1L×T3D monoreassortants containing reciprocal exchanges of the M1 gene, rsT1L-T3M1 and rsT3D-T1M1, were electrophoresed in an SDS–polyacrylamide gel, followed by ethidium bromide staining to visualize viral gene segments. Size classes of gene segments (L, M, S) are shown. Positions of the T1L and T3D M1 genes are indicated by round and diamond symbols, respectively.

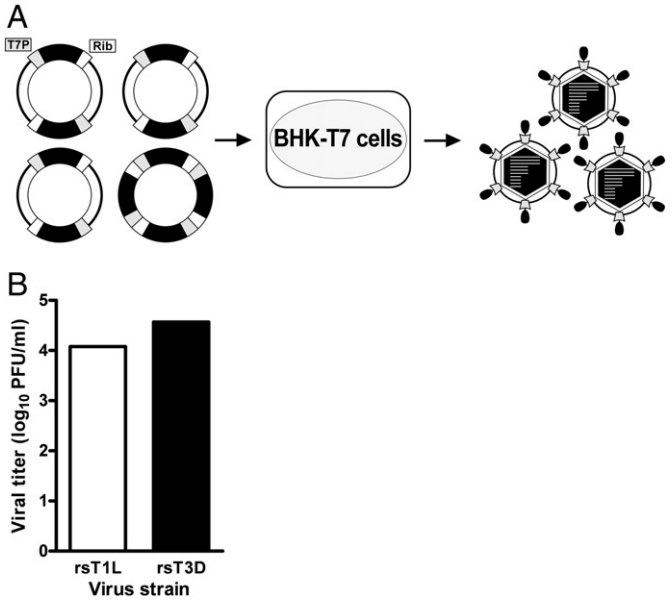

Fig. 5. Recombinant virus generated using BHK-T7 cells. (A) Schematic of reovirus reverse genetics system using BHK-T7 cells. (B) BHK-T7 cells were co-transfected with four rescue plasmids corresponding to the T1L and T3D genomes. Following 48-h incubation, transfected cells were lysed by freeze–thaw, and viral titers in cell lysates were determined by plaque assay.

over T3D in cell lines used for virus rescue, another possibility is that different gene arrangements between the T1L and T3D 4-plasmid systems contribute to higher yields of T1L. Whether genetic linkage within the rescue constructs affects virus production is unknown.

The 4-plasmid reverse genetics system reported here could conceivably enhance efficiency of virus recovery by three nonmutually exclusive mechanisms. First, since fewer plasmids are required to simultaneously enter a cell, the probability is increased that a full set of viral RNAs will accumulate to a critical threshold for replication initiation. While plasmids are provided in vast excess, there may be a limit to the amount of plasmid that can enter a single cell. Second, it is possible that only a small fraction of transfected plasmids avoid degradation and remain competent for transcription. By decreasing the number of plasmids from 10 to 4, the likelihood that a single cell will contain a sufficient number of intact transcription cassettes is enhanced. Third, it is possible that constraining transcription and translation of individual viral RNAs to the same intracellular microenvironment, as might be anticipated for multicistronic vectors, facilitates essential protein–protein or protein–RNA interactions required for virus recovery.

Technical complexities associated with manipulation of multicistronic vectors may limit their use for certain applications. Therefore, the 10-plasmid system remains a useful alterative for demanding cloning tasks. Tetracistronic vectors can be reduced to tricistronic constructs by simple endonucleolytic excision of a gene-segment cDNA and then complemented by co-transfection with the corresponding single-gene vector containing the desired mutations. We have found that the 4- and 10-plasmid vector systems are fully compatible for virus rescue. Hence, the monocistronic vectors remain important adjuncts to the 4-plasmid strategy by combining enhanced flexibility with gains in efficiency.

In our effort to improve reovirus reverse genetics, we found that BHK-T7 cells, which constitutively express T7 RNA polymerase (Buchholz et al., 1999), allow recovery of both rsT1L and rsT3D. The capacity of BHK-T7 cells to support virus rescue obviates the requirement for rDIs-T7pol and thereby greatly simplifies the rescue protocol. BHK-T7 cells are easier to maintain and propagate than rDIs-T7pol and thus provide an additional improvement to the reovirus rescue system.

Our progress with reovirus reverse genetics in many respects parallels the evolution of reverse genetics technology for influenza virus, which has also been modified to improve efficiency. Early reverse genetics systems for influenza virus required co-transfection of 12–16 plasmids encoding viral mRNAs or proteins (Neumann et al., 1999). Subsequently, the number of required plasmids was reduced to 8; each containing a viral gene flanked by both pol I and pol II promoters that drive viral genomic and messenger RNA expression, from the same cDNA (Hoffmann et al., 2000). As these systems were practical only in cell types supporting high transfection efficiencies, further improvements were achieved by combining eight RNA pol I transcription cassettes for viral RNA synthesis into a single plasmid and condensing three of the four protein expression cassettes onto one plasmid. The resulting 3-plasmid system increases efficiency of virus production in Vero cells, which are amenable to propagation of influenza vaccines for use in humans (Neumann et al., 2005). Hence, reverse genetics of viruses containing segmented genomes appears to be inherently inefficient, but this problem is surmountable through plasmid reduction.

We have established an improved reverse genetics system of reovirus that allows recovery of prototype strain T1L from plasmid vectors and reduces the number of plasmids for both the T1L and T3D systems. These enhancements have increased the flexibility and efficiency of reverse genetics for basic studies of reovirus biology and will accelerate development of reovirus for clinical and technological purposes.

Materials and methods

Cells and viruses

L cells were grown in Joklik's modified Eagle's minimal essential medium (Irvine Scientific) supplemented to contain 5% fetal calf serum (Gibco), 2 mM L-glutamine, 100 U of penicillin G/ml, 100 μg of streptomycin/ml, and 0.25 μg amphotericin B/ml (Gibco). BHK-T7 cells were grown in Dulbecco's modified Eagle's minimal essential medium (Invitrogen) supplemented to contain 5% fetal calf serum, 2 mM L-glutamine, 2% MEM amino acid solution (Invitrogen), and 1 mg/ml geneticin (Invitrogen). Reovirus strains T1L and T3D are laboratory stocks originally obtained from the laboratory of Dr. Bernard Fields. Strain rsT3D was produced by reverse genetics (Kobayashi et al., 2007). Virus was purified from L cells by CsCl-gradient centrifugation (Furlong et al., 1988). Viral titers were determined by plaque assay using L cell monolayers as described (Virgin et al., 1988). Attenuated vaccinia virus strain rDIs-T7pol expressing T7 RNA polymerase (Ishii et al., 2002) was propagated in chicken embryo fibroblasts.

Plasmid construction

T1L plasmid cDNAs for rescue of recombinant infectious reovirus were constructed using RT-PCR, viral genomic RNA, and gene-specific primer sets (Table 1). RT-PCR products were cloned into the SmaI–RsrII (L1, L2, and S3), SmaI–BseRI (S2), EcoRV–RsrII (M3), or EcoRV–BseRI (S4) sites of p3E5EGFP (Watanabe et al., 2004), resulting in pT7-L1T1L, pT7-L2T1L, pT7-M3T1L, pT7-S2T1L, pT7-S3T1L, and pT7-S4T1L. The T1L L3 gene cDNA, amplified from viral genomic RNA with specific primers (Table 1), was inserted into the EcoRI–RsrII site of pT7-L3T3D (Kobayashi et al., 2007), thereby replacing the T3D L3 cDNA and generating pT7-L3T1L. pT7-M2T1L was constructed by insertion into the p3E5EGFP RsrII site of RT-PCR amplification products generated with viral genomic RNA and specific primers (Table 1). The resulting construct containing the cloned T1L M2 gene was digested with SmaI and AvrII, followed by self-ligation to remove GFP-encoding sequences and the Ebola virus leader and trailer sequences. pT7-M1T1L and pBacT7-S1T1L, encoding T1L M1 and S1 genes, respectively, were described previously (Kobayashi et al., 2007, 2009).

Recombinant reovirus generation from four plasmids was facilitated by combining two or four viral gene transcription cassettes encoding T1L and T3D reovirus cDNAs flanked by the T7 RNA polymerase promoter (5′) and HDV ribozyme (3′) onto one plasmid. Bicistronic reovirus cDNA constructs pT7-L1-M2T1L (T1L L1 and M2), pT7-L2-M3T1L (T1L L2 and M3), pT7-L3-S3T1L (T1L L3 and S3), pT7-L1-S1T3D (T3D L1 and S1), pT7-L2-M3T3D (T3D L2 and M3), and pT7-L3-M1 (T3D L3 and M1) were generated by cloning PCR-amplified T1L M2, T1L M3, T1L S3, T3D S1, T3D M3, and T3D M1 gene transcription cassettes into the SphI site of pT7-L1T1L, NheI site of pT7-L2T1L, HindIII site of pT7-L3T1L, HindIII site of pT7-L1T3D, NheI site of pT7-L2T3D, and HindIII site of pT7-L3T3D, respectively. Tetracistronic reovirus cDNA constructs, pT7-M1-S1-S2-S4T1L (T1L S1, S2, S4, and M1) and pT7-M2-S2-S3-S4T3D (T3D S2, S3, S4, and M2), were generated by cloning PCR-amplified T1L S3, T1L S4, T1L M1, T3D S3, T3D S4, and T3D M2 gene transcription cassettes into the XbaI (T1L S1), SalI (T1L S4), or NheI (T1L M1) sites of pT7-S2T1L or SalI–HindIII (T3D S3), HindIII–NheI (T3D S4), or NheI (T3D M2) sites of pT7-S2T3D.

Plasmid transfection and recovery of recombinant virus using L cells

Monolayers of L cells at 90% confluency (approximately 3×10^6 cells) seeded in 60-mm dishes (Costar) were infected with rDIs-T7pol at an MOI of approximately 0.5 $TCID_{50}$. At 1 h post-infection, cells were co-transfected with plasmids representing the cloned reovirus genome using 3 μl of TransIT-LT1 transfection reagent (Mirus) per microgram of plasmid DNA. The amount of each plasmid used for transfection was given as follows: pT7-L1T1L, 2 μg; pT7-L2T1L, 2 μg; pT7-L3T1L, 2 μg; pT7-M1T1L, 1.75 μg; pT7-M2T1L, 1.75 μg; pT7-M3T1L, 1.75 μg; pBacT7-S1T1L, 2 μg; pT7-S2T1L, 1.5 μg; pT7-S3T1L, 1.5 μg; pT7-S4T1L, 1.5 μg; pT7-L1-M2T1L, 4.5 μg; pT7-L2-M3T1L, 4.5 μg; pT7-L3-M3T1L, 4.5 μg; pT7-M1-S1-S2-S4T1L, 4.5 μg; pT7-L1-S1T3D, 4.5 μg; pT7-L2-M3T3D, 4.5 μg; pT7-L3-M1T3D, 4.5 μg; and pT7-M2-S2-S3-S4T3D, 4.5 μg. Quantities of T3D monocistronic plasmid were used as previously described (Kobayashi et al., 2007). Following 1–5 days of incubation, recombinant virus was isolated from transfected cells by plaque purification using L cells (Virgin et al., 1988).

SDS–PAGE analysis of viral gene segments

Purified virions (5×10^{10} particles) were loaded into wells of 10% SDS–polyacrylamide gels. Gels were electrophoresed for approximately 600 m Amp-h. Gene segments were visualized by ethidium bromide staining.

Quantification of virus infectivity

Monolayers of L cells (5×10^5 cells) seeded in 24-well plates (Costar) were adsorbed with virus at an MOI of 2 PFU/cell. After 1 h adsorption at room temperature, the inoculum was removed, cells were washed with PBS, and fresh medium was added. Cells were incubated at 37 °C for various intervals, and viral titers in cell lysates were determined by plaque assay using L cells (Virgin et al., 1988).

Table 1
Oligodeoxynucleotide primers used for plasmid construction.

Plasmid DNA	Nucleotide sequence[a]	
pT7-L1T1L	Forward	5'-TAACCCGGGTAATACGACTCACTATAGCTACACGTTCCACGACAATGTCATCCA-3'
	Reverse	5'-GGTCGGACCGCGAGGAGGTGGAGATGCCATGCCGACCCGATGAGTTGACGCACCACGACCCAT-3'
pT7-L2T1L	Forward	5'-TAACCCGGGTAATACGACTCACTATAGCTATTGGCGCAATGGCGAACGTTTGGG-3'
	Reverse	5'-GGTCGGACCGCGAGGAGGTGGAGATGCCATGCCGACCCGATGAATTAGGCACGCTCACGAGGG-3'
pT7-L3T1L	Forward	5'-TAAGAATTCTAATACGACTCACTATAGCTAATCGTCAGGATGAAGCGGATTCCA-3'
	Reverse	5'-GGTCGGACCGCGAGGAGGTGGAGATGCCATGCCGACCCGATGAATCGGCCCAACTAGCATCGA-3'
pT7-M2T1L	Forward	5'-CCTCGCGGTCCGACCTGGGGTTAATACGACTCACTATAGCTAATCTGCTGACCGTCACTCT-3'
	Reverse	5'-GGTCGGACCGCGAGGAGGTGGAGATGCCATGCCGACCCGATGATGTGCCTGCACCCTTAACC-3'
pT7-M3T1L	Forward	5'-TAAGATATCTAATACGACTCACTATAGCTAAAGTGACCGTGGTCATGGCTTCAT-3'
	Reverse	5'-GGTCGGACCGCGAGGAGGTGGAGATGCCATGCCGACCCGATGAATAGGGGTCGGGAAGGCTTA-3'
pT7-S2T1L	Forward	5'-TAACCCGGGTAATACGACTCACTATAGCTATTCGCTGGTCAGTTATGGCT-3'
	Reverse	5'-ACCGCGAGGAGGTGGAGATGCCATGCCGACCCGATGAATGTGTGGTCAGTCGTGAGGGGTGTG-3'
pT7-S3T1L	Forward	5'-TAACCCGGGTAATACGACTCACTATAGCTAAAGTCACGCCTGTTGTCGTCAC-3'
	Reverse	5'-GGTCGGACCGCGAGGAGGTGGAGATGCCATGCCGACCCGATGATTAGGCGCCACCCACCACC-3'
pT7-S4T1L	Forward	5'-TAAGATATCTAATACGACTCACTATAGCTATTTTTGCCTCTTCCCAAACG-3'
	Reverse	5'-CGCGAGGAGGTGGAGATGCCATGCCGACCCGATGAATGGAGCCTGTCCCACGTC-3'

[a] The T7 RNA polymerase promoter sequence is underlined.

Immunofluorescence detection of reovirus infection

L cells were plated on glass coverslips in 24-well plates (Costar) and adsorbed at an MOI of 2 PFU/cell. Following incubation at 37 °C for 24 h, cells were fixed and stained with rabbit μNS antiserum followed by fluorophore-conjugated, goat anti-rabbit secondary antibody (Invitrogen). Images were acquired using a Zeiss LSM 510 META inverted confocal system (Carl Zeiss) with a Zeiss inverted Axiovert 200M microscope.

Plasmid transfection and recovery of recombinant virus using BHK-T7 cells

Monolayers of BHK-T7 cells at 90% confluency (approximately 3×10^6 cells) seeded in 60-mm dishes were co-transfected with plasmids representing the cloned reovirus genome using 3 μl of TransIT-LT1 transfection reagent (Mirus) per microgram of plasmid DNA. The amount of each plasmid used for transfection was identical to that described for L cell transfection. Following 1–5 days of incubation, recombinant virus was isolated from transfected cells by plaque purification using monolayers of L cells (Virgin et al., 1988).

Acknowledgments

We thank Yoshihiro Kawaoka for plasmid p3E5EGFP, Tatsuo Miyamura and Koji Ishii for vaccinia virus rDIs-T7pol, and Ulla Buchholz for BHK-T7 cells. This research was supported by a fellowship from the Naito Foundation (T.K.), K08 AI62862 (J.D.C.), R01 AI32539, R37 AI38296, and the Elizabeth B. Lamb Center for Pediatric Research.

References

Almazan, F., Gonzalez, J.M., Penzes, Z., Izeta, A., Calvo, E., Plana-Duran, J., Enjuanes, L., 2000. Engineering the largest RNA virus genome as an infectious bacterial artificial chromosome. Proc. Natl. Acad. Sci. U. S. A. 97 (10), 5516–5521.

Barton, E.S., Connolly, J.L., Forrest, J.C., Chappell, J.D., Dermody, T.S., 2001. Utilization of sialic acid as a coreceptor enhances reovirus attachment by multistep adhesion strengthening. J. Biol. Chem. 276, 2200–2211.

Becker, M.M., Peters, T.R., Dermody, T.S., 2003. Reovirus σNS and μNS proteins form cytoplasmic inclusion structures in the absence of viral infection. J. Virol. 77 (10), 5948–5963.

Boehme, K.W., Guglielmi, K.M., Dermody, T.S., 2009. Reovirus nonstructural protein σ1s is required for establishment of viremia and systemic dissemination. Proc. Natl. Acad. Sci. U. S. A. 106 (47), 19986–19991.

Bridgen, A., Elliott, R.M., 1996. Rescue of a segmented negative-strand RNA virus entirely from cloned complementary DNAs. Proc. Natl. Acad. Sci. U. S. A. 93 (26), 15400–15404.

Buchholz, U.J., Finke, S., Conzelmann, K.K., 1999. Generation of bovine respiratory syncytial virus (BRSV) from cDNA: BRSV NS2 is not essential for virus replication in tissue culture, and the human RSV leader region acts as a functional BRSV genome promoter. J. Virol. 73 (1), 251–259.

Coley, S.E., Lavi, E., Sawicki, S.G., Fu, L., Schelle, B., Karl, N., Siddell, S.G., Thiel, V., 2005. Recombinant mouse hepatitis virus strain A59 from cloned, full-length cDNA replicates to high titers in vitro and is fully pathogenic in vivo. J. Virol. 79 (5), 3097–3106.

Collins, P.L., Hill, M.G., Camargo, E., Grosfeld, H., Chanock, R.M., Murphy, B.R., 1995. Production of infectious human respiratory syncytial virus from cloned cDNA confirms an essential role for the transcription elongation factor from the 5′ proximal open reading frame of the M2 mRNA in gene expression and provides a capability for vaccine development. Proc. Natl. Acad. Sci. U. S. A. 92 (25), 11563–11567.

Danthi, P., Coffey, C.M., Parker, J.S., Abel, T.W., Dermody, T.S., 2008a. Independent regulation of reovirus membrane penetration and apoptosis by the μ1 ϕ domain. PLoS Pathog. 4 (12), e1000248.

Danthi, P., Kobayashi, T., Holm, G.H., Hansberger, M.W., Abel, T.W., Dermody, T.S., 2008b. Reovirus apoptosis and virulence are regulated by host cell membrane-penetration efficiency. J. Virol. 82 (1), 161–172.

Fodor, E., Devenish, L., Engelhardt, O.G., Palese, P., Brownlee, G.G., Garcia-Sastre, A., 1999. Rescue of influenza A virus from recombinant DNA. J. Virol. 73 (11), 9679–9682.

Furlong, D.B., Nibert, M.L., Fields, B.N., 1988. Sigma 1 protein of mammalian reoviruses extends from the surfaces of viral particles. J. Virol. 62 (1), 246–256.

Garcin, D., Pelet, T., Calain, P., Roux, L., Curran, J., Kolakofsky, D., 1995. A highly recombinogenic system for the recovery of infectious Sendai paramyxovirus from cDNA: generation of a novel copy-back nondefective interfering virus. EMBO J. 14 (24), 6087–6094.

Gritsun, T.S., Gould, E.A., 1995. Infectious transcripts of tick-borne encephalitis virus, generated in days by RT-PCR. Virology 214 (2), 611–618.

Hoffmann, E., Neumann, G., Hobom, G., Webster, R.G., Kawaoka, Y., 2000. "Ambisense" approach for the generation of influenza A virus: vRNA and mRNA synthesis from one template. Virology 267 (2), 310–317.

Ishii, K., Ueda, Y., Matsuo, K., Matsuura, Y., Kitamura, T., Kato, K., Izumi, Y., Someya, K., Ohsu, T., Honda, M., Miyamura, T., 2002. Structural analysis of vaccinia virus DIs strain: application as a new replication-deficient viral vector. Virology 302, 433–444.

Kelly, K., Nawrocki, S., Mita, A., Coffey, M., Giles, F.J., Mita, M., 2009. Reovirus-based therapy for cancer. Expert Opin. Biol. Ther. 9 (7), 817–830.

Kinney, R.M., Butrapet, S., Chang, G.J., Tsuchiya, K.R., Roehrig, J.T., Bhamarapravati, N., Gubler, D.J., 1997. Construction of infectious cDNA clones for dengue 2 virus: strain 16681 and its attenuated vaccine derivative, strain PDK-53. Virology 230 (2), 300–308.

Kirchner, E., Guglielmi, K.M., Strauss, H.M., Dermody, T.S., Stehle, T., 2008. Structure of reovirus σ1 in complex with its receptor junctional adhesion molecule-A. PLoS Pathog. 4 (12), e1000235.

Kobayashi, T., Chappell, J.D., Danthi, P., Dermody, T.S., 2006. Gene-specific inhibition of reovirus replication by RNA interference. J. Virol. 80 (18), 9053–9063.

Kobayashi, T., Antar, A.A.R., Boehme, K.W., Danthi, P., Eby, E.A., Guglielmi, K.M., Holm, G.H., Johnson, E.M., Maginnis, M.S., Naik, S., Skelton, W.B., Wetzel, J.D., Wilson, G.J., Chappell, J.D., Dermody, T.S., 2007. A plasmid-based reverse genetics system for animal double-stranded RNA viruses. Cell Host Microbe 1, 147–157.

Kobayashi, T., Ooms, L.S., Chappell, J.D., Dermody, T.S., 2009. Identification of functional domains in reovirus replication proteins μNS and μ2. J. Virol. 83 (7), 2892–2906.

Lawson, N.D., Stillman, E.A., Whitt, M.A., Rose, J.K., 1995. Recombinant vesicular stomatitis viruses from DNA. Proc. Natl. Acad. Sci. U. S. A. 92 (10), 4477–4481.

Miller, C.L., Parker, J.S., Dinoso, J.B., Piggott, C.D., Perron, M.J., Nibert, M.L., 2004. Increased ubiquitination and other covariant phenotypes attributed to a strain- and temperature-dependent defect of reovirus core protein μ2. J. Virol. 78 (19), 10291–10302.

Neumann, G., Watanabe, T., Ito, H., Watanabe, S., Goto, H., Gao, P., Hughes, M., Perez, D.R., Donis, R., Hoffmann, E., Hobom, G., Kawaoka, Y., 1999. Generation of influenza A viruses entirely from cloned cDNAs. Proc. Natl. Acad. Sci. U. S. A. 96 (16), 9345–9350.

Neumann, G., Fujii, K., Kino, Y., Kawaoka, Y., 2005. An improved reverse genetics system for influenza A virus generation and its implications for vaccine production. Proc. Natl. Acad. Sci. U. S. A. 102 (46), 16825–16829.

Nibert, M.L., Margraf, R.L., Coombs, K.M., 1996. Nonrandom segregation of parental alleles in reovirus reassortants. J. Virol. 70 (10), 7295–7300.

Parker, J.S., Broering, T.J., Kim, J., Higgins, D.E., Nibert, M.L., 2002. Reovirus core protein μ2 determines the filamentous morphology of viral inclusion bodies by interacting with and stabilizing microtubules. J. Virol. 76 (9), 4483–4496.

Racaniello, V.R., Baltimore, D., 1981. Cloned poliovirus complementary DNA is infectious in mammalian cells. Science 214 (4523), 916–919.

Rice, C.M., Grakoui, A., Galler, R., Chambers, T.J., 1989. Transcription of infectious yellow fever RNA from full-length cDNA templates produced by in vitro ligation. New Biol. 1 (3), 285–296.

Roner, M.R., Lin, P.N., Nepluev, I., Kong, L.J., Joklik, W.K., 1995. Identification of signals required for the insertion of heterologous genome segments into the reovirus genome. Proc. Natl. Acad. Sci. U. S. A. 92 (26), 12362–12366.

Schiff, L.A., Nibert, M.L., Tyler, K.L., 2007. Orthoreoviruses and their replication, In: Knipe, D.M., Howley, P.M. (Eds.), Fifth ed. Fields Virology, Vol. 2. Lippincott Williams & Wilkins, Philadelphia, pp. 1853–1915. 2 vols.

Schneider, U., Schwemmle, M., Staeheli, P., 2005. Genome trimming: a unique strategy for replication control employed by Borna disease virus. Proc. Natl. Acad. Sci. U. S. A. 102 (9), 3441–3446.

Schnell, M.J., Mebatsion, T., Conzelmann, K.K., 1994. Infectious rabies viruses from cloned cDNA. EMBO J. 13 (18), 4195–4203.

Virgin IV, H.W., Bassel-Duby, R., Fields, B.N., Tyler, K.L., 1988. Antibody protects against lethal infection with the neurally spreading reovirus type 3 (Dearing). J. Virol. 62 (12), 4594–4604.

Watanabe, S., Watanabe, T., Noda, T., Takada, A., Feldmann, H., Jasenosky, L.D., Kawaoka, Y., 2004. Production of novel Ebola virus-like particles from cDNAs: an alternative to Ebola virus generation by reverse genetics. J. Virol. 78, 999–1005.

Whelan, S.P., Ball, L.A., Barr, J.N., Wertz, G.T., 1995. Efficient recovery of infectious vesicular stomatitis virus entirely from cDNA clones. Proc. Natl. Acad. Sci. U. S. A. 92 (18), 8388–8392.

Yoneda, M., Guillaume, V., Ikeda, F., Sakuma, Y., Sato, H., Wild, T.F., Kai, C., 2006. Establishment of a Nipah virus rescue system. Proc. Natl. Acad. Sci. U. S. A. 103 (44), 16508–16513.

Yount, B., Curtis, K.M., Fritz, E.A., Hensley, L.E., Jahrling, P.B., Prentice, E., Denison, M.R., Geisbert, T.W., Baric, R.S., 2003. Reverse genetics with a full-length infectious cDNA of severe acute respiratory syndrome coronavirus. Proc. Natl. Acad. Sci. U. S. A. 100 (22), 12995–13000.

Yun, S.I., Kim, S.Y., Rice, C.M., Lee, Y.M., 2003. Development and application of a reverse genetics system for Japanese encephalitis virus. J. Virol. 77 (11), 6450–6465.

Zurney, J., Kobayashi, T., Holm, G.H., Dermody, T.S., Sherry, B., 2009. Reovirus μ2 protein inhibits interferon signaling through a novel mechanism involving nuclear accumulation of interferon regulatory factor 9. J. Virol. 83 (5), 2178–2187.

APPENDIX D

A POST-ENTRY STEP IN THE MAMMALIAN ORTHOREOVIRUS REPLICATION CYCLE IS A DETERMINANT OF CELL TROPISM

Laura S. Ooms, Takeshi Kobayashi, Terence S. Dermody, and James D. Chappell

Journal of Biological Chemistry. 285(53) 41604-13; 2010

THE JOURNAL OF BIOLOGICAL CHEMISTRY VOL. 285, NO. 53, pp. 41604–41613, December 31, 2010

A Post-entry Step in the Mammalian Orthoreovirus Replication Cycle Is a Determinant of Cell Tropism*

Received for publication, August 20, 2010, and in revised form, October 25, 2010 Published, JBC Papers in Press, October 26, 2010, DOI 10.1074/jbc.M110.176255

Laura S. Ooms[‡§], Takeshi Kobayashi[§¶1], Terence S. Dermody[§¶‖], and James D. Chappell[‡§¶2]

From the Departments of [‡]Pathology, [¶]Pediatrics, and [‖]Microbiology and Immunology and the [§]Elizabeth B. Lamb Center for Pediatric Research, Vanderbilt University School of Medicine, Nashville, Tennessee 37232

Mammalian reoviruses replicate in a broad range of hosts, cells, and tissues. These viruses display strain-dependent variation in tropism for different types of cells *in vivo* and *ex vivo*. Early steps in the reovirus life cycle, attachment, entry, and disassembly, have been identified as pivotal points of virus-cell interaction that determine the fate of infection, either productive or abortive. However, in studies of the differential capacity of reovirus strains type 1 Lang and type 3 Dearing to replicate in Madin-Darby canine kidney (MDCK) cells, we found that replication efficiency is regulated at a late point in the viral life cycle following primary transcription and translation. Results of genetic studies using recombinant virus strains show that reovirus tropism for MDCK cells is primarily regulated by replication protein μ2 and further influenced by the viral RNA-dependent RNA polymerase protein, λ3, depending on the viral genetic background. Furthermore, μ2 residue 347 is a critical determinant of replication efficiency in MDCK cells. These findings indicate that components of the reovirus replication complex are mediators of cell-selective viral replication capacity at a post-entry step. Thus, reovirus cell tropism may be determined at early and late points in the viral replication program.

Viral tropism, defined by the range of hosts and tissues productively infected, creates natural biologic groupings among viruses that correlate with infection pathology, clinical disease expression, and epidemiology. Delineating the molecular basis of viral cell tropism is fundamental to the elucidation of disease mechanisms and the identification of viral and cellular targets for treatment and prevention of infection. Growing threats posed by zoonotic viral diseases with global pandemic potential (1) underscore the necessity for an enhanced understanding of unifying principles that influence viral tropism and host range. We are conducting studies using mammalian reoviruses to better understand the nature of virus-cell interactions that dictate unique tropism properties.

Mammalian orthoreoviruses (hereafter referred to as reoviruses) are an established model for studies of viral replication and pathogenesis (2–6). Reoviruses have contributed to the development of paradigms of viral disease based on discrete patterns of viral tropism for particular host cells and tissues. The reovirus virion is a nonenveloped, double layered, icosahedral particle consisting of an outer shell surrounding an inner core that contains 10 double-stranded (ds) RNA gene segments. The viral genome encodes eight structural and three nonstructural proteins. Viral RNA gene segments can be resolved into small, medium, and large size classes by SDS-PAGE, corresponding to σ, μ, and λ proteins, respectively. Four reovirus serotypes have been identified based on neutralization and hemagglutination studies (7–9). Strains type 1 Lang (T1) [3] and type 3 Dearing (T3) serve as prototypes for serotype 1 and 3 reoviruses, respectively. T1 and T3 display numerous phenotypic differences, and the genetic basis of several biologic polymorphisms has been defined using reassortant viruses derived from co-infections of T1 and T3 (6). Such analyses have provided key insights into the mechanisms of viral replication and disease.

The reovirus replication program (reviewed in Ref. 6) begins with attachment using proteinaceous or carbohydrate receptors followed by entry into host cells by receptor-mediated endocytosis. Proteolytic disassembly of the outer capsid within endosomes facilitates membrane penetration, leading to release of transcriptionally active cores into the cytoplasm. Full-length, positive-strand, capped, and nonpolyadenylated RNAs synthesized by core particles serve as templates for translation and synthesis of new genomic dsRNA. Secondary viral mRNAs transcribed from new dsRNA templates fuel subsequent rounds of protein synthesis. The source of these late transcripts is presumed to be subviral particles. Virion assembly is completed by the addition of outer capsid proteins to core particles. Reovirus replication and assembly are thought to occur within viral intracytoplasmic inclusions (10), which strictly depend on nonstructural proteins σNS and μNS and structural protein μ2 for proper formation and function in reovirus-infected cells (11, 12). Inclusions are de-

* This work was supported, in whole or in part, by National Institutes of Health Grants K08 AI62862 (to J. D. C.) and R01 AI32539 (to T. S. D.) from the United States Public Health Service. This work was supported by the Vanderbilt Department of Pathology (to L. S. O.), a fellowship from the Naito Foundation (to T. K.), and the Elizabeth B. Lamb Center for Pediatric Research.

The nucleotide sequence(s) reported in this paper has been submitted to the GenBank™/EBI Data Bank with accession number(s) NC_004271, X59945, EF494435, and EF494438.

[1] Present address: Institute for Virus Research, Kyoto University, Kyoto 606-8507, Japan.

[2] To whom correspondence should be addressed: Lamb Center for Pediatric Research, D7235 MCN, Vanderbilt University School of Medicine, Nashville, TN 37232. Tel.: 615-322-3640; Fax: 615-343-9723; E-mail: jim.chappell@vanderbilt.edu.

[3] The abbreviations used are: T1, type 1 Lang; T3, type 3 Dearing; MDCK, Madin Darby canine kidney; L cells, murine 929 L cells; dsRNA, double-stranded RNA; RdRp, RNA-dependent RNA polymerase; pfu, plaque-forming unit; m.o.i., multiplicity of infection; qPCR, quantitative PCR.

tectable within 4 h post-infection, lack a delimiting membrane, contain viral proteins, dsRNA and virion particles at various stages of morphogenesis, and are composed of highly ordered arrays of mature virions at late times of infection (13–19).

The 83-kDa μ2 protein, encoded by the M1 gene segment, is essential for viral replication (20). The μ2 protein functions in viral transcription (21, 22) and virion particle assembly (22). As an integral component of viral inclusions, μ2 determines kinetics of inclusion formation (23) and inclusion morphology (24). Fluorescence microscopy performed on a variety of cell types has shown that T1 and T3 form filamentous and globular inclusions, respectively (11, 20, 23, 24), which is explained by a differential capacity of T1 and T3 μ2 proteins to bind microtubules and anchor inclusions to the cytoskeleton (24).

The μ2 protein is a component of the reovirus core, which contains ~20 molecules of μ2 per virion particle (6, 25, 26). Although the precise position of μ2 is unknown, several lines of evidence from biochemical, structural, and genetic studies indicate that μ2 resides at the vertex base in close approximation to λ3, the viral RNA-dependent RNA polymerase (RdRp) (22, 27–31). Single-stranded RNA and dsRNA (32) are bound by μ2, which possesses nucleotide triphosphatase and RNA triphosphatase activities enhanced by the presence of λ3 (27, 28). Two regions of μ2 sequence bare similarity to the nucleotide-binding motifs of ATPases and are essential for triphosphatase action (27). Strain-specific differences in transcriptional efficiency of core particles are determined by μ2 (21), and reovirus strains containing temperature-sensitive lesions in μ2 protein display defects in replication and particle assembly at restrictive temperatures (22). Thus, μ2 is a probable subunit of the functional reovirus polymerase complex.

In addition to its central place in viral replication, μ2 also regulates reovirus cell tropism and virulence. Strain-dependent viral replication efficiency has been genetically linked to μ2 in studies using primary and transformed cells, including murine cardiac cells (33–36), bovine aortic endothelial cells (37), and Madin-Darby canine kidney (MDCK) cells (38). The capacity of reovirus to cause myocarditis in neonatal mice is regulated by μ2 and tied to the innate antiviral response. Reovirus induction of and sensitivity to type 1 interferon (IFN) in cardiac myocytes is coupled through μ2 to viral replication efficiency, organ pathology, and survival (34–36). The μ2 protein of myocarditic strains such as T1 antagonizes the IFN response by mediating nuclear sequestration of interferon regulatory factor-9 (39).

A previous study using T1 × T3 reassortant viruses showed that the M1 and λ3-encoding L1 genes segregate with differences in the replication efficiency of T1 and T3 in MDCK cells (38). This dichotomy presents a useful experimental platform to rigorously address the individual and cooperative roles of μ2 and λ3 in reovirus cell tropism and identify μ2-sensitive steps in the viral life cycle. Therefore, we conducted studies to genetically and biochemically characterize strain-specific differences in reovirus replication efficiency in MDCK cells. Our findings indicate the μ2 protein is the primary determinant of viral replication efficiency in these cells and that λ3 is a conditional co-regulator of μ2 function depending on the viral genetic background. Furthermore, the critical μ2-dependent step in MDCK cells occurs at a later point in the reovirus replication program subsequent to primary rounds of viral transcription and translation. These results enhance our understanding of the viral replication apparatus and the viral and cellular requirements crucial for its activity.

EXPERIMENTAL PROCEDURES

Cells and Viruses—L cells were grown in Joklik's modified Eagle's minimal essential medium (Lonza, Walkersville, MD) supplemented to contain 5% fetal calf serum (Cellgro, Manassas, VA), 2 mM L-glutamine (Invitrogen), 100 units of penicillin G/ml (Invitrogen), 100 μg of streptomycin/ml (Invitrogen), and 0.25 μg of amphotericin B/ml (Sigma). MDCK cells were grown in DMEM supplemented to contain 4.5 g/liter sodium pyruvate (Cellgro), 10% fetal calf serum, 2 mM L-glutamine, 100 units of penicillin G/ml, 100 μg of streptomycin/ml, and 0.25 μg of amphotericin B/ml. BHK-T7 cells were grown in DMEM (Invitrogen) supplemented to contain 5% fetal calf serum, 2 mM L-glutamine, 2% minimal essential medium amino acid solution (Invitrogen), and 1 mg/ml geneticin (Invitrogen). Strains T1, T3, T1-T3M1, T3-T1M1, and all other reassortant strains used in this study were recovered by reverse genetics as described previously (40, 41). Virus was purified from L cells by CsCl gradient centrifugation (42). Viral titers were determined by plaque assay using L cell monolayers as described previously (43). Attenuated vaccinia virus strain rDIs-T7pol expressing T7 RNA polymerase (44) was propagated in chicken embryo fibroblasts (40).

Construction of Mutant Viruses—T1 × T3 M1 chimeric cDNAs were generated by inserting the EcoRV-RsrII (Ch1), MfeI-RsrII (Ch2), PsiI-RsrII (Ch3), and NdeI-RsrII (Ch4) fragments of pT7-M1T1L (41) into the pT7-M1T3D vector (40). M1 point mutants were generated using PCR with mutagenic primers and the pT7-M1T1L and pT7-M1T3D plasmids. Vectors containing mutant M1 genes were substituted for WT M1 to recover recombinant viruses using reverse genetics. Plasmid sequences were determined to confirm fidelity of mutagenesis and cloning.

Quantification of Virus Infectivity—Monolayers of L cells or MDCK cells (~5×10^5 cells) seeded in 24-well plates (Costar, Corning, NY) were adsorbed with virus at an m.o.i. of 2 pfu/cell. After 1 h of adsorption at room temperature, the viral inoculum was removed, cells were washed with PBS, and fresh medium was added. Cells were incubated at 37 °C for various intervals and removed to −80 °C. Viral titers in cell lysates were determined by plaque assay using L cells (43). Viral yield was calculated as the difference between $\log_{10}$ titer at 24 h and $\log_{10}$ titer at 0 h. Negative differences were assigned a value of zero. For the purpose of calculating fold differences in viral yields, non-log transformed data were used, and a yield of less than 1 was considered to be 1.

Immunofluorescence Detection of Reovirus Infection—L cells plated on untreated glass coverslips and MDCK cells plated on poly-L-lysine (Sigma)-treated glass coverslips in 24-well plates were adsorbed with virus at an m.o.i. of 20 pfu/cell. Fol-

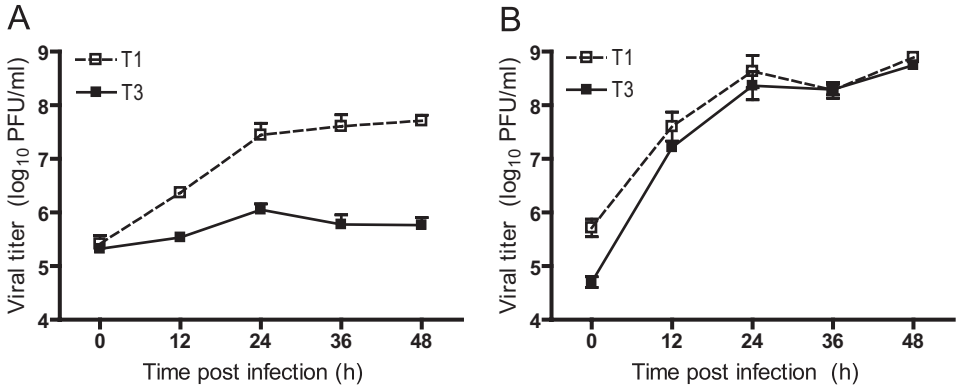

FIGURE 1. **Growth of reovirus in cultured cells.** MDCK cells (*A*) or L cells (*B*) were infected at an m.o.i. of 2 pfu/cell, and viral titers in cell lysates were determined at the time points shown by plaque assay using L cell monolayers. Results represent the mean of triplicate experiments. *Error bars* indicate S.D.

lowing incubation at 37 °C for various intervals, cells were fixed and stained with rabbit μ2-specific (45) and guinea pig σNS-specific (46) antisera followed by Alexa 546-conjugated goat anti-rabbit secondary antibody (Invitrogen), Alexa 488-conjugated goat anti-guinea pig secondary antibody (Invitrogen), and ToPro3 (Invitrogen). Images were acquired using a Zeiss LSM 510 META inverted confocal microscope.

Analysis of Viral RNA Production Using Reverse Transcription-Quantitative PCR—Monolayers of L cells or MDCK cells (~5×10^5 cells) seeded in 24-well plates were adsorbed with virus at an m.o.i. of 10 pfu/cell. After 1 h of adsorption at room temperature, the viral inoculum was removed; cells were washed with PBS, and fresh medium was added. Following incubation at 37 °C for various intervals, cultures were frozen at −80 °C, and total RNA was extracted from 140 μl of thawed lysate using the RNeasy mini kit (Qiagen, Valencia, CA). RNA was incubated at 95 °C for 3 min and immediately placed on ice. Reovirus S4 RNA in 10 μl of RNA extract was quantified using the SuperScript III Platinum One-Step qRT-PCR system (Invitrogen). PCRs were prepared according to the manufacturer's specifications with minor modifications. The S4-specific fluorogenic probe used was 5′-dFAM-AGCGCGCAAGAGGGATGGGA-BHQ-1–3′ (Biosearch Technologies, Novato, CA). Either forward (S4 83F, 5′-CGCTTTTGAAGGTCGTGTATCA-3′) or reverse (S4 153R, 5′-CTGGCTGTGCTGAGATTGTTTT-3′) primer corresponding to the viral S4 gene was used for reverse transcription performed at 50 °C for 15 min. Following 3 min of incubation at 95 °C, the second primer was added, and 40 cycles of quantitative PCR were performed at 95 °C for 15 s followed by 60 °C for 30 s. Total S4 RNA (combined dsRNA and mRNA) was quantified using the S4-specific reverse primer (complementary to the positive strand) in the reverse transcription step, and double-stranded S4 RNA was quantified using the S4-specific forward primer (complementary to the negative strand) in the reverse transcription step. Inclusion of only the reverse or forward primer in the reverse transcription step resulted in specific detection of the positive or negative strand of S4 RNA, respectively. Total S4 RNA is represented by the amount of positive-sense template, whereas dsRNA is equivalent to the amount of negative-sense template. S4 mRNA was calculated by subtracting the amount of dsRNA from total RNA. Standard curves relating *Ct* values to copies of positive- or negative-sense RNA template were generated using 10-fold dilutions of viral RNA extracted from purified virion particles (QIAamp viral RNA purification kit, Qiagen) and quantified by spectrophotometry. The amount of total and dsRNA in each sample was then extrapolated from standard curves generated with the reverse and forward primers, respectively. Standard curves generated using forward and reverse primers in the reverse transcription step were consistently similar, reflecting comparable amplification efficiencies of S4 RNA positive- and negative-sense strands.

Analysis of Viral Protein Synthesis—Monolayers of L cells or MDCK cells (~5×10^5 cells) seeded in 24-well plates were adsorbed with virus at an m.o.i. of 100 pfu/cell. After 1 h at room temperature, the inoculum was removed; fresh medium was added, and cells were incubated at 37 °C for various intervals. Cells were incubated with 50 mCi of [^{35}S]methionine-cysteine (PerkinElmer Life Sciences) in methionine-free medium (MP Biomedicals, Solon, OH) for 1 h prior to harvest; the medium was removed, and 50 μl of lysis buffer (0.1 M NaCl, 1 mM EDTA, 10 mM Tris (pH 7.4), and 0.5% IGEPAL) was added. Cell lysates were centrifuged at 14,000 × *g* at 4 °C for 15 min, and 20 μl of the resultant supernatant was mixed with an equal volume of Laemmli sample buffer (Bio-Rad). Samples were incubated at 95 °C for 5 min and electrophoresed in a 10% SDS-polyacrylamide gel, which was dried onto filter paper and exposed to film (BioMaz MR film, Eastman Kodak Co.).

RESULTS

Reovirus Strain-specific Replication in MDCK Cells—Previous studies revealed a strain-specific capacity of reovirus T1 and T3 to replicate in MDCK cells (38). Using classic reassortant analysis, this phenotype was genetically mapped to the λ3-encoding L1 and μ2-encoding M1 gene segments. To confirm that recombinant viruses recovered using reverse genetics (40, 41) recapitulate growth characteristics of native T1 and T3 in MDCK cells, recombinant strain T1 and recombinant strain T3 were used to infect MDCK cells at an m.o.i. of 2 pfu/cell, and viral titers in cell lysates were monitored over the course of infection. Consistent with previous findings, strain T1 achieved an ~100-fold increase in viral titer over 48 h of growth (Fig. 1*A*). Conversely, strain T3 exhibited a minimal increase in titer during the course of infection. In

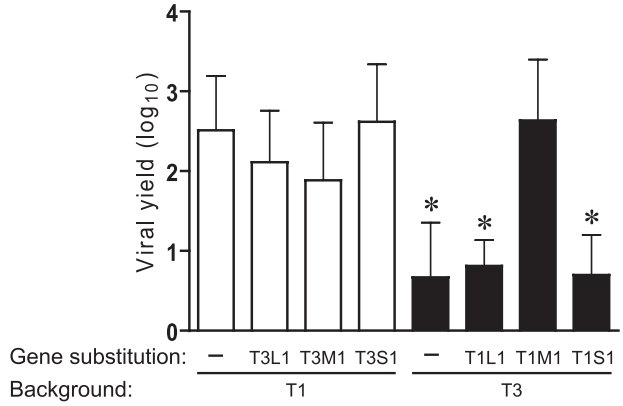

FIGURE 2. **Growth of monoreassortant viruses in MDCK cells.** Cells were infected with L1, M1, or S1 monoreassortant viruses at an m.o.i. of 2 pfu/cell, and viral yields (relative to 0 h) at 24 h post-infection were determined by plaque assay using L cell monolayers. Results represent the mean of triplicate experiments. *Error bars* indicate S.D. *, $p < 0.05$ in comparison with strain T1 (Student's *t* test).

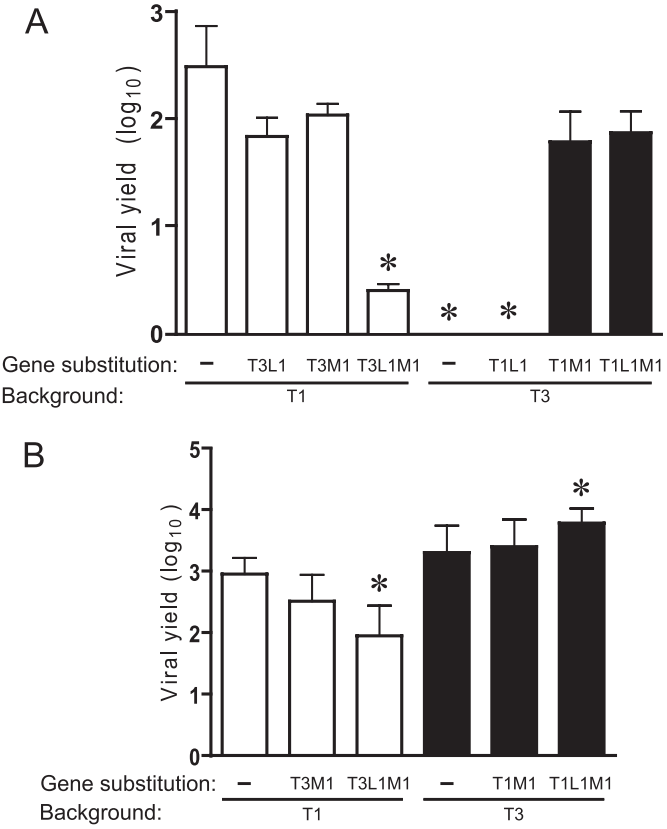

FIGURE 3. **Yields of L1/M1 reassortant viruses in cultured cells.** MDCK cells (*A*) or L cells (*B*) were infected at an m.o.i. of 2 pfu/cell, and viral yields (relative to 0 h) were determined at 24 h post-infection by plaque assay using L cell monolayers. Results represent the mean of triplicate experiments. *Error bars* indicate S.D. *, $p < 0.05$ in comparison with strain T1 (Student's *t* test).

contrast to growth in MDCK cells, both strains replicated with similar kinetics and produced equivalently high titers in L cells (Fig. 1*B*). These results demonstrate that differences in tropism for MDCK cells displayed by the native viruses are recapitulated by the recombinant strains.

Genetic Analysis of Reovirus Replication in MDCK Cells—To more fully understand the contributions of individual reovirus genes to viral replication efficiency in MDCK cells, we generated monoreassortant viruses (containing nine gene segments from one strain, denoted first in the virus name, and one gene derived from a different strain, indicated second in the virus name) and assessed production of infectious progeny virions. L1, M1, and S1 monoreassortant viruses were generated in both T1 and T3 genetic backgrounds. L1 and M1 were reassorted because these genes were previously identified as determinants of reovirus tropism for MDCK cells (38). Monoreassortant viruses encoding reciprocal exchanges of the S1 gene, encoding viral attachment protein σ1 and nonstructural protein σ1s, were tested for growth in MDCK cells because receptor engagement is responsible for differences in the infectivity of type 1 and type 3 reoviruses for a variety of cells and tissues (6, 47–50). Parental and monoreassortant viruses were used to infect MDCK cells at an m.o.i. of 2 pfu/cell, followed by quantification of viral yields after 24 h of growth. Consistent with the earlier mapping study (38), the T1 M1 gene was sufficient to support growth of T3 to the level of T1, whereas the S1 gene was not associated with strain-specific differences in viral yield (Fig. 2). However, contrary to previous findings (38), an independent association of the L1 gene with viral replication was not observed using L1 monoreassortant viruses; T1-T3L1 and T3-T1L1 displayed high and low yields, respectively, mimicking their parental strains. Furthermore, the effect of M1 on viral replication was unidirectional; the T3 M1 gene segment alone did not diminish T1 yield. These results indicate that the μ2 protein regulates reovirus replication efficiency in MDCK cells, but the effects of μ2 on replication are subject to modulation by other viral determinants. We assessed potential cooperativity between the L1 and M1 genes in viral yield experiments using L1/M1 double reassortant viruses in the T1 (T1-T3L1M1) and T3 (T3-T1L1M1) backgrounds. Pairing T3 L1 and T3 M1 genes in the T1 background significantly reduced T1 viral yield in MDCK cells at 24 h post-infection (Fig. 3*A*). In contrast, growth of T3-T1M1 was unaffected by the strain origin of the L1 gene.

Yields of M1 monoreassortant and L1/M1 double-reassortant viruses were also determined using L cells to control for potential constitutive effects of the T1 and T3 L1 and M1 genes on viral replication. In these experiments, all strains produced high yields in L cells (Fig. 3*B*). Reassortant strain T1-T3L1M1 grew less efficiently in L cells compared with the T1 parental strain. However, the reduction in viral yield was 10-fold compared with a 100-fold difference in MDCK cells. The yield of T3-T1L1M1 exceeded that of T3 by ~3-fold, but this difference was modest compared with the 70-fold increase in MDCK cells. Taken together, results of experiments using M1 and L1 reassortant viruses indicate that μ2 is a key determinant of reovirus tropism for MDCK cells and, additionally, provide evidence for co-regulation of viral replication by polymerase protein λ3, conditioned on the viral genetic background.

Identification of Sequences in μ2 That Mediate Reovirus Tropism for MDCK Cells—To identify μ2 sequence features of reovirus replication efficiency in MDCK cells, we generated a panel of T1 × T3 μ2-chimeric viruses in the T3 genetic

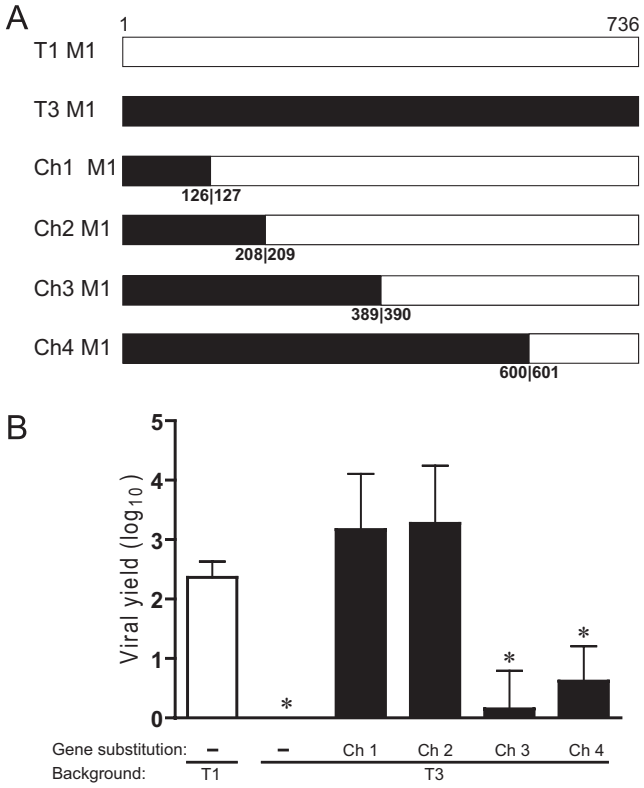

C

	93	208	300	342	347	434	458	652	726
T1	V	P	V	Q	F	V	H	M	N
T3	A	S	M	R	L	I	Q	I	S

FIGURE 4. **Identification of a μ2 domain that mediates reovirus tropism for MDCK cells.** *A,* schematic of T1 × T3 chimeric (*Ch*) M1 gene segments. Chimeric junctions were introduced at the nucleotide position corresponding to the amino acid numbers shown. Viruses containing M1 chimeric gene segments were generated in a T3 strain background. *B,* MDCK cells were infected with M1 chimeric viruses at an m.o.i. of 2 pfu/cell, and viral yields (relative to 0 h) were determined at 24 h post-infection by plaque assay using L cell monolayers. Results represent the mean of triplicate experiments. *Error bars* indicate S.D. *, $p < 0.05$ in comparison with strain T1 (Student's *t* test). *C,* T1 and T3 μ2 proteins differ at nine amino acid positions.

background (Fig. 4*A*). Chimera 1 and chimera 2, containing T3 μ2-derived sequences 1–126 and 1–208, respectively, produced high viral yields similar to T1, whereas chimera 3 and chimera 4, containing T3 μ2-derived sequences 1–389 and 1–600, respectively, produced low yields similar to T3 (Fig. 4*B*). Relative replication efficiencies of the four chimeric viruses suggest that μ2 sequences regulating reovirus replication in MDCK cells are bounded by amino acid residues 209 and 389.

Three sequence polymorphisms with respect to T1 and T3 (300, 342, and 347) are present within the μ2 region that controls viral growth efficiency in MDCK cells (Fig. 4*C*). The relative contribution of these amino acids to viral growth was assessed by reciprocal exchanges between the μ2 proteins of T1 and T3 using reverse genetics. Moderately increased yields (~4-fold) resulted from replacement of T3 μ2 amino acids with the corresponding T1 μ2 residues at positions 300 and 342. In contrast, substitution of Leu-347 in T3 μ2 with Phe (T3-M1L347F), which is found at this position in T1 μ2, enabled T3 to grow equivalently to T1 (~100-fold yield). The yield of T1-M1F347L, isogenic to T1 except for Leu at μ2 amino acid position 347, approximated that of T1 (Fig. 5*A*). Yields of μ2 point-mutant viruses T1-M1Q342R and T1-M1F347L, which contain T3 residues at μ2 amino acid positions 342 and 347, were modestly reduced in L cells, relative to parental strain T1 (Fig. 5*C*). However, the other μ2 point-mutant strains and the parental viruses all exhibited equivalently high yields in L cells, and no influence of the L1 gene was detected (Fig. 5, *C* and *D*). Therefore, constitutive replication defects are unlikely to account for disparities in yields of μ2-mutant viruses when propagated in MDCK cells.

Consistent with the cooperative relationship of WT λ3 and μ2 proteins in viral growth (Fig. 3), we observed a functional interaction between λ3 and mutant μ2 governed by the specific viral genetic environment; yield of T1-M1F347L in MDCK cells was reduced relative to WT parental strain T1 when the mutant μ2 protein was accompanied by the T3 (strain T1-T3L1-M1F347L), but not T1 (strain T1-M1F347L), λ3 protein (Fig. 5, *A* and *B*).

Interestingly, the T1 λ3 protein acted synergistically with the μ2 L347F mutation to moderately suppress (~13-fold reduction in yield) the growth of T3 (T3-T1L1-M1L347F) in MDCK cells (Fig. 5*B*), which further substantiates the functional linkage of λ3 and μ2 in reovirus tropism for these cells.

These results indicate that a sequence polymorphism at amino acid position 347 is the primary determinant of μ2-mediated reovirus replication efficiency in MDCK cells. Furthermore, the λ3 protein acts as a modifier of tropic phenotypes manifested by sequence variation at this position in μ2.

Viral Inclusion Formation in Reovirus-infected Cells—As an initial approach to delineating the μ2-sensitive step in viral replication in MDCK cells, we imaged viral inclusions over a time course of infection using confocal immunofluorescence microscopy. Cells were infected with T1 or T3, fixed at various intervals, and stained with anti-μ2 and anti-σNS antisera. In both T1- and T3-infected MDCK cells, inclusions initially appeared as small, punctate structures that gradually enlarged and assumed strain-dependent filamentous and globular features characteristic of T1 and T3, respectively, in L cells (Fig. 6) (23, 24). However, T1 inclusions in MDCK cells also displayed globular structures intermingled with filamentous forms, resulting in a more intermediate phenotype. Although the progress of inclusion formation for both T1 and T3 was slightly delayed in MDCK cells in comparison with L cells, inclusion development was comparable between MDCK cells and L cells by 12 h post-infection. Thus, kinetics of T3 inclusion maturation in MDCK cells was not overtly impaired. Typical inclusion maturation and abundant expression of σNS, a nonstructural protein, in T3-infected MDCK cells indicate that viral attachment, entry, and early rounds of transcription and translation proceed normally.

Quantification of Reovirus RNA in Infected Cells—Although the presence of viral inclusions in T3-infected MDCK cells confirms the occurrence of viral transcription and translation, these findings cannot distinguish possible temporal defects occurring during primary and secondary rounds of gene expression. To monitor production of viral RNA over the course

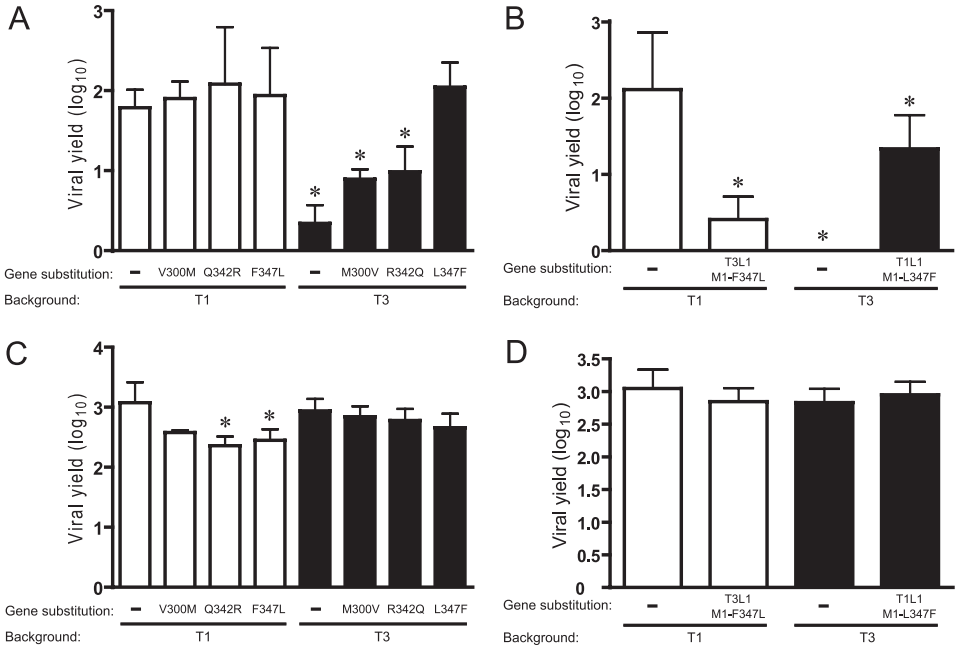

FIGURE 5. **Identification of residues in μ2 that mediate reovirus tropism for MDCK cells.** MDCK cells (*A*) or L cells (*C*) were infected with μ2 point-mutant viruses at an m.o.i. of 2 pfu/cell, and viral yields (relative to 0 h) were determined at 24 h post-infection by plaque assay using L cell monolayers. MDCK cells (*B*) or L cells (*D*) were infected at an m.o.i. of 2 pfu/cell with L1 monoreassortant viruses containing point mutations at residue 347 of μ2, and viral yields (relative to 0 h) were determined at 24 h post-infection by plaque assay using L cell monolayers. Results represent the mean of triplicate experiments. *Error bars* indicate S.D. *, $p < 0.05$ in comparison with strain T1 (Student's *t* test).

of infection, we used an RT-qPCR approach to specifically quantify positive and negative sense S4 gene RNA, which encodes viral structural protein σ3. Standard curves relating total viral genomic RNA to *Ct* were used for calculations of S4 total, double-stranded, and mRNA in RNA extracts from virus-infected cells. MDCK cells and L cells were infected at an m.o.i. of 10 pfu/cell with either T3-T1M1 or T3. Strain T3-T1M1 was used in place of T1 because the T3 and T3-T1M1 S4 alleles are identical. Growth of T3-T1M1 in MDCK cells recapitulated that of T1 (Fig. 2). At 12 h post-infection and the following time points, high levels of total S4 RNA were detected in T3-T1M1-infected MDCK cells compared with the minimal amount of RNA produced in T3-infected cells (Fig. 7*A*). Conversely, in L cells, significant levels of total RNA were present in both T3-T1M1- and T3-infected cells at 12 h post-infection and beyond (Fig. 7*B*). Similar patterns of S4 dsRNA production by T3-T1M1 and T3 were observed (Fig. 7, *C* and *D*). Significant levels of S4 mRNA were detected in MDCK cells at 12, 18, and 24 h post-infection with strain T3-T1M1 (Fig. 7*E*), whereas little S4 mRNA was detected in T3-infected cells at 12 and 18 h post-infection (Fig. 7*E*). The amount of S4 mRNA in T3-infected cells at 24 h post-infection was below the limit of detection (<10 copies of S4 RNA (data not shown)). These results indicate roughly equivalent efficiencies of early viral RNA synthesis in T3-T1M1- and T3-infected MDCK cells. However, late RNA synthesis is markedly diminished in T3-infected cells in comparison with that in T3-T1M1-infected cells, consistent with attenuated dsRNA production by T3 in MDCK cells.

Protein Synthesis in Reovirus-infected Cells—We next assessed viral protein synthesis in infected MDCK cells and L cells. Strains T1 and T3 differ in the capacity to inhibit host cell protein synthesis, a phenotype unrelated to the M1 gene segment (51, 52). Therefore, T3-T1M1 was used instead of T1 to remove this variable. MDCK cells and L cells were infected at an m.o.i. of 100 pfu/cell with either T3-T1M1 or T3. One hour prior to harvest, cells were incubated with 50 mCi [^{35}S]methionine-cysteine, and solubilized whole-cell proteins were resolved using SDS-PAGE, followed by autoradiography. New viral protein synthesis was observed at 12, 18, and 24 h post-infection in T3-T1M1-infected MDCK cells, yet only at 12 h post-infection in T3-infected cells (Fig. 8*A*). These data generally mirror T3-T1M1 and T3 RNA production in MDCK cells. In contrast, the kinetics and magnitude of new viral protein synthesis by T3-T1M1 and T3 did not significantly differ in infected L cells (Fig. 8*B*). Thus, early viral protein synthesis was roughly equivalent between T3-T1M1 and T3 in MDCK cells, but late protein synthesis by T3 was undetectable, consistent with diminished mRNA production at later time points.

DISCUSSION

The purpose of this study was to define post-receptor control mechanisms of reovirus cell tropism. Our primary findings emerging from this study are the following: 1) μ2 controls efficiency of reovirus growth in MDCK cells; 2) residue 347 is the primary determinant of μ2-mediated viral replication potential in these cells; 3) polymerase protein λ3 is a co-regulator of viral replication in a strain-dependent manner; and 4) μ2 protein appears to regulate a later step in the reovirus replication program subsequent to primary rounds of viral transcription and translation. These findings suggest a unique structural or functional interaction between μ2 and λ3 that

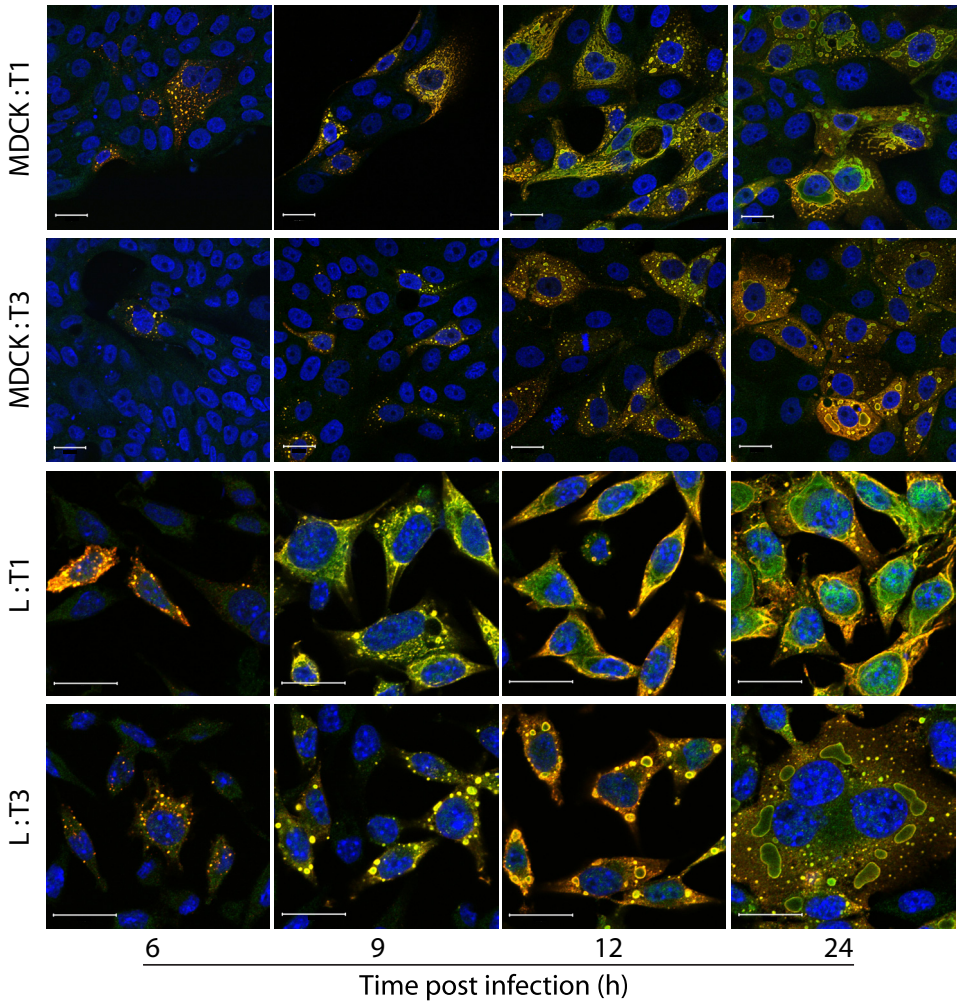

FIGURE 6. **Reovirus inclusion formation.** MDCK or L cells were infected with T1 or T3 at an m.o.i. of 20 pfu/cell, fixed at the time points shown, stained with anti-μ2 (*green*) and anti-σNS (*red*) antibodies and ToPro3 (*blue*, nuclear), and imaged using confocal microscopy. *Scale bars,* 20 μm.

facilitates productive viral replication in a manner responsive to specific viral and host-cell environments.

Initial studies of reovirus replication in MDCK cells revealed a genetic association of the λ3 and μ2 proteins with viral replication efficiency using classical reassortant analysis (38). A reverse genetics system for reovirus has permitted us to generate viruses containing specific combinations of T1 and T3 gene segments and clearly define the relative contributions of μ2 and λ3 to this phenotype (Figs. 2 and 3). T1 μ2 is associated with efficient reovirus replication in MDCK cells irrespective of the viral genetic background. The influence of T3 μ2 on viral replication is more complex; its quantitative effect on production of infectious progeny requires the co-association of T3 λ3. The μ2 protein is thought to be a cofactor of the viral RdRp (6). However, there is limited insight into interactions between μ2 and λ3. Biochemical data show that the nucleotide triphosphatase and RNA triphosphatase activities of μ2 are enhanced in the presence of λ3, and the two proteins interact in immunoprecipitation assays (27). Furthermore, the L1 and M1 genes display nonrandom segregation in T1 × T3 reassortant viruses (53), suggesting co-evolution of λ3 and μ2 to optimize concerted roles in viral replication. Data presented in this study showing the unidirectional μ2-mediated regulation of replication efficiency in MDCK cells and viral background-dependent co-regulation by λ3 suggest a unique structural or functional interaction between μ2 and λ3 in specific viral and cellular contexts. Our findings provide additional genetic evidence linking the function of these two proteins and implicate the role of the polymerase complex in determining viral cell tropism.

Using recombinant viruses containing chimeric and point-mutant μ2 proteins, we were able to systematically define sequence determinants of reovirus replication efficiency in MDCK cells. Our results indicate that residue 347 is primarily responsible (Fig. 5*A*). The influence of this polymorphic position on viral replication potential is modulated by λ3 in a manner consistent with the effect of λ3 on full-length μ2 (Fig. 5*B*). A crystal structure of μ2 has not been reported; however, a number of functional sequence determinants have been defined (20, 22, 24, 27, 28). It is possible that critical residues identified in this study are part of a larger domain of μ2 that controls reovirus tropism for different types of cells. For example, a temperature-sensitive strain of reovirus (tsH11.2) containing mutations at residues 399 and 414 of μ2 displays defective dsRNA synthesis and particle assembly at restrictive temperatures. The proximity of these residues to amino acid

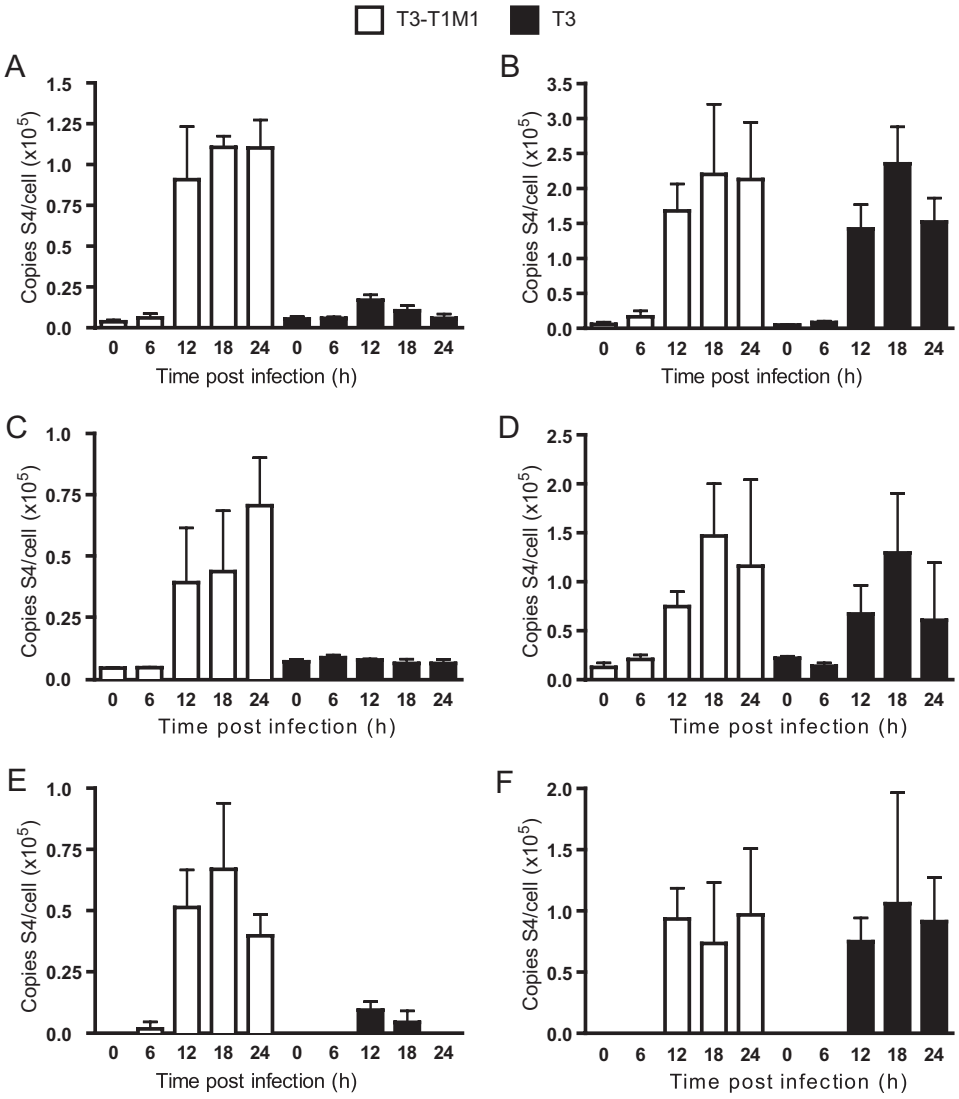

FIGURE 7. **Analysis of viral RNA synthesis.** Cells were infected with T3-T1M1 or T3 at an m.o.i. of 10 pfu/cell, and total RNA was extracted from cell lysates at the indicated time points. RT-qPCR of total S4 RNA in MDCK cells (*A*) and L cells (*B*) was performed using an S4-specific reverse primer (complementary to the (+)-strand) in the reverse transcription step, followed by qPCR. A standard curve relating *Ct* to the amount of S4 RNA isolated from purified virion particles was used to determine S4 (+)-strand RNA copy number. RT-PCR of dsRNA in infected MDCK cells (*C*) and L cells (*D*) was performed using an S4-specific forward primer (complementary to the (−)-strand) in the reverse transcription step, followed by qPCR. A standard curve relating *Ct* to the amount of S4 RNA isolated from purified virion particles was used to determine S4 (−)-strand RNA copy number. Amounts of viral mRNA in MDCK cells (*E*) and L cells (*F*) are expressed as the difference between total RNA and dsRNA at each time point shown. Results represent the mean of triplicate experiments. *Error bars* indicate S.D.

position 347 in primary sequence raises the possibility that all three are part of a functional unit responsive to the host cell environment. Residue 347 is also near a predicted leucine-rich nuclear export signal spanning residues 328–335 (NetNES 1.1 (54)). Because μ2 distributes to both the cytoplasm and nucleus (Fig. 6) (20, 24) and contains two predicted nuclear localization signals, one of which has been shown to be important for viral replication (20), it is plausible that a polymorphism at position 347 could deleteriously shift the nucleocytoplasmic balance of μ2.

The three-dimensional structure of the μ2 protein is unknown; therefore, it is not possible to rule out an interaction of residue 347 with other structural or functional domains distantly located in the primary sequence, such as the nucleotide-binding motifs located at residues 414–420 and 445–450 (27). These sequences are required for nucleotide triphosphatase and RNA triphosphatase activities of μ2 (27), and we found them necessary for viral replication using an RNAi trans-complementation system (20). Therefore, changes at μ2 residue 347 plausibly could alter the function of these domains, with a resultant impact on viral replication efficiency in MDCK cells.

Although negative-stand RNA synthesis and particle assembly have been ascribed to viral inclusions, the discrete series of steps that occur between entry of transcriptionally active core particles into the cytoplasm and the appearance of mature progeny particles within viral inclusions remain poorly defined. The absence of detectable viral RNA and protein synthesis at late times of infection in T3-infected MDCK cells (Figs. 7 and 8) despite normal-appearing inclusions (Fig. 6) indicates that the impasse occurs at one or more of these undefined steps. Several potential but nonmutually exclusive

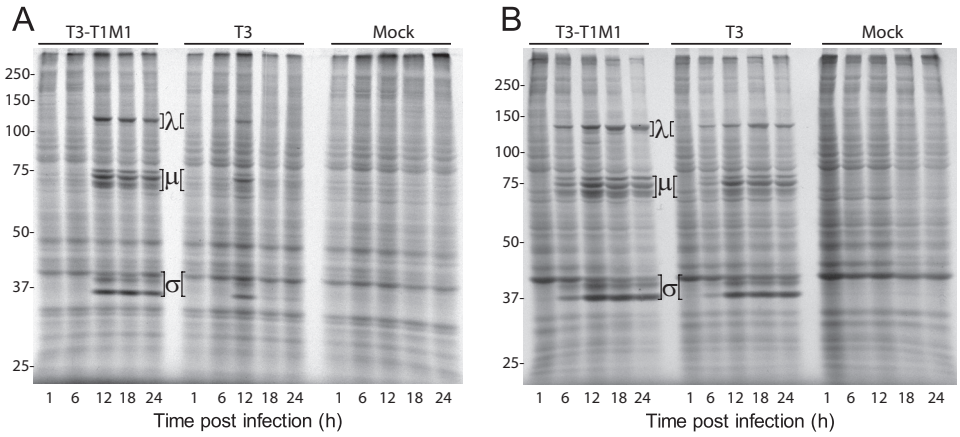

FIGURE 8. **Analysis of viral protein synthesis.** MDCK cells (*A*) or L cells (*B*) were infected at an m.o.i. of 100 pfu/cell with reovirus strain T3-T1M1 or T3 and incubated for 1 h with [^{35}S]methionine/cysteine at the indicated times post-infection. Radiolabeled polypeptides were resolved by SDS-PAGE and visualized using autoradiography. Positions of viral λ, μ, and σ proteins are indicated. Molecular mass standards (in kDa) are shown.

mechanisms can be proposed to explain the replication block in T3-infected MDCK cells, including the following: 1) mislocalization of RNA; 2) decreased RNA stability; 3) malfunction of the viral replicase during positive- or negative-strand synthesis; and 4) defective genome packaging or particle assembly. Each of these possibilities is currently under investigation. Notably, by confocal immunofluorescence microscopy, core protein λ2 (which serves as the viral RNA-capping enzyme) exhibits the expected pattern of localization to inclusions in T3- and T3-T1M1-infected MDCK cells, using infected L cells as a reference for λ2 distribution in permissive cells (data not shown). These results suggest that recruitment of virion core proteins occurs normally in T3-infected MDCK cells and the defect in viral replication is not ascribable to mislocalization of replicase components.

The capacity of MDCK cells to discriminate reovirus strains T1 and T3 in a μ2- and λ3-dependent manner at a later point in the viral life cycle indicates the existence of a tightly controlled post-entry replication checkpoint responsive to structural or functional features of the viral polymerase complex. Conceivably, the regulatory mechanism could be positive or negative, *i.e.* active stimulation of T1 replication or suppression of T3 replication. A passive mechanism also is possible in which MDCK cells fail to provide a function essential for T3, but not T1, replication. The mediator of replication permissivity might be as simple as a single protein or as intricate as a biochemical pathway.

RdRp complexes of diverse RNA viruses may function in viral adaptation to different intracellular environments (55–57). In the influenza A paradigm, host-range restriction involves an active inhibitory process that protects against cross-species transmission of nonadapted viruses. It is provocative that reovirus strains T1 and T3 sharply contrast in their capacities to grow in canine cells, whereas both strains productively infect cells derived from several other species, including mouse (L (Fig. 1)), human (HeLa and 293T (11, 58)), and primate (Vero and CV-1 (59, 60)), raising the possibility that μ2 is a host-range determinant of reovirus infection. However, this hypothesis awaits formal testing.

The reovirus μ2 protein is a pleiotropic mediator of reovirus replication operating at the intersection of virus multiplication, cellular regulation of infection, and host disease. Based on this study, the capacity of μ2 to mediate viral tropism at the post-entry level can be added to the list of μ2 functions in the reovirus replication program. Further investigation of μ2 interactions with the viral and cellular metabolic machineries will provide sharper insights into mechanisms of cellular permissivity to reovirus infection and create a framework for conceptualizing and testing general models of viral pathogenesis, epidemiology, and adaptation.

Acknowledgments—Acquisition and analysis of confocal imaging data were performed in part through the use of the Vanderbilt University Medical Center Imaging Shared Resource.

REFERENCES

1. Taubenberger, J. K., and Kash, J. C. (2010) *Cell Host Microbe* **7,** 440–451
2. Guglielmi, K. M., Johnson, E. M., Stehle, T., and Dermody, T. S. (2006) *Curr. Top. Microbiol. Immunol.* **309,** 1–38
3. Clarke, P., Debiasi, R. L., Meintzer, S. M., Robinson, B. A., and Tyler, K. L. (2005) *Apoptosis* **10,** 513–524
4. Forrest, J. C., and Dermody, T. S. (2003) *J. Virol.* **77,** 9109–9115
5. Sherry, B. (2002) *Viral Immunol.* **15,** 17–28
6. Schiff, L. A., Nibert, M. L., and Tyler, K. L. (2007) in *Fields Virology* (Knipe, D. M., and Howley, P. M., eds) 5th Ed., pp. 1853–1915, Lippincott Williams & Wilkins, Philadelphia, PA
7. Rosen, L. (1962) *Ann. N. Y. Acad. Sci.* **101,** 461–465
8. Sabin, A. B. (1959) *Science* **130,** 1387–1389
9. Attoui, H., Biagini, P., Stirling, J., Mertens, P. P., Cantaloube, J. F., Meyer, A., de Micco, P., and de Lamballerie, X. (2001) *Biochem. Biophys. Res. Commun.* **287,** 583–588
10. Fields, B. N. (1971) *Virology* **46,** 142–148
11. Kobayashi, T., Chappell, J. D., Danthi, P., and Dermody, T. S. (2006) *J. Virol.* **80,** 9053–9063
12. Arnold, M. M., Murray, K. E., and Nibert, M. L. (2008) *Virology* **375,** 412–423
13. Gomatos, P. J., Tamm, I., Dales, S., and Franklin, R. M. (1962) *Virology* **17,** 441–454
14. Spendlove, R. S., Lennette, E. H., Knight, C. O., and Chin, J. N. (1963) *J. Immunol.* **90,** 548–553
15. Dales, S., Gomatos, P. J., and Hsu, K. C. (1965) *Virology* **25,** 193–211
16. Silverstein, S. C., and Schur, P. H. (1970) *Virology* **41,** 564–566
17. Anderson, N., and Doane, F. W. (1966) *J. Pathol. Bacteriol.* **92,** 433–439
18. Sharpe, A. H., Chen, L. B., and Fields, B. N. (1982) *Virology* **120,** 399–411

19. Silverstein, S. C., and Dales, S. (1968) *J. Cell Biol.* **36,** 197–230
20. Kobayashi, T., Ooms, L. S., Chappell, J. D., and Dermody, T. S. (2009) *J. Virol.* **83,** 2892–2906
21. Yin, B., Whyatt, R. M., Perera, F. P., Randall, M. C., Cooper, T. B., and Santella, R. M. (1995) *Free Radic. Biol. Med.* **18,** 1023–1032
22. Coombs, K. M. (1996) *J. Virol.* **70,** 4237–4245
23. Mbisa, J. L., Becker, M. M., Zou, S., Dermody, T. S., and Brown, E. G. (2000) *Virology* **272,** 16–26
24. Parker, J. S., Broering, T. J., Kim, J., Higgins, D. E., and Nibert, M. L. (2002) *J. Virol.* **76,** 4483–4496
25. Coombs, K. M. (1998) *Virology* **243,** 218–228
26. Coombs, K. M. (1998) *Curr. Top. Microbiol. Immunol.* **233,** 69–107
27. Kim, J., Parker, J. S., Murray, K. E., and Nibert, M. L. (2004) *J. Biol. Chem.* **279,** 4394–4403
28. Noble, S., and Nibert, M. L. (1997) *J. Virol.* **71,** 7728–7735
29. Reinisch, K. M., Nibert, M. L., and Harrison, S. C. (2000) *Nature* **404,** 960–967
30. Yin, P., Cheang, M., and Coombs, K. M. (1996) *J. Virol.* **70,** 1223–1227
31. Zhang, X., Walker, S. B., Chipman, P. R., Nibert, M. L., and Baker, T. S. (2003) *Nat. Struct. Biol.* **10,** 1011–1018
32. Brentano, L., Noah, D. L., Brown, E. G., and Sherry, B. (1998) *Virology* **72,** 8354–8357
33. Matoba, Y., Sherry, B., Fields, B. N., and Smith, T. W. (1991) *J. Clin. Invest.* **87,** 1628–1633
34. Sherry, B., Schoen, F. J., Wenske, E., and Fields, B. N. (1989) *J. Virol.* **63,** 4840–4849
35. Sherry, B., and Blum, M. A. (1994) *J. Virol.* **68,** 8461–8465
36. Sherry, B. (1998) *Curr. Top. Microbiol. Immunol.* **233,** 51–66
37. Matoba, Y., Colucci, W. S., Fields, B. N., and Smith, T. W. (1993) *J. Clin. Invest.* **92,** 2883–2888
38. Rodgers, S. E., Barton, E. S., Oberhaus, S. M., Pike, B., Gibson, C. A., Tyler, K. L., and Dermody, T. S. (1997) *J. Virol.* **71,** 2540–2546
39. Zurney, J., Kobayashi, T., Holm, G. H., Dermody, T. S., and Sherry, B. (2009) *J. Virol.* **83,** 2178–2187
40. Kobayashi, T., Antar, A. A., Boehme, K. W., Danthi, P., Eby, E. A., Guglielmi, K. M., Holm, G. H., Johnson, E. M., Maginnis, M. S., Naik, S., Skelton, W. B., Wetzel, J. D., Wilson, G. J., Chappell, J. D., and Dermody, T. S. (2007) *Cell Host Microbe* **1,** 147–157
41. Kobayashi, T., Ooms, L. S., Ikizler, M., Chappell, J. D., and Dermody, T. S. (2010) *Virology* **398,** 194–200
42. Furlong, D. B., Nibert, M. L., and Fields, B. N. (1988) *J. Virol.* **62,** 246–256
43. Virgin, H. W., 4th., Bassel-Duby, R., Fields, B. N., and Tyler, K. L. (1988) *J. Virol.* **62,** 4594–4604
44. Ishii, K., Ueda, Y., Matsuo, K., Matsuura, Y., Kitamura, T., Kato, K., Izumi, Y., Someya, K., Ohsu, T., Honda, M., and Miyamura, T. (2002) *Virology* **302,** 433–444
45. Zou, S., and Brown, E. G. (1996) *Virology* **217,** 42–48
46. Becker, M. M., Goral, M. I., Hazelton, P. R., Baer, G. S., Rodgers, S. E., Brown, E. G., Coombs, K. M., and Dermody, T. S. (2001) *J. Virol.* **75,** 1459–1475
47. Tyler, K. L., McPhee, D. A., and Fields, B. N. (1986) *Science* **233,** 770–774
48. Kaye, K. M., Spriggs, D. R., Bassel-Duby, R., Fields, B. N., and Tyler, K. L. (1986) *J. Virol.* **59,** 90–97
49. Weiner, H. L., Drayna, D., Averill, D. R., Jr., and Fields, B. N. (1977) *Proc. Natl. Acad. Sci. U.S.A.* **74,** 5744–5748
50. Dermody, T. S., Nibert, M. L., Bassel-Duby, R., and Fields, B. N. (1990) *J. Virol.* **64,** 5173–5176
51. Zweerink, H. J., and Joklik, W. K. (1970) *Virology* **41,** 501–518
52. Sharpe, A. H., and Fields, B. N. (1982) *Virology* **122,** 381–391
53. Nibert, M. L., Margraf, R. L., and Coombs, K. M. (1996) *J. Virol.* **70,** 7295–7300
54. la Cour, T., Kiemer, L., Mølgaard, A., Gupta, R., Skriver, K., and Brunak, S. (2004) *Protein Eng. Des. Sel.* **17,** 527–536
55. Neumann, G., and Kawaoka, Y. (2006) *Emerg. Infect. Dis.* **12,** 881–886
56. Mehle, A., and Doudna, J. A. (2008) *Cell Host Microbe* **4,** 111–122
57. Neumann, G., Noda, T., and Kawaoka, Y. (2009) *Nature* **459,** 931–939
58. Campbell, J. A., Schelling, P., Wetzel, J. D., Johnson, E. M., Forrest, J. C., Wilson, G. A., Aurrand-Lions, M., Imhof, B. A., Stehle, T., and Dermody, T. S. (2005) *J. Virol.* **79,** 7967–7978
59. Berry, J. M., Barnabé, N., Coombs, K. M., and Butler, M. (1999) *Biotechnol. Bioeng.* **62,** 12–19
60. Carvalho, J., Arnold, M. M., and Nibert, M. L. (2007) *Virology* **364,** 301–316

APPENDIX E

A SINGLE-AMINO-ACID POLYMORPHISM IN REOVIRUS PROTEIN μ2 DETERMINES REPRESSION OF INTERFERON SIGNALING AND MODULATES MYOCARDITIS

Susan C. Irvin, Jennifer Zurney, Laura S. Ooms, James D. Chappell, Terence S. Dermody, and Barbara Sherry

Journal of Virology. 86(4) 2302-11; 2012

JVI Journals.ASM.org

A Single-Amino-Acid Polymorphism in Reovirus Protein $\mu 2$ Determines Repression of Interferon Signaling and Modulates Myocarditis

Susan C. Irvin,[a] Jennifer Zurney,[a]* Laura S. Ooms,[b,d] James D. Chappell,[b,c,d] Terence S. Dermody,[b,c,d] and Barbara Sherry[a]

Department of Molecular Biomedical Sciences, North Carolina State University, Raleigh, North Carolina, USA,[a] and Departments of Pathology, Microbiology, and Immunology[b] and Pediatrics[c] and Elizabeth B. Lamb Center for Pediatric Research, Vanderbilt University School of Medicine, Nashville, Tennessee, USA[d]

Myocarditis is indicated as the second leading cause of sudden death in young adults. Reovirus induces myocarditis in neonatal mice, providing a tractable model system for investigation of this important disease. Alpha/beta-interferon (IFN-α/β) treatment improves cardiac function and inhibits viral replication in patients with chronic myocarditis, and the host IFN-α/β response is a determinant of reovirus strain-specific differences in induction of myocarditis. Virus-induced IFN-β stimulates a signaling cascade that establishes an antiviral state and further induces IFN-α/β through an amplification loop. Reovirus strain-specific differences in induction of and sensitivity to IFN-α/β are associated with the viral M1, L2, and S2 genes. The reovirus M1 gene-encoded $\mu 2$ protein is a strain-specific repressor of IFN-β signaling, providing one possible mechanism for the variation in resistance to IFN and induction of myocarditis between different reovirus strains. We report here that $\mu 2$ amino acid 208 determines repression of IFN-β signaling and modulates reovirus induction of IFN-β in cardiac myocytes. Moreover, $\mu 2$ amino acid 208 determines reovirus replication, both in initially infected cardiac myocytes and after viral spread, by regulating the IFN-β response. Amino acid 208 of $\mu 2$ also influences the cytopathic effect in cardiac myocytes after spread. Finally, $\mu 2$ amino acid 208 modulates myocarditis in neonatal mice. Thus, repression of IFN-β signaling mediated by reovirus $\mu 2$ amino acid 208 is a determinant of the IFN-β response, viral replication and damage in cardiac myocytes, and myocarditis. These results demonstrate that a single amino acid difference between viruses can dictate virus strain-specific differences in suppression of the host IFN-β response and, consequently, damage to the heart.

Viral infection is the leading cause of myocarditis in North America and Europe (12). This disease can be fatal in infants and, although usually resolved in adults, can lead to dilated cardiomyopathy and cardiac failure. Importantly, myocarditis is indicated as the second leading cause of sudden death in young adults (10). Most virus families are implicated in myocarditis in humans (12), with enteroviruses, such as coxsackievirus B (8, 12), adenoviruses (8, 12), and more recently parvovirus B19 (8, 22, 24) as the most frequently identified. While enterovirus-induced myocarditis in mice is predominantly immune mediated, cardiac damage is also due to direct viral cytopathic effect (CPE). Indeed, immunosuppressive therapy is only minimally beneficial in affected humans (30, 40). Furthermore, adenovirus-positive cardiac sections from patients with myocarditis often lack inflammatory cell infiltrates (29). Therefore, the importance of immune-mediated damage in myocarditis is unclear. Reovirus induction of cardiac lesions in newborn mice reflects direct viral CPE in cardiac myocytes (2, 47) and is virus strain specific (46). Thus, reovirus infection in mice provides a useful experimental system to study the direct effects of viral infection on the heart.

The type I interferon (IFN) response is critical for protection of cardiac cells against reovirus infection *in vitro* (48). Accordingly, nonmyocarditic reoviruses induce myocarditis in mice depleted of alpha/beta IFN (IFN-α/β) (48) or lacking a transcription factor critical for the induction of IFN (15). Reoviruses that are either strong inducers of IFN or are most sensitive to IFN-mediated antiviral effects, such as strain type 3 Dearing (T3D), do not induce myocarditis (48). Conversely, reoviruses that are weak inducers of IFN or are highly resistant to its effects, such as strain type 1 Lang (T1L), induce myocarditis (48). Given that cardiac myocytes are essentially nonreplenishable (4) and thus vulnerable to systemic viral infections, the IFN response provides a critical first-line of protection for these cells. Indeed, cardiac myocytes are pre-armed with higher basal expression of IFN-β than neighboring cardiac fibroblasts (55). Moreover, IFN-α (9, 32) and IFN-β (23) treatment has improved cardiac function and inhibited viral replication in patients with chronic myocarditis.

Viral nucleic acids can be recognized by pattern recognition receptors (PRRs), including RIG-I-like receptors, to stimulate intracellular signaling cascades that result in the induction and secretion of IFN-α/β (52). Through autocrine and paracrine signaling, IFN-α/β induces expression of IFN-stimulated genes (ISGs), including those with antiviral activity (37), and the transcription factor, IRF7, which further amplifies IFN expression (17, 42). Viruses have evolved mechanisms to inhibit the induction of IFN, IFN signaling, and ISG protein function (5, 13, 41, 51). Reovirus subverts IFN signaling by a novel mechanism associated with nuclear accumulation of IRF9 (56). Reovirus strain-specific differences in this subversion are determined by the M1 gene-encoded protein $\mu 2$ (56). While strain-specific differences in reovirus re-

Received 6 September 2011 **Accepted** 26 November 2011
Published ahead of print 7 December 2011
Address correspondence to Barbara Sherry, barbara_sherry@ncsu.edu.
* Present address: Burleson Research Technologies, Morrisville, North Carolina, USA.

doi:10.1128/JVI.06236-11

pression of IFN signaling correlate with induction of myocarditis (56), the role of this repression in disease is not known.

The M1 gene is the primary determinant of reovirus strain-specific differences in murine myocarditis (45, 46). Reovirus strain-specific differences in induction of and sensitivity to IFN are also determined by the M1 gene in concert with the L2 and S2 genes (44). In the present study, we investigated μ2 determinants of IFN induction, repression of IFN signaling, viral replication and CPE in cardiac myocytes, and reovirus-induced myocarditis in mice. We found that μ2 amino acid 208 is a determinant of IFN responses, viral spread, and damage in cardiac cells and that this amino acid modulates myocarditis.

MATERIALS AND METHODS

Cells and mice. Mouse L929 cells were maintained in minimal essential medium (SAFC Biosciences) supplemented to contain 5% fetal calf serum (FCS) (Atlanta Biologicals) and 2 mM L-glutamine (Mediatech, Inc.). L929 cells were plated at 5×10^5 cells per well in 24-well clusters and allowed to adhere 2 h prior to infection.

Timed-pregnant Cr:NIH(S) mice from the National Cancer Institute were maintained as a colony in a facility that is accredited by the Association for Assessment and Accreditation of Laboratory Animal Care. All animal procedures were approved by the North Carolina State University Institutional Animal Care and Use Committee.

Primary cardiac myocyte and fibroblast cultures were generated from 1-day-old neonatal or term fetal Cr:NIH(S) mice resulting from timed pregnancies. Neonatal or term fetal mice were euthanized, and the apical two-thirds of hearts were excised and treated with trypsin (2). Cardiac myocytes were separated from cardiac fibroblasts by differential adherence to culture wells and resuspended in Dulbecco modified Eagle medium (Gibco) supplemented to contain 7% FCS (Atlanta Biologicals) and 10 μg of gentamicin (Sigma-Aldrich Corp.)/ml. Myocyte culture medium also contained 0.06% thymidine (Sigma-Aldrich Corp.). Myocyte cultures contain $\leq$5% fibroblasts, and fibroblast cultures contain $<$1% myocytes (55). Myocyte cultures were plated at 1.5×10^5 cells per well in 96-well clusters or at 5×10^5 cells per well in 48-well clusters. Fibroblast cultures were plated at one-half those densities in 96-well or 48-well clusters, were confluent by the day of infection, and were assumed to double from the initial plating density. Cells were incubated for 2 days prior to infection. Myocyte and fibroblast cultures were not passaged before use.

Two-day-old mice from timed litters were injected in the left hind limb with 20 μl of gel saline (46) containing 10^6 PFU of various virus strains or gel saline as a mock infection. At 7 days postinjection, mice were euthanized, and hearts were removed, fixed in 10% buffered formalin, and sectioned for hematoxylin and eosin (H&E) staining. Sections were photographed with a Nikon AZ100 zoom microscope at $\times$75 magnification. A minimum of eight hearts (with a minimum of 15 sections per heart) were scored as blinded cardiac sections for each virus. Mice were considered "positive" if more than a single lesion was detected in the $\geq$15 sections examined. Lesions in adjacent sections were not scored as independent lesions.

Viruses. All viruses were generated from plasmids by reverse genetics as described previously (20, 38). The recombinant viruses were plaque purified, amplified using L929 cells, purified using CsCl gradients (49), and stored as diluted aliquots at -80°C.

Virus replication. Primary cardiac myocyte and cardiac fibroblast cultures were plated in 96-well clusters. Cells were infected at a multiplicity of infection (MOI) of 3 PFU per cell for single-cycle assays and 0.1 PFU per cell for multicycle assays. After 1 h of incubation at 37°C, additional supplemented medium was added to each well. For some experiments, this overlay also contained 640 neutralizing units per ml (final concentration) of anti-IFN-β antibody (catalog no. 32400-1; PBL, Inc., Piscataway, NJ) and, at 2 days postinfection, these cells were again treated with anti-IFN-β antibody (320 neutralizing units per ml). Cells were incubated for various times before freezing at -80°C. Plates of cells were frozen and thawed twice more, and cells were lysed in 0.5% Nonidet P-40. For plaque assays, serial dilutions of the lysates were used to infect monolayers of L929 cells, which were subsequently overlaid with agar and stained with neutral red as described previously (44). In each experiment, duplicate or triplicate wells of cardiac cells were each assessed for viral replication by duplicate plaque assay wells.

SDS-PAGE and immunoblotting. Primary cardiac myocyte cultures were plated in 24-well clusters, infected at an MOI of 10 PFU per cell, incubated for 24 h, and lysed to generate total cellular protein extracts using radioimmunoprecipitation assay lysis buffer (50 mM Tris-HCl [pH 7.4], 1% NP-40, 0.25% sodium deoxycholate, 150 mM NaCl, 1 mM EDTA) supplemented to contain 1% SDS and a cocktail of protease and phosphatase inhibitors (Sigma-Aldrich, catalog numbers P8340 and P2850, respectively). Cells were rocked on ice for 25 min and centrifuged at $10{,}000 \times g$ for 10 min at 4°C to remove cellular debris. Protein concentrations were determined by using a bicinchoninic acid protein assay (Thermo Fisher Scientific, catalog no. 23227), and 10 μg of protein from each lysate was boiled for 5 min in 1$\times$ Laemmli sample buffer and resolved using 10% SDS-polyacrylamide gel electrophoresis (PAGE). After protein transfer onto nitrocellulose, membranes were blocked for 1 h in phosphate-buffered saline (PBS) containing 5% bovine serum albumin. Membranes were incubated overnight at 4°C with a rabbit anti-μ2 polyclonal antibody (1:500; generated against two μ2 peptides by Open Biosystems, Huntsville, AL). Membranes were washed three times for 5 min each in PBS containing 0.05% Tween 20 (PBS-T) and then incubated for 1 h at room temperature with a goat anti-rabbit horseradish peroxidase-conjugated polyclonal (secondary) antibody (1:2,000; Millipore, catalog no. AP132P). The membranes were washed, and proteins were visualized using enhanced chemiluminescence (GE Healthcare, catalog no. RPN2108) according to the manufacturer's instructions. Membranes were exposed to film and converted to digital format using an HP Scanjet G4050.

CPE. Primary cardiac myocyte and cardiac fibroblast cultures were plated in 96-well clusters. Cells were infected at an MOI of 10 PFU per cell (single-cycle assays) or 0.1 PFU per cell (multicycle assays) in five replicate wells. After 1 h of incubation at 37°C, additional supplemented medium was added to each well. At 7 days (multicycle assay), the cultures were photographed using a Nikon TE-200 inverted microscope (phase contrast). At 2 days (single-cycle assays) or 5 or 7 days (multicycle assays) postinfection, an MTT assay was performed to quantify cell viability (48). An automated microplate reader (TECAN Sunrise Microplate Reader) was used to determine the optical density at 570 (OD_{570}) and the OD_{650}. The absorbance was determined by subtracting OD_{650} from OD_{570}.

Quantitative (real-time) reverse transcription-PCR (qRT-PCR). Duplicate wells were plated in 24-well (L929 cells) or 48-well (primary cardiac cell cultures) clusters. Cells were infected at an MOI of 25 PFU per cell (L929 cells) or 10 PFU per cell (primary cardiac cell cultures). After 1 h of incubation at 37°C, additional supplemented medium was added to each well. L929 cells were incubated for 20 h, treated with 100 or 1,000 U of IFN-β (catalog no. 12400-1; PBL, Inc.)/ml, and incubated for an additional 5 h. Primary cardiac myocyte and cardiac fibroblast cultures were incubated for 8 and 24 h postinfection. All cells were lysed with an RNeasy kit (Qiagen, Inc.), and total RNA was harvested and treated with RNase-free DNase I (Qiagen, Inc.). From each harvested well, one-third of the total RNA was used to generate cDNA by reverse transcription in a 100-μl reaction containing 5 μM oligo(dT) (Invitrogen Corp.), 1$\times$ *Taq* buffer (Promega Corp.), 7.5 mM $MgCl_2$ (Promega Corp.), 1 mM dithiothreitol (Promega Corp.), 1 mM concentrations of each deoxynucleoside triphosphate (Roche), 0.67 U of RNasin (Promega Corp.)/μl, and 0.20 U of avian myeloblastosis virus reverse transcriptase (Promega Corp.)/μl. Then, 5% of the reverse transcription product was amplified on an iCycler iQ fluorescence thermocycler (Bio-Rad Laboratories) in 96-well plates. Each duplicate 25-μl reaction contained 1$\times$ Quantitech SYBR green master mix (Qiagen, Inc.), 10 mM fluorescein, and 0.3 μM concentrations of each

forward and reverse primer. Primer sequences were as previously published (50). The relative abundance of IRF7, IFN-β, and GAPDH (glyceraldehyde-3-phosphate dehydrogenase) mRNA was determined by comparison to a standard curve generated from serial dilutions of a DNA standard; IRF7 and IFN-β expression and IRF7 fold repressions were normalized to GAPDH expression.

Statistical analysis. A Student two-sample *t* test (pooled variance; Systat 9.0) was applied to all data except those for Fig. 6, where a chi-square test was applied. The results were considered significant if the *P* value was <0.05.

RESULTS

Amino acid (aa) 208 in reovirus protein μ2 determines reovirus repression of IFN signaling. The M1 gene product, μ2, of reovirus strain T1L but not that of strain T3D represses IFN signaling in L929 cells (56). To identify the μ2 amino acids responsible for repression of IFN signaling, viruses containing T1L-T3D chimeric M1 genes or viruses containing mutations in the M1 gene (Fig. 1A) were tested for the capacity to repress IFN signaling in L929 cells (Fig. 1B). A recombinant virus containing nine genes from T3D and a chimeric M1 gene expressing the N-terminal 126 μ2 amino acids from T3D and remaining amino acids from T1L (Ch1) was as effective as T1L at repressing IFN induction of IRF7. In contrast, viruses containing a chimeric M1 gene expressing the N-terminal 208 μ2 amino acids (Ch2) or more (Ch3 and Ch4) from T3D failed to repress IFN signaling. Strains T1L and T3D differ at only aa 208 in the μ2 region spanning aa 127 through aa 208. Remarkably, a T3D virus mutated at only μ2 residue 208 (T3D-S208P), changing it from the T3D serine (S) to a T1L proline (P), repressed IFN signaling as effectively as T1L. Conversely, a virus containing nine T3D genes and the T1L M1 gene mutated to T3D serine at μ2 residue 208 (T3D-T1LM1-P208S) failed to repress IFN signaling. Together, these data demonstrate that T1L μ2 aa 208 is both required and sufficient for reovirus repression of IFN signaling.

μ2 aa 208 modulates reovirus induction of IFN-β in cardiac cells. As anticipated from previous reports (48, 55), in cardiac myocytes, T3D induced IFN-β well and T1L induced IFN-β poorly (Fig. 2A, $P < 0.001$ at 8 and 24 h). Differences in T3D and T1L induction of IFN in cardiac myocytes segregate with the M1, L2, and S2 genes (48). Reovirus infection stimulates PRRs to induce IFN-β (16, 18, 26). While strain-specific differences in induction of IFN could reflect differences in this stimulation, they also could reflect differences in repression of IFN signaling since reovirus-mediated induction of IFN involves the positive feedback loop in cardiac myocytes (50, 56). T3D-T1LM1 induced markedly less IFN-β than did T3D (Fig. 2A, $P < 0.001$ at 8 and 24 h), a finding consistent with the association of the T1L M1 gene with poor induction of IFN (48). T1L-T3DM1 also induced minimal IFN-β ($P < 0.001$ relative to T3D at 8 and 24 h), which is consistent with the association of the T1L L2 and S2 genes with poor induction of this cytokine (48). Thus, the T3D M1 gene is not sufficient for strong induction of IFN. Instead, a full response requires the T3D L2 and S2 genes in addition to the T3D M1 gene.

To determine the effect of μ2 aa 208 on reovirus induction of IFN, viruses with single aa substitutions at that site were tested. At 8 h postinfection in cardiac myocytes (Fig. 2A), viral induction of IFN-β was decreased almost 3-fold by changing T3D μ2 aa 208 to that of T1L (T3D-S208P; $P < 0.001$), indicating that μ2 aa 208 modulates reovirus induction of IFN-β at this early time. However, by 24 h postinfection, T3D and T3D-S208P induction of

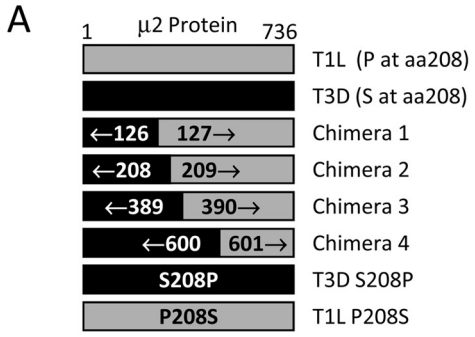

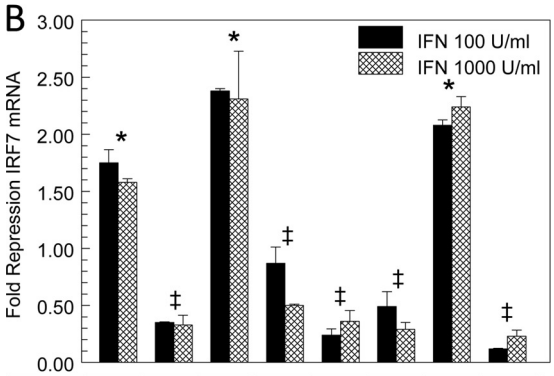

Virus Name	T1L	T3D	Ch 1	Ch 2	Ch 3	Ch 4	T3D-S208P	T3D-T1LM1-P208S
9 Genes	T1L	T3D	T3D	T3D	T3D	T3D	T3D	T3D
Substitute M1 Gene	–	–	Ch 1	Ch 2	Ch 3	Ch 4	–	T1L
T1L μ2 Amino Acids	–	–	127-736	209-736	390-736	601-736	208	all except 208

FIG 1 μ2 aa 208 determines reovirus repression of IFN signaling. (A) Viruses with a chimeric M1 gene or viruses with a mutated amino acid at position 208 of μ2 were generated by reverse genetics (21, 38). (B) L929 cells were infected with the indicated viruses, cells were treated with IFN, and mRNA was harvested for qRT-PCR. The fold repression was calculated as ([copies IRF7/GAPDH in IFN-treated mock-infected cells]/[copies IRF7/GAPDH in IFN-treated virus-infected cells]). Viruses that induce high levels of IFN resulted in values <1, but the relative repression between viruses was the same (56). The results are means $\pm$ the standard deviation (SD) (average of replicate wells; representative of four experiments). *, Different from T3D ($P < 0.05$); ‡, different from T1L ($P < 0.05$).

IFN-β (Fig. 2A, $P > 0.05$) and IRF7 (Fig. 2B, $P > 0.05$) were similar, indicating that repression of IFN signaling is not the primary determinant of strain-specific differences in reovirus induction of IFN-β. The similar induction of IRF7 by T3D and T3D-S208P (Fig. 2B) contrasts with T3D-S208P repression of exogenous IFN induction of IRF7 (Fig. 1B), likely reflecting the difference between induction of IRF7 concomitant with (Fig. 2B) or after (Fig. 1B) the majority of μ2 expression. Interestingly, other sequences in the T1L M1 gene also affected induction of IFN-β. Specifically, in contrast to the minimal effect of changing T3D μ2 aa 208 to that of T1L (T3D-S208P), induction of IFN-β and IRF7 was significantly increased by changing T1L μ2 aa 208 of T3D-T1LM1 to that of T3D (T3D-T1LM1-P208S, Fig. 2A and B, $P < 0.01$ at 8 and 24 h for both IFN-β and IRF7). In addition, the substantial increase in the induction of IFN-β at 24 h by T3D-T1LM1-P208S relative to T3D (Fig. 2A, $P < 0.001$) suggests that

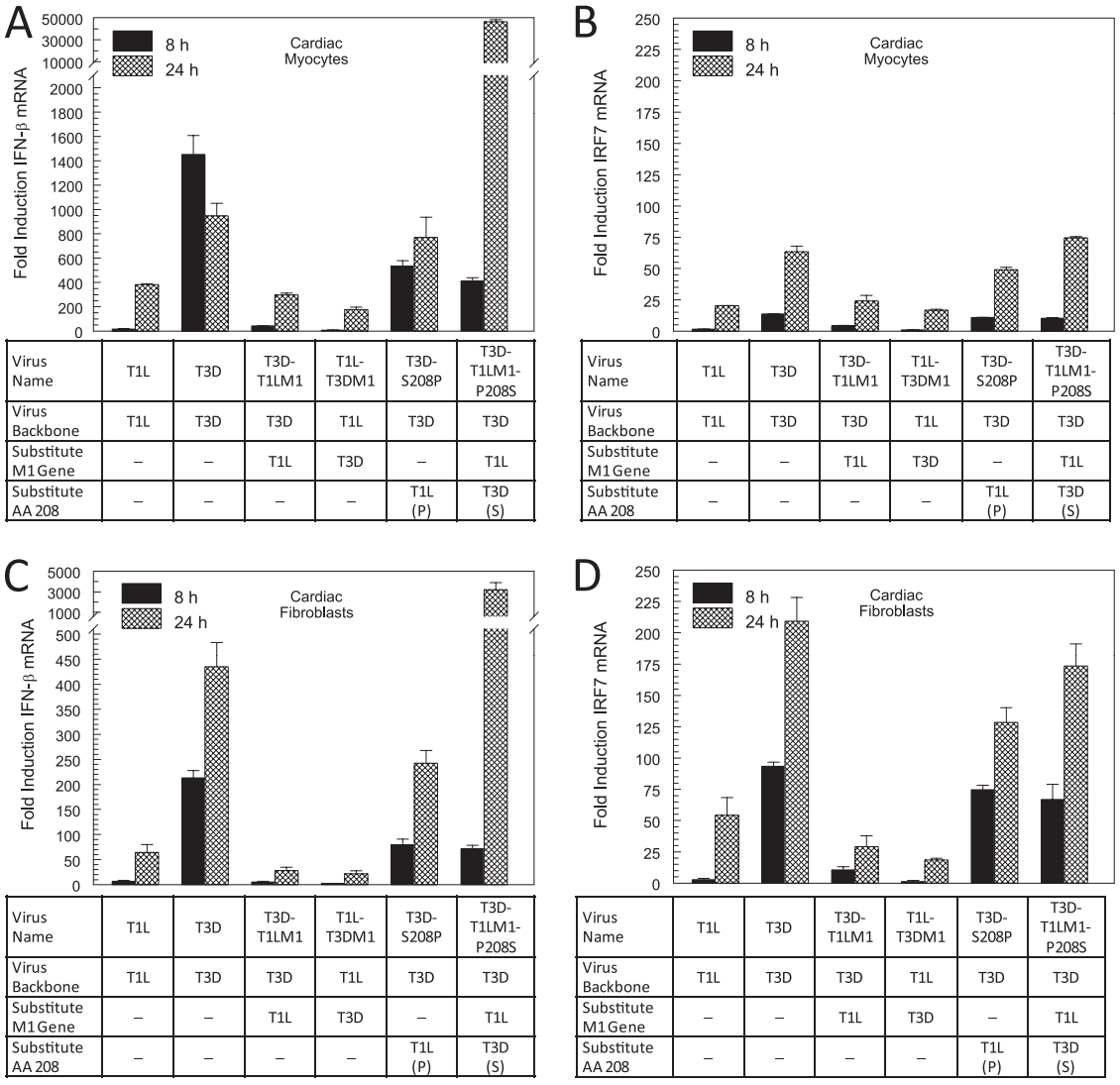

FIG 2 μ2 aa 208 modulates reovirus induction of IFN in cardiac cells. Primary cardiac myocyte (A and B) or fibroblast (C and D) cultures were infected with the indicated viruses, and mRNA was harvested for qRT-PCR using primers specific for IFN-β (A and C) or IRF7 (B and D) and GAPDH. The fold induction was calculated as copies IFN-β or IRF7/GAPDH in infected cultures relative to uninfected cultures. (A and C) Results are means ± the standard errors of the mean (SEM) (average of two experiments); (B and D) results are means ± the SD (average of replicate wells; representative of two experiments). See the statistical analyses in the text.

T1L M1 sequences other than aa 208 influence induction of this cytokine. The results for cardiac fibroblasts (Fig. 2C and D) were similar to those for cardiac myocytes, with the notable and expected difference (50, 55) that reovirus induction of IFN-β is much higher in cardiac myocytes than in cardiac fibroblasts (compare scales between Fig. 2A and C), but the opposite is true for reovirus induction of ISGs (Fig. 2B and D). Thus, reovirus μ2 proline 208 (the T1L residue) represses the induction of IFN-β in both cardiac myocytes and cardiac fibroblasts, but predominantly when expressed in the context of the entire T1L M1 gene.

***μ2* aa 208 determines reovirus single-cycle and multicycle replication in cardiac myocytes.** As expected (48, 50), T1L achieved higher titers in cardiac myocytes than did T3D after single or multiple cycles of replication (Fig. 3A and 3B; $P < 0.005$ for both cases). Differences between T1L and T3D could reflect IFN-dependent, IFN-independent, or both mechanisms. After single or multiple cycles of replication, T1L-T3DM1 titers were as low ($P > 0.05$) or lower than those for T3D, whereas T3D-T1LM1 titers were as high ($P > 0.05$) as those for T1L, demonstrating that the T1L M1 gene is both required and sufficient for reovirus to replicate maximally in cardiac myocytes. After single (Fig. 3A) or multiple (Fig. 3B) cycles of replication, the titers for T3D-T1LM1-P208S were as low ($P > 0.05$) or lower than those for T3D, demonstrating that T1L μ2 aa 208 is required for production of high titers in cardiac myocytes. Conversely, after a single round of replication, titers for T3D-S208P were even higher ($P < 0.05$) than those for T1L, demonstrating that T1L μ2 aa 208 is sufficient for high titers in cardiac myocytes. As expected, levels of μ2 protein paralleled levels of infectious virus (Fig. 3A).

To determine whether T1L μ2 aa 208 regulates replication in cardiac myocytes solely by regulating the IFN response, titers were compared after multiple cycles of replication in the absence or

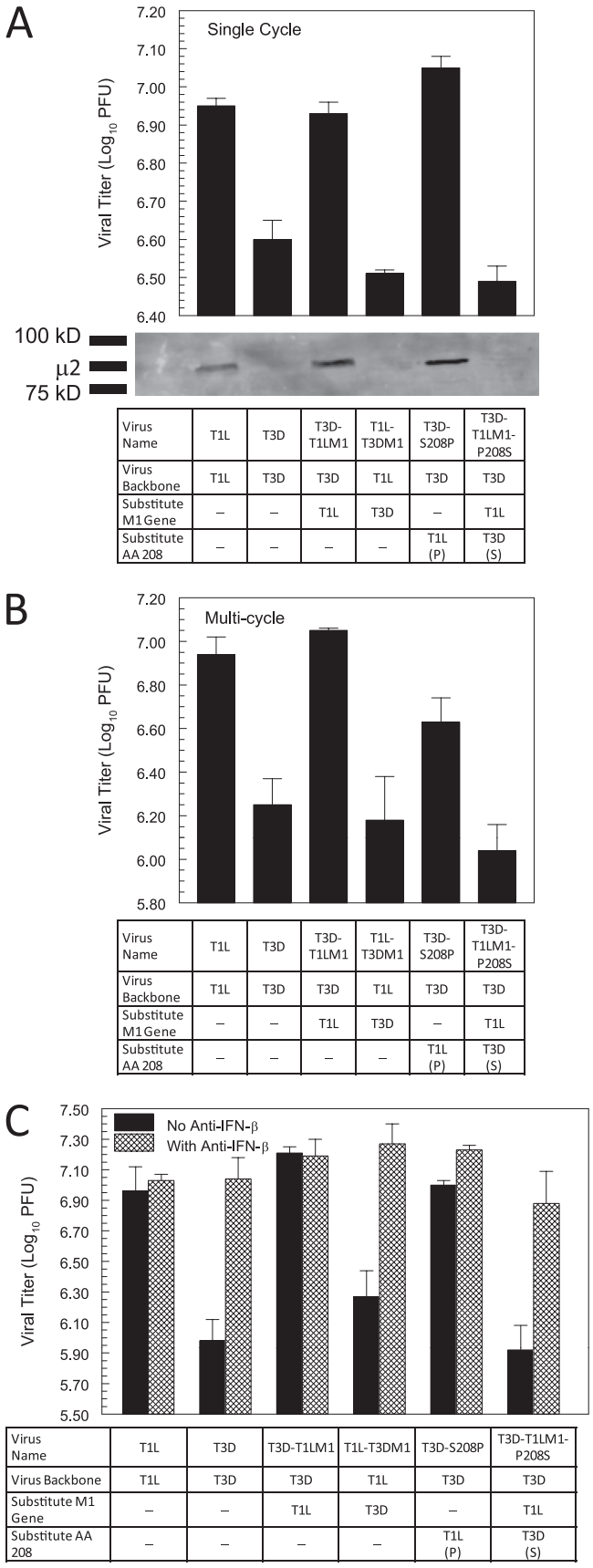

Virus Name	T1L	T3D	T3D-T1LM1	T1L-T3DM1	T3D-S208P	T3D-T1LM1-P208S
Virus Backbone	T1L	T3D	T3D	T1L	T3D	T3D
Substitute M1 Gene	–	–	T1L	T3D	–	T1L
Substitute AA 208	–	–	–	–	T1L (P)	T3D (S)

presence of anti-IFN-β antibody (Fig. 3C). As anticipated (48), elimination of the IFN response in cardiac myocytes increased T3D replication 11.5-fold ($P = 0.001$), which is consistent with evidence that the IFN response dictates the replication efficiency of this strain in these cells. Furthermore, elimination of the IFN response increased replication of all viruses tested to the level of T1L ($P > 0.05$) or higher, demonstrating that μ2 aa 208 regulates reovirus multicycle replication in cardiac myocytes by regulating the IFN response.

μ2 aa 208 influences reovirus single-cycle and multicycle replication in cardiac fibroblasts. In contrast to results obtained in experiments using cardiac myocytes, differences in yields of T1L and T3D were apparent in cardiac fibroblasts only after multiple cycles of replication, suggesting that the IFN response has little effect on initial infection in cardiac fibroblasts (Fig. 4A and B). This finding is consistent with the dramatically lower induction of IFN by reovirus in cardiac fibroblasts (Fig. 2C) than in cardiac myocytes (Fig. 2A). Indeed, in contrast to cardiac myocytes, the T1L M1 gene did not result in a higher yield of T3D (T3D-T1LM1) after a single cycle of replication in cardiac fibroblasts (Fig. 4A, $P > 0.05$). Replication of T3D-T1LM1-P208S was markedly reduced relative to the parent T3D-T1LM1 virus, most likely reflecting the effect of the single aa 208 substitution on induction of IFN (Fig. 2C. $P = 0.002$) and suggesting that the IFN response can modulate reovirus replication in cardiac fibroblasts if the IFN response is sufficiently strong. Replication of T1L-T3DM1 was reduced relative to both T1L and T3D after a single cycle of replication (Fig. 4A, $P < 0.001$), but intermediate between these two viruses after multiple cycles (Fig. 4B, $P < 0.001$). While reproducible, the underlying mechanism is unclear but may reflect heterologous gene combinations that are detrimental only in certain cell types (33). After multiple cycles of replication in cardiac fibroblasts, T3D replicated less well than T1L ($P < 0.001$), a property determined by the M1 gene (Fig. 4B). T3D-T1LM1-P208S produced the lowest titers of the viruses tested, a finding consistent with its dramatically higher induction of IFN (Fig. 2C).

To test the role of IFN in μ2 aa 208 effects on reovirus replication in cardiac fibroblasts, virus titers in the presence or absence of anti-IFN-β antibody were compared (Fig. 4C). In comparison to results using cardiac myocytes, all viruses achieved only slightly higher titers when IFN was eliminated, consistent with the low level of IFN induced in cardiac fibroblasts relative to cardiac myocytes (Fig. 2).

μ2 aa 208 determines reovirus CPE in cardiac myocytes only after spread. Results thus far suggested that T1L μ2 aa 208 influences the IFN response to reovirus in both cardiac myocytes and cardiac fibroblasts but that the effect on viral replication is greater in cardiac myocytes than in cardiac fibroblasts. To determine the

Virus Name	T1L	T3D	T3D-T1LM1	T1L-T3DM1	T3D-S208P	T3D-T1LM1-P208S
Virus Backbone	T1L	T3D	T3D	T1L	T3D	T3D
Substitute M1 Gene	–	–	T1L	T3D	–	T1L
Substitute AA 208	–	–	–	–	T1L (P)	T3D (S)

FIG 3 μ2 aa 208 determines reovirus single-cycle and multicycle replication in cardiac myocytes. (A) Primary cardiac myocyte cultures were infected with the indicated viruses at an MOI of 3 PFU per cell and harvested for plaque assay after 24 h or infected at 10 PFU per cell and harvested for immunoblotting after 24 h. The leftmost lane contains mock-infected sample. (B) Primary cardiac myocyte cultures were infected at an MOI of 0.1 PFU per cell and harvested for plaque assay after 5 days. (C) Primary cardiac myocyte cultures were infected as in panel B, treated with anti-IFN-β antibody where indicated, and harvested for plaque assay. All results are means ± the SD (average of replicate wells; representative of two to four experiments). See the statistical analyses in the text.

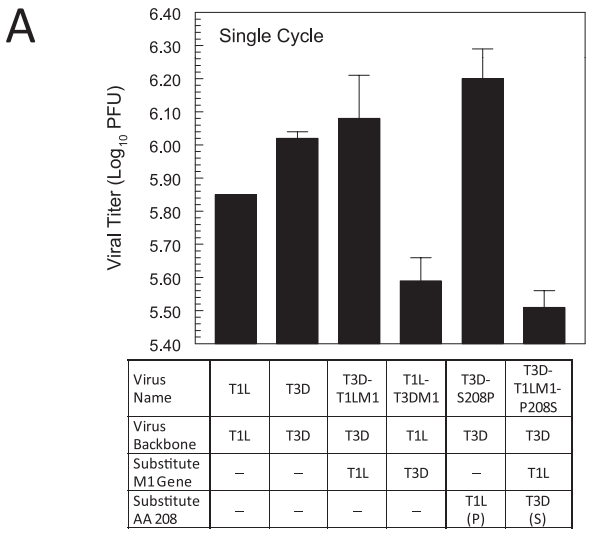

Virus Name	T1L	T3D	T3D-T1LM1	T1L-T3DM1	T3D-S208P	T3D-T1LM1-P208S
Virus Backbone	T1L	T3D	T3D	T1L	T3D	T3D
Substitute M1 Gene	–	–	T1L	T3D	–	T1L
Substitute AA 208	–	–	–	–	T1L (P)	T3D (S)

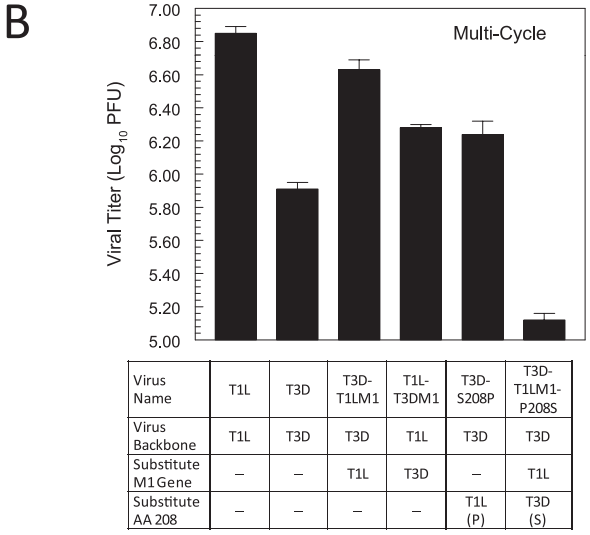

Virus Name	T1L	T3D	T3D-T1LM1	T1L-T3DM1	T3D-S208P	T3D-T1LM1-P208S
Virus Backbone	T1L	T3D	T3D	T1L	T3D	T3D
Substitute M1 Gene	–	–	T1L	T3D	–	T1L
Substitute AA 208	–	–	–	–	T1L (P)	T3D (S)

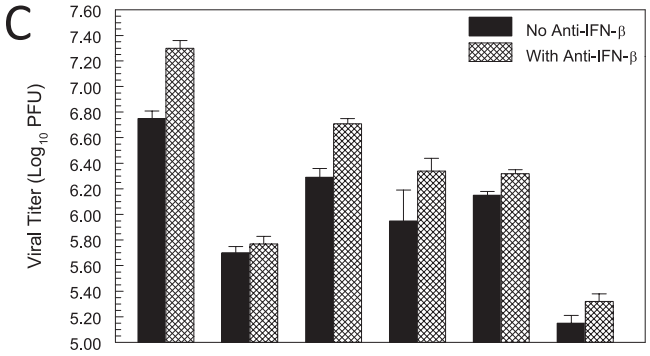

Virus Name	T1L	T3D	T3D-T1LM1	T1L-T3DM1	T3D-S208P	T3D-T1LM1-P208S
Virus Backbone	T1L	T3D	T3D	T1L	T3D	T3D
Substitute M1 Gene	–	–	T1L	T3D	–	T1L
Substitute AA 208	–	–	–	–	T1L (P)	T3D (S)

FIG 4 μ2 aa 208 influences reovirus single-cycle and multicycle replication in cardiac fibroblasts. Primary cardiac fibroblast cultures were infected with the indicated viruses at an MOI of 3 PFU per cell and incubated for 24 h (A) or at an MOI of 0.1 PFU per cell and incubated for 5 days (B) and harvested for plaque assay. (C) Primary cardiac fibroblast cultures were infected as in panel B, treated with anti-IFN-β where indicated, and harvested for plaque assay. All results are means ± the SD (average of replicate wells; representative of two to four experiments). See the statistical analyses in the text.

contribution of μ2 aa 208 to viral CPE, cardiac cells were infected at a high MOI (10 PFU per cell) and cell viability was quantified after a single cycle of replication (2 days) or the cells were infected at a low MOI (0.1 PFU per cell) and cell viability was quantified after multiple cycles of replication (5 days and 7 days). PFU are quantified using L929 cells, and virus is less infectious in cardiac cells than in L929 cells (data not shown). Therefore, even at an MOI of 10 PFU per cell, not all cardiac cells are infected (44). In cardiac fibroblasts, none of the viruses were cytopathic after a single cycle of replication, and CPE increased only minimally after multiple cycles (data not shown). As expected (48), T1L and T3D were similarly cytopathic in cardiac myocytes after a single cycle of replication (Fig. 5). However, after multiple cycles of replication, T1L and T3D clearly differed in the induction of CPE ($P < 0.001$ at 5 and 7 days), as did the entire panel of viruses. The overall trend inversely correlated with viral replication in cardiac myocytes (Fig. 3A and B): viruses that replicated to the highest titers left the fewest cells viable. More specifically, after 5 or 7 days, T3D-T1LM1 was even more cytopathic than T1L ($P < 0.001$), while T1L-T3DM1 was as noncytopathic as T3D at 5 days ($P > 0.05$) and only slightly more cytopathic at 7 days. Moreover, changing only T3D μ2 aa 208 to that of T1L (T3D-S208P) increased cytopathicity to even greater than that of T1L ($P < 0.002$). Finally, T3D-T1LM1-P208S cytopathicity was markedly reduced relative to the parent T3D-T1LM1 virus ($P < 0.001$). Gross CPE paralleled MTT results (Fig. 5B). Together, these results demonstrate that T1L μ2 aa 208 determines CPE after viral spread, likely through repression of the IFN signaling that is required for the positive feedback loop of induction of IFN-β.

***μ*2 aa 208 modulates myocarditis.** To determine the effect of μ2 aa 208 on viral myocarditis, mice were inoculated with the panel of recombinant viruses, and cardiac lesions were quantified. As expected (45), T1L induced cardiac lesions in all mice, while T3D induced few lesions (Fig. 6). Reovirus strain-specific differences in the capacity to induce myocarditis segregate with the M1, L1, and L2 genes (45, 46), but the role of the M1 gene alone has not been previously determined. A virus containing the T1L M1 gene in the T3D genetic background (T3D-T1LM1) induced a higher frequency of myocarditis than did T3D ($P < 0.05$), demonstrating that the T1L M1 gene when introduced into the genetic background of T3D is sufficient to cause myocarditis. The T3D M1 gene in the T1L genetic background (T1L-T3DM1) induced a lower frequency of myocarditis than did T1L ($P < 0.05$), confirming the importance of the T1L M1 gene in this phenotype. Furthermore, although not statistically significant, T1L-T3DM1 appeared to induce myocarditis more efficiently than did T3D, providing evidence to support previous conclusions that genes in T1L in addition to M1 contribute to myocarditis (45, 46). Finally, changing T3D μ2 aa 208 to that of T1L (T3D-S208P) dramatically increased the frequency of myocarditis ($P < 0.05$) compared to that caused by T3D ($P < 0.05$), suggesting that repression of IFN signaling alone can modulate this disease. T3D-T1LM1-P208S appeared to be less myocarditic than the parental T3D-T1LM1 virus but more myocarditic than T3D (not statistically significant), supporting the importance of repression of IFN signaling but indicat-

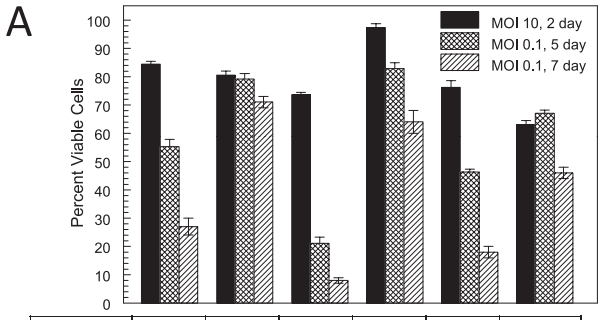

Virus Name	T1L	T3D	T3D-T1LM1	T1L-T3DM1	T3D-S208P	T3D-T1LM1-P208S
Virus Backbone	T1L	T3D	T3D	T1L	T3D	T3D
Substitute M1 Gene	–	–	T1L	T3D	–	T1L
Substitute AA 208	–	–	–	–	T1L (P)	T3D (S)

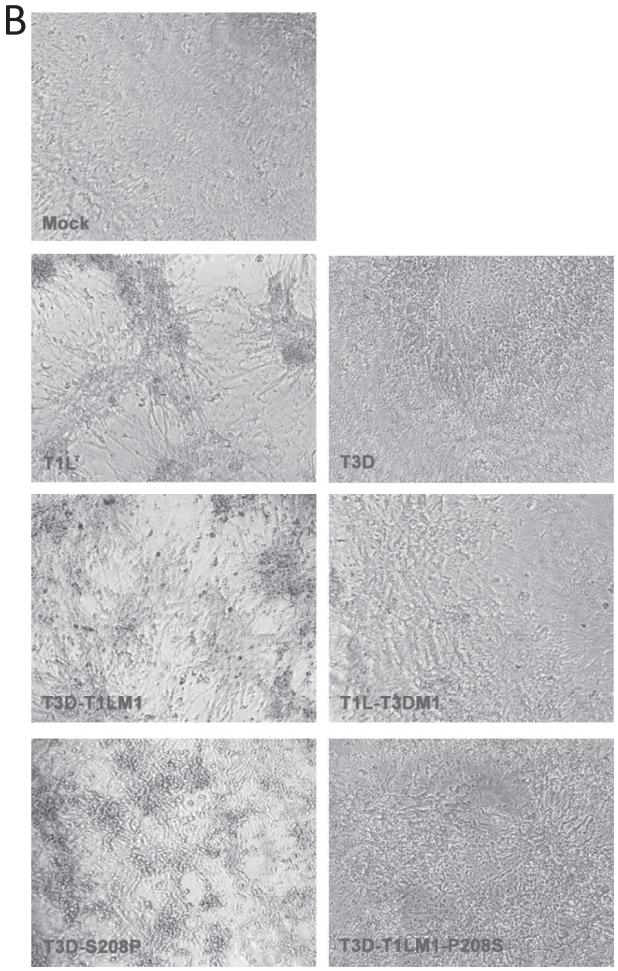

FIG 5 μ2 aa 208 determines reovirus CPE in cardiac myocytes only after spread. (A) Primary cardiac myocyte cultures were infected with the indicated viruses at an MOI of 10 PFU per cell and incubated for 2 days (single cycle) or at an MOI 0.1 PFU per cell and incubated for 5 or 7 days (multicycle) and harvested for MTT assay. The percent viable cells was calculated relative to mock-infected cells. The results at 2 and 5 days are means ± the SEM (average of at least two experiments); results at 7 days are means ± the SD (average of replicate wells for a single experiment). See the statistical analyses in the text. (B) Primary cardiac myocyte cultures were infected at an MOI of 0.1 PFU per cell, incubated for 7 days, and photographed at a final magnification of ×100 (representative fields shown).

ing that other T1L M1 functions are also determinants of myocarditis. Collectively, these results demonstrate that μ2 aa 208 modulates myocarditis, suggesting that repression of IFN signaling is a determinant of reovirus-induced cardiac disease.

DISCUSSION

The IFN-α/β response is essential for protection against reovirus infection of cardiac cells *in vitro* and reovirus-induced myocarditis in mice (48). We demonstrated here that sequence polymorphisms at reovirus protein μ2 aa 208 are both required and sufficient for strain-specific differences in reovirus repression of IFN-β signaling. Furthermore, μ2 aa 208 modulation of IFN expression and signaling determines viral replication and spread in cardiac myocytes and modulates myocarditis in mice.

Virus-induced IFN-β stimulates the expression of antiviral ISGs, as well as transcription factor IRF7, which results in further induction of IFN-β in a positive amplification loop. Viral repression of IFN signaling could: (i) limit IFN expression to that initiated by PRRs and (ii) suppress IFN-induced expression of antiviral genes. Viruses have evolved many mechanisms to antagonize IFN signaling, including inactivation of JAKs, degradation or sequestration of STATs, and inhibition of karyopherins required for ISGF3 nuclear translocation (41). Only two viruses are known to repress IFN signaling through IRF9: human papillomavirus type 16 sequesters IRF9 to inhibit its nuclear translocation (1), and adenovirus infection leads to a decrease in IRF9 levels (25). The μ2 protein from reovirus strain T1L but not strain T3D represses IFN-β signaling, and this repression is associated with nuclear accumulation of IRF9 (56). However, it is not known whether alterations in IRF9 mediate repression or are merely a consequence of that event. In the present study, we found that sequence variation in μ2 aa 208 determines these reovirus strain-specific differences in repression of IFN-β signaling (Fig. 1).

The M1 gene sequences of nine field isolate reovirus strains are available, and while all nine contain a proline or serine at μ2 residue 208, eight contain a proline-like T1L, suggesting a selective advantage (53). Interestingly, μ2 aa 208 governs several differences displayed by strains T1L and T3D. Reovirus replicates and assembles in viral inclusion bodies (VIBs). While T3D induces formation of globular VIBs, T1L induces formation of filamentous VIBs, reflecting T1L μ2-stimulated hyperacetylation and stabilization of microtubules (39). While these T1L μ2-stimulated events are disrupted when the T1L proline at aa 208 is substituted with the T3D serine (39), substitutions at μ2 aa 383 also prevent T1L formation of filamentous VIBs (21). Importantly, aa 208 mediates greater ubiquitylation and aggregation of T3D μ2 than T1L μ2, suggesting that the capacity of T1L μ2 to stabilize microtubules and induce filamentous VIBs may be a consequence of virus strain-specific posttranslational μ2 modifications (31). The results presented here identify T1L μ2 aa 208 as both required and sufficient for reovirus repression of IFN signaling and suggest two possible models: (i) repression of IFN signaling requires the cytoskeletal changes that accompany formation of filamentous VIBs or (ii) ubiquitylated and aggregated μ2 cannot function to repress IFN signaling. Future studies are planned to discriminate between these possibilities.

Strain-specific differences in reovirus induction of IFN-α/β genetically segregate with the reovirus M1, L2, and S2 genes (48). While T3D induces IFN well and T1L induces IFN poorly (48), it is unclear whether this polymorphism reflects differences in PRR-

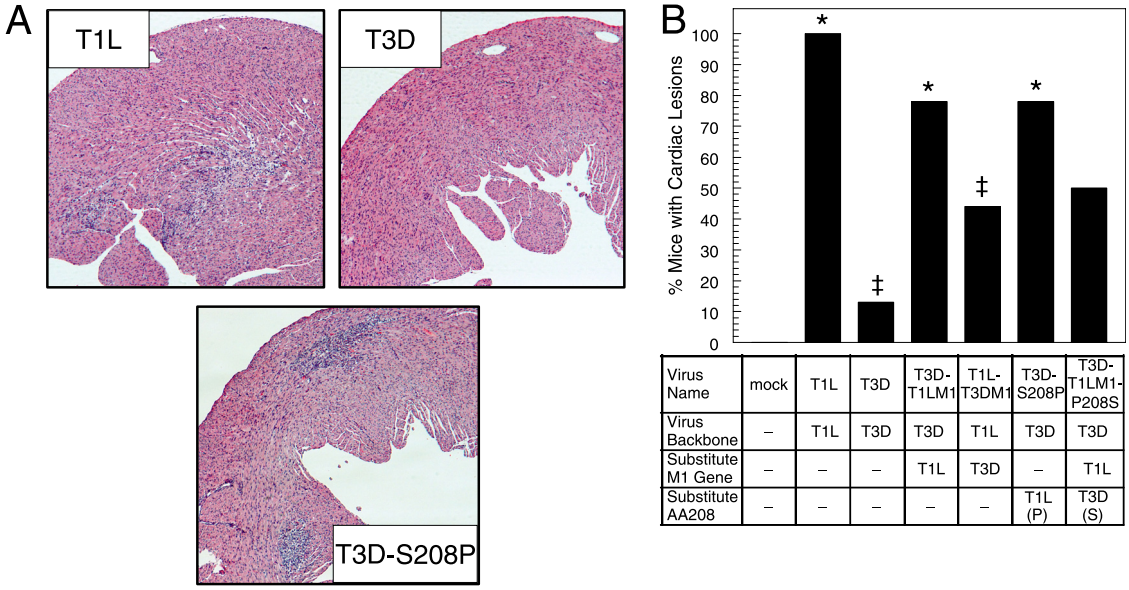

Virus Name	mock	T1L	T3D	T3D-T1LM1	T1L-T3DM1	T3D-S208P	T3D-T1LM1-P208S
Virus Backbone	–	T1L	T3D	T3D	T1L	T3D	T3D
Substitute M1 Gene	–	–	–	T1L	T3D	–	T1L
Substitute AA208	–	–	–	–	–	T1L (P)	T3D (S)

FIG 6 μ2 aa 208 modulates myocarditis. Neonatal mice were inoculated with the indicated viruses and euthanized 7 days postinjection. Hematoxylin-eosin-stained cardiac sections were scored for lesions. (A) Representative sections. (B) A minimum of eight hearts (minimum of 15 sections per heart) were scored for each virus. Lesions in adjacent sections were not scored as independent lesions. Hearts were considered "positive" if more than a single lesion was detected in the $\geq$ 15 sections examined. *, Different from T3D; ‡, different from T1L (chi square, $P < 0.05$). The results are representative of two independent experiments.

stimulated induction, IRF7-mediated amplification, or both effects. The roles of the L2-encoded λ2 and S2-encoded σ2 proteins in these processes have not been reported, but one possible role for the M1-encoded μ2 protein could be to suppress IFN induction of IRF7, thereby inhibiting further induction of IFN. Indeed, substitution of only μ2 aa 208 in T3D to provide a repressor of IFN signaling (T3D-S208P), significantly reduced reovirus induction of IFN in both cardiac myocytes and cardiac fibroblasts at 8 h postinfection (Fig. 2). Interestingly, the converse substitution, in which only μ2 aa 208 in T3D-T1LM1 is replaced to remove the repressor of IFN signaling (T3D-T1LM1-P208S), had a much more substantial effect on reovirus induction of IFN in both cell types (Fig. 2). Specifically, T3D-T1LM1-P208S induced 10-fold more IFN-β than did T3D-T1LM1 at 8 h and a remarkable 150-fold more at 24 h (Fig. 2A) with a concomitant increase in induction of IRF7 (Fig. 2B). Therefore, in the context of the T1L M1 gene, T1L μ2 aa 208 repression of IFN signaling dramatically affected reovirus induction of IRF7 and consequently IFN-β. Importantly, viruses with a T1L M1 gene display enhanced kinetics of viral RNA synthesis in cardiac myocytes in comparison to those with a T3D M1 gene (44). Thus, T1L μ2 should be synthesized earlier than T3D μ2, offering T3D-T1LM1 greater opportunity than T3D-S208P to repress induction of IRF7. The substantial increase in the induction of IFN-β at 24 h by T3D-T1LM1-P208S relative to T3D (Fig. 2A) is consistent with both the absence of the T1L μ2 aa 208 repressor of IFN signaling and the T1L M1-associated rapid RNA synthesis phenotype facilitating RNA-stimulated activation of IRF7 (44). Together, these data indicate that reovirus induction of IFN in cardiac cells involves a positive amplification loop and that repression of IFN signaling reduces reovirus induction of IFN-β.

The reovirus M1-, L2-, and S2-encoded proteins also could modulate reovirus activation of PRRs. Depending on the cell type or perhaps infection stage (14), reovirus activates the PRRs RIG-I, MDA5, or both molecules to induce IFN (16, 18, 26), although the specific nucleic acid stimulus remains unclear. While reovirus particles contain genomic double-stranded RNA (dsRNA), virions are not thought to fully uncoat during viral replication (43), and thus genomic dsRNA should be protected from PRRs. Instead, reovirus cores synthesize single-stranded RNA, which is extruded and then complexed into new subviral particles for RNA second-strand synthesis (43). The μ2 protein is found at the icosahedral vertices of viral cores as part of a probable RNA-synthesizing complex (19, 54), has both NTPase (19, 35) and RNA-binding activity (6, 19, 35), and determines the rate of viral RNA synthesis in cardiac myocytes (44). However, reoviruses with a T1L M1 gene synthesize RNA more rapidly than those with a T3D M1 gene (44), the opposite of what would be predicted if μ2-stimulated viral RNA synthesis solely determined the level of IFN induction. It is possible that the location of both μ2 and λ2 at the icosahedral vertices (7, 11) influences particle stability. Virions contain not only genomic dsRNA, a potential RIG-I and MDA5 ligand, but also short oligonucleotides with free 5′ triphosphates (3, 34, 43), an additional potential RIG-I ligand, although shorter than other RIG-I agonists (27, 28). Therefore, T3D particles may aberrantly disassemble more readily than T1L particles, resulting in commensurately greater PRR activation and induction of IFN. We found that T3D induction of IFN in cardiac cells was reduced when its M1 gene was replaced with that of T1L (T3D-T1LM1, Fig. 2A and C). However, the striking increase in induction of IFN when the T1LM1 repressor of IFN signaling was removed (T3D-T1LM1-P208S), particularly later during infection, suggests that the main function of μ2 in the IFN response is to repress IFN signaling (as in T1L) rather than to shield PRR ligands from the innate immune surveillance machinery.

The protective effects of secreted IFN should be greater in cells that have not been infected, i.e., as a paracrine signal, than in cells already infected, i.e., as an autocrine signal, since the former have

more time to induce antiviral proteins. In addition, IFN-mediated reductions in viral yield should result in fewer secondary infections. Therefore, the effect of the IFN response on viral yield should be amplified following viral spread. The IFN response determines reovirus yields in primary cardiac myocyte cultures and, as expected, the effect is increased following viral spread (48). We found that μ2 aa 208 determines strain-specific differences in viral replication in cardiac myocytes even after a single cycle of replication (Fig. 3A), suggesting that IFN can reduce viral replication in these cells even after infection is initiated. As expected, the effect was enhanced after multiple cycles (Fig. 3B), and all viruses achieved equivalent titers when IFN was removed (Fig. 3C). Together, the data demonstrate that μ2 aa 208 regulation of the IFN response determines reovirus replication and spread between cardiac myocytes.

Virus strain-specific differences in the induction of myocarditis correlate with differences in CPE in primary cardiac myocyte cultures only after viral spread (2, 48), which is consistent with the IFN response regulating viral spread *in vitro* and *in vivo* (15, 36, 48). Many investigations have used IFN-deficient mice or viruses that are defective in repressing the IFN response to demonstrate the importance of the IFN response in protection against virus-induced disease, but few have pinpointed the populations of differentiated cells in which IFN critically acts to limit progression of viral infection. Here, we found that a serine-proline polymorphism at aa 208 in the reovirus μ2 protein influences CPE after multiple cycles of replication in cardiac myocytes (Fig. 5) and modulates myocarditis (Fig. 6), providing evidence that viral repression of IFN signaling in a target differentiated cell can determine disease outcome.

ACKNOWLEDGMENTS

We thank Lianna Li and Ray Pickles for insightful discussions and Lance Johnson for excellent technical assistance.

This research was supported by Public Health Service awards R01 AI32539 (T.S.D.), R37 AI38296 (T.S.D.), and R01 A1083333 (B.S.) and the Elizabeth B. Lamb Center for Pediatric Research. Additional support was provided by Public Health Service awards CA68485 for the Vanderbilt-Ingram Cancer Center and DK20593 for the Vanderbilt Diabetes Research and Training Center.

REFERENCES

1. **Barnard P, McMillan NA.** 1999. The human papillomavirus E7 oncoprotein abrogates signaling mediated by interferon-alpha. Virology **259**:305–313.
2. **Baty CJ, Sherry B.** 1993. Cytopathogenic effect in cardiac myocytes but not in cardiac fibroblasts is correlated with reovirus-induced acute myocarditis. J. Virol. **67**:6295–6298.
3. **Bellamy AR, Joklik WK.** 1967. Studies on the A-rich RNA of reovirus. Proc. Natl. Acad. Sci. U. S. A. **58**:1389–1395.
4. **Bergmann O, et al.** 2009. Evidence for cardiomyocyte renewal in humans. Science **324**:98–102.
5. **Bowie AG, Unterholzner L.** 2008. Viral evasion and subversion of pattern-recognition receptor signalling. Nat. Rev. Immunol. **8**:911–922.
6. **Brentano L, Noah D, Brown EG, Sherry B.** 1998. The reovirus protein mu 2, encoded by the M1 gene, is an RNA-binding protein. J. Virol. **72**:8354–8357.
7. **Coombs KM.** 1998. Stoichiometry of reovirus structural proteins in virus, ISVP, and core particles. Virology **243**:218–228.
8. **Cooper LT, Jr.** 2009. Myocarditis. N. Engl. J. Med. **360**:1526–1538.
9. **Daliento L, et al.** 2003. Successful treatment of enterovirus-induced myocarditis with interferon-alpha. J. Heart Lung Transplant. **22**:214–217.
10. **Drory Y, et al.** 1991. Sudden unexpected death in persons less than 40 years of age. Am. J. Cardiol. **68**:1388–1392.
11. **Dryden KA, et al.** 1998. Internal structures containing transcriptase-related proteins in top component particles of mammalian orthoreovirus. Virology **245**:33–46.
12. **Feldman AM, McNamara D.** 2000. Myocarditis. N. Engl. J. Med. **343**:1388–1398.
13. **Fensterl V, Sen GC.** 2009. Interferons and viral infections. Biofactors **35**:14–20.
14. **Fredericksen BL, Keller BC, Fornek J, Katze MG, Gale M, Jr.** 2008. Establishment and maintenance of the innate antiviral response to West Nile virus involves both RIG-I and MDA5 signaling through IPS-1. J. Virol. **82**:609–616.
15. **Holm GH, et al.** 2010. Interferon regulatory factor 3 attenuates reovirus myocarditis and contributes to viral clearance. J. Virol. **84**:6900–6908.
16. **Holm GH, et al.** 2007. Retinoic acid-inducible gene-I and interferon-beta promoter stimulator-1 augment proapoptotic responses following mammalian reovirus infection via interferon regulatory factor-3. J. Biol. Chem. **282**:21953–21961.
17. **Honda K, et al.** 2005. IRF-7 is the master regulator of type-I interferon-dependent immune responses. Nature **434**:772–777.
18. **Kato H, et al.** 2008. Length-dependent recognition of double-stranded ribonucleic acids by retinoic acid-inducible gene-I and melanoma differentiation-associated gene 5. J. Exp. Med. **205**:1601–1610.
19. **Kim J, Parker JS, Murray KE, Nibert ML.** 2004. Nucleoside and RNA triphosphatase activities of orthoreovirus transcriptase cofactor mu2. J. Biol. Chem. **279**:4394–4403.
20. **Kobayashi T, et al.** 2007. A plasmid-based reverse genetics system for animal double-stranded RNA viruses. Cell Host Microbe **1**:147–157.
21. **Kobayashi T, Ooms LS, Chappell JD, Dermody TS.** 2009. Identification of functional domains in reovirus replication proteins muNS and mu2. J. Virol. **83**:2892–2906.
22. **Kuhl U, et al.** 2005. High prevalence of viral genomes and multiple viral infections in the myocardium of adults with "idiopathic" left ventricular dysfunction. Circulation **111**:887–893.
23. **Kuhl U, et al.** 2003. Interferon-beta treatment eliminates cardiotropic viruses and improves left ventricular function in patients with myocardial persistence of viral genomes and left ventricular dysfunction. Circulation **107**:2793–2798.
24. **Kuhl U, et al.** 2005. Viral persistence in the myocardium is associated with progressive cardiac dysfunction. Circulation **112**:1965–1970.
25. **Leonard GT, Sen GC.** 1996. Effects of adenovirus E1A protein on interferon-signaling. Virology **224**:25–33.
26. **Loo YM, et al.** 2008. Distinct RIG-I and MDA5 signaling by RNA viruses in innate immunity. J. Virol. **82**:335–345.
27. **Loo YM, Gale M, Jr.** 2011. Immune signaling by RIG-I-like receptors. Immunity **34**:680–692.
28. **Marques JT, et al.** 2006. A structural basis for discriminating between self and nonself double-stranded RNAs in mammalian cells. Nat. Biotechnol. **24**:559–565.
29. **Martin A, et al.** 1994. Acute myocarditis: rapid diagnosis by PCR in children. Circulation **90**:330–339.
30. **Mason JW, et al.** 1995. A clinical trial of immunosuppressive therapy for myocarditis. N. Engl. J. Med. **333**:269–275.
31. **Miller CL, et al.** 2004. Increased ubiquitination and other covariant phenotypes attributed to a strain- and temperature-dependent defect of reovirus core protein mu2. J. Virol. **78**:10291–10302.
32. **Miric M, et al.** 1996. Long-term follow-up of patients with dilated heart muscle disease treated with human leukocytic interferon alpha or thymic hormones: initial results. Heart **75**:596–601.
33. **Nibert ML, Margraf RL, Coombs KM.** 1996. Nonrandom segregation of parental alleles in reovirus reassortants. J. Virol. **70**:7295–7300.
34. **Nichols JL, Bellamy AR, Joklik WK.** 1972. Identification of the nucleotide sequences of the oligonucleotides present in reovirions. Virology **49**:562–572.
35. **Noble S, Nibert ML.** 1997. Core protein mu 2 is a second determinant of nucleoside triphosphatase activities in the reovirus core. J. Virol. **71**:7728–7735.
36. **O'Donnell SM, et al.** 2005. Organ-specific roles for transcription factor NF-κB in reovirus-induced apoptosis and disease. J. Clin. Invest. **115**:2341–2350.
37. **O'Neill LA, Bowie AG.** 2010. Sensing and signaling in antiviral innate immunity. Curr. Biol. **20**:R328–R333.
38. **Ooms LS, Kobayashi T, Dermody TS, Chappell JD.** 2010. A post-entry

step in the mammalian orthoreovirus replication cycle is a determinant of cell tropism. J. Biol. Chem. **285**:41604–41613.
39. **Parker JSL, Broering TJ, Kim J, Higgins DE, Nibert ML.** 2002. Reovirus core protein mu2 determines the filamentous morphology of viral inclusion bodies by interacting with and stabilizing microtubules. J. Virol. **76**: 4483–4496.
40. **Parrillo JE, et al.** 1989. A prospective, randomized, controlled trial of prednisone for dilated cardiomyopathy. N. Engl. J. Med. **321**:1061–1068.
41. **Randall RE, Goodbourn S.** 2008. Interferons and viruses: an interplay between induction, signaling, antiviral responses and virus countermeasures. J. Gen. Virol. **89**:1–47.
42. **Sato M, et al.** 1998. Postive feedback regulation of type 1 IFN genes by the IFN-inducible transcription factor IRF-7. FEBS Lett. **441**:106–110.
43. **Schiff LA, Nibert ML, Tyler KL.** 2007. Orthoreoviruses and their replication, p 1853–1915. *In* Knipe DM, Howley PM (ed), Fields virology, 5th ed, **vol 2**. Lippincott/The Williams & Wilkins Co, Philadelphia, PA.
44. **Sherry B, Baty CJ, Blum MA.** 1996. Reovirus-induced acute myocarditis in mice correlates with viral RNA synthesis rather than generation of infectious virus in cardiac myocytes. J. Virol. **70**:6709–6715.
45. **Sherry B, Blum MA.** 1994. Multiple viral core proteins are determinants of reovirus-induced acute myocarditis. J. Virol. **68**:8461–8465.
46. **Sherry B, Fields BN.** 1989. The reovirus M1 gene, encoding a viral core protein, is associated with the myocarditic phenotype of a reovirus variant. J. Virol. **63**:4850–4856.
47. **Sherry B, Li X, Tyler KL, Cullen JM, Virgin HW.** 1993. Lymphocytes protect against and are not required for reovirus-induced myocarditis. J. Virol. **67**:6119–6124.
48. **Sherry B, Torres J, Blum MA.** 1998. Reovirus induction of and sensitivity to beta-interferon in cardiac myocyte cultures correlate with induction of myocarditis and are determined by viral core proteins. J. Virol. **72**:1314–1323.
49. **Smith RE, Zweerink HJ, Joklik WK.** 1969. Polypeptide components of virions, top component and cores of reovirus type 3. Virology **39**:791–810.
50. **Stewart MJ, Smoak K, Blum MA, Sherry B.** 2005. Basal and reovirus-induced beta interferon (IFN-beta) and IFN-beta-stimulated gene expression are cell type specific in the cardiac protective response. J. Virol. **79**: 2979–2987.
51. **Takeuchi O, Akira S.** 2009. Innate immunity to virus infection. Immunol. Rev. **227**:75–86.
52. **Wilkins C, Gale M, Jr.** 2010. Recognition of viruses by cytoplasmic sensors. Curr. Opin. Immunol. **22**:41–47.
53. **Yin P, et al.** 2004. Comparisons of the M1 genome segments and encoded mu2 proteins of different reovirus isolates. Virol. J. **1**:6.
54. **Zhang X, Walker SB, Chipman PR, Nibert ML, Baker TS.** 2003. Reovirus polymerase lambda 3 localized by cryo-electron microscopy of virions at a resolution of 7.6 Å. Nat. Struct. Biol. **10**:1011–1018.
55. **Zurney J, Howard KE, Sherry B.** 2007. Basal expression levels of IFNAR and Jak-STAT components are determinants of cell-type-specific differences in cardiac antiviral responses. J. Virol. **81**:13668–13680.
56. **Zurney J, Kobayashi T, Holm GH, Dermody TS, Sherry B.** 2009. Reovirus mu2 protein inhibits interferon signaling through a novel mechanism involving nuclear accumulation of interferon regulatory factor 9. J. Virol. **83**:2178–2187.

APPENDIX F

MOLECULAR DETERMINANTS OF PROTEOLYTIC DISASSEMBLY OF THE REOVIRUS OUTER CAPSID

Joshua D. Doyle, Pranav Danthi, Emily A. Kendall, Laura S. Ooms, J. Denise Wetzel, and Terence S. Dermody

Journal of Biological Chemistry. 287(11) 8029-38; 2012

THE JOURNAL OF BIOLOGICAL CHEMISTRY VOL. 287, NO. 11, pp. 8029–8038, March 9, 2012

Molecular Determinants of Proteolytic Disassembly of the Reovirus Outer Capsid*

Received for publication, December 16, 2011, and in revised form, January 16, 2012 Published, JBC Papers in Press, January 17, 2012, DOI 10.1074/jbc.M111.334854

Joshua D. Doyle[‡§], Pranav Danthi[§¶1], Emily A. Kendall[§¶2], Laura S. Ooms[‡§], J. Denise Wetzel[§¶], and Terence S. Dermody[‡§¶3]

From the Departments of [‡]Pathology, Microbiology, and Immunology and [¶]Pediatrics and the [§]Elizabeth B. Lamb Center for Pediatric Research, Vanderbilt University School of Medicine, Nashville, Tennessee 37232

Background: The reovirus outer capsid protein σ3 acts as a substrate for intracellular proteases.
Results: Two polymorphic amino acids in σ3 act in opposition to determine protease sensitivity, disassembly kinetics, and biochemical stability.
Conclusion: A regulatory network of residues maintains optimal reovirus outer capsid function.
Significance: The balance between stability and instability of capsid structures is likely to be an important determinant of viral fitness.

Following attachment and internalization, mammalian reoviruses undergo intracellular proteolytic disassembly followed by viral penetration into the cytoplasm. The initiating event in reovirus disassembly is the cathepsin-mediated proteolytic degradation of viral outer capsid protein σ3. A single tyrosine-to-histidine mutation at amino acid 354 (Y354H) of strain type 3 Dearing (T3D) σ3 enhances reovirus disassembly and confers resistance to protease inhibitors such as E64. The σ3 amino acid sequence of strain type 3 Abney (T3A) differs from that of T3D at eight positions including Y354H. However, T3A displays disassembly kinetics and protease sensitivity comparable with T3D. We hypothesize that one or more additional σ3 polymorphisms suppress the Y354H phenotype and restore T3D disassembly characteristics. To test this hypothesis, we engineered a panel of reovirus variants with T3A σ3 polymorphisms introduced individually into T3D-σ3Y354H. We evaluated E64 resistance and *in vitro* cathepsin L susceptibility of these viruses and found that one containing a glycine-to-glutamate substitution at position 198 (G198E) displayed disassembly kinetics and E64 sensitivity similar to those properties of T3A and T3D. Additionally, viruses containing changes at positions 233 and 347 (S233L and I347T) developed *de novo* compensatory mutations at position 198, strengthening the conclusion that residue 198 is a key determinant of σ3 proteolytic susceptibility. Variants with Y354H in σ3 lost infectivity more rapidly than T3A or T3D following heat treatment, an effect abrogated by G198E. These results identify a regulatory network of residues that control σ3 cleavage and capsid stability, thus providing insight into the regulation of nonenveloped virus disassembly.

All viruses must transit host cell membranes, either at the cell surface or following particle internalization, to productively infect cells. Enveloped viruses, such as orthomyxoviruses (1, 2), paramyxoviruses (3), and retroviruses (4, 5), encode proteins that mediate fusion of the viral envelope with target cell membranes, thus facilitating viral cell entry. Nonenveloped viruses, such as adenovirus (6) and reovirus (7), traverse cellular membranes despite the absence of a viral envelope. The capsid proteins of nonenveloped viruses often contain hydrophobic motifs that are exposed in response to receptor binding or endosomal cues. These motifs in turn disrupt host cell membranes and mediate viral access to the cytosol. The viral machinery that guides the virus into the cell interior must be tightly regulated to ensure its activation only at the appropriate time and in the correct compartment to ensure productive infection.

Mammalian orthoreoviruses (reoviruses) are nonenveloped, icosahedral viruses that contain a double-stranded RNA genome housed within two concentric protein shells, an outer capsid, composed primarily of viral proteins σ3 and μ1, and an inner core (8, 9). Following binding to cell-surface receptors, including sialylated glycans and junctional adhesional molecule-A (JAM-A), reovirus particles are internalized via β1 integrin-dependent, clathrin-mediated endocytosis (10–13). Internalized viral particles undergo a stepwise disassembly process. The initial event in reovirus disassembly is the proteolytic cleavage of σ3 protein, which is catalyzed by endosomal cathepsin proteases (14–16). Ablation of cathepsin activity by either pharmacological (7, 14) or genetic (16) means abolishes reovirus infectivity, suggesting that σ3 cleavage is essential for reovirus disassembly and productive infection. Proteolytic removal of σ3 facilitates cleavage of μ1 to generate the fragments δ and φ, resulting in formation of infectious subvirion particles (7, 17, 18). Infectious subvirion particles feature exposed membrane interaction motifs and transit across membranes, leading to the delivery of viral core particles into the cytosol (19). Infectious subvirion particles can be generated *in vitro* using several proteases, including cathepsins B and L (7, 16, 20).

* This work was supported, in whole or in part, by National Institutes of Health Grants T32 GM008554 from USPHS (to J. D. D.) and R01 AI032539 (to T. S. D.). This work was also supported by the Elizabeth B. Lamb Center for Pediatric Research.
[1] Present address: Dept. of Biology, Indiana University, Bloomington, IN 47405.
[2] Present address: Dept. of Medicine, Massachusetts General Hospital, Boston, MA 02114.
[3] To whom correspondence should be addressed: Lamb Center for Pediatric Research, D7235 MCN, Vanderbilt University School of Medicine, Nashville, TN 37232. Tel.: 615-343-9943; Fax: 615-343-9723; E-mail: terry.dermody@vanderbilt.edu.

Structural determinants of σ3 cathepsin-cleavage susceptibility are not well defined. Putative cathepsin L cleavage sites between residues 243–244 and 250–251 have been identified in reovirus strain type 1 Lang (T1L)[4] σ3 (16), and this region is conserved between T1L and strain type 3 Dearing (T3D). However, structural models of σ3 (21) indicate that these cleavage sites are masked by the σ3 carboxyl-terminal domain (C terminus). Additional evidence suggests that the C terminus determines σ3 protease susceptibility (22). Mutant viruses isolated from persistently infected cultures have increased protease susceptibility (23), a phenotype that genetically segregates with a tyrosine-to-histidine mutation at amino acid position 354 (Y354H) in σ3 (22), which is located in the C terminus of the protein. The Y354H mutation increases the rate at which σ3 is cleaved by proteases *in vitro* and confers resistance to protease inhibitors, such as the pan-cysteine protease inhibitor E64 and ammonium chloride, which inhibits vacuolar acidification (14, 22, 24). The mechanism by which Y354H enhances the protease sensitivity of σ3 is unclear, but it is possible that His-354 alters the intramolecular localization of the C terminus and exposes the normally occluded protease cleavage sites (22).

The relationship between the stability of nonenveloped virus capsid structures and viral fitness is poorly defined. Mutations that enhance outer capsid proteolysis, such as Y354H, accelerate the kinetics of viral entry into tissue culture cells and enable viral replication in settings of diminished protease availability. However, this mutation is absent from most primary reovirus isolates (25), suggesting that it imposes a fitness penalty on the virus. Interestingly, the deduced σ3 amino acid sequence of strain type 3 Abney (T3A) (26) contains a native histidine at residue 354 (25). Determining how His-354 in T3A σ3 affects cell entry, viral disassembly, and viral replication should provide information about how nonenveloped viruses maintain the optimum balance between capsid stability and instability and further an understanding of the fitness implications of perturbing that balance.

In this study, we compared disassembly kinetics and sensitivity to protease inhibitors of T3A and T3D. The deduced σ3 amino acid sequence of T3D contains a tyrosine at residue 354, and there are seven additional amino acid polymorphisms between T3A and T3D σ3 sequence. We engineered a panel of reovirus variants containing each of these native σ3 polymorphisms in the context of σ3-Y354H to identify residues in σ3 that modulate protease sensitivity. The panel of variants was tested for growth inhibition by E64 and disassembly mediated by cathepsin L *in vitro*. We identified a glycine-to-aspartate polymorphism at position 198 in σ3 that is capable of independently suppressing the Y354H phenotype. We propose that residues 198 and 354 act in concert to maintain optimum stability of the reovirus capsid.

EXPERIMENTAL PROCEDURES

Cells and Viruses—Spinner-adapted murine L929 cells were grown in either suspension or monolayer cultures in Joklik's spinner-modified Eagle's minimal essential medium (SMEM; Lonza, Walkersville, MD) supplemented to contain 5% fetal bovine serum (Invitrogen), 2 mM L-glutamine (Invitrogen), 100 units of penicillin/ml, 100 units of streptomycin/ml (Invitrogen), and 0.25 μg of amphotericin/ml (Sigma-Aldrich). BHK-T7 (baby hamster kidney-T7) cells were grown in Dulbecco's modified Eagle's minimal essential medium (Invitrogen) supplemented to contain 5% fetal calf serum, 2 mM L-glutamine, 2% minimal essential medium amino acid solution (Invitrogen), and 1 mg of Geneticin/ml (Invitrogen).

Reovirus strain T3A is maintained as a laboratory stock. Recombinant strain (rs) T3D is a stock generated by plasmid-based reverse genetics from cloned T3D cDNAs (27). The engineered reovirus mutant rsT3D-σ3Y354H was generated as described (28).

Generation of Reovirus Variants—Viruses containing engineered changes in σ3 protein were generated using reverse genetics (27). The S4 gene was excised from the pT7-M2-S2-S3-S4T3D plasmid (27) using HindIII and NheI to generate the tricistronic plasmid pT7-M2-S2-S3T3D. The pT7-S4T3D plasmid was used as template to generate pT7-S4T3DA28T+Y354H, pT7-S4T3DE108A+Y354H, pT7-S4T3DI180V+ Y354H, pT7-S4T3DG198E+Y354H, pT7-S4T3DS215D+Y354H, pT7-S4T3DS233L+ Y354H, and pT7-S4T3DI347T+Y354H using QuikChange mutagenesis (Stratagene, La Jolla, CA). Monolayers of BHK-T7 cells (27) at 90% confluency (~3×10^6 cells) seeded in 60-mm dishes (Costar; Corning Inc., Corning, NY) were co-transfected with 3.5 μg each of five plasmids representing the cloned reovirus T3D genome using 3 μl of TransIT-LT1 transfection reagent (Mirus Bio LLC; Madison, WI) per μg of plasmid DNA. Following 72 h of incubation, recombinant virus was isolated from transfected cells by plaque purification using monolayers of L929 cells (29). Virus stocks were passaged, and titers were determined as described (30).

Growth of Virus in Cells Treated with E64—Confluent monolayers of L929 cells (~2×10^5 cells/well) in 24-well plates (Costar) were preincubated in SMEM supplemented to contain 0–200 μM E64 (Sigma-Aldrich) at 37 °C for 4 h. The medium was removed, and cells were adsorbed with second- or third-passage virus stocks at an m.o.i. of 2 pfu/cell. After incubation at 4 °C for 1 h, the inoculum was removed, cells were washed with PBS, and 1 ml of fresh SMEM supplemented to contain 0–200 μM E64 was added. Cells were incubated at 37 °C for 24 h and frozen and thawed twice. Viral titer in cell lysates was determined by plaque assay (29).

Treatment of Reovirus Virions with Cathepsin L—Purified reovirus virions at a concentration of 2×10^{12} particles/ml in reaction buffer L (100 mM NaCl, 15 mM $MgCl_2$, 50 mM sodium acetate (pH 5.0)) were treated with 50 μg of purified, recombinant human cathepsin L (7) per ml in the presence of 5 mM dithiothreitol at 37 °C for 0–4 h. Aliquots were removed at various intervals, mixed with SDS sample buffer supplemented to contain 500 μM E64, and incubated on ice for 5 min to terminate protease activity. Reaction mixtures were analyzed by SDS-PAGE.

SDS-PAGE of Reovirus Structural Proteins—Discontinuous SDS-PAGE was performed as described (31). Samples were incubated at 98 °C for 5 min, loaded into wells of precast 4–20%

[4] The abbreviations used are: T1L, type 1 Lang; T3A, type 3 Abney; T3D, type 3 Dearing; SMEM, spinner-modified Eagle's minimal essential medium; Tricine, *N*-[2-hydroxy-1,1-bis(hydroxymethyl)ethyl]glycine; m.o.i., multiplicity of infection; rs, recombinant strain.

gradient Tris-Tricine polyacrylamide gels (Bio-Rad Laboratories), and electrophoresed at a constant voltage of 180 V for 1 h. Following electrophoresis, gels were stained using a Novex colloidal blue staining kit (Invitrogen) according to the manufacturer's instructions.

Densitometric Analysis of Reovirus Structural Proteins—Stained gels were visualized using an infrared imaging system (LI-COR Biosciences, Lincoln, NE). Band intensities in the scanned images were quantified using Odyssey Application software version 3.0.16 (LI-COR). The relative amount of σ3 protein was determined by comparing the intensity of bands corresponding to σ3, which has an apparent molecular mass of ~41 kDa, with bands corresponding to viral core protein σ2, which has an apparent molecular mass of ~47 kDa and is not affected by protease treatment under these conditions (14).

Heat Resistance of Reovirus Virions—Purified reovirus virions at a concentration of 2×10^8 particles/ml in virion storage buffer (150 mM NaCl, 15 mM $MgCl_2$, 10 mM Tris (pH 7.4)) were treated at 55 °C for 60 min. At 15-min intervals, samples were removed and placed on ice. Viral titers were determined by plaque assay (28).

Specific Infectivity of Reovirus Virions—Fresh preparations of reovirus virions were generated in triplicate from second-passage lysate stocks as described (27). Particle density of each viral preparation was determined by quantifying absorbance at 260 nm and calculated using the equivalence of 1 $A_{260} = 2.1 \times 10^{12}$ particles/ml (32). Titer of each preparation was determined by plaque assay (28).

Kinetic Ammonium Chloride Protection Assay—Confluent monolayers of L929 cells (~2×10^5 cells/well) in 24-well plates were adsorbed with second- or third-passage virus stocks at an m.o.i. of 25 pfu/cell. After incubation at 4 °C for 1 h, the inoculum was removed, cells were washed with PBS at 4 °C, and 1 ml of prewarmed SMEM was added. At various times after adsorption, 25 μl of 1 M NH_4Cl was added to the medium to give a final concentration of 25 mM. At 20 h after adsorption, the medium was removed, and cell monolayers were fixed with 1 ml of methanol at −20 °C for a minimum of 30 min. Fixed monolayers were washed twice with PBS, blocked with 5% immunoglobulin-free BSA (Sigma-Aldrich) in PBS, and incubated at 37 °C for 30 min with rabbit polyclonal anti-reovirus serum at a 1:1000 dilution in PBS plus 0.5% Triton X-100. Monolayers were washed twice with PBS and incubated at 37 °C for 30 min with a 1:1000 dilution of anti-rabbit goat immunoglobulin conjugated with Alexa Fluor 488 (Molecular Probes, Inc., Eugene, OR). Monolayers were washed twice and visualized by indirect immunofluorescence. Reovirus antigen-positive cells were quantitated by enumerating fluorescent cells in three random fields of view per well at 100–400× magnification. Total cell number was quantified by enumerating 4′,6-diamidino-2-phenylindole (DAPI)-stained nuclei.

RESULTS

T3A and T3D Are Sensitive to Protease Inhibitor E64—The deduced amino acid sequences of T3A and T3D σ3 proteins contain eight polymorphic residues (Table 1). Several of the T3A-T3D polymorphic residues including 354 are found in the virion-distal region of σ3, which is predicted to be accessible to protease (Fig. 1). To determine whether the Y354H polymorphism in T3A σ3 confers resistance to protease inhibitors, T3A, T3D, and T3D-σ3Y354H were tested for the capacity to replicate in the presence of protease inhibitor E64. L929 cells were incubated in medium supplemented to contain 100 or 200 μM E64, adsorbed with T3A, T3D, and T3D-σ3Y354H, and incubated in the presence or absence of E64 for 24 h. Cells were lysed, and viral titers in cell lysates were determined by plaque assay (Fig. 2). Despite the presence of histidine at position 354 in T3A σ3, yields of T3A were reduced 259-fold, approximating the reduction observed for T3D, 195-fold, in the presence of 100 μM E64, whereas yields of T3D-σ3Y354H were diminished less than 10-fold at this E64 concentration. Replication of T3A and T3D was completely ablated in the presence of 200 μM E64, but yields of T3D-σ3Y354H were not further diminished. These findings suggest that one or more of the additional polymorphisms displayed by T3A σ3 suppresses the Y354H phenotype and restores optimal σ3 stability.

TABLE 1
Polymorphic residues between T3A and T3D σ3
T3A and T3D differ at the eight indicated positions in the σ3 open reading frame.

	Amino acid position							
Virus strain	**28**	**108**	**180**	**198**	**215**	**233**	**347**	**354**
T3A	Thr	Ala	Val	Glu	Asn	Leu	Thr	His
T3D	Ala	Glu	Ile	Gly	Ser	Ser	Ile	Tyr

G198E Confers Susceptibility to E64 in Context of Y354H—To identify residues in T3A σ3 that suppress the capacity of the Y354H polymorphism to confer viral growth in the presence of protease inhibitors, we engineered a panel of reovirus variants that incorporate single T3A-T3D polymorphisms in the context of T3D-σ3Y354H but are otherwise isogenic with T3D (Table 2). Despite several attempts, we could not recover T3D-σ3A28T,Y354H. In addition, T3D-σ3 S233L,Y354H was recovered only with a concomitant glycine-to-tryptophan mutation at position 198 of σ3. Each of the other variants was rescued and propagated to high titer working stocks.

We tested each of the variant viruses for replication in the presence of E64 (Fig. 3). As before, yields of T3A and T3D were diminished substantially by this inhibitor, whereas yields of T3D-σ3Y354H were only modestly impaired. Similarly, yields of T3D-σ3E108A, T3D-σ3I180V, T3D-σ3S215N, and T3D-σ3I347T were only slightly diminished by E64. In sharp contrast, yields of T3D-σ3G198E,Y354H were markedly decreased in the presence of E64, approximating those of T3A and T3D. These findings suggest that a glycine-to-glutamic acid mutation at position 198 independently suppresses the Y354H phenotype in T3A and enhances its sensitivity to the protease inhibitor E64.

Cathepsin L Sensitivity of T3A-T3D Variant Viruses—Cathepsin proteases catalyze reovirus disassembly within cellular endosomes (16, 33). To determine whether T3A-T3D polymorphisms alter capsid disassembly when treated with endosomal proteases, virions of T3A, T3D, T3D-σ3Y354H, and the T3A-T3D variants were digested *in vitro* with purified human cathepsin L (34). At 30-min intervals, aliquots were removed from the digestion mixtures, and viral proteins were resolved by SDS-PAGE and visualized using colloidal blue staining (Fig.

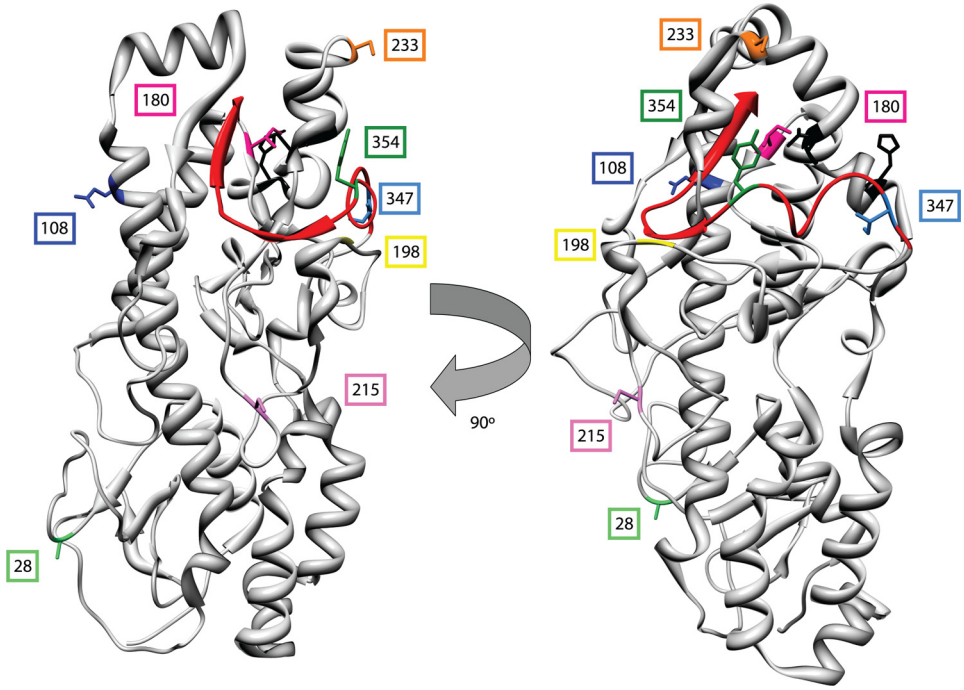

FIGURE 1. **Location of polymorphic residues in strains T3A and T3D σ3 proteins.** A crystal structure of T3D σ3 (21) is shown highlighting polymorphic residues in T3A and T3D σ3 proteins, including Tyr-354 (*dark green*), which is altered in reovirus variants selected for enhanced disassembly kinetics (23, 24, 39). The virion-distal domain of σ3 including the C terminus (depicted in *red*) is at the *top* of the figure. The virion-proximal region including the N terminus is at the *bottom*. Putative cathepsin L cleavage sites (determined for strain type 1 Lang) between amino acids 243 and 244 and between 250 and 251 are depicted in *black* (16).

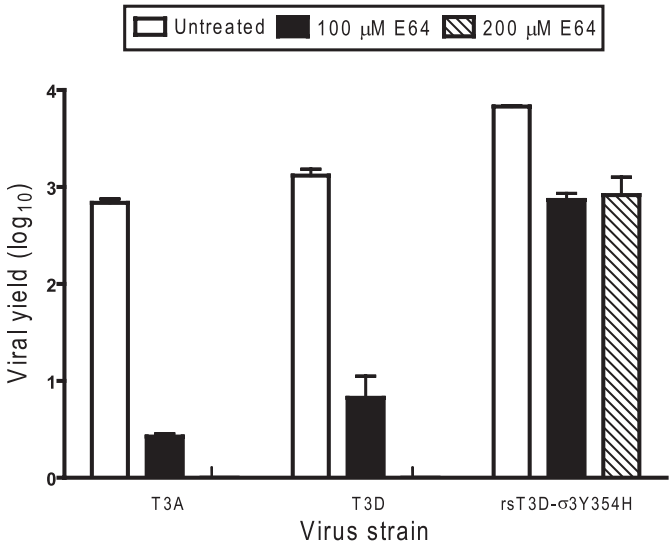

FIGURE 2. **Replication of T3A, T3D, and rsT3D-σ3Y354H in L929 cells treated with E64.** Monolayers of L929 cells were preincubated for 4 h in medium supplemented with or without E64 at the concentrations shown. The medium was removed, and cells were adsorbed with virus at an m.o.i. of 2 pfu/cell. After adsorption for 1 h, the inoculum was removed, and fresh medium with or without E64 was added. After incubation at 37 °C for 24 h, cells were frozen and thawed twice, and viral titers were determined by plaque assay. The results are presented as the mean viral yields, calculated by dividing titer at 24 h by titer at 0 h for each concentration of E64, for triplicate experiments. Yields of less than zero are not shown. *Error bars* indicate S.D.

TABLE 2

Reovirus variants in which polymorphic residues in T3D σ3 are exchanged with those in T3A σ3

Reovirus variants were engineered using plasmid-based reverse genetics. Each reovirus variant is isogenic with T3D with the exception of His-354 and a single additional T3A residue as shown. Bold and italics indicate viruses that were not successfully recovered.

Virus strain	Amino acid position							
	28	108	180	198	215	233	347	354
T3D	A	E	I	G	S	S	I	Y
T3A	T	A	V	E	N	L	T	H
T3D-σ3Y354H	A	E	I	G	S	S	I	H
T3D-σ3A28T,Y354H	*T*	*E*	*I*	*G*	*S*	*S*	*I*	*H*
T3D-σ3E108A,Y354H	A	A	I	G	S	S	I	H
T3D-σ3I180V,Y354H	A	E	V	G	S	S	I	H
T3D-σ3G198E,Y354H	A	E	I	E	S	S	I	H
T3D-σ3S215N,Y354H	A	E	I	G	N	S	I	H
T3D-σ3S233L,Y354H	*A*	*E*	*I*	*G*	*S*	*L*	*I*	*H*
T3D-σ3I347T,Y354H	A	E	I	G	S	S	T	H

4*A*). Intensity of the band corresponding to σ3 remained relatively constant for T3A and T3D over the 240-min time course, as did the band corresponding to μ1C. However, in these experiments, T3D-σ3Y354H displayed almost complete loss of σ3 protein within 60 min. In addition, the band corresponding to μ1C in T3D-σ3Y354H diminished in intensity over the course of protease treatment, and the appearance of a band corresponding to the δ fragment of μ1C was noted for this virus. Each of the variant viruses was observed to undergo disassembly with kinetics similar to those of T3D-σ3Y354H (Fig. 4*A*) with the exception of T3D-σ3G198E,Y354H, which displayed a digestion profile similar to that of T3A and T3D.

We quantified the intensity of protein bands corresponding to σ3 using an Odyssey infrared imaging system (Fig. 4*B*). To control for differences in gel loading, the band intensity of σ3 protein was normalized to that of reovirus core protein σ2, which is resistant to protease cleavage under these conditions. The σ3/σ2 ratio of T3A and T3D slightly decreased over the time course tested. The σ3/σ2 ratio of T3D-σ3Y354H and the variant viruses rapidly approached zero (Fig. 4*B*), with the nota-

ble exception of T3D-σ3G198E,Y354H. For this virus, the σ3/σ2 ratio approximated the T3D σ3/σ2 ratio throughout the digestion time course. We conclude that G198E stabilizes σ3 in the context of Y354H.

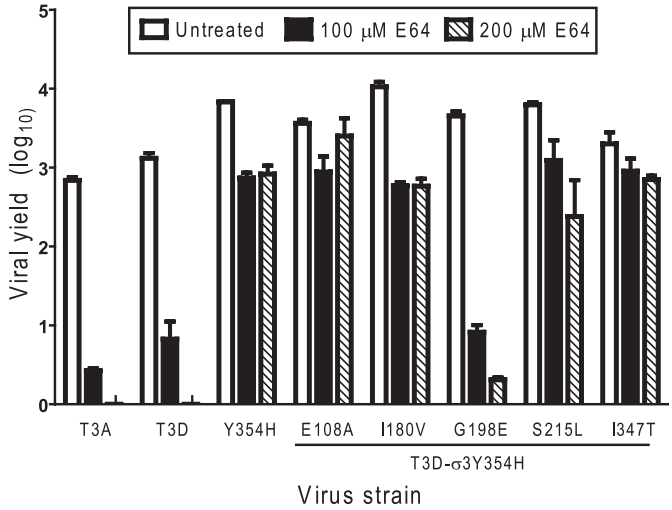

FIGURE 3. **E64 susceptibility of T3A-T3D variant viruses.** Monolayers of L929 cells were preincubated for 4 h in medium supplemented with or without E64 at the concentrations shown. The medium was removed, and cells were adsorbed with virus at an m.o.i. of 2 pfu/cell. After adsorption for 1 h, the inoculum was removed, and fresh medium with or without E64 was added. After incubation at 37 °C for 24 h, cells were frozen and thawed twice, and viral titers were determined by plaque assay. The results are presented as the mean viral yields, calculated by dividing titer at 24 h by titer at 0 h for each concentration of E64, for triplicate experiments. Yields of less than zero are not shown. *Error bars* indicate S.D.

Specific Infectivity of Reovirus Variants—We next considered the possibility that one or more of the σ3 polymorphisms in our panel of variant reovirus strains might affect assembly of σ3 onto nascent virions and thus compromise infectivity. To test this hypothesis, we examined the specific infectivity of our variant panel by calculating particle/pfu ratios for several independent preparations of each virus (Fig. 5). We observed that most of the virion stocks tested displayed particle/pfu ratios between 300 and 1000, consistent with reported values for type 3 reovirus strains (35) and our previous observations (data not shown). Although we observed some prep-to-prep variation, there were no significant differences between the variant and parental viruses (analysis of variance, $p > 0.05$). Therefore, the σ3 mutations introduced in our variant panel do not substantially affect reovirus replicative efficiency and thus are not likely to alter capsid assembly.

Outer Capsid Mutations Affect Reovirus Heat Sensitivity—To assess whether the differences in protease sensitivity of our variant viruses correlate with biochemical measures of capsid stability, we determined the relative loss of titer of our variant panel following heat treatment. Samples of each virus were diluted to a titer of 2×10^8 and placed at 55 °C for 1 h. Aliquots were removed at 15-min intervals, and titers were determined by plaque assay (Fig. 6). We observed that T3D-σ3Y354H lost titer significantly more rapidly (Student's *t* test, $p < 0.05$) at elevated temperature than did either T3A or T3D. Additionally, each of the variant viruses tested lost titer at rates similar to T3D-σ3Y354H, again with the exception

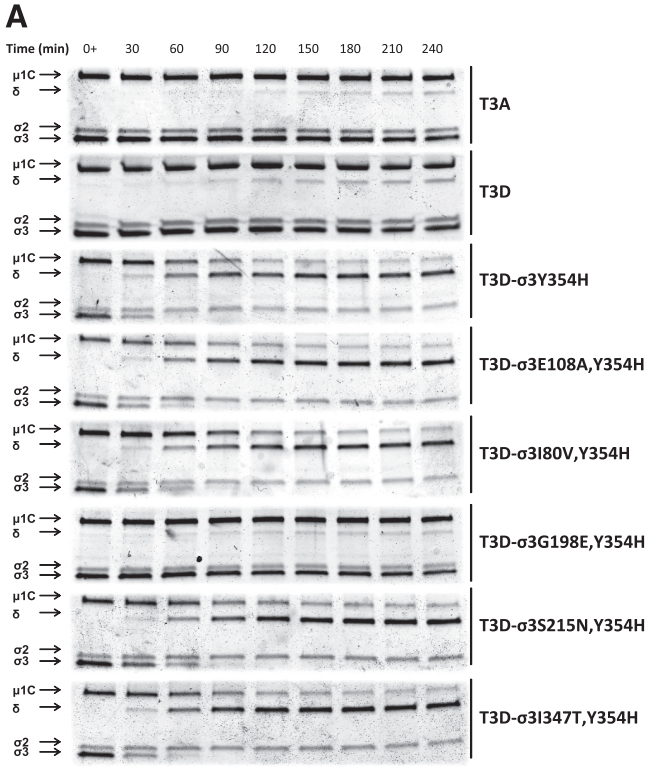

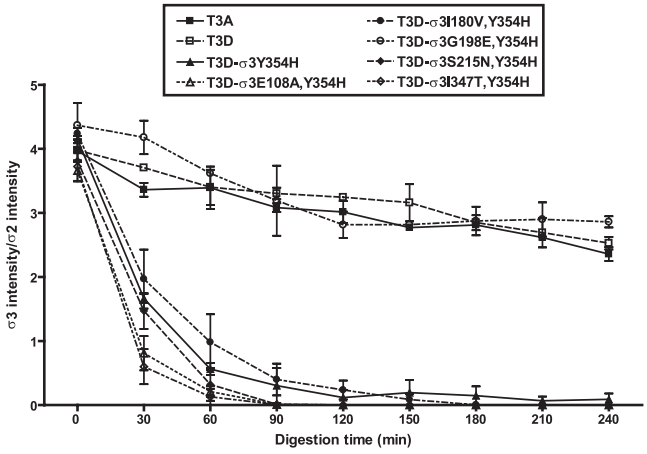

FIGURE 4. **Digestion of reovirus strains with cathepsin L.** *A*, purified virions were treated with human cathepsin L (34) for the intervals shown and loaded into wells of 4–20% gradient polyacrylamide gels. After electrophoresis, the gels were stained with colloidal blue (Invitrogen). Viral proteins μ1C, δ, σ2, and σ3 are labeled at the *left*. The experiments shown are representative of two performed for each virus. *B*, intensities of bands corresponding to reovirus proteins were quantified using the Odyssey software package (LI-COR). Results are expressed as the ratio of σ3 band intensity to σ2 band intensity to control for differences in loading for two independent experiments. *Error bars* indicate S.D.

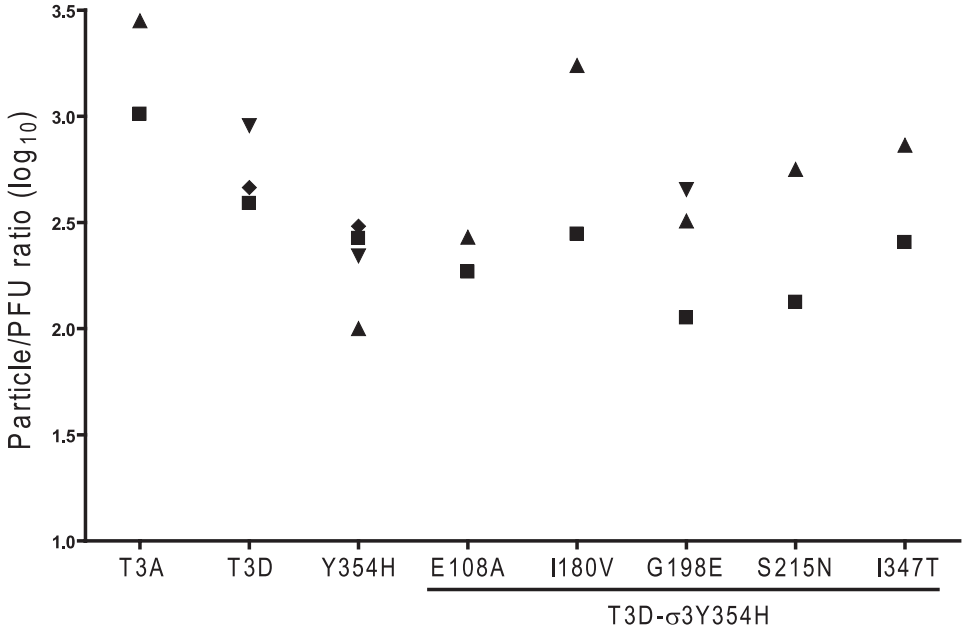

FIGURE 5. **Infectivity of reovirus variants.** Purified virions of variant viruses were generated from independent cultures of L929 cells (~4×10^8 cells) using CsCl gradient centrifugation. Particle number was quantified using the equivalence of 1 $A_{260} = 2.1 \times 10^{12}$ particles/ml. The titer of each preparation was determined by plaque assay. The results are presented as particle/pfu ratio. Data points indicate independent viral purifications.

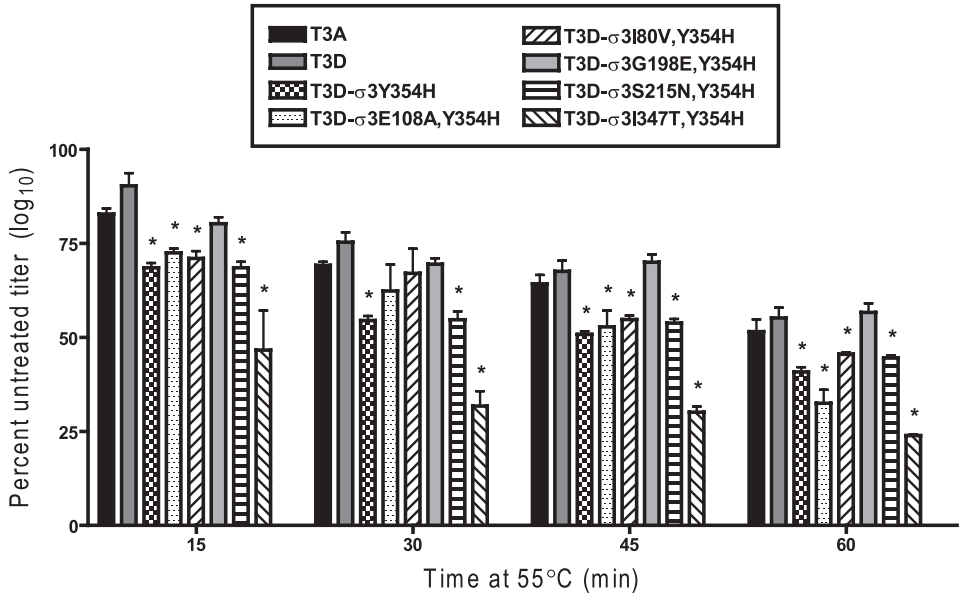

FIGURE 6. **Resistance of reovirus variants to inactivation by heat.** Purified virions of reovirus variants were diluted to a concentration of 2×10^8 particles/ml in virion storage buffer and incubated at 55 °C for 60 min. At 15-min intervals, samples were removed and placed on ice for 15 min. Titers were determined by plaque assay. Results are presented as the percentage of mean viral titer of untreated samples per interval of incubation, for triplicate experiments. *Error bars* indicate S.D.; *, $p \leq 0.05$ in comparison with T3D.

of T3D-σ3G198E,Y354H. The rate of titer loss for that virus did not significantly differ from T3D. The fact that enhanced protease sensitivity and altered sensitivity to heat are correlated in the context of Y354H suggests that this residue controls both properties through a common structural mechanism.

Enhanced Outer Capsid Protease Sensitivity Facilitates Endosomal Escape—Following binding to cell-surface receptors, reovirus particles are thought to be internalized via clathrin-dependent endocytosis (10–12, 36). Cleavage of σ3 by endosomal cathepsins is required for particle disassembly and subsequent escape from the endosome into the cytoplasm (14–19, 37). To determine whether the enhanced susceptibility to proteolytic cleavage mediated by σ3-Y354H alters the kinetics with which reovirus particles escape host cell endosomes, we took advantage of the fact that reovirus disassembly is abrogated by preventing the pH drop required for efficient cathepsin cleavage when intact particles are still resident in endosomes (7, 38). We adsorbed monolayers of L929 cells with variant reovirus strains at 4 °C for 1 h to synchronize viral attachment, warmed the cells to 37 °C, and added ammonium chloride at various intervals following

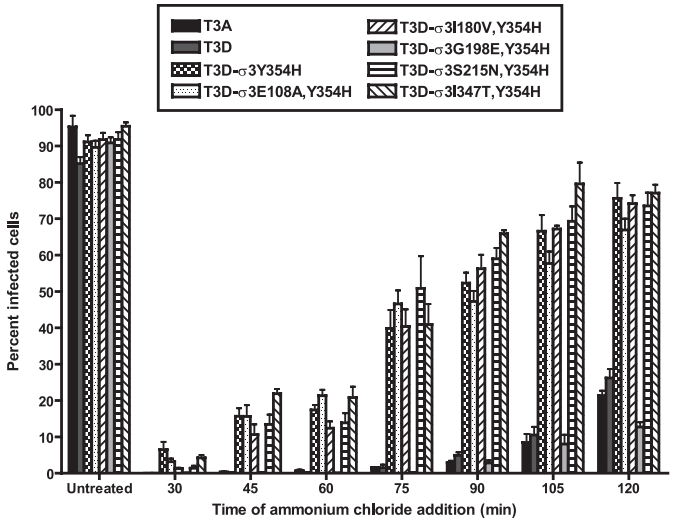

FIGURE 7. **Kinetics of ammonium chloride bypass by reovirus variants.** Monolayers of L929 cells were adsorbed with reovirus variants at an m.o.i. of 25 pfu/cell at 4 °C. After adsorption for 1 h, the inoculum was removed, fresh prewarmed medium was added, and cells were warmed to 37 °C. At the times shown after adsorption, ammonium chloride was added to a final concentration of 25 mM. After incubation at 37 °C for 20 h, cells were fixed with methanol at −20 °C, and infectivity was assessed by indirect immunofluorescence. The results are presented as the percentage of cells infected, normalized to untreated wells, for triplicate experiments. *Error bars* indicate S.D.

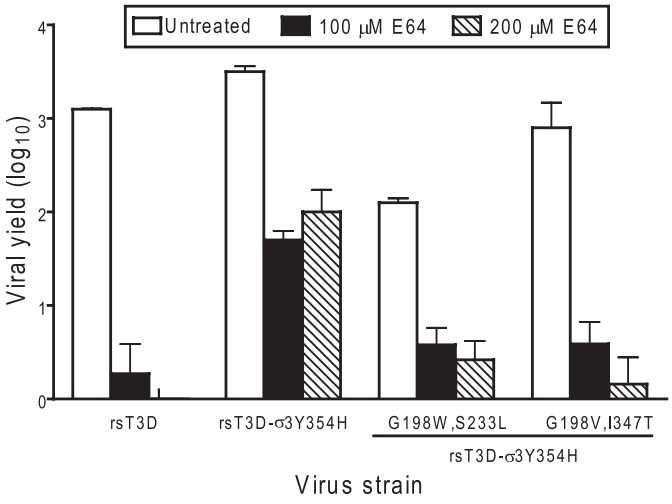

FIGURE 8. **E64 sensitivity of reovirus strains with second-site mutations.** Monolayers of L929 cells were preincubated for 4 h in medium supplemented with or without E64 at the concentrations shown. The medium was removed, and cells were adsorbed with reovirus strains at an m.o.i. of 2 pfu/cell. After adsorption for 1 h, the inoculum was removed, and fresh medium with or without E64 was added. After incubation at 37 °C for 24 h, cells were frozen and thawed twice, and viral titers were determined by plaque assay. The results are presented as the mean viral yields, calculated by dividing titer at 24 h by titer at 0 h for each concentration of E64, for triplicate experiments. Yields of less than zero are not shown. *Error bars* indicate S.D.

warming to prevent endosome acidification. Cells were incubated overnight and scored for viral infectivity by indirect immunofluorescence (Fig. 7). Variant viruses containing the σ3-Y354H mutation, with the exception of T3D-σ3G198E,Y354H, escaped ammonium chloride blockade as much as 60 min earlier than either T3A or T3D. These findings indicate that enhanced outer capsid protease sensitivity accelerates access of reovirus to the cytoplasm for subsequent steps in its replication cycle.

Residue 198 Second-site Changes—One of the variant viruses, T3D-σ3S233L,Y354H, could be recovered only in combination with a glycine-to-tryptophan substitution at position 198. In addition, multiple isolates of T3D-σ3I347T,Y354H contained *de novo* glycine-to-valine mutations at position 198. To determine whether these second-site mutations affect reovirus disassembly, we tested the effect of E64 treatment on the replication of variants containing these alterations (Fig. 8). Viruses containing either Val-198 or Trp-198 in the context of Y354H had modestly enhanced E64 sensitivity in comparison with that of T3D-σ3Y354H. In particular, introduction of Val-198 restored the E64 sensitivity of T3D-σ3G198V,I347T,Y354H to that of T3D. The E64 sensitivity of T3D-σ3G198W,S233L,Y354H was intermediate between that of T3D and T3D-σ3Y354H, although T3D-σ3G198W,S233L,Y354H produced lower peak titers in the absence of protease inhibitor than did T3D. These findings underscore the importance of residue 198 in determining σ3 stability and suggest that the molecular basis of Y354H suppression may differ depending on the biochemical nature of the amino acid at that position.

DISCUSSION

Nonenveloped viruses must undergo particle disassembly to initiate an infectious cycle. The rate-limiting step in reovirus disassembly is the enzyme-mediated cleavage of σ3 protein in endosomes of infected cells (7, 11, 14, 17, 18). Surface features of σ3 that influence its capacity to serve as an enzyme substrate are not well understood. A single mutation in reovirus T3D σ3 protein, Y354H, enhances susceptibility of the reovirus virion to protease and confers viral resistance to protease inhibitors (14, 22, 24, 39). Structural evidence suggests that enhanced susceptibility to protease conferred by Y354H is due to an intramolecular rearrangement of domains in σ3 that enhances access to internal protease cleavage sites (22). However, this model has not been explicitly tested. Selection of reovirus mutants under conditions that diminish endosomal protease activity yields viruses containing the σ3-Y354H mutation (14, 24, 39), suggesting that capsid-destabilizing mutations are advantageous in certain settings. The importance of capsid stability in other phases of the reovirus life cycle is unclear.

In this study, we identified a new surface determinant of reovirus capsid stability located at position 198 in σ3. To our knowledge, reovirus strain T3A is the only field isolate strain reported to date that contains a histidine at position 354 (25). Based on our previous understanding of the phenotype of virus strains containing σ3-Y354H, we anticipated that T3A would be resistant to protease inhibitors and display enhanced susceptibility to proteases in comparison with T3D. Surprisingly, we found that T3A has E64 sensitivity similar to that of T3D despite the presence of His-354 in σ3. We also observed that T3A and T3D have similar *in vitro* disassembly kinetics when treated with the endosomal protease cathepsin L. Based on these observations, we hypothesized that other residues in T3A σ3 that differ from T3D σ3 suppress the Y354H phenotype.

We used plasmid-based reverse genetics to generate a panel of reovirus variants to test the contributions made by each T3A-T3D polymorphic residue to capsid stability in an other-

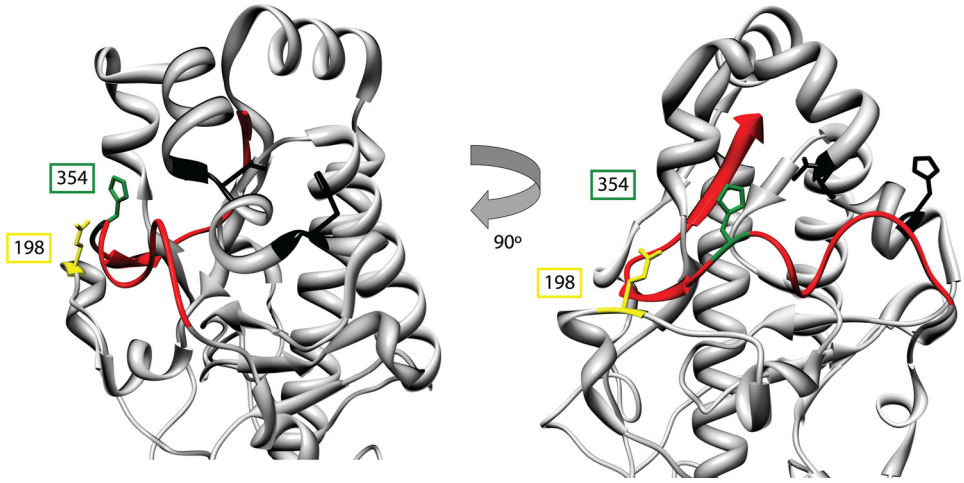

FIGURE 9. **Residues 198 and 354 define an amino acid network regulating σ3 proteolysis.** The virion-distal domain of T3D σ3 is shown. The C terminus is depicted in *red*. Glu-198 and His-354 are modeled in *yellow* and *green*, respectively, and are drawn in *stick representation*. The amino acids corresponding to the two putative cathepsin L cleavage sites, residues Val-243-Thr-244 and Gly-250-His251 (16), are shown in *black* in *stick representation*.

wise isogenic background that includes Y354H. Despite numerous attempts, a virus containing an aspartate-to-threonine change at position 28, T3D-σ3D28T,Y354H, could not be recovered. Amino acid 28 is located in a virion-proximal domain of σ3 (Fig. 1) that is important for interactions of σ3 with μ1 during virion assembly (40). It is possible that mutations at position 28 impair interactions between σ3 and μ1 (40), hindering recovery of T3D-σ3D28T,Y354H. The recovered variant viruses had no overt defects in replication or specific infectivity (Fig. 5). All of the T3A-T3D variant viruses are resistant to cysteine protease inhibitor E64 and thus phenocopy T3D-σ3Y354H, except the virus containing a glycine-to-glutamate change at position 198, T3D-σ3G198E,Y354H. Yields of T3D-σ3G198E,Y354H are markedly diminished in cells treated with E64. Concordantly, all members of the T3A-T3D variant panel except T3D-σ3G198E,Y354H display kinetics of digestion by cathepsin L similar to T3D-σ3Y354H. Moreover, we also observed that all of the variant viruses escape an endosomal infectivity block more rapidly than T3A or T3D, again excepting T3D-σ3G198E,Y354H. Together, these results provide strong evidence that suppression of the Y354H phenotype in T3A is solely attributable to the glycine-to-glutamate polymorphism at position 198.

Another virus, T3D-σ3S233L,Y354H, could be recovered only with an accompanying glycine-to-tryptophan mutation at position 198. In addition, four of the seven T3D-σ3I347T,Y354H clones sequenced contained a second-site mutation at position 198, specifically, a glycine-to-valine substitution. We found that T3D-σ3G198W,S233L,Y354H and T3D-σ3G198V,I347T,Y354H had increased E64 susceptibility in comparison with that of T3D-σ3Y354H, although neither virus was as sensitive to this protease inhibitor as was T3A or T3D. The observation of two different, independently arising mutations at position 198 in σ3 supports the conclusion that residue 198 is a key determinant of σ3 protease susceptibility. It is plausible that mutations at positions 233 and 347 enhance the selection of Y354H-suppressive mutations, perhaps by further destabilizing σ3.

The σ3 C terminus is thought to control the rate of σ3 cleavage by restricting protease access to cleavage sites located internally within the protein (16, 22, 40). The C-terminal domain of σ3 localizes to a solvent-exposed surface of the σ3/μ1 heterohexamer and is not predicted to directly interact with other viral proteins (40). There is some structural evidence suggesting that the Y354H mutation accelerates σ3 cleavage by dislocating the σ3 C terminus, affording easier access to internal cleavage sites (22). The observation that residue 198 suppresses Y354H indirectly supports this model (Fig. 9). The σ3 C terminus (*red*) overlies the putative cathepsin L cleavage sites (*black*), located between residues 243–244 and 250–251. Substitution of Tyr-354 in the C terminus (*green*) with histidine, a basic amino acid, may disrupt hydrophobic interactions required for proper folding of the σ3 C terminus. Low resolution cryo-EM reconstructions of σ3-Y354H reveal added density in a hinge region between the virion-proximal and virion-distal σ3 lobes that is absent in T3D σ3 (22). This increase in density may represent the dislocated C terminus of the molecule. Residue 198 in σ3 is located on a loop directly opposed to residue 354. It is possible that the glycine-to-glutamate polymorphism observed in T3A stabilizes the C terminus through charge-charge interactions with His-354. Substitution of residue 198 with hydrophobic amino acids, such as tryptophan and valine as observed in this study, may also stabilize the σ3 C terminus, perhaps by steric interactions that limit its mobility. Our finding that alterations at positions 233 and 347 elicit compensatory hydrophobic mutations at position 198 suggests that more complex intramolecular rearrangements of σ3 may occur in those viruses. Interestingly, a virus selected for growth in the presence of E64, D-EA3, contains two mutations in σ3, the expected Y354H and a glycine-to-arginine change at position 198 (39). In that study, Arg-198 failed to suppress Y354H, perhaps because it fails to neutralize the basic charge of His-354. Although our results suggest that σ3 residue 198 is a key surface determinant of reovirus outer capsid stability, the ready selection of mutations at position 198 that incorporate amino acids with a range of biochemical properties may point to subtle roles

for residue 198 either in maintaining capsid stability or in other aspects of reovirus replication.

The observation that σ3-Y354H is rare in circulating reovirus strains and exists coincident with suppressor mutations in T3A σ3 suggests that reovirus strains suffer a fitness penalty for mutations that destabilize the outer capsid. The reovirus life cycle involves fecal-oral transmission between infected hosts, a step that requires some degree of resistance to degradation. Viruses with diminished outer capsid stability may have decreased viability outside a mammalian host, which would reduce their likelihood of encountering a new host. We note that viruses containing uncompensated σ3-Y354H lose titer more rapidly at elevated temperature than T3A or T3D (Fig. 6), suggesting that such viruses may have diminished environmental persistence or decreased infectivity from fomite surfaces. However, it is possible that destabilization of the outer capsid adversely affects other aspects of viral replication or virus-host interactions. The optimum stability of reovirus capsid structures may also depend on the specific proteolytic milieu of the various physiological compartments encountered by viral particles during the course of infection. More work is necessary to define the precise constraints on reovirus capsid stability throughout the viral life cycle. The findings reported in this study identify a network of residues that determine the stability of reovirus σ3 and provide insight into mechanisms used by nonenveloped viruses to maintain optimum capsid stability.

Acknowledgments—We express our appreciation to Karl Boehme and Greg Wilson for careful review of the manuscript and to Chris Aiken for helpful suggestions. We thank John Mort for the kind gift of purified cathepsin L. Additional support was provided by United States Public Health Service Awards CA68485 for the Vanderbilt Cancer Center and DK20593 for the Vanderbilt Diabetes Research and Training Center.

REFERENCES

1. Wilson, I. A., Skehel, J. J., and Wiley, D. C. (1981) Structure of the hemagglutinin membrane glycoprotein of influenza virus at 3 Å resolution. *Nature* **289,** 366–373
2. Skehel, J. J., Bayley, P. M., Brown, E. B., Martin, S. R., Waterfield, M. D., White, J. M., Wilson, I. A., and Wiley, D. C. (1982) Changes in the conformation of influenza virus hemagglutinin at the pH optimum of virus-mediated membrane fusion. *Proc. Natl. Acad. Sci. U.S.A.* **79,** 968–972
3. Baker, K. A., Dutch, R. E., Lamb, R. A., and Jardetzky, T. S. (1999) Structural basis for paramyxovirus-mediated membrane fusion. *Mol. Cell* **3,** 309–319
4. Chan, D. C., Fass, D., Berger, J. M., and Kim, P. S. (1997) Core structure of gp41 from the HIV envelope glycoprotein. *Cell* **89,** 263–273
5. Weissenhorn, W., Dessen, A., Harrison, S. C., Skehel, J. J., and Wiley, D. C. (1997) Atomic structure of the ectodomain from HIV-1 gp41. *Nature* **387,** 426–430
6. Wiethoff, C. M., Wodrich, H., Gerace, L., and Nemerow, G. R. (2005) Adenovirus protein VI mediates membrane disruption following capsid disassembly. *J. Virol.* **79,** 1992–2000
7. Sturzenbecker, L. J., Nibert, M., Furlong, D., and Fields, B. N. (1987) Intracellular digestion of reovirus particles requires a low pH and is an essential step in the viral infectious cycle. *J. Virol.* **61,** 2351–2361
8. Dryden, K. A., Wang, G., Yeager, M., Nibert, M. L., Coombs, K. M., Furlong, D. B., Fields, B. N., and Baker, T. S. (1993) Early steps in reovirus infection are associated with dramatic changes in supramolecular structure and protein conformation: analysis of virions and subviral particles by cryo-electron microscopy and image reconstruction. *J. Cell Biol.* **122,** 1023–1041
9. Schiff, L. A., Nibert, M. L., and Tyler, K. L. (2007) in *Fields Virology* (Knipe, D. M., and Howley, P. M., eds), Fifth Ed., pp. 1853–1915, Lippincott Williams & Wilkins, Philadelphia
10. Borsa, J., Morash, B. D., Sargent, M. D., Copps, T. P., Lievaart, P. A., and Szekely, J. G. (1979) Two modes of entry of reovirus particles into L cells. *J. Gen. Virol.* **45,** 161–170
11. Borsa, J., Sargent, M. D., Lievaart, P. A., and Copps, T. P. (1981) Reovirus: evidence for a second step in the intracellular uncoating and transcriptase activation process. *Virology* **111,** 191–200
12. Ehrlich, M., Boll, W., Van Oijen, A., Hariharan, R., Chandran, K., Nibert, M. L., and Kirchhausen, T. (2004) Endocytosis by random initiation and stabilization of clathrin-coated pits. *Cell* **118,** 591–605
13. Maginnis, M. S., Forrest, J. C., Kopecky-Bromberg, S. A., Dickeson, S. K., Santoro, S. A., Zutter, M. M., Nemerow, G. R., Bergelson, J. M., and Dermody, T. S. (2006) β1 integrin mediates internalization of mammalian reovirus. *J. Virol.* **80,** 2760–2770
14. Baer, G. S., and Dermody, T. S. (1997) Mutations in reovirus outer capsid protein σ3 selected during persistent infections of L cells confer resistance to protease inhibitor E64. *J. Virol.* **71,** 4921–4928
15. Baer, G. S., Ebert, D. H., Chung, C. J., Erickson, A. H., and Dermody, T. S. (1999) Mutant cells selected during persistent reovirus infection do not express mature cathepsin L and do not support reovirus disassembly. *J. Virol.* **73,** 9532–9543
16. Ebert, D. H., Deussing, J., Peters, C., and Dermody, T. S. (2002) Cathepsin L and cathepsin B mediate reovirus disassembly in murine fibroblast cells. *J. Biol. Chem.* **277,** 24609–24617
17. Chang, C. T., and Zweerink, H. J. (1971) Fate of parental reovirus in infected cell. *Virology* **46,** 544–555
18. Silverstein, S. C., Astell, C., Levin, D. H., Schonberg, M., and Acs, G. (1972) The mechanisms of reovirus uncoating and gene activation *in vivo*. *Virology* **47,** 797–806
19. Ivanovic, T., Agosto, M. A., Zhang, L., Chandran, K., Harrison, S. C., and Nibert, M. L. (2008) Peptides released from reovirus outer capsid form membrane pores that recruit virus particles. *EMBO J.* **27,** 1289–1298
20. Ebert, D. H., Kopecky-Bromberg, S. A., and Dermody, T. S. (2004) Cathepsin B is inhibited in mutant cells selected during persistent reovirus infection. *J. Biol. Chem.* **279,** 3837–3851
21. Olland, A. M., Jané-Valbuena, J., Schiff, L. A., Nibert, M. L., and Harrison, S. C. (2001) Structure of the reovirus outer capsid and dsRNA-binding protein σ3 at 1.8 Å resolution. *EMBO J.* **20,** 979–989
22. Wilson, G. J., Nason, E. L., Hardy, C. S., Ebert, D. H., Wetzel, J. D., Venkataram Prasad, B. V., and Dermody, T. S. (2002) A single mutation in the carboxyl terminus of reovirus outer capsid protein σ3 confers enhanced kinetics of σ3 proteolysis, resistance to inhibitors of viral disassembly, and alterations in σ3 structure. *J. Virol.* **76,** 9832–9843
23. Wetzel, J. D., Wilson, G. J., Baer, G. S., Dunnigan, L. R., Wright, J. P., Tang, D. S., and Dermody, T. S. (1997) Reovirus variants selected during persistent infections of L cells contain mutations in the viral S1 and S4 genes and are altered in viral disassembly. *J. Virol.* **71,** 1362–1369
24. Clark, K. M., Wetzel, J. D., Gu, Y., Ebert, D. H., McAbee, S. A., Stoneman, E. K., Baer, G. S., Zhu, Y., Wilson, G. J., Prasad, B. V., and Dermody, T. S. (2006) Reovirus variants selected for resistance to ammonium chloride have mutations in viral outer capsid protein σ3. *J. Virol.* **80,** 671–681
25. Kedl, R., Schmechel, S., and Schiff, L. (1995) Comparative sequence analysis of the reovirus S4 genes from 13 serotype 1 and serotype 3 field isolates. *J. Virol.* **69,** 552–559
26. Rosen, L., Hovis, J. F., Mastrota, F. M., Bell, J. A., and Huebner, R. J. (1960) Observations on a newly recognized virus (Abney) of the reovirus family. *American Journal of Hygiene* **71,** 258–265
27. Kobayashi, T., Ooms, L. S., Ikizler, M., Chappell, J. D., and Dermody, T. S. (2010) An improved reverse genetics system for mammalian orthoreoviruses. *Virology* **398,** 194–200
28. Kobayashi, T., Antar, A. A., Boehme, K. W., Danthi, P., Eby, E. A., Guglielmi, K. M., Holm, G. H., Johnson, E. M., Maginnis, M. S., Naik, S., Skelton, W. B., Wetzel, J. D., Wilson, G. J., Chappell, J. D., and Dermody, T. S. (2007) A plasmid-based reverse genetics system for animal double-

stranded RNA viruses. *Cell Host Microbe.* **1,** 147–157
29. Virgin, H. W., 4th, Bassel-Duby, R., Fields, B. N., and Tyler, K. L. (1988) Antibody protects against lethal infection with the neurally spreading reovirus type 3 (Dearing). *J. Virol.* **62,** 4594–4604
30. Furlong, D. B., Nibert, M. L., and Fields, B. N. (1988) σ1 protein of mammalian reoviruses extends from the surfaces of viral particles. *J. Virol.* **62,** 246–256
31. Laemmli, U. K. (1970) Cleavage of structural proteins during the assembly of the head of bacteriophage T4. *Nature* **227,** 680–685
32. Smith, R. E., Zweerink, H. J., and Joklik, W. K. (1969) Polypeptide components of virions, top component, and cores of reovirus type 3. *Virology* **39,** 791–810
33. Johnson, E. M., Doyle, J. D., Wetzel, J. D., McClung, R. P., Katunuma, N., Chappell, J. D., Washington, M. K., and Dermody, T. S. (2009) Genetic and pharmacologic alteration of cathepsin expression influences reovirus pathogenesis. *J. Virol.* **83,** 9630–9640
34. Carmona, E., Dufour, E., Plouffe, C., Takebe, S., Mason, P., Mort, J. S., and Ménard, R. (1996) Potency and selectivity of the cathepsin L propeptide as an inhibitor of cysteine proteases. *Biochemistry* **35,** 8149–8157
35. Hand, R., and Tamm, I. (1973) Reovirus: effect of noninfective viral components on cellular deoxyribonucleic acid synthesis. *J. Virol.* **11,** 223–231
36. Maginnis, M. S., Mainou, B. A., Derdowski, A., Johnson, E. M., Zent, R., and Dermody, T. S. (2008) NP*X*Y motifs in the β1 integrin cytoplasmic tail are required for functional reovirus entry. *J. Virol.* **82,** 3181–3191
37. Chandran, K., Farsetta, D. L., and Nibert, M. L. (2002) Strategy for nonenveloped virus entry: a hydrophobic conformer of the reovirus membrane penetration protein μ1 mediates membrane disruption. *J. Virol.* **76,** 9920–9933
38. Dermody, T. S., Nibert, M. L., Wetzel, J. D., Tong, X., and Fields, B. N. (1993) Cells and viruses with mutations affecting viral entry are selected during persistent infections of L cells with mammalian reoviruses. *J. Virol.* **67,** 2055–2063
39. Ebert, D. H., Wetzel, J. D., Brumbaugh, D. E., Chance, S. R., Stobie, L. E., Baer, G. S., and Dermody, T. S. (2001) Adaptation of reovirus to growth in the presence of protease inhibitor E64 segregates with a mutation in the carboxyl terminus of viral outer capsid protein σ3. *J. Virol.* **75,** 3197–3206
40. Liemann, S., Chandran, K., Baker, T. S., Nibert, M. L., and Harrison, S. C. (2002) Structure of the reovirus membrane penetration protein, μ1, in a complex with is protector protein, σ3. *Cell* **108,** 283–295

APPENDIX G

REOVIRUS REPLICATION PROTEIN μ2 INFLUENCES CELL TROPISM BY PROMOTING PARTICLE ASSEMBLY WITHIN VIRAL INCLUSIONS

Laura S. Ooms, W. Gray Jerome, Terence S. Dermody, and James D. Chappell

Manuscript provisionally accepted in *Journal of Virology*

Reovirus Replication Protein μ2 Influences Cell Tropism by Promoting Particle Assembly within Viral Inclusions

Laura S. Ooms,[1,4] W. Gray Jerome,[1,2] Terence S. Dermody,[1,3,4] and James D. Chappell[1,3,4#]

Departments of Pathology, Microbiology, and Immunology[1], Cancer Biology[2], and Pediatrics[3] and Elizabeth B. Lamb Center for Pediatric Research,[4] Vanderbilt University School of Medicine, Nashville, Tennessee 37232 USA

[#]Corresponding author. Mailing address: Lamb Center for Pediatric Research, D7235 MCN, Vanderbilt University School of Medicine, Nashville, TN 37232. Phone: (615) 322-3640 Fax: (615) 343-9723. Email: jim.chappell@vanderbilt.edu

Running title: Reovirus μ2 protein promotes particle assembly

Abstract word count: 228

Text word count: 4960

ABSTRACT

The double-stranded RNA virus, mammalian reovirus, displays broad cell, tissue, and host tropism. A critical checkpoint in the reovirus replication cycle resides within viral cytoplasmic inclusions, which are biosynthetic centers of genome multiplication and new particle assembly. Replication of strain type 3 Dearing (T3) is arrested in Madin-Darby canine kidney (MDCK) cells at a step subsequent to inclusion development and prior to formation of genomic double-stranded RNA. This phenotype is primarily regulated by viral replication protein μ2. To understand how reovirus inclusions differ in productively and abortively infected MDCK cells, we used confocal immunofluorescence and thin-section transmission electron microscopy (TEM) to probe inclusion organization and particle morphogenesis. Although no abnormalities in inclusion morphology or viral protein localization were observed in T3-infected MDCK cells using confocal microscopy, TEM revealed markedly diminished production of mature progeny virions. Compared to T3-T1M1, a productively replicating reovirus strain, T3 inclusions were less frequent, smaller, and contained decreased numbers of complete particles. T3 replication was enhanced when cells were cultivated at 31ºC, and inclusion ultrastructure at low-temperature infection more closely resembled that of a productive infection. These results indicate that particle assembly in T3-infected MDCK cells is defective, possibly due to a temperature-sensitive structural or functional property of μ2. Thus, reovirus cell tropism can be governed by interactions between viral replication proteins and the unique cell environment that modulate efficiency of particle assembly.

41 INTRODUCTION

42

43 A common strategy shared by numerous viruses is the formation of specialized sites within a
44 host cell to compete viral replication. Animal double-stranded (ds) RNA viruses generate
45 nonmembranous intracytoplasmic structures—termed inclusions or factories—that have a
46 characteristic morphology, contain viral proteins and RNA, and constitute the presumed site of (-
47)-strand RNA synthesis and particle assembly (11, 35, 48). We are studying replication
48 mechanisms of the dsRNA virus, mammalian orthoreoviruses (reovirus), to better understand the
49 function of viral inclusions and how these novel organelles influence viral tropism.

50 Reoviruses are nonenveloped, double-shelled, icosahedral particles containing a genome
51 of 10 dsRNA segments (40). The viral replication cycle is entirely cytoplasmic. Following
52 internalization of virions, the viral outer capsid disassembles to generate transcriptionally active
53 core particles (3, 15, 49), which are released into the cytoplasm and synthesize full-length,
54 message-sense, capped and nonpolyadenylated ssRNAs (32, 42, 45). Viral inclusions are
55 detectable as early as 4 h post-infection by confocal immunofluorescence microscopy, lack a
56 delimiting membrane, and contain viral proteins and dsRNA, virion particles at various stages of
57 morphogenesis, and at late times of infection, paracrystalline arrays of virion particles (12, 13,
58 37). Studies of viral inclusions in infected cells and viral inclusion-like structures formed by
59 ectopic protein expression indicate that higher-order multimers of viral nonstructural protein
60 μNS establish inclusions by forming an essential matrix to which μ2, nonstructural protein σNS,
61 and other viral structural proteins are recruited (1, 4, 5, 7-9, 13, 16, 17, 22, 23, 26, 27, 34, 37, 41,
62 43, 44, 46). The μNS, μ2, and σNS proteins participate in inclusion formation and maturation as
63 indispensable components of viral replication (23). However, the nature of ribonucleoprotein

(RNP) intermediates linking the initial round of viral gene expression to the emergence of mature progeny virions has been only partially defined.

Although viral RNA assortment, genome replication, secondary transcription, and particle formation are presumed to occur within reovirus inclusions (2, 13, 14, 29, 30, 37, 58, 59), individual steps of particle assembly remain largely unknown. However, this process likely begins with assortment of positive-sense viral RNAs by a specific mechanism. Available data are congruous with an assembly model wherein equimolar amounts of the 10 viral mRNAs associate with nonstructural and core proteins and condense to form "replicase particles" (2, 14) capable of synthesizing complementary negative-sense RNA to generate the dsRNA genome. Populations of particles with distinctive complements of viral RNA and protein, as well as specific transcriptional activities (i.e., positive- or negative-strand synthesis), can be separated physiochemically and are thought to represent intermediates on a pathway toward virion assembly (29, 30, 58, 59). Current concepts of sequential steps in virion assembly are rooted mainly in biochemical analyses of these subvirion forms. However, the proposed assembly intermediates have not been correlated with specific morphogenic events in viral inclusions.

Reovirus inclusions are implicated functionally as determinants of viral cell tropism (33), where tropism is defined as the range of hosts, tissues, and cells productively infected. Reovirus strains type 1 Lang (T1) and type 3 Dearing (T3) display differential capacity to replicate in Madin Darby canine kidney (MDCK) cells (33, 39). Strain T1 replicates efficiently, while T3 replicates poorly. Analysis of recombinant reovirus strains derived from reverse genetics revealed that the M1-encoded μ2 protein of strain T1 in a T3 genetic background independently promotes reovirus replication in MDCK cells (33). The L1-encoded λ3 protein is a modulator of μ2 effects on replication efficiency, although λ3 does not display an independent association

87 with replication capacity in MDCK cells. Furthermore, the influence of λ3 on μ2-mediatied
88 replication efficiency is manifest only in the T1 genetic background. These findings indicate that
89 μ2 is the primary determinant of reovirus replication capacity in MDCK cells and λ3 is a
90 conditional co-regulator of infectivity dependent on the viral genetic context. In the same study,
91 we found that the μ2-sensitive step in replication occurs at a point in the reovirus life cycle
92 subsequent to primary rounds of viral transcription and translation but prior to dsRNA synthesis,
93 which suggests that μ2 and λ3 mediate differences in strain-specific replication efficiency at a
94 life-cycle stage occurring within viral inclusions.

95 The reovirus RNA-dependent RNA polymerase (RdRp) is thought to be composed of two
96 subunits, λ3 and μ2. The λ3 protein is the RdRp catalytic subunit (47, 50, 56), and numerous
97 biochemical, structural, and genetic studies indicate that μ2 lies proximal to λ3 and forms a
98 subunit of the fully assembled polymerase complex (6, 10, 21, 31, 36, 54, 56). The μ2 protein
99 also represents an essential component of viral inclusions required for productive viral
100 replication (24, 34). It binds inclusion-forming protein μNS (9) and determines strain-specific
101 differences in inclusion morphology—filamentous or globular—based on the relative capacity to
102 bind microtubules and tether inclusions to the cytoskeleton (34). Although the μ2 protein
103 coordinates diverse events during the reovirus replication cycle, a mechanistic understanding of
104 the role of μ2 in replication remains unknown, primarily because its functions have not been
105 linked to specific steps in the viral life cycle.

106 In work described here, we used confocal immunofluorescence and transmission electron
107 microscopy to more precisely define the role of μ2 protein in productive reovirus replication and
108 virion particle production. The results indicate that particle assembly in T3-infected MDCK cells
109 is defective and dependent on μ2 protein in a cell type-specific and temperature-dependent

manner. Thus, permissivity of some cell types to reovirus infection is governed by interactions between viral replication proteins and the unique cell environment that promote genesis of functional viral inclusions.

MATERIALS and METHODS

Cells and viruses. L929 (L) cells were grown in Joklik's modified Eagle's minimal essential medium (Lonza, Walkersville, MD) supplemented to contain 5% fetal calf serum (Cellgro, Manassas, VA), 2 mM $_{L}$-glutamine (Gibco, Grand Island, NY), 100 U/ml penicillin (Gibco), 100 μg/ml streptomycin (Gibco), and 0.25 μg/ml amphotericin B (Sigma, St. Louis, MO). MDCK cells were grown in DMEM supplemented to contain 4.5 μg/ml sodium pyruvate (Cellgro), 10% fetal calf serum, 2 mM $_{L}$-glutamine, 100 U/ml penicillin G, 100 μg/ml streptomycin, and 0.25 μg/ml amphotericin B. Strains T3 and T3-T1M1 were recovered by reverse genetics as described (22, 25). Viral titers were determined by plaque assay using L cells (51).

Quantification of virus infectivity. Monolayers of L cells or MDCK cells (approximately 5 x 10^5 cells) seeded in 24-well plates (Corning, Tewksbury, MA) were adsorbed with virus at a multiplicity of infection (MOI) of 2 PFU/cell at room temperature (RT) for 1 h. The viral inoculum was removed, cells were washed with PBS, fresh medium was added, and cells were incubated at 31ºC or 37ºC for various intervals, followed by removal to -80ºC. Viral titers in cell lysates were determined by plaque assay. Viral yield was calculated as the difference between $\log_{10}$ titer at the indicated time points and $\log_{10}$ titer at 0 h.

Immunofluorescence detection of reovirus infection. L cells plated on untreated glass coverslips and MDCK cells plated on poly-$_{L}$-lysine (Sigma)-treated glass coverslips in 24-well plates were adsorbed with virus at an MOI of 20 PFU/cell. Following incubation at 37ºC for 24 h, cells were fixed with 10% formalin and stained with guinea pig σNS-specific (4) and either rabbit μNS-specific (23), rabbit μ2-specific (57), mouse σ3-specific (4F2, [52]), mouse μ1-specific (8H6, [52]), or rabbit λ2-specific (7F4, [52]) antibodies, followed by Alexa 488-

conjugated goat anti-guinea pig secondary antibody (Invitrogen, Eugene, OR), Alexa 546-conjugated goat anti-rabbit secondary antibody (Invitrogen), or Alexa 546-conjugated goat anti-mouse antibody (Invitrogen). ToPro3 (Invitrogen) was used to stain the nucleus. Images were acquired using a Zeiss LSM 510 META inverted confocal microscope.

Electron microscopy. L cells or MDCK cells grown in T75 flasks (Corning) were adsorbed at RT for 1 h with virus at an MOI of 100 PFU/cell. Following adsorption, cells were incubated at 31ºC or 37ºC for 24 or 72 h. Cells were trypsinized, pelleted, washed with PBS, fixed at room temperature for at least 1 h with 2.5% glutaraldehyde buffered with 0.1 M sodium cacodylate, and stored at 4ºC. Following fixation, cells were washed with 0.1 M sodium cacodylate, postfixed in 1% osmium tetroxide/0.1 M sodium cacodylate for 1 h, washed in 0.1 M sodium cacodylate, and dehydrated using a graded series of ethanols. After dehydration, cells were subjected to two changes of propylene oxide and embedded in epoxy resin. Ultra-thin (65-70 nm) serial sections were obtained using a Leica Ultracut microtome and collected on copper grids. Samples were contrast stained with 2% uranyl acetate followed by Reynold's lead citrate and examined using a Phillips CM10 transmission electron microscope or FEI T-12 transmission electron microscope operated at 80 KeV.

Quantification of TEM images. The fraction of cytoplasm containing virion particles or inclusion matrix in electron micrographs was quantified using point counting stereology (53). Images were collected in a systematic, unbiased fashion using a FEI T-12 transmission electron microscope at a magnification of 30,000x. Thirty-six images were collected for each sample. A grid of points was superimposed over the images (grid size 43 x 43 nm), and points overlying cytoplasm or virus-specific material were counted. The volume of virus-occupied cytoplasm was calculated by dividing the number of points that superimposed on virus-specific material by the

160 total number points on cytoplasm. Particle diameters were measured using ImageJ
161 (http://rsb.info.nih.gov/ij/index.html). A Student's *t*-test was used to determine statistical
162 significance of differences among groups. The fraction of viral inclusion matrix occupied by
163 particles was calculated from the images collected for point counting. Particle area was estimated
164 by assuming that particles are spherical and calculating area using πr^2, where r is half the mean
165 diameter of mature and empty particles measured using imageJ. Areas of mature and empty
166 particles were calculated independently using their respective diameters and combined to yield
167 total particle area.

RESULTS

Reovirus replication in MDCK cells. Our previous studies of T3-infected MDCK cells revealed that inclusions produced by strain T3 display normal morphologic and kinetic development despite an apparent functional abnormality leading to arrest of replication (33). To more precisely define viral inclusion composition and ultrastructure in T3-infected MDCK cells, we used both confocal immunofluorescence microscopy and thin-section TEM. Strain T3-T1M1, containing the T1 M1 gene in an otherwise T3 genetic background, served as a reference for efficient μ2-regulated reovirus replication. Consistent with our previous results (33), T3-T1M1 replicated to high titers, whereas T3 exhibited minimal titer increase over a 48 h incubation interval (Fig. 1A).

Viral protein recruitment in MDCK cells. To determine whether protein recruitment to inclusions differs in productively and non-productively infected cells, we visualized individual viral proteins using confocal microscopy. Nonstructural proteins σNS and μNS physically associate in the formation of an inclusion scaffold (27). In cells infected with T3 or T3-T1M1, σNS and μNS displayed co-localization, forming large inclusions with usual strain-dependent morphology (globular for T3 and filamentous for T3-T1M1 [34]) at 24 h post-infection (Fig. 1 B, C). No alterations in σNS or μNS localization were apparent in T3-infected cells. These data indicate that the viral proteins required to form inclusions are properly recruited and assembled in T3-infected MDCK cells.

We next examined the localization of viral core proteins μ2 and λ2 and outer-capsid proteins μ1 and σ3 in T3- and T3-T1M1-infected MDCK cells (Fig. 2A) and L cells (Fig. 2B). In MDCK cells, the μ2 and λ2 proteins of both T3 and T3-T1M1 were found throughout the

cytoplasm and concentrated in viral inclusions (Fig. 2A). A similar distribution of these proteins was observed in L cells. Outer-capsid protein σ3 was highly abundant in both T3- and T3-T1M1-infected MDCK cells. It was found distributed throughout the cytoplasm, colocalized with σNS in inclusion puncta, and frequently in the nucleus (Fig. 2A). The distribution of σ3 in L cells was similar except for reduced distribution to the nucleus compared with MDCK cells. Outer-capsid protein μ1 was observed diffusely throughout the cytoplasm and in punctate structures associated with inclusions (Fig. 2). Fewer μ1-containing punctate structures were observed in T3- vs. T3-T1M1-infected MDCK cells (Fig. 2A). However, this quantitative difference correlated with diminished levels of μ1 expression overall. Viral proteins also were visualized at earlier times post-infection. Inclusions were less developed, but patterns of protein distribution were similar to those observed at 24 h (data not shown). In summary, no qualitative differences in the distribution of non-structural, core, and outer-capsid viral proteins were discernable in comparison of T3 - and T3-T1M1-infected MDCK cells, indicating that viral protein recruitment to inclusions occurs normally for both strains.

Ultrastructural analysis of viral inclusions in MDCK cells. As confocal microscopy did not reveal overt abnormalities in the morphology or viral protein composition of T3 inclusions in MDCK cells, we used thin-section TEM to visualize viral particles within inclusions. In both T3- and T3-T1M1-infected cells, mature virion particles (i.e., containing electron-dense centers representing genomic viral RNA [13, 38]) and empty virion particles were observed in a variety of arrangements. Some sections contained only a few scattered mature virions, whereas others contained large groups of viral particles surrounded by material having a consistency clearly distinct from cytoplasm. The latter structures presumably correspond to the filamentous or globular inclusions observed using confocal microscopy; we refer to these as

214 particle-containing inclusions. Representative images of particle-containing inclusions in T3-
215 T1M1-infected MDCK cells are shown in Fig. 3A. These large aggregates of virions contain a
216 significant fraction of complete particles in paracrystalline array. In marked contrast, T3 particle-
217 containing inclusions were less frequent, smaller, displayed decreased organization, and
218 harbored fewer mature particles. Inclusions containing T3 particles like those shown in Fig. 3A
219 were rare and required extensive searching to locate. The size, frequency, and particle content of
220 T3 and T3-T1M1 inclusions in L cells were similar to each other and to those in T3-T1M1-
221 infected MDCK cells (Fig. 3B).
222 To systematically confirm our impressions of T3 and T3-T1M1 inclusion ultrastructural
223 morphology, we quantified certain features of inclusions captured in electron micrographic
224 images. The fraction of cytoplasm containing virion particles or inclusion matrix was measured
225 using the point counting stereology method (53). We defined the viral fraction of cytoplasm to be
226 viral particles and surrounding milieu (i.e., inclusion matrix) that was clearly distinct from
227 cytoplasm. Structures resembling viral inclusions but devoid of viral particles were counted as
228 cytoplasm since we could not be certain that these were of viral origin. However, such "empty
229 inclusions" were infrequent. In T3-T1M1-infected MDCK cells, 19.2% of the cytoplasm was
230 occupied by inclusion matrix, whereas this fraction was only 2.9% in T3-infected cells (Table 1).
231 The corresponding values in L cells were 27.8% and 14.9%, respectively. The proportion of
232 inclusion matrix occupied by particles was 11.2% and 17.8% in T3- and T3-T1M1-infected
233 MDCK cells, respectively, and 23.4% and 32.1% in L cells. These data are consistent with our
234 observation that particles within inclusions of T3-infected MDCK cells were less densely packed.
235 Finally, we determined the ratios of complete and empty particles in inclusions formed in both
236 cell types. The fraction of complete particles in T3- and T3-T1M1-infected MDCK cells was

36.3% and 76.7%, respectively. The corresponding values in L cells were 79.7% and 94.9%, respectively. The smaller fraction of inclusion matrix observed in T3-infected MDCK cells suggests that particle assembly is defective and dependent on μ2 protein. While T3 infection of L cells resulted in lower fractional inclusion matrix, particle density, and particle maturity vs. T3-T1M1, differences in the fraction of inclusion matrix and mature particles were clearly more pronounced in MDCK cells infected with these strains. Furthermore T3 particles assumed definite order in inclusions of L cells, unlike the irregular arrangements typical of T3-infected MDCK cells. Taken together, qualitative and quantitative TEM analysis of reovirus inclusions under conditions of productive and abortive infection of MDCK cells points to viral assembly as a μ2-sensitive step in viral replication.

While examining the ultrastructure of reovirus inclusions in MDCK cells, we observed that empty T3 particles appeared smaller than empty T3-T1M1 particles. Therefore, we quantified and compared the diameters of complete and empty particles. A high-magnification image of virion particles in T3-T1M1-infected MDCK cells (Fig. 4) illustrates the specific diameter measurements recorded: (1) electron-dense centers of mature particles, (2) outer rim of mature particles, and (3) outer rim of empty particles. Large numbers of observations (110-417) for each category were made to statistically validate the size differences. The mean inner diameter of mature T3 and T3-T1M1 particles in both MDCK and L cells was ~ 38 nm, whereas the mean outer diameter of mature particles was ~ 72 nm (MDCK cells) or 71 nm (L cells) (Table 2). In contrast, the mean diameter of empty particles in T3-infected MDCK cells was significantly less than the empty-particle diameters in T3-T1M1-infected MDCK cells, 67.3 ±0.27 nm vs. 73.5 ±0.34 nm, respectively. Diameters of empty particles of T3 and T3-T1M1 in L cells, 71.2 ±0.40 nm vs. 72.0 ±0.42 nm, respectively, were not significantly different. These

results reveal a difference in the size of T3 and T3-T1M1 empty particles produced in MDCK cells but not L cells, indicating that some aspect of T3 particle assembly in MDCK cells follow an anomalous path. Furthermore, these findings are consistent with a μ2-associated block to morphogenesis of mature T3 virions in MDCK cells.

Replication of reovirus at low temperature. A previous study suggested that the T3 μ2 protein is subject to temperature-dependent misfolding (28), which led us to consider whether strain-dependent differences in viral replication efficiency in MDCK cells might be influenced by the temperature of infection. To test this hypothesis, viral titers were monitored in MDCK cells (Fig. 5A, 5B) and L cells (Fig. 5C, 5D) infected with either T3 or T3-T1M1 and incubated at either 31ºC (Fig. 5A, 5C) or 37ºC (Fig. 5B, 5D) for 96 h post-infection. Replication of T3 in MDCK cells at 31ºC greatly exceeded that at 37ºC, closely approaching the yield of T3-T1M1 at 31ºC. In L cells infected at 31ºC, T3 displayed significantly lower yield at 24 h post-infection compared to T3-T1M1, but attained a similarly high level of replication at later times post-infection. T3-T1M1 replicated efficiently in both cell types at 31ºC. However, the rise in titer was delayed relative to 37ºC. Taken together, these results indicate that replication of T3 in MDCK cells is temperature-dependent.

We used thin-section TEM of MDCK cells infected at the lower temperature to determine whether enhanced replication kinetics of T3 in MDCK cells at 31ºC correlates with restoration of normal inclusion ultrastructure. At 72 h post-infection, large particle-containing inclusions enclosing mature and empty particles were observed in both T3- and T3-T1M1-infected cells (Fig. 6). The fraction of cytoplasm occupied by viral inclusion matrix was 17% and 28% in T3- and T3-T1M1-infected cells, respectively, while the proportion of inclusion matrix occupied by particles was 12.7% in T3-infected cells and 16.8% in T3-T1M1-infected cells (Table 3).

283 Complete particles comprised 29.7% and 36.3% of total virions in T3- and T3-T1M1-infected
284 cells, respectively. The substantial increase in the fraction of inclusion matrix from 2.9% to 17%
285 in T3-infected MDCK cells incubated at 31ºC vs. 37ºC provides further evidence that the
286 restriction to T3 replication in MDCK cells relaxes at low temperature. Additionally, the mean
287 diameters of empty particles in MDCK cells infected with T3 (72.6 ±0.29 nm) and T3-T1M1
288 (71.9 ± 0.20 nm) were equivalent at reduced incubation temperature (Table 4). Thus, lowering
289 the temperature of infection partially relieved μ2-mediated restriction of T3 replication in
290 MDCK cells and reversed the block to mature particle assembly, consistent with the hypothesis
291 that the conformational state of μ2 influences efficiency of the reovirus life cycle through a
292 mechanism involving virion morphogenesis.
293

DISCUSSION

A common strategy of virus replication is formation of neo-organelles—i.e., inclusions—that concentrate and protect viral components required for genome multiplication and particle assembly. An understanding of viral inclusion composition and organization is essential to illuminate strategies by which viruses direct a successful replication program. In this study, we characterized a post entry-determined, strain-specific replication defect in MDCK cells to enhance knowledge of critical activities within reovirus inclusions that depend on the particular cell environment. Our findings suggest that reovirus tropism for some types of cells is governed by interactions between viral replication proteins and cell-type-specific factors that favor development of inclusions capable of generating fully assembled infectious particles.

Original studies of reovirus replication in MDCK cells revealed a genetic association of polymerase proteins μ2 and λ3 with viral replication efficiency (39). We subsequently showed that the μ2-sensitive step of replication in these cells occurs following the formation of viral inclusions but prior to dsRNA synthesis, leading us to propose that reovirus strain-specific replication efficiency in MDCK cells is determined at a post-entry replication checkpoint responsive to the composition of the viral polymerase complex (33). Here, we report findings of a more comprehensive analysis of viral protein trafficking to inclusions conducted to determine whether one or more inclusion components displays abnormal localization in non-productively infected MDCK cells. Using confocal immunofluorescence microscopy, no discernable cell-type-specific differences in the distribution of μ2, other major inclusion proteins μNS and σNS, core protein λ2, or outer-capsid proteins μ1 and σ3 were observed in T3-infected MDCK cells (Figs. 1, 2A). Although a relative reduction (compared with T3-T1M1) in the expression of μ1

317 was observed, the significance of this reduction to T3 replication in MDCK cells is unclear as
318 expression of all viral proteins markedly declines at late times post-infection (33). Thus, results
319 of our confocal microscopy studies confirm the expected pattern of viral protein localization to
320 T3 inclusions in MDCK cells, indicating structurally or functionally abnormal interactions within
321 the inclusion that prevent production of infectious progeny.
322 TEM analysis of MDCK cells infected with T3 revealed a much smaller fraction of
323 cytoplasm containing particles and inclusion matrix compared with strain T3-T1M1 (2.9% vs.
324 19.2%) (Fig. 3, Table 1). Mature particles with electron-dense (i.e., genome-containing) centers
325 and empty particles were observed in MDCK cells infected with either T3 or T3-T1M1.
326 However, the mature fraction of T3 particles was less than that of T3-T1M1 (36% vs. 77%)
327 (Table 1). Assembly intermediates that escape the restrictive step appear competent to reach full
328 structural maturity, consistent with the finding that conditions can be modified to permit partial
329 relief of the restriction to T3 replication in MDCK cells. Collectively, the substantial decrease in
330 particle-containing inclusion matrix and mature virion particles suggest that assembly of T3
331 particles is restricted in MDCK cells, leading to a significant reduction in viral yield. It is
332 possible that decreased protein synthesis leads to diminished mature particle yields in T3-
333 infected cells. However, we think our results are more consistent with a model wherein
334 replication fails due to inefficient production of replicase particles. We previously observed that
335 new T3 virion proteins are expressed through 12 h post infection in MDCK cells (33).
336 Additionally results of the current study confirm that no overt impediments exist to the
337 morphogenesis of T3 inclusions in these cells, and we found no obvious abnormalities in the
338 levels or localization of T3 protein relative to T3-T1M1 (Figs. 1, 2). Biochemical analysis of
339 reovirus RNA synthesis has demonstrated that 80-95% of viral mRNA is transcribed by progeny

340 particles made in the infected cells (55), and these transcripts serve as templates for protein
341 translation during latter portions of the viral life cycle (40). Taken together, results from our
342 work and other published studies best support the conclusion that diminished viral RNA and
343 protein production in T3-infected MDCK cells is secondary to a defect in particle assembly.
344 Although results of confocal microscopy studies indicate that a majority of cells are
345 infected (Figs. 1, 2), not all TEM sections contained identifiable viral structures. We defined
346 inclusions in electron micrographs by the presence of virion particles. Structures resembling
347 particle-free inclusions were rarely observed, and inclusion matrix could not be determined with
348 complete confidence in the absence of particles. It is possible that our TEM method lacks the
349 sensitivity necessary to identify particle-free inclusion matrix. Alternatively, the large difference
350 in section thickness between the two methods (900 nm confocal z-slice vs. 70 nm EM thin
351 section) may explain preferential detection of infected cells using confocal microscopy.
352 The observation that empty particles are smaller in T3- vs. T3-T1M1-infected MDCK
353 cells offers corroborating evidence of aberrant assembly of T3 virion particles. It is not known
354 whether empty particles represent precursors to mature virions or replication byproducts, but the
355 latter possibility is generally favored (18, 40). In either case, these structures inevitably share
356 some assembly steps with complete virion particles and highlight the potential for a global μ2-
357 dependent defect in particle assembly. Possible explanations for the smaller size of empty T3
358 particles include missing or stoichiometrically incorrect protein subassemblies or misfolding of
359 key protein constituents. The cell-type-specific nature of this phenotype further suggests that
360 discrete cellular factors are essential to coordinate successful particle maturation.
361 TEM ultrastructural analysis reveals a 6.6-fold decrease in the fraction of cytoplasm
362 containing virion particles or inclusion matrix in T3-infecected MDCK cells in comparison to

363 T3-T1M1 (Table 1). This difference correlates with an approximate 100-fold decrease in T3 viral
364 yield compared with T3-T1M1 (Fig. 5). Numerous factors may contribute to disproportionate
365 changes in virion production as measured by TEM and viral plaque assay. First, the mature, and
366 presumably infectious, fraction of virion particles is significantly less in T3-infected (36%) vs.
367 T3-T1M1-infected (77%) MDCK cells. Also, TEM almost exclusively identifies intracellular
368 virus, whereas replication experiments measure both intracellular and released virus. Finally, the
369 two analytical methods are subject to non-equivalent sampling bias. For example, in the
370 replication experiments, virus particles moving randomly in a fluid matrix are equally likely to
371 undergo sampling in a plaque titration assay, in contrast to TEM-based virus detection, where
372 virion particles are immobilized within structures that have non-uniform boundaries and
373 represent fewer members of the total virus population for quantification. These technical
374 differences could account in part for the greater discriminatory power of a viral replication assay
375 compared with TEM for enumeration of viable virion particles.
376 The capacity of T3 to replicate in MDCK cells at 31ºC provides insight into a possible
377 mechanism of the μ2-regulated replication phenotype. The T3 μ2 protein is highly ubiquitylated
378 in a temperature-dependent manner, and ubiquitylation is reduced when the temperature of viral
379 infection is lowered (28). These findings suggest that T3 μ2 misfolds at higher temperature and
380 raise the possibility that temperature-sensitive conformations of μ2 influence a critical early step
381 in viral assembly. The μ2 ubiquitylation phenotype segregates with a polymorphism at amino
382 acid position 208 (28), while temperature-dependent replication efficiency in MDCK cells is
383 regulated by amino acid position 347, without detectable contribution by the residue at position
384 208 (33). The effect of amino acid variability at position 347 on μ2 conformational states has not
385 been examined. However, reversal of the block to T3 replication at decreased temperature

386 suggests that residue 347 modulates a temperature-sensitive property of μ2, possibly protein-
387 folding, which in turn governs reovirus strain-specific interactions with the host-cell environment
388 during viral assembly. These interactions could involve stimulation of replication complexes
389 containing T1 μ2 or inhibition of complexes containing T3 μ2. Alternatively, the replication
390 block could be passive in nature, caused by a failure of T3 μ2 to successfully interact with
391 cellular factors. In either model, conformational variation in μ2 could conceivably influence a
392 critical association of viral and host-cell factors required for virion assembly.

393 T3 replication phenotype in MDCK cells is similar to that of reovirus strain tsH11.2,
394 which contains lesions in μ2 protein that restrict viral replication to low temperature. Like T3
395 infection of MDCK cells, tsH11.2 synthesizes normal amounts of ssRNA but displays
396 significantly diminished dsRNA production and secondary translation (10). However, unlike T3
397 infection of MDCK cells, tsH11.2 μ2 does not concentrate in viral inclusions at restrictive
398 temperature (26). Thus, the replication block to tsH11.2 might operate through mechanisms
399 affecting μ2 localization. Although the precise step in viral replication blocked in tsH11.2 may
400 differ from or complement that of T3 in MDCK cell at non-permissive temperature, both of these
401 models of conditional reovirus replication confirm the importance of μ2 protein for progression
402 of the viral life cycle beyond primary rounds of RNA and protein synthesis.

403 Reovirus inclusions are generally thought to contain cellular proteins repurposed for viral
404 use. Identities of these molecules remain mostly unknown. Early studies using electron
405 microscopy identified inclusion-associated cytoskeletal elements, including coated microtubules
406 and thick, kinked fibrils interspersed among viral particles (13, 16). Known cellular proteins
407 recruited to reovirus inclusions include chaperone Hsc70 (20) and clathrin (19). The roles played
408 by these proteins in inclusion formation and function await further investigation. A

409 comprehensive study of cellular factors required for reovirus replication, in particular those
410 required for inclusion development and maturation, will further define post-entry mechanisms of
411 viral tropism and the precise activities of μ2 and other viral replication proteins in virion
412 morphogenesis.

413 In summary, we used microscopic techniques to characterize functionally abnormal
414 reovirus inclusions that form in non-permissive cells to more fully understand the role played by
415 μ2 in promoting productive viral replication and tropism for host cells. Findings made in this
416 study establish virion particle assembly as a μ2-regulated step in the reovirus replication program
417 and suggest that a temperature-sensitive property of μ2, perhaps protein conformation, controls
418 key events within inclusions that culminate in assembly of mature particles. Additional
419 characterization of this system may identify novel cellular regulators of reovirus infection that
420 participate in virion morphogenesis and serve as determinants of viral cell tropism.
421

ACKNOWLEDGEMENTS

Acquisition and analysis of confocal and transmission electron microscopic images were made possible in part through use of the Vanderbilt University Medical Center Cell Imaging Shared Resource that is supported in part by Public Health Service awards DK58404, HD15052, DK59637, and EY08126. Funding for this work was provided by the Department of Pathology, Microbiology, and Immunology, Elizabeth B. Lamb Center for Pediatric Research, and Public Health Service awards R01 AI32539 (T.S.D.) and K08 AI062862 (J.D.C.). Additional support was provided by Public Health Service awards CA68485 for the Vanderbilt-Ingram Cancer Center and DK20593 for the Vanderbilt Diabetes Research and Training Center.

REFERENCES

1. **Anderson, N., and F. W. Doane.** 1966. An electron-microscope study of reovirus type 2 in L cells. J. Pathol. Bacteriol. **92:**433-439.
2. **Antczak, J. B., and W. K. Joklik.** 1992. Reovirus genome segment assortment into progeny genomes studied by the use of monoclonal antibodies directed against reovirus proteins. Virology **187:**760-776.
3. **Baer, G. S., D. H. Ebert, C. J. Chung, A. H. Erickson, and T. S. Dermody.** 1999. Mutant cells selected during persistent reovirus infection do not express mature cathepsin L and do not support reovirus disassembly. J. Virol. **73:**9532-9543.
4. **Becker, M. M., M. I. Goral, P. R. Hazelton, G. S. Baer, S. E. Rodgers, E. G. Brown, K. M. Coombs, and T. S. Dermody.** 2001. Reovirus σNS protein is required for nucleation of viral assembly complexes and formation of viral inclusions. J. Virol. **75:**1459-1475.
5. **Becker, M. M., T. R. Peters, and T. S. Dermody.** 2003. Reovirus σNS and μNS proteins form cytoplasmic inclusion structures in the absence of viral infection. J. Virol. **77:**5948-63.
6. **Brentano, L., D. L. Noah, E. G. Brown, and B. Sherry.** 1998. The reovirus μ2, encoded by the M1 gene, is an RNA-binding protein. Virology **72:**8354-8357.
7. **Broering, T. J., M. M. Arnold, C. L. Miller, J. A. Hurt, P. L. Joyce, and M. L. Nibert.** 2005. Carboxyl-proximal regions of reovirus nonstructural protein μNS necessary and sufficient for forming factory-like inclusions. J. Virol. **79:**6194-206.
8. **Broering, T. J., J. Kim, C. L. Miller, C. D. Piggott, J. B. Dinoso, M. L. Nibert, and J. S. Parker.** 2004. Reovirus nonstructural protein μNS recruits viral core surface proteins and entering core particles to factory-like inclusions. J. Virol. **78:**1882-1892.
9. **Broering, T. J., J. S. Parker, P. L. Joyce, J. Kim, and M. L. Nibert.** 2002. Mammalian reovirus nonstructural protein μNS forms large inclusions and colocalizes with reovirus microtubule-associated protein μ2 in transfected cells. J. Virol. **76:**8285-8297.
10. **Coombs, K. M.** 1996. Identification and characterization of a double-stranded RNA-reovirus temperature-sensitive mutant defective in minor core protein μ2. J. Virol. **70:**4237-4245.
11. **Coombs, K. M.** 2006. Reovirus structure and morphogenesis. Curr Top Microbiol Immunol **309:**117-67.
12. **Dales, S.** 1963. Association between the spindle apparatus and reovirus. Pro. Nat. Acad. Sci. **50:**268-275.
13. **Dales, S., P. Gomatos, and K. C. Hsu.** 1965. The uptake and development of reovirus in strain L cells followed with labelled viral ribonucleic acid and ferritin-antibody conjugates. Virology **25:**193-211.
14. **Dermody, T. S., J. Parker, and B. Sherry.** In Press. Orthoreovirus. *In* D. M. K. a. P. M. Howley (ed.), Fields Virology, 6 ed, vol. 2. Lippincott Williams & Wilkins, Philadelphia.
15. **Ebert, D. H., J. Deussing, C. Peters, and T. S. Dermody.** 2002. Cathepsin L and cathepsin B mediate reovirus disassembly in murine fibroblast cells. J. Biol. Chem. **277:**24609-24617.
16. **Fields, B. N.** 1971. Temperature-sensitive mutants of reovirus type 3 features of genetic recombination. Virology **46:**142-148.

17. **Gomatos, P. J., I. Tamm, S. Dales, and R. M. Franklin.** 1962. Reovirus type 3: physical characteristics and interactions with L cells. Virology **17:**441-454.
18. **Hazelton, P. R., and K. M. Coombs.** 1995. The reovirus mutant tsA279 has temperature-sensitive lesions in the M2 and L2 genes: the M2 gene is associated with decreased viral protein production and blockade in transmembrane transport. Virology **207:**46-58.
19. **Ivanovic, T., S. Boulant, M. Ehrlich, A. A. Demidenko, M. M. Arnold, T. Kirchhausen, and M. L. Nibert.** 2011. Recruitment of cellular clathrin to viral factories and disruption of clathrin-dependent trafficking. Traffic **12:**1179-95.
20. **Kaufer, S., C. M. Coffey, and J. S. Parker.** 2012. The cellular chaperone hsc70 is specifically recruited to reovirus viral factories independently of its chaperone function. J. Virol. **86:**1079-89.
21. **Kim, J., J. S. Parker, K. E. Murray, and M. L. Nibert.** 2004. Nucleoside and RNA triphosphatase activities of orthoreovirus transcriptase cofactor μ2. J. Biol. Chem. **279:**4394-403.
22. **Kobayashi, T., A. A. R. Antar, K. W. Boehme, P. Danthi, E. A. Eby, K. M. Guglielmi, G. H. Holm, E. M. Johnson, M. S. Maginnis, S. Naik, W. B. Skelton, J. D. Wetzel, G. J. Wilson, J. D. Chappell, and T. S. Dermody.** 2007. A plasmid-based reverse genetics system for animal double-stranded RNA viruses. Cell Host Microbe **1:**147-157.
23. **Kobayashi, T., J. D. Chappell, P. Danthi, and T. S. Dermody.** 2006. Gene-specific inhibition of reovirus replication by RNA interference. J. Virol. **80:**9053-9063.
24. **Kobayashi, T., L. S. Ooms, J. D. Chappell, and T. S. Dermody.** 2009. Identification of functional domains in reovirus replication proteins μNS and μ2. J. Virol. **83:**2892-2906.
25. **Kobayashi, T., L. S. Ooms, M. Ikizler, J. D. Chappell, and T. S. Dermody.** 2010. An improved reverse genetics system for mammalian orthoreoviruses. Virology **2:**194-200.
26. **Mbisa, J. L., M. M. Becker, S. Zou, T. S. Dermody, and E. G. Brown.** 2000. Reovirus μ2 protein determines strain-specific differences in the rate of viral inclusion formation in L929 cells. Virology **272:**16-26.
27. **Miller, C. L., T. J. Broering, J. S. Parker, M. M. Arnold, and M. L. Nibert.** 2003. Reovirus σNS protein localizes to inclusions through an association requiring the μNS amino terminus. J. Virol. **77:**4566-4576.
28. **Miller, C. L., J. S. Parker, J. B. Dinoso, C. D. Piggott, M. J. Perron, and M. L. Nibert.** 2004. Increased ubiquitination and other covariant phenotypes attributed to a strain- and temperature-dependent defect of reovirus core protein μ2. J. Virol. **78:**10291-10302.
29. **Morgan, E. M., and H. J. Zweerink.** 1975. Characterization of transcriptase and replicase particles isolated from reovirus infected cells. Virology **68:**455-466.
30. **Morgan, E. M., and H. J. Zweerink.** 1974. Reovirus morphogenesis: core-like particles in cells infected at 39^{o} with wild-type reovirus and temperature-sensitive mutants of groups B and G. Virology **59:**556-565.
31. **Noble, S., and M. L. Nibert.** 1997. Core protein μ2 is a second determinant of nucleoside triphosphatase activities by reovirus cores. J. Virol. **71:**7728-7735.
32. **Nonoyama, M., S. Millward, and A. F. Graham.** 1974. Control of transcription of the reovirus genome. Nucleic Acids Res. **1:**373-385.

33. **Ooms, L. S., T. Kobayashi, T. S. Dermody, and J. D. Chappell.** 2010. A post-entry step in the mammalian orthoreovirus replication cycle is a determinant of cell tropism. J. Biol. Chem. **285:**41604-41613.
34. **Parker, J. S., T. J. Broering, J. Kim, D. E. Higgins, and M. L. Nibert.** 2002. Reovirus core protein m2 determines the filamentous morphology of viral inclusion bodies by interacting with and stabilizing microtubules. J. Virol. **76:**4483-4496.
35. **Patton, J. T., L. S. Silvestri, M. A. Tortorici, R. Vasquez-Del Carpio, and Z. F. Taraporewala.** 2006. Rotavirus genome replication and morphogenesis: role of the viroplasm. Curr. Top. Microbiol. Immunol. **309:**169-87.
36. **Reinisch, K. M., M. L. Nibert, and S. C. Harrison.** 2000. Structure of the reovirus core at 3.6 Å resolution. Nature **404:**960-967.
37. **Rhim, J. S., L. E. Jordan, and H. D. Mayor.** 1962. Cytochemical, fluorescent-antibody and electron microscopic studies on the growth of reovirus (ECHO 10) in tissue culture. Virology **17:**342-355.
38. **Rhim, J. S., K. O. Smith, and J. L. Melnick.** 1961. Complete and coreless forms of reovirus (ECHO 10): ratio of number of virus particles to infective units in the one-step growth cycle. Virology **15:**428-435.
39. **Rodgers, S. E., E. S. Barton, S. M. Oberhaus, B. Pike, C. A. Gibson, K. L. Tyler, and T. S. Dermody.** 1997. Reovirus-induced apoptosis of MDCK cells is not linked to viral yield and is blocked by Bcl-2. J. Virol **71:**2540-2546.
40. **Schiff, L. A., M. L. Nibert, and K. L. Tyler.** 2007. Orthoreoviruses and their replication, p. 1853-1915. *In* D. M. Knipe and P. M. Howley (ed.), Fields Virology, Fifth ed, vol. 2. Lippincott Williams & Wilkins, Philadelphia.
41. **Sharpe, A. H., L. B. Chen, and B. N. Fields.** 1982. The interaction of mammalian reoviruses with the cytoskeleton of monkey kidney CV-1 cells. Virology **120:**399-411.
42. **Shatkin, A. J., and A. J. LaFiandra.** 1972. Transcription by infectious subviral particles of reovirus. J. Virol. **10:**698-706.
43. **Silverstein, S. C., and S. Dales.** 1968. The penetration of reovirus RNA and initiation of its genetic function in L-strain fibroblasts. J. Cell Biol. **36:**197-230.
44. **Silverstein, S. C., and P. H. Schur.** 1970. Immunofluorescent localization of double-stranded RNA in reovirus-infected cells. Virology **41:**564-566.
45. **Skehel, J. J., and W. K. Joklik.** 1969. Studies on the in vitro transcription of reovirus RNA catalyzed by reovirus cores. Virology **39:**822-831.
46. **Spendlove, R. S., E. H. Lennette, C. O. Knight, and J. N. Chin.** 1963. Development of viral antigens and infectious virus on HeLa cells infected with reovirus. J. Immunol. **90:**548-553.
47. **Starnes, M. C., and W. K. Joklik.** 1993. Reovirus protein λ3 is a poly(C)-dependent poly(G) polymerase. Virology **193:**356-366.
48. **Stuart, D. I., and J. M. Grimes.** 2006. Structural studies on orbivirus proteins and particles. Curr. Top. Microbiol. Immunol. **309:**221-44.
49. **Sturzenbecker, L. J., M. L. Nibert, D. B. Furlong, and B. N. Fields.** 1987. Intracellular digestion of reovirus particles requires a low pH and is an essential step in the viral infectious cycle. J. Virol. **61:**2351-2361.
50. **Tao, Y., D. L. Farsetta, M. L. Nibert, and S. C. Harrison.** 2002. RNA synthesis in a cage -- structural studies of reovirus polymerase λ3. Cell **111:**733-745.

51. **Virgin, H. W., IV, R. Bassel-Duby, B. N. Fields, and K. L. Tyler.** 1988. Antibody protects against lethal infection with the neurally spreading reovirus type 3 (Dearing). J. Virol. **62:**4594-4604.
52. **Virgin, H. W., and K. L. Tyler.** 1991. Role of immune cells in protection against and control of reovirus infection in neonatal mice. Journal of Virology **65:**5157-5164.
53. **Weibel, E. R.** 1979. Stereological Methods: Practical Methods for Biological Morphometry., vol. 1. Academic Press, London.
54. **Yin, P., M. Cheang, and K. M. Coombs.** 1996. The M1 gene is associated with differences in the temperature optimum of the transcriptase activity in reovirus core particles. J. Virol. **70:**1223-1227.
55. **Zarbl, H., and S. Millward.** 1983. The reovirus multiplication cycle, p. 107-196. *In* W. K. Joklik (ed.), The Reoviridae. Plenum Press, New York.
56. **Zhang, X., S. B. Walker, P. R. Chipman, M. L. Nibert, and T. S. Baker.** 2003. Reovirus polymerase λ3 localized by cryo-electron microscopy of virions at a resolution of 7.6 A. Nat. Struct. Biol. **10:**1011-1018.
57. **Zou, S., and E. G. Brown.** 1996. Stable expression of the reovirus μ2 protein in mouse L cells complements the growth of a reovirus ts mutant with a defect in its M1 gene. Virology **217:**42-48.
58. **Zweerink, H. J., Y. Ito, and T. Matsuhisa.** 1972. Synthesis of reovirus double-stranded RNA within virion-like particles. Virology **50:**349-358.
59. **Zweerink, H. J., E. M. Morgan, and J. S. Skyler.** 1976. Reovirus morphogenesis: characterization of subviral particles in infected cells. Virology **73:**442-453.

FIGURE LEGENDS

FIG 1. Reovirus replication and inclusion formation. (A) MDCK cells were adsorbed with T3 or T3-T1M1 at an MOI of 2 PFU/cell, and viral titers in cell lysates were determined at the times shown by plaque assay using L cells. Results represent the mean of triplicate experiments. Error bars indicate S.D. (B, C) MDCK cells were adsorbed with T3 (B) or T3-T1M1 (C) at an MOI of 100 PFU/cell, fixed at 24 h post-infection, stained with anti-σNS (green) and anti-μNS (red) antibodies and ToPro3 (blue, nuclear), and imaged using confocal microscopy. Scale bar, 50 μm.

FIG 2. Distribution of reovirus proteins μ2, σ3, μ1, and λ2 in infected cells. MDCK cells (A) and L cells (B) were absorbed with either T3 or T3-T1M1 at an MOI of 20 PFU/cell, fixed at 24 h post-infection, stained with anti-σNS (green) and anti-μ2, anti-σ3, anti-μ1, or anti-λ2 (red) antibodies. Nuclei were visualized using ToPro3 (blue). Images were captured using confocal microscopy. Scale bar, 20 μm.

FIG 3. Ultrastructural analysis of viral inclusions. MDCK cells (A) and L cells (B) were adsorbed with either T3 or T3-T1M1 at an MOI of 100 PFU/cell and fixed at 24 h post-infection. Ultra-thin sections (65-70 nm) were examined using transmission electron microscopy. Boxed regions correspond to high-magnification images shown below. Scale bars: low-magnification images, 2 μm; high-magnification images, 500 nm.

FIG 4. High-magnification image of T3-T1M1-infected MDCK cells. The diameter of the inner electron dense center of complete particles (Inner), the outer diameter of complete particles (Outer), and outer diameter of empty particles (Empty) are demarcated by horizontal bars. Scale bar, 100 nm.

FIG 5. Temperature-dependence of reovirus replication in MDCK cells. MDCK cells (A, B) or L cells (C, D) were adsorbed at an MOI of 2 PFU/cell and incubated at 31ºC (A, C) or 37ºC (B, D) for the times shown. Viral titers in cell lysates were determined by plaque assay using L cells. Viral yields were calculated as the difference between $\log_{10}$ titer at the indicated times and $\log_{10}$ titer at 0 h. Results represent the mean of triplicate experiments. Error bars indicate S.D. *, $P < 0.05$ in comparison to T3-T1M1 (Student's *t* test).

FIG 6. Ultrastructural analysis of viral inclusions in MDCK cells infected at low temperature. MDCK cells were adsorbed with either T3 or T3-T1M1 at an MOI of 100 PFU/cell, incubated at 31ºC, and fixed at 72 h post-infection. Ultra-thin sections (65-70 nm) were examined using transmission electron microscopy. Boxed regions correspond to high-magnification images shown below. Scale bars: low-magnification images, 2 μm; high-magnification images, 500 nm.

Table 1. Quantitative analysis of reovirus replication using thin-section electron micrographs of reovirus-infected MDCK and L cells*

Cell type	Virus strain	Fraction of cytoplasm containing virion particles or inclusion matrix	Fraction of viral inclusion matrix occupied by particles	Mature fraction of virion particles
MDCK	T3	2.9%	11.2%	36.3%
MDCK	T3-T1M1	19.2%	17.8%	76.7%
L	T3	14.9%	23.4%	79.7%
L	T3-T1M1	27.8%	32.1%	94.9%

*36 images examined for each sample condition

Table 2: Quantification of viral particle diameters in reovirus-infected MDCK and L cells

Cell type	Virus strain	Mature particle outer diameter (nm)*	n§	Mature particle inner diameter (nm)	n	Empty particle outer diameter (nm)	n
MDCK	T3	72.3 ± 0.44	110	38.3 ± 0.22	116	67.3 ± 0.27	306
	T3-T1M1	72.0 ± 0.21#	311	37.9 ± 0.12#	323	73.5 ± 0.34&	177
L	T3	71.3 ± 0.24	380	38.5 ± 0.11	417	71.2 ± 0.40	119
	T3-T1M1	71.0 ± 0.22#	385	38.3 ± 0.11#	413	72.0 ± 0.42#	138

*Values represent mean ± S.E.M.
§n, number of particles measured
#*t*-test, not significant (vs. T3)
&*t*-test, $P < 0.0001$ (vs. T3)

Table 3. Quantitative analysis of reovirus replication at 31ºC using thin-section electron micrographs of reovirus-infected MDCK cells*

Virus strain	Fraction of cytoplasm containing virion particles or inclusion matrix	Fraction of viral inclusion matrix occupied by particles	Mature fraction of virion particles
T3	17.2%	12.7%	29.7%
T3-T1M1	28.0%	16.8%	36.3%

*36 images examined for each sample condition

Table 4. Quantification of viral particle diameters following infection of MDCK cells at 31ºC

Virus strain	Mature particle outer diameter (nm)*	n[§]	Mature particle inner diameter (nm)	n	Empty particle outer diameter (nm)	n
T3	71.9 ± 0.35	203	38.0 ± 0.16	225	72.6 ± 0.29	284
T3-T1M1	71.5 ± 0.23[#]	306	37.9 ± 0.13[#]	312	71.9 ± 0.20[#]	472

650 *Values represent mean ± S.E.M.
651 [§]n, number of particles measured
652 [#]*t*-test, not significant (vs. T3)
653

Figure 1

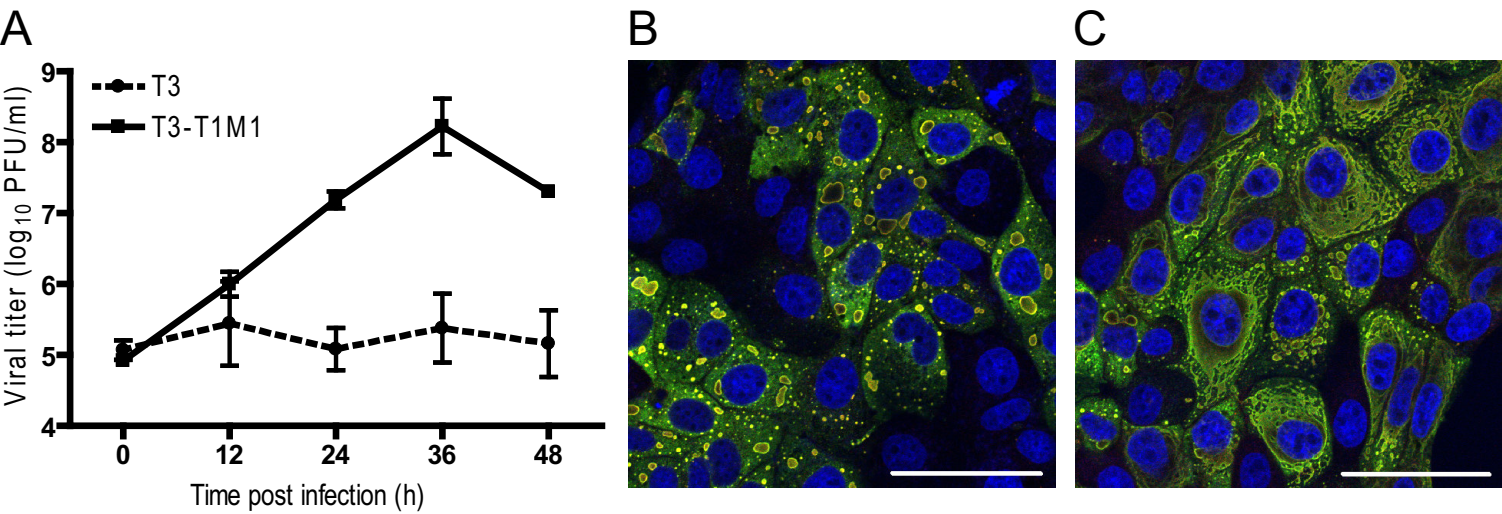
A
B
C
T3
T3-T1M1
Viral titer (log10 PFU/ml)
9
8
7
6
5
4
0
12
24
36
48
Time post infection (h)

Figure 2

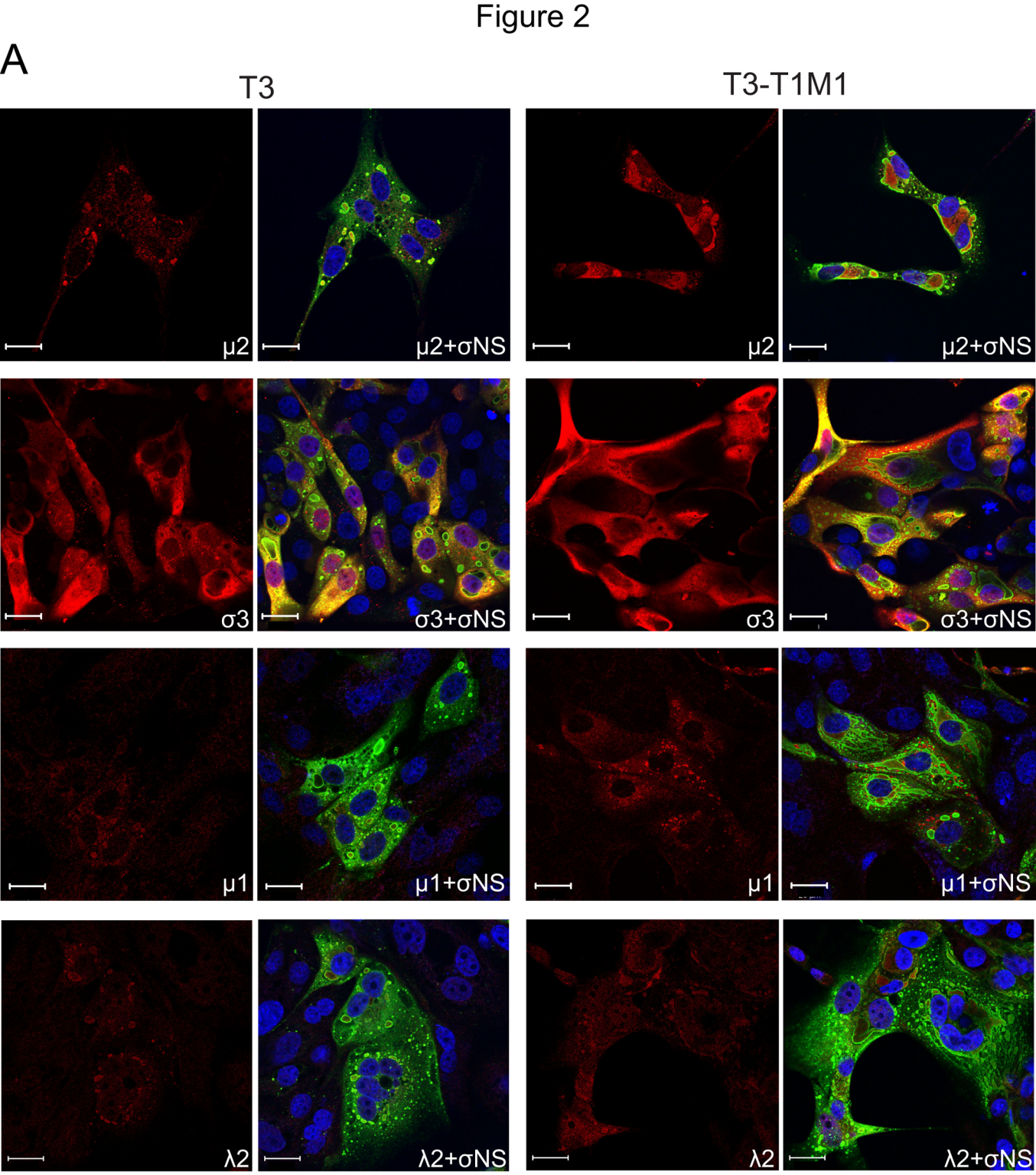
A
T3
T3-T1M1
μ2
μ2+σNS
μ2
μ2+σNS
σ3
σ3+σNS
σ3
σ3+σNS
μ1
μ1+σNS
μ1
μ1+σNS
λ2
λ2+σNS
λ2
λ2+σNS

Figure 2

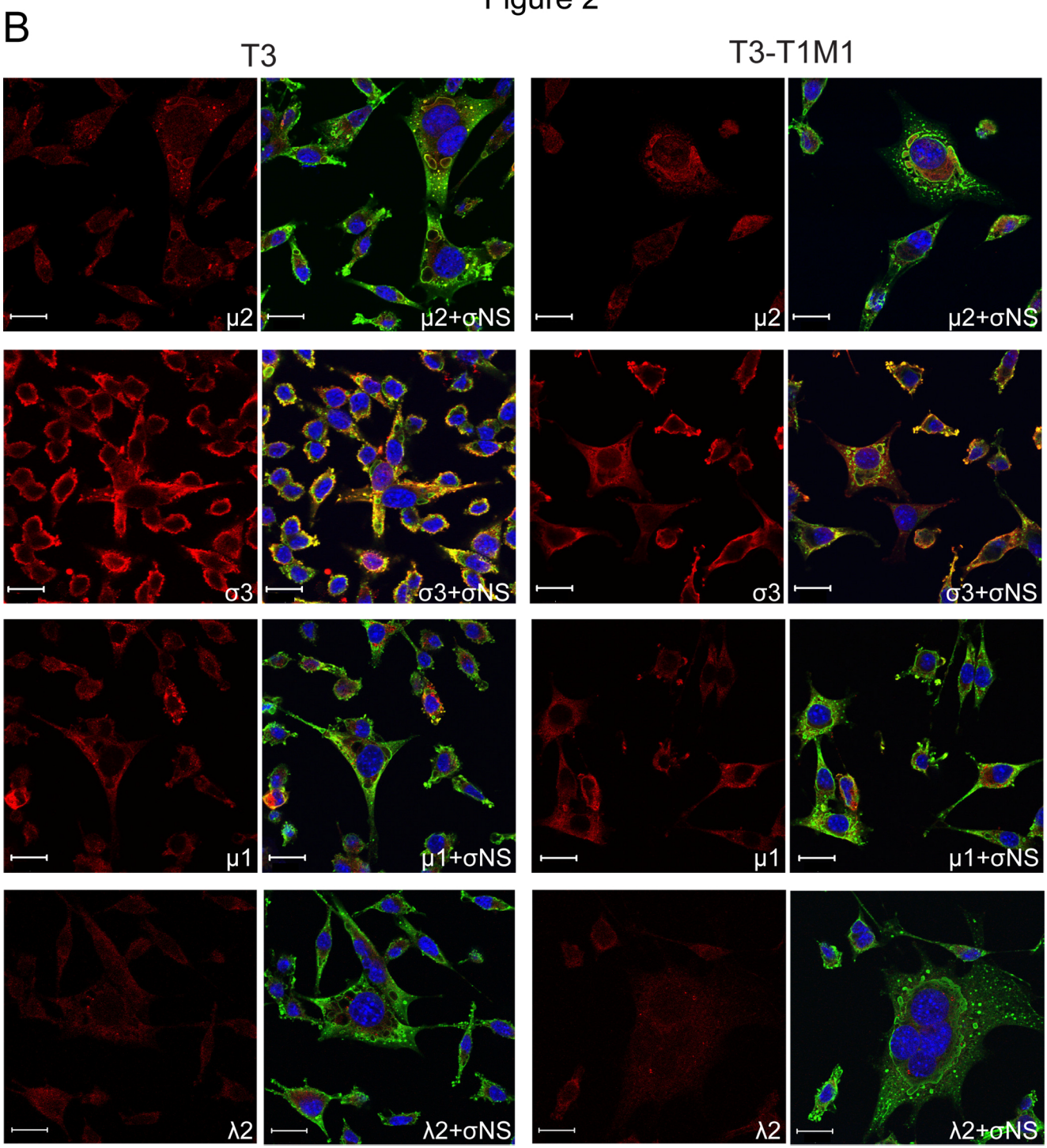
B
T3
T3-T1M1
μ2
μ2+σNS
μ2
μ2+σNS
σ3
σ3+σNS
σ3
σ3+σNS
μ1
μ1+σNS
μ1
μ1+σNS
λ2
λ2+σNS
λ2
λ2+σNS

Figure 3

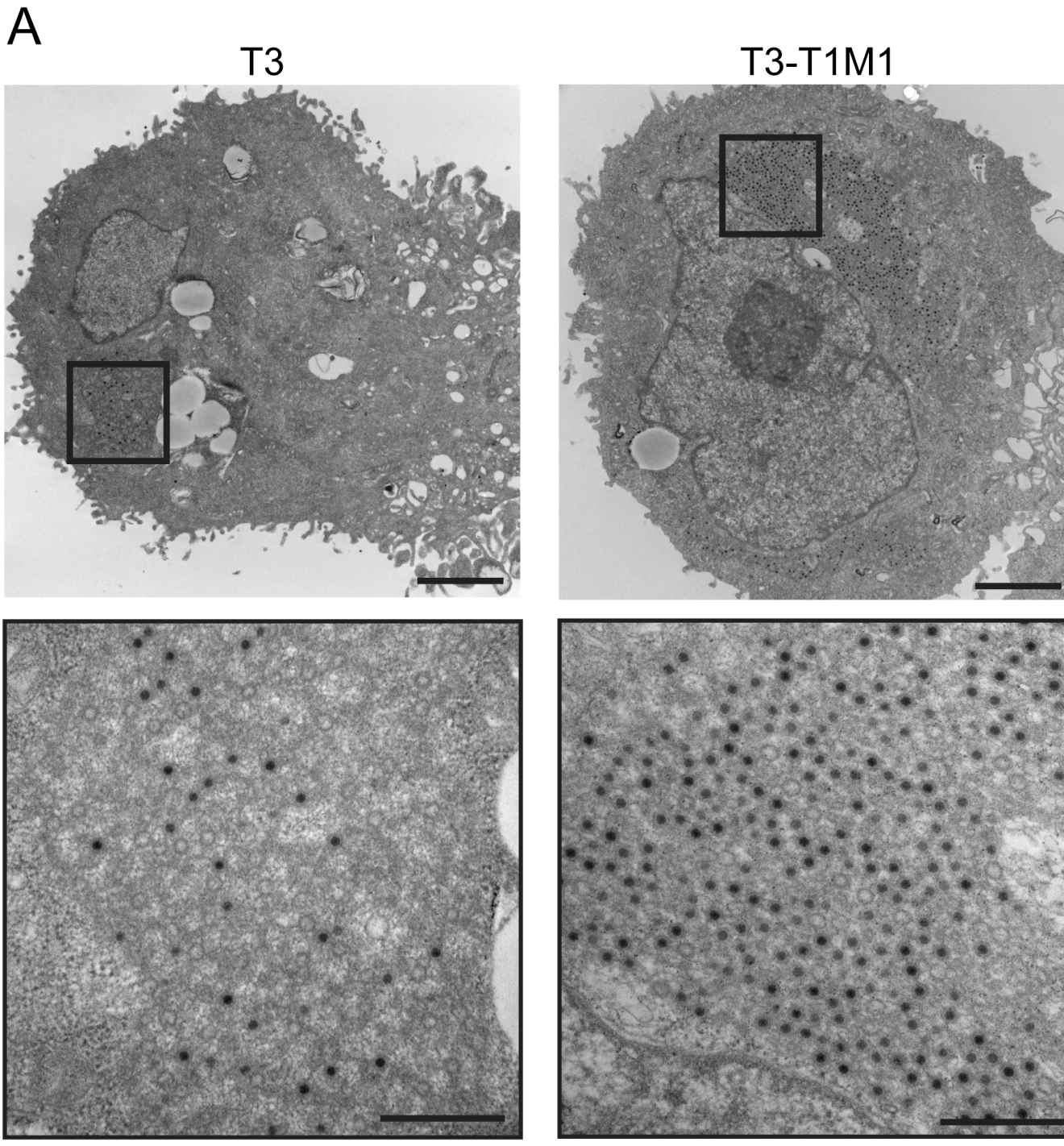

Figure 3

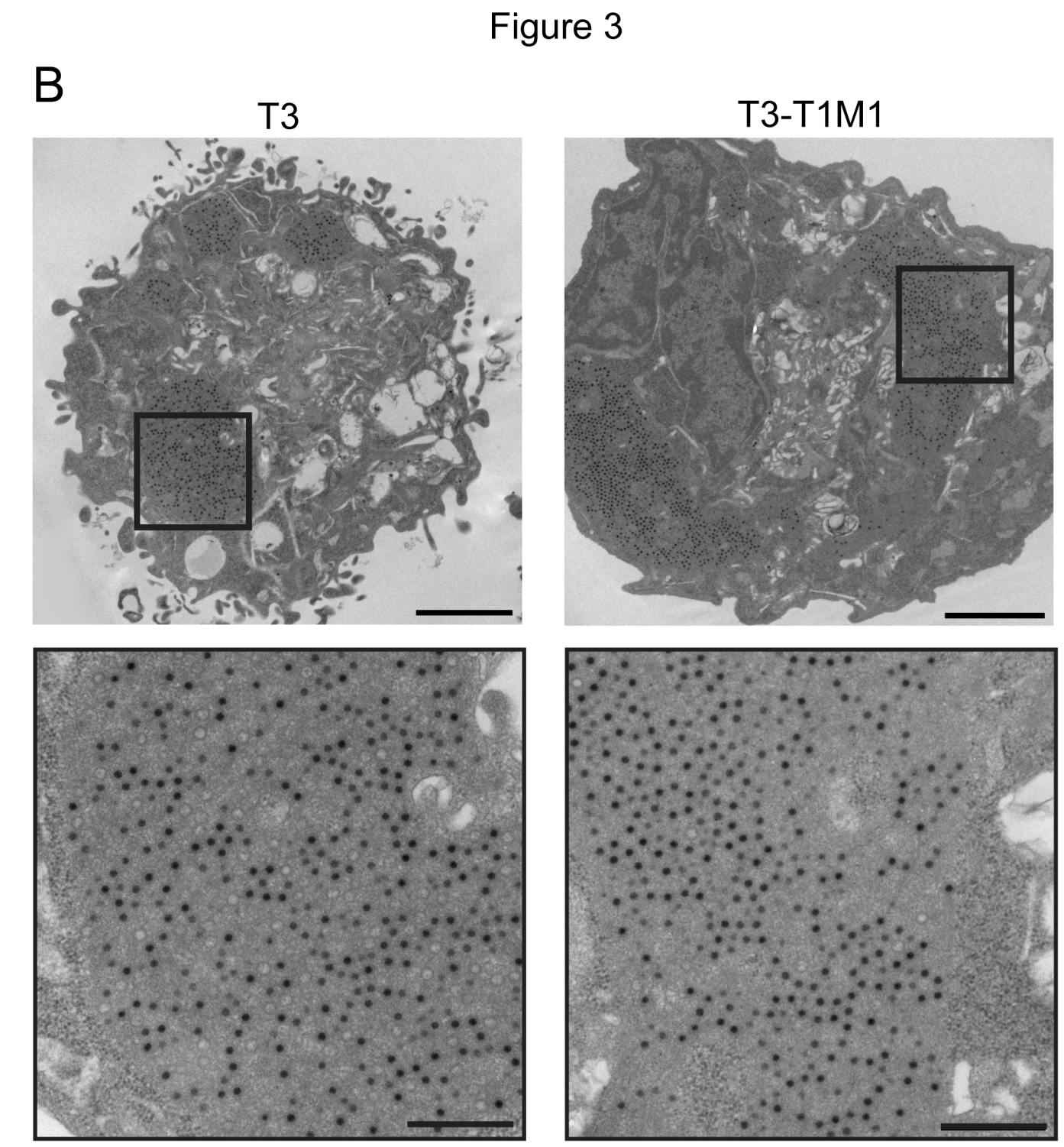

Figure 4

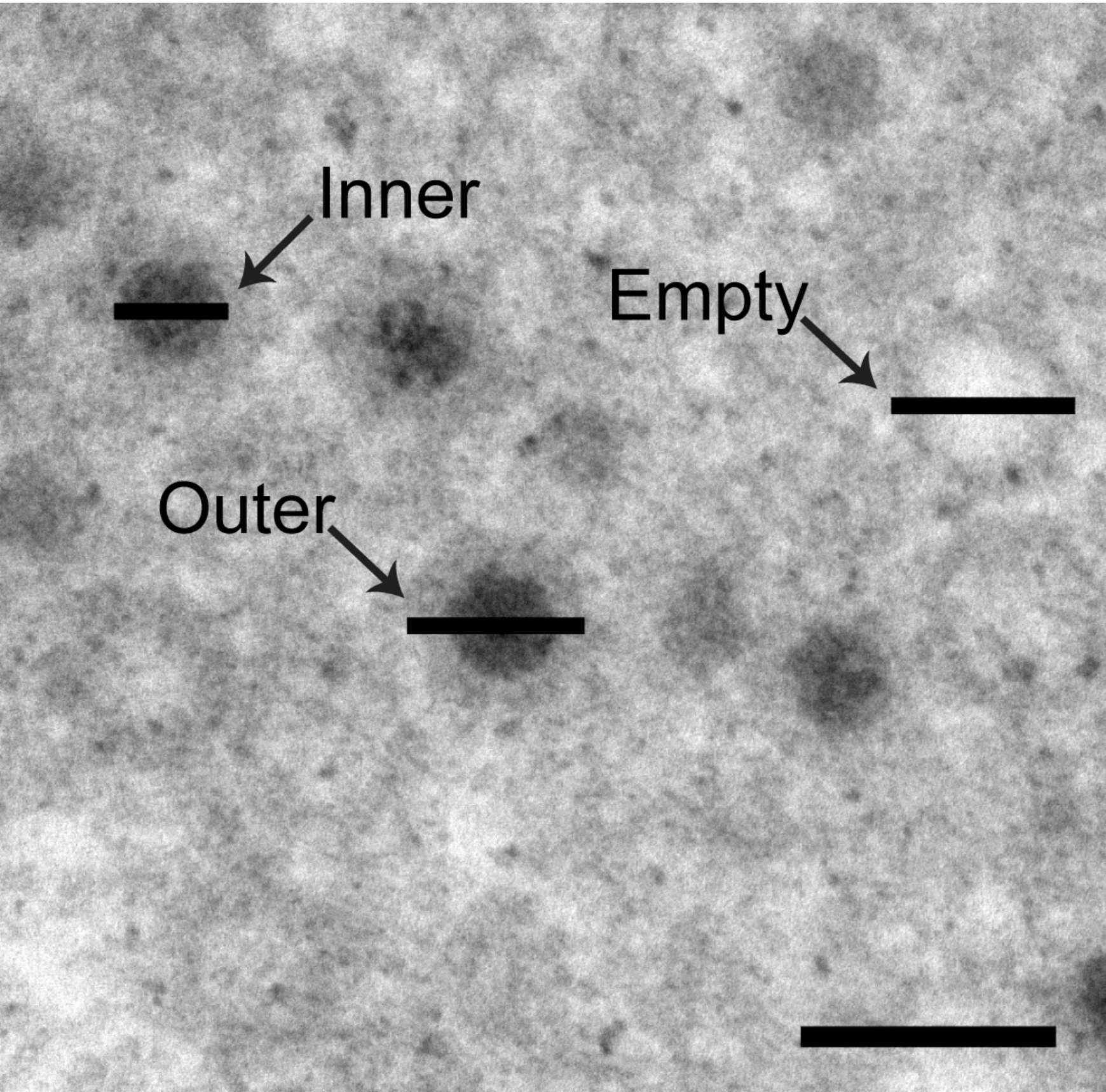

Figure 5

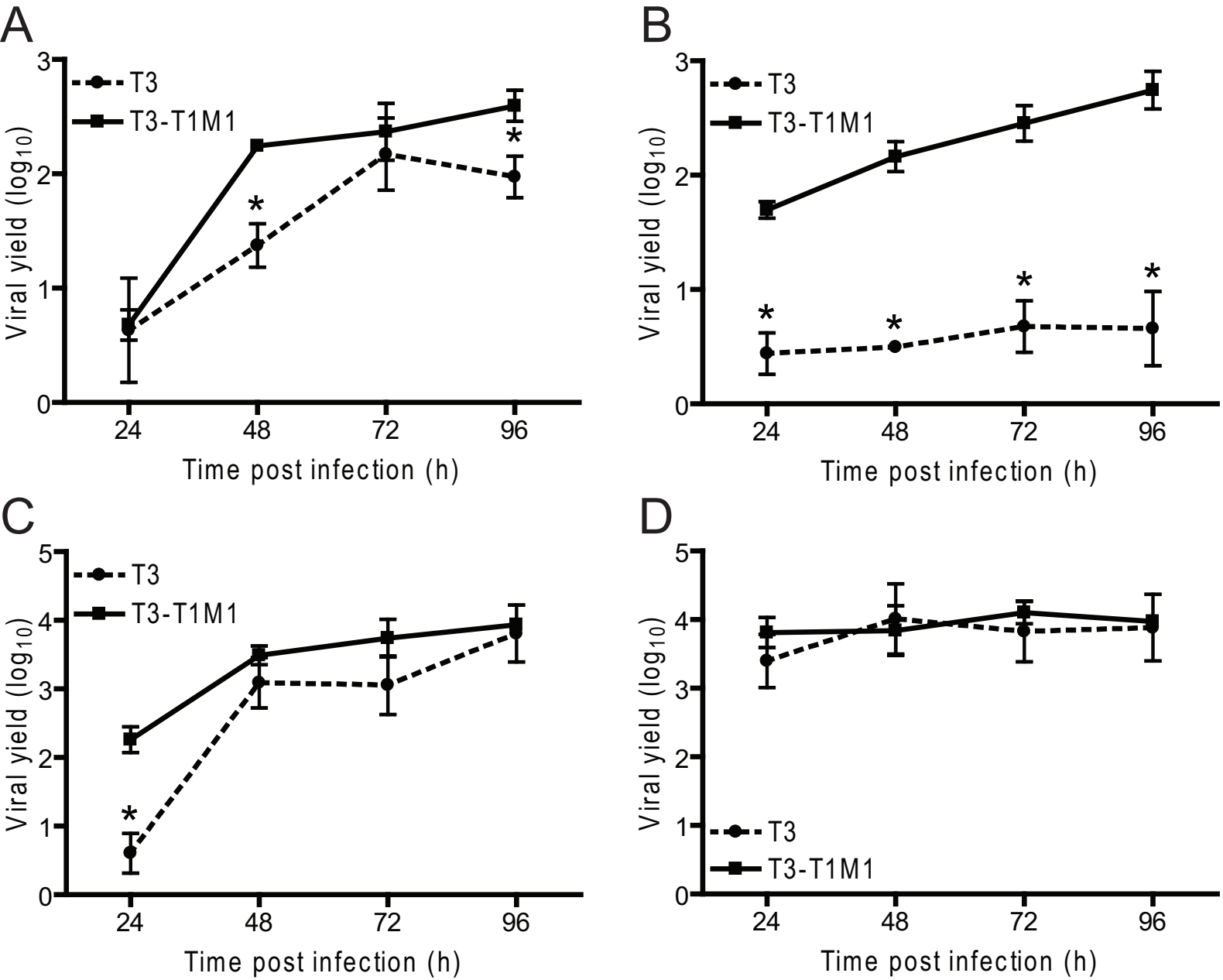
A
B
C
D
T3
T3-T1M1
Viral yield (log10)
Time post infection (h)
24
48
72
96
0
1
2
3
4
5
*

Figure 6

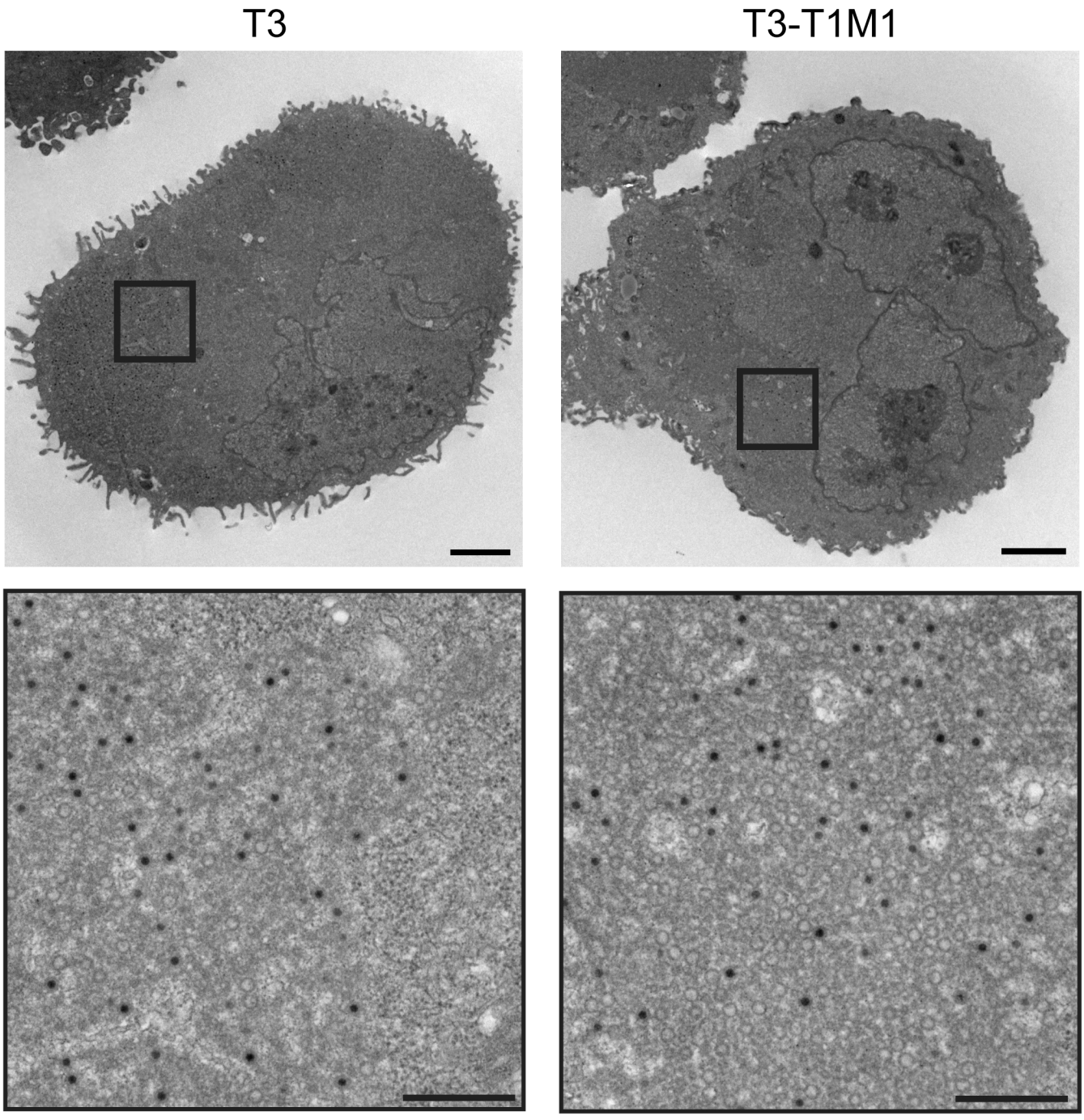

REFERENCES

1. **Ahlquist, P.** 2006. Parallels among positive-strand RNA viruses, reverse-transcribing viruses and double-stranded RNA viruses. Nature Reviews Microbiology **4:**371-382.
2. **Antczak, J. B., and W. K. Joklik.** 1992. Reovirus genome segment assortment into progeny genomes studied by the use of monoclonal antibodies directed against reovirus proteins. Virology **187:**760-776.
3. **Arnold, M. M., K. E. Murray, and M. L. Nibert.** 2008. Formation of the factory matrix is an important, though not a sufficient function of nonstructural protein μNS during reovirus infection. Virology **375:**412-23.
4. **Attoui, H., P. Biagini, J. Stirling, P. P. Mertens, J. F. Cantaloube, A. Meyer, P. de Micco, and X. de Lamballerie.** 2001. Sequence characterization of Ndelle virus genome segments 1, 5, 7, 8, and 10: evidence for reassignment to the genus Orthoreovirus, family Reoviridae. Biochemical and Biophysical Research Communications **287:**583-588.
5. **Babiss, L. E., R. B. Luftig, J. A. Weatherbee, R. R. Weihing, U. R. Ray, and B. N. Fields.** 1979. Reovirus serotypes 1 and 3 differ in their in vitro association with microtubules. Journal of Virology **30:**863-874.
6. **Banerjee, A. K., and A. J. Shatkin.** 1970. Transcription in vitro by reovirus-associated ribonucleic acid-dependent polymerase. Journal of Virology **6:**1-11.
7. **Barton, E. S., J. C. Forrest, J. L. Connolly, J. D. Chappell, Y. Liu, F. Schnell, A. Nusrat, C. A. Parkos, and T. S. Dermody.** 2001. Junction adhesion molecule is a receptor for reovirus. Cell **104:**441-451.
8. **Becker, M. M., M. I. Goral, P. R. Hazelton, G. S. Baer, S. E. Rodgers, E. G. Brown, K. M. Coombs, and T. S. Dermody.** 2001. Reovirus σNS protein is required for nucleation of viral assembly complexes and formation of viral inclusions. Journal of Virology **75:**1459-1475.
9. **Becker, M. M., T. R. Peters, and T. S. Dermody.** 2003. Reovirus σNS and μNS proteins form cytoplasmic inclusion structures in the absence of viral infection. Journal of Virology **77:**5948-63.
10. **Berry, J. M., N. Barnabe, K. M. Coombs, and M. Butler.** 1999. Production of reovirus type-1 and type-3 from Vero cells grown on solid and macroporous microcarriers. Biotechnology and Bioengineering **62:**12-19.
11. **Bisaillon, M., and G. Lemay.** 1997. Characterization of the reovirus λ1 protein RNA 5'-triphosphatase activity. Journal of Biological Chemistry **272:**29954-7.
12. **Bisaillon, M., and G. Lemay.** 1997. Molecular dissection of the reovirus λ1 protein nucleic acids binding site. Virus Research **51:**231-7.
13. **Bonner, W. M.** 1978. Protein migration and accumulation in nuclei, p. 97-148. *In* H. Busch (ed.), The Cell Nucleus, vol. 6. Academic Press, New York.
14. **Brentano, L., D. L. Noah, E. G. Brown, and B. Sherry.** 1998. The reovirus μ2, encoded by the M1 gene, is an RNA-binding protein. Virology **72:**8354-8357.
15. **Broering, T. J., J. Kim, C. L. Miller, C. D. Piggott, J. B. Dinoso, M. L. Nibert, and J. S. Parker.** 2004. Reovirus nonstructural protein μNS recruits viral core

surface proteins and entering core particles to factory-like inclusions. Journal of Virology **78:**1882-1892.

16. **Broering, T. J., A. M. McCutcheon, V. E. Centonze, and M. L. Nibert.** 2000. Reovirus nonstructural protein μNS binds to core particles but does not inhibit their transcription and capping activities. Journal of Virology **74:**5516-5524.
17. **Broering, T. J., J. S. Parker, P. L. Joyce, J. Kim, and M. L. Nibert.** 2002. Mammalian reovirus nonstructural protein μNS forms large inclusions and colocalizes with reovirus microtubule-associated protein μ2 in transfected cells. Journal of Virology **76:**8285-8297.
18. **Campbell, J. A., P. Shelling, J. D. Wetzel, E. M. Johnson, G. A. R. Wilson, J. C. Forrest, M. Aurrand-Lions, B. Imhof, T. Stehle, and T. S. Dermody.** 2005. Junctional adhesion molecule-A serves as a receptor for prototype and field-isolate strains of mammalian reovirus. Journal of Virology **79:**7967-7978.
19. **Carvalho, J., M. M. Arnold, and M. L. Nibert.** 2007. Silencing and complementation of reovirus core protein μ2: functional correlations with μ2-microtubule association and differences between virus- and plasmid-derived μ2. Virology **364:**301-16.
20. **Chelsky, D., R. Ralph, and G. Jonak.** 1989. Sequence requirements for synthetic peptide-mediated translocation to the nucleus. Molecular and Cellular Biology **9:**2487-2492.
21. **Cleveland, D. R., H. Zarbl, and S. Millward.** 1986. Reovirus guanyltransferase is L2 gene product λ2. Journal of Virology **60:**307-311.
22. **Coffey, M. C., J. E. Strong, P. A. Forsyth, and P. W. Lee.** 1998. Reovirus therapy of tumors with activated Ras pathway. Science **282:**1332-1334.
23. **Coombs, K. M.** 1996. Identification and characterization of a double-stranded RNA-reovirus temperature-sensitive mutant defective in minor core protein μ2. Journal of Virology **70:**4237-4245.
24. **Coombs, K. M.** 2006. Reovirus structure and morphogenesis. Current Topics in Microbiology and Immunology **309:**117-67.
25. **Coombs, K. M.** 1998. Stoichiometry of reovirus structural proteins in virus, ISVP, and core particles. Virology **243:**218-228.
26. **Cross, R. K., and B. N. Fields.** 1972. Temperature-sensitive mutants of reovirus type 3: studies on the synthesis of viral RNA. Journal of Virology **50:**799-809.
27. **Dales, S., P. Gomatos, and K. C. Hsu.** 1965. The uptake and development of reovirus in strain L cells followed with labeled viral ribonucleic acid and ferritin-antibody conjugates. Virology **25:**193-211.
28. **Danthi, P., K. M. Guglielmi, E. Kirchner, B. Mainou, T. Stehle, and T. S. Dermody.** 2010. From touchdown to transcription: the reovirus cell entry pathway. Current Topics in Microbiology and Immunology **343:**91-119.
29. **den Boon, J. A., and P. Ahlquist.** 2010. Organelle-like membrane Compartmentalization of positive-strand RNA virus replication factories. Annual Review of Microbiology **64:**241-256.
30. **den Boon, J. A., A. Diaz, and P. Ahlquist.** 2010. Cytoplasmic viral replication complexes. Cell Host & Microbe **8:**77-85.

31. **Dermody, T. S., J. Parker, and B. Sherry.** In Press. Orthoreovirus. *In* D. M. K. a. P. M. Howley (ed.), Fields Virology, 6 ed, vol. 2. Lippincott Williams & Wilkins, Philadelphia.
32. **Dermody, T. S., M. L. Nibert, R. Bassel-Duby, and B. N. Fields.** 1990. A σ1 region important for hemagglutination by serotype 3 reovirus strains. Journal of Virology **64:**5173-5176.
33. **Drayna, D., and B. N. Fields.** 1982. Biochemical studies on the mechanism of chemical and physical inactivation of reovirus. Journal of General Virology **63:**161-170.
34. **Dryden, K. A., G. Wang, M. Yeager, M. L. Nibert, K. M. Coombs, D. B. Furlong, B. N. Fields, and T. S. Baker.** 1993. Early steps in reovirus infection are associated with dramatic changes in supramolecular structure and protein conformation: analysis of virions and subviral particles by cryoelectron microscopy and image reconstruction. Journal of Cell Biology **122:**1023-1041.
35. **Fields, B. N.** 1971. Temperature-sensitive mutants of reovirus type 3 features of genetic recombination. Virology **46:**142-148.
36. **Furlong, D. B., M. L. Nibert, and B. N. Fields.** 1988. σ1 protein of mammalian reoviruses extends from the surfaces of viral particles. Journal of Virology **62:**246-256.
37. **Furuichi, Y., S. Muthukrishnan, J. Tomasz, and A. J. Shatkin.** 1976. Mechanism of formation of reovirus mRNA 5'-terminal blocked and methylated sequence M^7 $GpppG^m$ pC. Journal of Biological Chemistry **251:**5043-5053.
38. **Gale, M., and G. C. Sen.** 2009. Viral evasion of the interferon system. Journal of Interferon & Cytokine Research **29:**475-6.
39. **Garcia-Bustos, J., J. Heitman, and M. N. Hall.** 1991. Nuclear protein localization. Biochimica et Biophysa Acta **1071:**83-101.
40. **Gillies, S., S. Bullivant, and A. R. Bellamy.** 1971. Viral RNA polymerases: electron microscopy of reovirus reaction cores. Science **174:**694-696.
41. **Golden, J. W., J. Linke, S. Schmechel, K. Thoemke, and L. A. Schiff.** 2002. Addition of exogenous protease facilitates reovirus infection in many restrictive cells. Journal of Virology **76:**7430-7443.
42. **Gomatos, P. J., I. Tamm, S. Dales, and R. M. Franklin.** 1962. Reovirus type 3: physical characteristics and interactions with L cells. Virology **17:**441-454.
43. **Gottesman, A., J. Milazzo, and Y. Lazebnik.** 2010. V-fusions: a convenient, nontoxic method for cell fusions. BioTechniques **49:**747-750.
44. **Haller, B. L., M. L. Barkon, G. P. Vogler, and H. W. Virgin, IV.** 1995. Genetic mapping of reovirus virulence and organ tropism in severe combined immunodeficient mice: organ-specific virulence genes. Journal of Virology **69:**357-364.
45. **Hatziioannou, T., S. Cowan, S. P. Goff, P. D. Bieniasz, and G. J. Towers.** 2003. Restriction of multiple divergent retroviruses by Lv1 and Ref1. The EMBO Journal **22:**385-94.
46. **Hazelton, P. R., and K. M. Coombs.** 1995. The reovirus mutant tsA279 has temperature-sensitive lesions in the M2 and L2 genes: the M2 gene is associated with decreased viral protein production and blockade in transmembrane transport. Virology **207:**46-58.

47. **Heinrich, B. S., D. K. Cureton, A. A. Rahmeh, and S. P. Whelan.** 2010. Protein expression redirects vesicular stomatitis virus RNA synthesis to cytoplasmic inclusions. PLoS Pathogens **6:**e1000958.
48. **Hermann, L. L., and K. M. Coombs.** 2004. Inhibition of reovirus by mycophenolic acid is associated with the M1 genome segment. Journal of Virology **78:**6171-6179.
49. **Irvin, S. C., J. Zurney, L. S. Ooms, J. D. Chappell, T. S. Dermody, and B. Sherry.** 2012. A single amino acid polymorphism in reovirus protein μ2 determines repression of interferon signaling and modulates myocarditis. Journal of Virology **86:**2302-11.
50. **Ito, Y., and W. K. Joklik.** 1972. Temperature-sensitive mutants of reovirus. I. Patterns of gene expression by mutants of groups C, D, and E. Virology **50:**189-201.
51. **Ivanovic, T., S. Boulant, M. Ehrlich, A. A. Demidenko, M. M. Arnold, T. Kirchhausen, and M. L. Nibert.** 2011. Recruitment of cellular clathrin to viral factories and disruption of clathrin-dependent trafficking. Traffic **12:**1179-95.
52. **Joklik, W. K.** 1985. Recent progress in reovirus research. Annual Review of Genetics **19:**537-575.
53. **Kauder, S. E., and V. R. Racaniello.** 2004. Poliovirus tropism and attenuation are determined after internal ribosome entry. Journal of Clinical Investigation **113:**1743-53.
54. **Kaufer, S., C. M. Coffey, and J. S. Parker.** 2012. The cellular chaperone hsc70 is specifically recruited to reovirus viral factories independently of its chaperone function. Journal of Virology **86:**1079-89.
55. **Kauffman, R. S., J. L. Wolf, R. Finberg, J. S. Trier, and B. N. Fields.** 1983. The σ1 protein determines the extent of spread of reovirus from the gastrointestinal tract of mice. Virology **124:**403-410.
56. **Kaukinen, P., A. Vaheri, and A. Plyusnin.** 2005. Hantavirus nucleocapsid protein: a multifunctional molecule with both housekeeping and ambassadorial duties. Archives of Virology **150:**1693-713.
57. **Kaye, K. M., D. R. Spriggs, R. Bassel-Duby, B. N. Fields, and K. L. Tyler.** 1986. Genetic basis for altered pathogenesis of an immune-selected antigenic variant of reovirus type 3 Dearing. Journal of Virology **59:**90-97.
58. **Kim, J., J. S. Parker, K. E. Murray, and M. L. Nibert.** 2004. Nucleoside and RNA triphosphatase activities of orthoreovirus transcriptase cofactor μ2. Journal of Biological Chemistry **279:**4394-403.
59. **Kobayashi, T., A. A. R. Antar, K. W. Boehme, P. Danthi, E. A. Eby, K. M. Guglielmi, G. H. Holm, E. M. Johnson, M. S. Maginnis, S. Naik, W. B. Skelton, J. D. Wetzel, G. J. Wilson, J. D. Chappell, and T. S. Dermody.** 2007. A plasmid-based reverse genetics system for animal double-stranded RNA viruses. Cell Host & Microbe **1:**147-157.
60. **Kobayashi, T., J. D. Chappell, P. Danthi, and T. S. Dermody.** 2006. Gene-specific inhibition of reovirus replication by RNA interference. Journal of Virology **80:**9053-9063.

61. **Kobayashi, T., L. S. Ooms, J. D. Chappell, and T. S. Dermody.** 2009. Identification of functional domains in reovirus replication proteins μNS and μ2. Journal of Virology **83:**2892-2906.
62. **Kobayashi, T., L. S. Ooms, M. Ikizler, J. D. Chappell, and T. S. Dermody.** 2010. An improved reverse genetics system for mammalian orthoreoviruses. Virology **2:**194-200.
63. **la Cour, T., L. Kiemer, A. Molgaard, R. Gupta, K. Skriver, and S. Brunak.** 2004. Analysis and prediction of leucine-rich nuclear export signals. Protein Engineering Design and Selection **17:**527-536.
64. **Lopez-Lastra, M., P. Ramdohr, A. Letelier, M. Vallejos, J. Vera-Otarola, and F. Valiente-Echeverria.** 2010. Translation initiation of viral mRNAs. Reviews in Medical Virology **20:**177-95.
65. **Luongo, C. L., K. M. Reinisch, S. C. Harrison, and M. L. Nibert.** 2000. Identification of the mRNA guanylyltransferase region and active site in reovirus λ2 protein. Journal of Biological Chemistry **275:**2804-2810.
66. **Matoba, Y., W. S. Colucci, B. N. Fields, and T. W. Smith.** 1993. The reovirus M1 gene determines the relative capacity of growth of reovirus in cultured bovine aortic endothelial cells. Journal of Clinical Investigation **92:**2883-2888.
67. **Matoba, Y., B. Sherry, B. N. Fields, and T. W. Smith.** 1991. Identification of the viral genes responsible for growth of strains of reovirus in cultured mouse heart cells. Journal of Clinical Investigation **87:**1628-1633.
68. **Mbisa, J. L., M. M. Becker, S. Zou, T. S. Dermody, and E. G. Brown.** 2000. Reovirus μ2 protein determines strain-specific differences in the rate of viral inclusion formation in L929 cells. Virology **272:**16-26.
69. **McCrae, M. A., and W. K. Joklik.** 1978. The nature of the polypeptide encoded by each of the ten double-stranded RNA segments of reovirus type 3. Virology **89:**578-593.
70. **Medina, R. A., and A. Garcia-Sastre.** 2011. Influenza A viruses: new research developments. Nature Reviews Microbiology **9:**590-603.
71. **Mehle, A., and J. A. Doudna.** 2008. An inhibitory activity in human cells restricts the function of an avian-like influenza virus polymerase. Cell Host & Microbe **4:**111-122.
72. **Miller, C. L., M. M. Arnold, T. J. Broering, C. Eichwald, J. Kim, J. B. Dinoso, and M. L. Nibert.** 2007. Virus-derived platforms for visualizing protein associations inside cells. Molecular & Cellular Proteomics **6:**1027-38.
73. **Miller, C. L., M. M. Arnold, T. J. Broering, C. E. Hastings, and M. L. Nibert.** 2010. Localization of mammalian orthoreovirus proteins to cytoplasmic factory-like structures via nonoverlapping regions of μNS. Journal of Virology **84:**867-82.
74. **Miller, C. L., T. J. Broering, J. S. Parker, M. M. Arnold, and M. L. Nibert.** 2003. Reovirus σNS protein localizes to inclusions through an association requiring the μNS amino terminus. Journal of Virology **77:**4566-4576.
75. **Miller, C. L., J. S. Parker, J. B. Dinoso, C. D. Piggott, M. J. Perron, and M. L. Nibert.** 2004. Increased ubiquitination and other covariant phenotypes attributed to a strain- and temperature-dependent defect of reovirus core protein μ2. Journal of Virology **78:**10291-10302.

76. **Mora, M., K. Partin, M. Bhatia, J. Partin, and C. Carter.** 1987. Association of reovirus proteins with the structural matrix of infected cells. Virology **159:**265-277.
77. **Morgan, E. M., and H. J. Zweerink.** 1975. Characterization of transcriptase and replicase particles isolated from reovirus infected cells. Virology **68:**455-466.
78. **Morgan, E. M., and H. J. Zweerink.** 1974. Reovirus morphogenesis: core-like particles in cells infected at 39^{o} with wild-type reovirus and temperature-sensitive mutants of groups B and G. Virology **59:**556-565.
79. **Mustoe, T. A., R. F. Ramig, A. H. Sharpe, and B. N. Fields.** 1978. Genetics of reovirus: identification of the dsRNA segments encoding the polypeptides of the μ and σ size classes. Virology **89:**594-604.
80. **Nakayama, E. E., and T. Shioda.** 2010. Anti-retroviral activity of TRIM5α. Reviews in Medical Virology **20:**77-92.
81. **Netherton, C. L., and T. Wileman.** 2011. Virus factories, double membrane vesicles and viroplasm generated in animal cells. Current Opinion in Virology **1:**381-7.
82. **Neumann, G., and Y. Kawaoka.** 2006. Host range restriction and pathogenicity in the context of influenza pandemic. Emerging Infectious Diseases **12:**881-886.
83. **Neumann, G., T. Noda, and Y. Kawaoka.** 2009. Emergence and pandemic potential of swine-origin H1N1 influenza virus. Nature **459:**931-939.
84. **Nibert, M. L., R. L. Margraf, and K. M. Coombs.** 1996. Nonrandom segregation of parental alleles in reovirus reassortants. Journal of Virology **70:**7295-7300.
85. **Noble, S., and M. L. Nibert.** 1997. Core protein μ2 is a second determinant of nucleoside triphosphatase activities by reovirus cores. Journal of Virology **71:**7728-7735.
86. **Nonoyama, M., S. Millward, and A. F. Graham.** 1974. Control of transcription of the reovirus genome. Nucleic Acids Research **1:**373-385.
87. **Paine, P. L., L. C. Moore, and S. B. Horowitz.** 1975. Nuclear envelope permeability. Nature Reviews Microbiology **254:**109-114.
88. **Parker, J. S., T. J. Broering, J. Kim, D. E. Higgins, and M. L. Nibert.** 2002. Reovirus core protein μ2 determines the filamentous morphology of viral inclusion bodies by interacting with and stabilizing microtubules. Journal of Virology **76:**4483-4496.
89. **Patton, J. T., L. S. Silvestri, M. A. Tortorici, R. Vasquez-Del Carpio, and Z. F. Taraporewala.** 2006. Rotavirus genome replication and morphogenesis: role of the viroplasm. Current Topics in Microbiology and Immunology **309:**169-87.
90. **Racaniello, V. R.** 2007. Picornaviridae: The Viruses and Their Replication, p. 796-838. *In* D. M. Knipe and P. M. Howley (ed.), Fields Virology, 5 ed. Lippincott Williams & Wilkins, Philadelphia.
91. **Reinisch, K. M., M. L. Nibert, and S. C. Harrison.** 2000. Structure of the reovirus core at 3.6 Å resolution. Nature **404:**960-967.
92. **Rhim, J. S., L. E. Jordan, and H. D. Mayor.** 1962. Cytochemical, fluorescent-antibody and electron microscopic studies on the growth of reovirus (ECHO 10) in tissue culture. Virology **17:**342-355.

93. **Rodgers, S. E., E. S. Barton, S. M. Oberhaus, B. Pike, C. A. Gibson, K. L. Tyler, and T. S. Dermody.** 1997. Reovirus-induced apoptosis of MDCK cells is not linked to viral yield and is blocked by Bcl-2. Journal of Virology **71:**2540-2546.
94. **Rosen, L.** 1962. Reoviruses in animals other than man. Annals of the New York Academy of Science **101:**461-465.
95. **Sabin, A. B.** 1959. Reoviruses: a new group of respiratory and enteric viruses formerly classified as ECHO type 10 is described. Science **130:**1387-1389.
96. **Schiff, L. A., M. L. Nibert, and K. L. Tyler.** 2007. Orthoreoviruses and their replication, p. 1853-1915. *In* D. M. Knipe and P. M. Howley (ed.), Fields Virology, Fifth ed, vol. 2. Lippincott Williams & Wilkins, Philadelphia.
97. **Schmaljohn, C. S., and S. T. Nichol.** 2007. Bunyaviridae, p. 1742-1789. *In* D. M. Knipe and P. M. Howley (ed.), Fields Virology, 5 ed. Lippincott Williams & Wilkins, Philadelphia.
98. **Sharpe, A. H., L. B. Chen, and B. N. Fields.** 1982. The interaction of mammalian reoviruses with the cytoskeleton of monkey kidney CV-1 cells. Virology **120:**399-411.
99. **Shatkin, A. J., and A. J. LaFiandra.** 1972. Transcription by infectious subviral particles of reovirus. Journal of Virology **10:**698-706.
100. **Shatkin, A. J., J. D. Sipe, and P. C. Loh.** 1968. Separation of 10 reovirus genome segments by polyacrylamide gel electrophoresis. Journal of Virology **12:**986-991.
101. **Sherry, B.** 1998. Pathogenesis of reovirus myocarditis. Current Topics in Microbiology and Immunology **233:**51-66.
102. **Sherry, B., and M. A. Blum.** 1994. Multiple viral core proteins are determinants of reovirus-induced acute myocarditis. Journal of Virology **68:**8461-8465.
103. **Sherry, B., and B. N. Fields.** 1989. The reovirus M1 gene, encoding a viral core protein, is associated with the myocarditic phenotype of a reovirus variant. Journal of Virology **63:**4850-4856.
104. **Sherry, B., J. Torres, and M. A. Blum.** 1998. Reovirus induction of and sensitivity to beta interferon in cardiac myocyte cultures correlate with induction of myocarditis and are determined by viral core proteins. Journal of Virology **72:**1314-1323.
105. **Silverstein, S. C., and P. H. Schur.** 1970. Immunofluorescent localization of double-stranded RNA in reovirus-infected cells. Virology **41:**564-566.
106. **Skehel, J. J., and W. K. Joklik.** 1969. Studies on the in vitro transcription of reovirus RNA catalyzed by reovirus cores. Virology **39:**822-831.
107. **Smith, J. A., S. C. Schmechel, A. Raghavan, M. Abelson, C. Reilly, M. G. Katze, R. J. Kaufman, P. R. Bohjanen, and L. A. Schiff.** 2006. Reovirus induces and benefits from an integrated cellular stress response. Journal of Virology **80:**2019-2033.
108. **Starnes, M. C., and W. K. Joklik.** 1993. Reovirus protein λ3 is a poly(C)-dependent poly(G) polymerase. Virology **193:**356-366.
109. **Stoeckel, J., and J. G. Hay.** 2006. Drug evaluation: Reolysin--wild-type reovirus as a cancer therapeutic. Current Opinion in Molecular Therapeutics **8:**249-260.

110. **Stuart, D. I., and J. M. Grimes.** 2006. Structural studies on orbivirus proteins and particles. Current Topics in Microbiology and Immunology **309:**221-44.
111. **Sturzenbecker, L. J., M. L. Nibert, D. B. Furlong, and B. N. Fields.** 1987. Intracellular digestion of reovirus particles requires a low pH and is an essential step in the viral infectious cycle. Journal of Virology **61:**2351-2361.
112. **Tao, Y., D. L. Farsetta, M. L. Nibert, and S. C. Harrison.** 2002. RNA synthesis in a cage -- structural studies of reovirus polymerase λ3. Cell **111:**733-745.
113. **Taraporewala, Z. F., and J. T. Patton.** 2004. Nonstructural proteins involved in genome packaging and replication of rotaviruses and other members of the Reoviridae. Virus Research **101:**57-66.
114. **Twigger, K., L. Vidal, C. L. White, J. S. De Bono, S. Bhide, M. Coffey, B. Thompson, R. G. Vile, L. Heinemann, H. S. Pandha, F. Errington, A. A. Melcher, and K. J. Harrington.** 2008. Enhanced in vitro and in vivo cytotoxicity of combined reovirus and radiotherapy. Clinical Cancer Research **14:**912-923.
115. **Tyler, K. L., D. A. McPhee, and B. N. Fields.** 1986. Distinct pathways of viral spread in the host determined by reovirus S1 gene segment. Science **233:**770-774.
116. **Virgin, H. W., IV, R. Bassel-Duby, B. N. Fields, and K. L. Tyler.** 1988. Antibody protects against lethal infection with the neurally spreading reovirus type 3 (Dearing). Journal of Virology **62:**4594-4604.
117. **Virgin, H. W., IV, M. A. Mann, B. N. Fields, and K. L. Tyler.** 1991. Monoclonal antibodies to reovirus reveal structure/function relationships between capsid proteins and genetics of susceptibility to antibody action. Journal of Virology **65:**6772-6781.
118. **Virgin, S.** 2007. Pathogenesis of viral infection, p. 327-388. *In* D. M. Knipe and P. M. Howley (ed.), Fields Virology, 5 ed. Lippincott Williams & Wilkins, Philadelphia.
119. **Walker, J. E., M. Saraste, M. J. Runswick, and N. J. Gay.** 1982. Distantly related sequences in the α- and β-subunits of ATP synthase, myosin, kinases and other ATP-requiring enzymes and a common nucleotide binding fold. The EMBO Journal **1:**945-951.
120. **Weibel, E. R.** 1979. Stereological Methods: Practical Methods for Biological Morphometry., vol. 1. Academic Press, London.
121. **Weiner, H. L., D. Drayna, D. R. Averill, Jr, and B. N. Fields.** 1977. Molecular basis of reovirus virulence: role of the S1 gene. Proceedings of the National Academy of Sciences USA **74:**5744-5748.
122. **Whitton, J. L., C. T. Cornell, and R. Feuer.** 2005. Host and virus determinants of picornavirus pathogenesis and tropism. Nature reviews Microbiology **3:**765-76.
123. **Yin, P., M. Cheang, and K. M. Coombs.** 1996. The M1 gene is associated with differences in the temperature optimum of the transcriptase activity in reovirus core particles. Journal of Virology **70:**1223-1227.
124. **Yin, P., N. D. Keirstead, T. J. Broering, M. M. Arnold, J. S. Parker, M. L. Nibert, and K. M. Coombs.** 2004. Comparisons of the M1 genome segments and encoded μ2 proteins of different reovirus isolates. Virology Journal **1:**6.
125. **Yue, Z., and A. J. Shatkin.** 1998. Enzymatic and control functions of reovirus structural proteins. Current Topics in Microbiology and Immunology **233:**31-56.

126. **Zhang, X., S. B. Walker, P. R. Chipman, M. L. Nibert, and T. S. Baker.** 2003. Reovirus polymerase λ3 localized by cryo-electron microscopy of virions at a resolution of 7.6 A. Nature Structural Biology **10:**1011-1018.
127. **Zou, S., and E. G. Brown.** 1996. Stable expression of the reovirus μ2 protein in mouse L cells complements the growth of a reovirus ts mutant with a defect in its M1 gene. Virology **217:**42-48.
128. **Zurney, J., T. Kobayashi, G. H. Holm, T. S. Dermody, and B. Sherry.** 2009. The reovirus μ2 protein inhibits interferon signaling through a novel mechanism involving nuclear accumulation of interferon regulatory factor 9. Journal of Virology **83:**2178-2187.
129. **Zweerink, H. J.** 1974. Multiple forms of ss-dsRNA polymerase activity in reovirus-infected cells. Nature **247:**313-315.
130. **Zweerink, H. J., Y. Ito, and T. Matsuhisa.** 1972. Synthesis of reovirus double-stranded RNA within virion-like particles. Virology **50:**349-358.
131. **Zweerink, H. J., and W. K. Joklik.** 1970. Studies on the intracellular synthesis of reovirus-specified proteins. Virology **41:**501-518.
132. **Zweerink, H. J., E. M. Morgan, and J. S. Skyler.** 1976. Reovirus morphogenesis: characterization of subviral particles in infected cells. Virology **73:**442-453.